PB81-228587

Time-Settlement Behavior of Processed Refuse
Part IV: Consolidation of Milled Refuse
Volume 1, Volume 2-Appendix

Northwestern Univ.
Evanston, IL

Prepared for

Municipal Environmental Research Lab.
Cincinnati, OH

Jul 81

U.S. Department of Commerce
National Technical Information Service
NTIS

EPA-600/2-81-136
August 1981

PB81-228587

TIME-SETTLEMENT BEHAVIOR OF PROCESSED REFUSE

Part IV - Consolidation of Milled Refuse
Volume 1
Volume 2 - Appendix

by

W.H. Chen
A.G. Franklin
J.E. Quon
The Technological Institute
Department of Civil Engineering
Northwestern University
Evanston, Illinois 60201

Grant No. 800654

Project Officer

Norbert B. Schomaker
Solid and Hazardous Waste Research Division
Municipal Environmental Research Laboratory
Cincinnati, Ohio 45268

MUNICIPAL ENVIRONMENTAL RESEARCH LABORATORY
OFFICE OF RESEARCH AND DEVELOPMENT
U.S. ENVIRONMENTAL PROTECTION AGENCY
CINCINNATI, OHIO 45268

REPRODUCED BY
NATIONAL TECHNICAL
INFORMATION SERVICE
U.S. DEPARTMENT OF COMMERCE
SPRINGFIELD, VA 22161

NOTICE

THIS DOCUMENT HAS BEEN REPRODUCED FROM THE BEST COPY FURNISHED US BY THE SPONSORING AGENCY. ALTHOUGH IT IS RECOGNIZED THAT CERTAIN PORTIONS ARE ILLEGIBLE, IT IS BEING RELEASED IN THE INTEREST OF MAKING AVAILABLE AS MUCH INFORMATION AS POSSIBLE.

TECHNICAL REPORT DATA

(Please read Instructions on the reverse before completing)

1. REPORT NO. EPA-600/2-81-136	2. ORD Report	3. RECIPIENT'S ACCESSION NO. PB81 228587
4. TITLE AND SUBTITLE TIME SETTLEMENT BEHAVIOR OF PROCESSED REFUSE FINAL REPORT, Part IV - Consolidation of Milled Refuse Volume 1 Volume 2 - Appendix		5. REPORT DATE July 1981 6. PERFORMING ORGANIZATION CODE
7. AUTHOR(S) A.G. Franklin, W.H. Chen, J.E. Quon		8. PERFORMING ORGANIZATION REPORT NO.
9. PERFORMING ORGANIZATION NAME AND ADDRESS The Technological Institute Department of Civil Engineering Northwestern University Evanston, Illinois 60201		10. PROGRAM ELEMENT NO. 11. CONTRACT/GRANT NO. 800654
12. SPONSORING AGENCY NAME AND ADDRESS Municipal Environmental Research Laboratory Office of Research and Development U.S. Environmental Protection Agency Cincinnati, Ohio 45268		13. TYPE OF REPORT AND PERIOD COVERED 3/1/71 -- 5-31-75 14. SPONSORING AGENCY CODE EPA/600/14

15. SUPPLEMENTARY NOTES

Project Officer: Norbert B. Schomaker (513) 684-7871

16. ABSTRACT

A previously developed mathematical model for the prediction of the time-settlement behavior of a sanitary landfill of milled refuse, taking into account the effects of finite deformations, large creep strains, and biological and chemical decomposition of the material with accompanying gas and liquid generation, is reviewed. Modifications and refinements of this model have been made in light of consolidation test data obtained in the present study from the laboratory testing of both raw and laboratory aged milled refuse samples. An apparatus for the consolidation testing of milled refuse was developed in which a back pressure of up to 100 psi can be applied to insure essentially complete saturation of the sample. Laboratory aging of samples was conducted in an insulated chamber maintained at a constant temperature of about 125 F. Consolidation tests were performed on 4 raw samples and 11 samples aged for periods of up to 12 months. A general equation of continuity based on the theory of mixture was combined with a rate process function based on the micropore structure to represent the modified model for the time-settlement behavior of this material. Encouraging agreement between the theoretical time-settlement predictions and experimental results was obtained. Limitations of the modified mathematical model and of the experimental program are discussed and a simplified method which is convenient for practical use to represent the time-settlement behavior of miled refuse is discussed.

17. KEY WORDS AND DOCUMENT ANALYSIS

a. DESCRIPTORS		b. IDENTIFIERS/OPEN ENDED TERMS	c. COSATI Field/Group
Sanitary Landfill Mathematical Model Milled Refuse Biological Decomposition Chemical Decomposition Finite Strain Finite Deformation	Creep Strain Variation of Saturation Rate Process Function Testing Apparatus Settlement Behavior Secondary Comparison	Sanitary Landfill Milled Refuse Settlement Behaviors	68C

18. DISTRIBUTION STATEMENT RELEASE TO PUBLIC	19. SECURITY CLASS *(This Report)* UNCLASSIFIED	21. NO. OF PAGES
	20. SECURITY CLASS *(This page)* UNCLASSIFIED	22.

EPA Form 2220-1 (9-73)

TYPING GUIDE SHEET
BEGIN FIRST LINE OF TEXT HERE
CENTER OF PAGE
TOP OF IMAGE AREA
DROPPED HEAD BEGIN SECTIONS HERE

DISCLAIMER

This report has been reviewed by the Municipal Environmental Research Laboratory, U.S. Environmental Protection Agency, and approved for publication. Approval does not signify that the contents necessarily reflect the views and policies of the U.S. Environmental Protection Agency, nor does mention of trade names or commercial products constitute endorsement or recommendation for use.

BEGIN LAST LINE OF TEXT
BOTTOM OF IMAGE AREA, OUTSIDE DIMENSION FOR TABLES AND ILLUSTRATIONS
5/8"

PAGE NUMBER
EPA-287 (Cin.)
(4-76)

FOREWORD

The Environmental Protection Agency was created because of increasing public and government concern about the dangers of pollution to the health and welfare of the American people. Noxious air, foul water, and spoiled land are tragic testimony to the deterioration of our natural environment. The complexity of that environment and the interplay between its components require a concentrated and integrated attack on the problem.

Research and development is that necessary first step in problem solution and it involves defining the problem, measuring its impact, and searching for solutions. The Municipal Environmental Research Laboratory develops new and improved technology and systems for the prevention, treatment, and management of wastewater and solid and hazardous waste pollutant discharges from municipal and community sources, for the preservation and treatment of public drinking water supplies, and to minimize the adverse economic, social, health, and aesthetic effects of pollution. This publication is one of the products that research; a most vital communications link between the researcher and the user community.

A previously proposed mathematical model of the time-settlement behavior of a sanitary landfill containing milled refuse is reviewed and refined in the context of the new data obtained in the study. The report includes discussion of a simplified practical method for representing the time-settlement behavior of milled refuse.

Francis T. Mayo
Director
Municipal Environmental Research
Laboratory

ABSTRACT

A previously developed mathematical model for the prediction of the time-settlement behavior of a sanitary landfill of milled refuse, taking into account the effects of finite deformations, large creep strains, and biological and chemical decomposition of the material with accompanying gas and liquid generation, is reviewed. Modifications and refinements of this model have been made in light of consolidation test data obtained in the present study from the laboratory testing of both raw and laboratory aged milled refuse samples.

An apparatus for the consolidation testing of milled refuse was developed in which a back pressure of up to 100 psi can be applied to insure essentially complete saturation of the sample. Laboratory aging of samples was conducted in an insulated chamber maintained at a constant temperature of about 125 F. Consolidation tests were performed on 4 raw samples and 11 samples aged for periods of up to 12 months.

A general equation of continuity based on the theory of mixture was combined with a rate process function based on the micropore structure to represent the modified model for the time-settlement behavior of this material. Encouraging agreement between the theoretical time-settlement predictions and experimental results was obtained. Limitations of the modified mathematical model and of the experimental program are discussed and a simplified method which is convenient for practical use to represent the time-settlement behavior of milled refuse is discussed.

CONTENTS

Foreword iii
Abstract iv
Figures viii
Tables xx
Symbols xxi

1. Introduction 1
2. Milled Refuse 4

    Introduction 4
    Characteristics of Milled Refuse 6
    Decomposition of Milled Refuse 12
    The Structure of Milled Refuse 14
    Permeability 17

3. Consolidation Theory 24

    Terzaghi's Theory of Consolidation 25
    Validity of Terzaghi's Assumptions 28
    Mechanisms of Secondary Consolidation 29

        Terzaghi-Taylor Concept of Structural Viscosity 30
        Tan's Concept of The Jumping of Bounds 31
        The Concept of Two Levels of Structure 31

    Modified Theory of Consolidation 32

        Multi-dimensional Compression 33
        Validity of Darcy's Law 35
        Finite Strain and Variable Permeability and Compressibility 36
        Nonlinear Void Ratio - Effective Stress Relationship 37

    Summary 39

4. Consolidation Model of Milled Refuse 43

    Equation of Continuity 43
    Generized Darcy's Law 46

TYPING GUIDE SHEET
BEGIN FIRST LINE OF TEXT HERE
CENTER OF PAGE
TOP OF IMAGE AREA
DROPPED HEAD BEGIN SECTIONS HERE

General Equation of Pore Pressure Dissipation 47
Earlier Consolidation Model for Milled Refuse 50
Modified Consolidation Model of Milled Refuse 52
Summary 62

5. Creep Models 63

Parameter Study of Creep Model Based On Structural Viscosity 64
Parameter Study of Creep Model Based On Micropore Structure 67
Summary 70

6. Consolidation Tests of Milled Refuse 73

Consolidometer for Milled Refuse 73

  Development of Consolidometer 73
  The Consolidation Cell 75
  Loading and Back Pressure System 78
  Pore Pressure Measurement 82

Preparation of Samples 83
Aging of Samples 84
Testing Procedures 85
Summary 89

7. Determination of Model Parameters 92

8. Experimental Results 108

Experimental Program 108
Temperature Data From Laboratory Aged Milled Refuse Samples 109
The Rate Constant of Milled Refuse Decomposition 111
Test Results 119
Discussion of Test Results 148

  Effect of the Load Increment Ratio on the Shape of the Time-deformation Cueve 148
  Effect of the Load Increment Ratio on the Relative Amount of Secondary Compression 150
  Effect of Aging and Load Increment on Consolidation Behavior 150

BEGIN LAST LINE OF TEXT
BOTTOM OF IMAGE AREA OUTSIDE DIMENSION FOR TABLES AND ILLUSTRATIONS
PAGE NUMBER
EPA-287 (Cin.)
(4-78)

Effect of the Rate of Decomposition of Solid on the Consolidation Behavior of Milled Refuse 163

Summary 168

9. Applicability of the Model 171

Effect of the Degree of Saturation 171
Effect of the Generation of Gases and Liquids 173
Limitations of the Model and the Test Program 177
Practical Applications 182
Summary 183

10. Simplified Method of Analysis 184

Simplified Creep Expressions 184
Simplified Method 189
Summary 195

11. Summary, Conclusions, and Recommendations 196

References 202

Appendices

A. The Numerical Solution of the Governing Nonlinear Partial Differential Equations 212

B. Listing of Computer Program and Flow Chart 221

C. Computer Input Data for the Samples Tested 246

D. Results of the Parameter Study of Creep Models 259

FIGURES

Number Page

2-1 Effect of grate size on the particle size distribution of milled refuse.................. 9

2-2 Data from Greater London, England, 1969, showing effect of various grate spacing on pulverized refuse density...................... 10

2-3 A photomicrograph of handsheets made from bleached unbeaten paper pulp.................. 16

2-4 A micromigragraph of a non-woody fine fibrous peat................................ 18

2-5 A photomicrograph of fine peat fibers.......... 20

2-6 Permeability versus dry density of milled refuse.. 21

2-7 Permeability versus solid content of paper-mill sludge................................ 22

3-1 Rheological models............................ 40

4-1 Rheological model based on the micropore mechanism.................................... 54

4-2 Rheological model based on the structural viscosity.................................... 59

5-1 Settlement vs. time factor of the creep model based on structural viscosity for various value of stress increment: $\alpha_o p_o$=10, (p_f/p_o)x $(\alpha_f/\alpha_o)^{0.5}$=1................................ 71

5-2 Settlement vs. time factor of the creep model based on micropore structure for various values of p_f/p_o: B_o = 10....................... 72

6-1 The consolidation cell for 6.75 in. diameter sample...................................... 76

6-2a Schematical overall experimental set-up........ 79

6-2b Overall experimental set-up.................... 80

6-2c Consolidation test cell....................... 81

6-3 Typical relationship of thermistor resistance to its temperature............................ 86

FIGURES

Number		Page
7-1	Void ratio versus log time record for sample R3-4-1	93
7-2	Strain versus log strain rate of sample R3-4-1	95
7-3	Log strain rate versus log time plot of sample R3-4-1	96
7-4	Permeability versus void ratio used in the present study	107
8-1	Milled refuse cell temperature vs. time	110
8-2	Temperature difference vs. time for sample A2-2-1	112
8-3	Temperature difference vs. time for sample A3-2-1	113
8-4	Temperature difference vs. time for sample A3-4-1	114
8-5	Temperature difference vs. time for sample A4-2-1	115
8-6	Void ratio vs. log time plot for sample A3-8-1	120
8-7	Experimental and theoretical void ratio vs. log time curve for sample R3-2-1	123
8-8	Experimental and theoretical void ratio vs. log time curve for sample R3-2-2	124
8-9	Experimental and theoretical void ratio vs. log time curve for sample R3-4-1	125
8-10	Experimental and theoretical void ratio vs. log time curve for sample R3-4-2	126
8-11	Experimental and theoretical void ratio vs. log time curve for sample R3-8-1	127
8-12	Experimental and theoretical void ratio vs. log time curve for sample R3-16-1	128
8-13	Experimental and theoretical void ratio vs. log time curve for sample A2-2-1	129

FIGURES

Number		Page
8-14	Experimental and theoretical void ratio vs. log time curve for sample A2-2-2.............	130
8-15	Experimental and theoretical void ratio vs. log time curve for sample A2-4-1.............	131
8-16	Experimental and theoretical void ratio vs. log time curve for sample A2-4-2.............	132
8-17	Experimental and theoretical void ratio vs. log time curve for sample A2-8-1.............	133
8-18	Experimental and theoretical void ratio vs. log time curve for sample A2-16-1............	134
8-19	Experimental and theoretical void ratio vs. log time curve for sample A3-2-1.............	135
8-20	Experimental and theoretical void ratio vs. log time curve for sample A3-2-2.............	136
8-21	Experimental and theoretical void ratio vs. log time curve for sample A3-4-1.............	137
8-22	Experimental and theoretical void ratio vs. log time curve for sample A3-4-2.............	138
8-23	Experimental and theoretical void ratio vs. log time curve for sample A3-8-1.............	139
8-24	Experimental and theoretical void ratio vs. log time curve for sample A3-16-1............	140
8-25	Experimental and theoretical void ratio vs. log time curve for sample A4-2-1.............	141
8-26	Experimental and theoretical void ratio vs. log time curve for sample A4-2-2.............	142
8-27	Experimental and theoretical void ratio vs. log time curve for sample A4-4-1.............	143
8-28	Experimental and theoretical void ratio vs. log time curve for sample A4-4-2.............	144
8-29	Experimental and theoretical void ratio vs. log time curve for sample A4-8-1.............	145

Reproduced from
best available copy.

FIGURES

Number Page

8-30 Experimental and theoretical pore pressure dissipation curve for sample A3-8-1........... 147

8-31 Effect of load increment on shape of settlement versus time curve, undisturbed Mexico City clay 149

8-32 Effect of load increment ratio on consolidation behavior of raw milled refuse samples......... 151

8-33 Effect of load increment ratio on consolidation behavior of aged milled refuse samples........ 152

8-34 Strain vs. log time curves for various value of P_f/p_o: sample R3......................... 153

8-35 Strain vs. log time curves for various value of p_f/p_o: sample A2......................... 154

8-36 Influence of effective stress ratio on the initial value of creep index.................. 161

8-37 Influence of effective stress ratio on the final value of creep index.................... 162

8-38 Influence of effective stress ratio on strain rate for sample R3.......................... 164

8-39 Influence of effective stress ratio on strain rate for sample A2.......................... 165

8-40 Influence of effective stress ratio on strain rate for sample A3.......................... 166

8-41 Influence of sample aging on the strain rate.. 167

9-1 Time-settlement curves showing the effect of biological and/or chemical activity........... 176

9-2 Time-effective saturation curves showing the effect of the biological and/or chemical activity.................................... 178

9-3 Strain vs. log time plot showing the effect of the sample thickness......................... 180

10-1 Log (de/dt) versus log time graphs for individual variations of H, p, and e_o......... 186

FIGURES

Number Page

10-2 Nomograph for settlement predictions........... 187

10-3 Log strain rate versus log time plot of sample R3-4-1.................................. 191

A-1 Boundary conditions for W and V................ 215

A-2 Time-space grid................................ 216

D-1 Settlement vs. time factor of the creep model based on structural viscosity for various value of stress increment: $\alpha_o p_o=10$, (p_f/p_o)x $(\alpha_f/\alpha_o)^{0.5}=1$.................................. 260

D-2 Settlement vs. time factor of the creep model based on structural viscosity for various value of stress increment: $\alpha_o p_o=15$, (p_f/p_o)x $(\alpha_f/\alpha_o)^{0.5}=1$.................................. 261

D-3 Settlement vs. time factor of the creep model based on structural viscosity for various value of stress increment: $\alpha_o p_o=20$, (p_f/p_o)x $(\alpha_f/\alpha_o)^{0.5}=1$................................. 262

D-4 Settlement vs. time factor of the creep model based on structural viscosity for various values of stress increment: $\alpha_o p_o=25$, (p_f/p_o)x $(\alpha_f/\alpha_o)^{0.5}=1$................................. 263

D-5 Settlement vs. time factor of the creep model based on structural viscosity for various values of stress increment: $\alpha_o p_o=30$, (p_f/p_o)x $(\alpha_f/\alpha_o)^{0.5}=1$................................. 264

D-6 Settlement vs. time factor of the creep model based on structural viscosity for various values of $\alpha_o p_o$: $(p_f/p_o)=1.5$, $(p_f/p_o)(\alpha_f/\alpha_o)^{0.5}=1$ 265

D-7 Settlement vs. time factor of the creep model based on structural viscosity for various values of $\alpha_o p_o$: $(p_f/p_o)=2$, $(p_f/p_o)(\alpha_f/\alpha_o)^{0.5}=1$.. 266

D-8 Settlement vs. time factor of the creep model based on structural viscosity for various values of $\alpha_o p_o$: $(p_f/p_o)=4$, $(p_f/p_o)(\alpha_f/\alpha_o)^{0.5}=1$ 267

FIGURES

Number | Page

D-9 Settlement vs. time factor of the creep model based on structural viscosity for various values of stress increment: $\alpha_o p_o=10, (p_f/p_o) \times (\alpha_f/\alpha_o)=1$ 268

D-10 Settlement vs. time factor of the creep model based on structural viscosity for various values of stress increment: $\alpha p_o=15, (p_f/p_o) \times (\alpha_f/\alpha_o)=1$ 269

D-11 Settlement vs. time factor of the creep model based on structural viscosity for various values of stress increment: $\alpha p_o=20, (p_f/p_o) \times (\alpha_f/\alpha_o)=1$ 270

D-12 Settlement vs. time factor of the creep model based on structural viscosity for various values of stress increment: $\alpha p_o=25, (p_f/p_o) \times (\alpha_f/\alpha_o)=1$ 271

D-13 Settlement vs. time factor of the creep model based on structural viscosity for various values of stress increment: $\alpha p_o=30, (p_f/p_o) \times (\alpha_f/\alpha_o)=1$ 272

D-14 Settlement vs. time factor of the creep model based on structural viscosity for various values of $\alpha_o p_o : p_f/p_o=1.5, (p_f/p_o)(\alpha_f/\alpha_o)=1$ 273

D-15 Settlement vs. time factor of the creep model based on structural viscosity for various values of $\alpha_o p_o : p_f/p_o=2, (p_f/p_o)(\alpha_f/\alpha_o)=1$ 274

D-16 Settlement vs. time factor of the creep model based on structural viscosity for various values of $\alpha_o p_o : p_f/p_o=4, (p_f/p_o)(\alpha_f/\alpha_o)=1$ 275

D-17 Settlement vs. time factor of the creep model based on structural viscosity for various values of stress increment: $\alpha_o p_o=10, (p_f/p_o) \times (\alpha_f/\alpha_o)^{1.5}=1$ 276

D-18 Settlement vs. time factor of the creep model based on structural viscosity for various values of stress intensity: $\alpha_o p_o=15, (p_f/p_o) \times (\alpha_f/\alpha_o)^{1.5}=1$ 277

FIGURES

Number Page

D-19 Settlement vs. time factor of the creep model based on structural viscosity for various values of stress increment: $\alpha_o p_o=20$, $(p_f/p_o)\times(\alpha_f/\alpha_o)^{1.5}=1$ 278

D-20 Settlement vs. time factor of the creep model based on structural viscosity for various values of stress increment: $\alpha_o p_o=25$, $(p_f/p_o)\times(\alpha_f/\alpha_o)^{1.5}=1$ 279

D-21 Settlement vs. time factor of the creep model based on structural viscosity for various values of stress increment: $\alpha_o p_o=30$, $(p_f/p_o)\times(\alpha_f/\alpha_o)^{1.5}=1$ 280

D-22 Settlement vs. time factor of the creep model based on structural viscosity for various values of $\alpha_o p_o$: $p_f/p_o=1.5$ $(p_f/p_o)(\alpha_f/\alpha_o)^{1.5}=1$.. 281

D-23 Settlement vs. time factor of the creep model based on structural viscosity for various values of $\alpha_o p_o$: $p_f/p_o=2$, $(p_f/p_o)(\alpha_f/\alpha_o)^{1.5}=1$... 282

D-24 Settlement vs. time factor of the creep model based on structural viscosity for various values of $\alpha_o p_o$: $p_f/p_o=4$, $(p_f/p_o)(\alpha_f/\alpha_o)^{1.5}=1$... 283

D-25 Settlement vs. time factor of the creep model based on structural viscosity for various values of the ratio of the slope of the e_b-log p line to the slope of the e_b - logα line: $\alpha_o p_o=10$, $p_f/p_o=4$ 284

D-26 Settlement vs. time factor of the creep model based on structural viscosity for various values of the ratio of the slope of the e_b-log p line to the slope of the e_b - logα line: $\alpha_o p_o=20$, $p_f/p_o=4$ 285

D-27 Settlement vs. time factor of the creep model based on structural viscosity for various values of the ratio of the slope of the e_b-log p line to the slope of the e_b - logα line: $\alpha_o p_o=30$, $p_f/p_o=4$ 286

Reproduced from best available copy.

FIGURES

Number		Page
D-28	Settlement vs. time factor of the creep model based on micropore structure for various values of p_f/p_o: B_o=10	287
D-29	Settlement vs. time factor of the creep model based on micropore structure for various values of p_f/p_o: B_o=11	288
D-30	Settlement vs. time factor of the creep model based on micropore structure for various values of p_f/p_o: B_o=12	289
D-31	Settlement vs. time factor of the creep model based on micropore structure for various values of p_f/p_o: B_o=13	290
D-32	Settlement vs. time factor of the creep model based on micropore structure for various values of p_f/p_o: B_o=14	291
D-33	Settlement vs. time factor of the creep model based on micropore structure for various values of p_f/p_o: B_o=15	292
D-34	Settlement vs. time factor of the creep model based on micropore structure for various values of p_f/p_o: B_o=16	293
D-35	Settlement vs. time factor of the creep model based on micropore structure for various values of p_f/p_o: B_o=17	294
D-36	Settlement vs. time factor of the creep model based on micropore structure for various values of p_f/p_o: B_o=18	295
D-37	Settlement vs. time factor of the creep model based on micropore structure for various values of p_f/p_o: B_o=19	296
D-38	Settlement vs. time factor of the creep model based on micropore structure for various values of p_f/p_o: B_o=20	297
D-39	Settlement vs. time factor of the creep model based on micropore structure for various values of p_f/p_o: B_o=25	298

FIGURES

Number		Page
D-40	Settlement vs. time factor of the creep model based on micropore structure for various values of p_f/p_o; $B_o=30$	299
D-41	Settlement vs. time factor of the creep model based on micropore structure for various values of p_f/p_o; $B_o=10$	300
D-42	Settlement vs. time factor of the creep model based on micropore structure for various values of p_f/p_o; $B_o=11$	301
D-43	Settlement vs. time factor of the creep model based on micropore structure for various values of p_f/p_o; $B_o=12$	302
D-44	Settlement vs. time factor of the creep model based on micropore structure for various values of p_f/p_o; $B_o=13$	303
D-45	Settlement vs. time factor of the creep model based on micropore structure for various values of p_f/p_o; $B_o=14$	304
D-46	Settlement vs. time factor of the creep model based on micropore structure for various values of p_f/p_o; $B_o=15$	305
D-47	Settlement vs. time factor of the creep model based on micropore structure for various values of p_f/p_o; $B_o=16$	306
D-48	Settlement vs. time factor of the creep model based on micropore structure for various values of p_f/p_o; $B_o=17$	307
D-49	Settlement vs. time factor of the creep model based on micropore structure for various values of p_f/p_o; $B_o=18$	308
D-50	Settlement vs. time factor of the creep model based on micropore structure for various values of p_f/p_o; $B_o=19$	309
D-51	Settlement vs. time factor of the creep model based on micropore structure for various values of p_f/p_o; $B_o=20$	310

FIGURES

Number Page

D-52 Settlement vs. time factor of the creep model based on micropore structure for various values of $p_f/p_o : B_o=25$ 311

D-53 Settlement vs. time factor of the creep model based on micropore structure for various values of $p_f/p_o : B_o=30$ 312

D-54 Settlement vs. time factor of the creep model based on micropore structure for various values of $p_f/p_o : B_o=10$ 313

D-55 Settlement vs. time factor of the creep model based on micropore structure for various values of $p_f/p_o : B_o=11$ 314

D-56 Settlement vs. time factor of the creep model based on micropore structure for various values of $p_f/p_o : B_o=12$ 315

D-57 Settlement vs. time factor of the creep model based on micropore structure for various values of $p_f/p_o : B_o=13$ 316

D-58 Settlement vs. time factor of the creep model based on micropore structure for various values of $p_f/p_o : B_o=14$ 317

D-59 Settlement vs. time factor of the creep model based on micropore structure for various values of $p_f/p_o : B_o=15$ 318

D-60 Settlement vs. time factor of the creep model based on micropore structure for various values of $p_f/p_o : B_o=16$ 319

D-61 Settlement vs. time factor of the creep model based on micropore structure for various values of $p_f/p_o : B_o=17$ 320

D-62 Settlement vs. time factor of the creep model based on micropore structure for various values of $p_f/p_o : B_o=18$ 321

D-63 Settlement vs. time factor of the creep model based on micropore structure for various values of $p_f/p_o : B_o=19$ 322

FIGURES

Number Page

D-64 Settlement vs. time factor of the creep model based on micropore structure for various values of p_f/p_o:$B_o=20$........................ 323

D-65 Settlement vs. time factor of the creep model based on micropore structure for various values of p_f/p_o:$B_o=25$........................ 324

D-66 Settlement vs. time factor of the creep model based on micropore structure for various values of p_f/p_o:$B_o=30$........................ 325

D-67 Settlement vs. time factor of the creep model based on micropore structure for various values of B_o:$p_f/p_o=1.5$........................ 326

D-68 Settlement vs. time factor of the creep model based on micropore structure for various values of B_o:$p_f/p_o=4$.......................... 327

D-69 Settlement vs. time factor of the creep model based on micropore structure for various values of B_o:$p_f/p_o=16$........................ 328

D-70 Settlement vs. time factor of the creep model based on micropore structure for various values of B_o:$p_f/p_o=1.5$........................ 330

D-71 Settlement vs. time factor of the creep model based on micropore structure for various values of B_o:$p_f/p_o=4$.......................... 330

D-72 Settlement vs. time factor of the creep model based on micropore structure for various values of B_o:$p_f/p_o=16$........................ 331

D-73 Settlement vs. time factor of the creep model based on micropore structure for various values of B_o:$p_f/p_o=1.5$........................ 332

D-74 Settlement vs. time factor of the creep model based on micropore structure for various values of B_o:$p_f/p_o=4$.......................... 333

D-75 Settlement vs. time factor of the creep model based on micropore structure for various values of B_o:$p_f/p_o=16$........................ 334

Reproduced from best available copy.

FIGURES

Number		Page
D-76	Settlement vs. time factor of the creep model based on micropore structure for various values of the ratio of the slope of the e_b-log p line to the slope of the e_b-log B line: $B_o=10$, $p_f/p_o=4$	335
D-77	Settlement vs. time factor of the creep model based on micropore structure for various values of the ratio of the slope of the e_b-log p line to the slope of the e_b-log B line: $B_o=20$, $p_f/p_o=4$	336
D-78	Settlement vs. time factor of the creep model based on micropore structure for various values of the ratio of the slope of the e_b-log p line to the slope of the e_b-log B line: $B_o=30$, $p_f/p_o=4$	337

TABLES

Number		Page
2-1	Composition of Solid Waste (Wet Basis) Madison, Wisconsin	7
2-2	Effect of grate size on effective density and machine capacity	11
6-1	Burette reading for sample R3-4-1	91
6-2	Burette readings for sample A4-4-1	91
7-1	Curve-fitting data for sample R3-4-1	100
8-1	Rate constant for digestion of cellulose and cellulosic materials	117
8-2	Values of rheological parameters	121
8-3	Values of creep index and apparent permeability	159
10-1	Values of parameters for simplified method	193

SYMBOLS

a_{vo} = initial value of compressibility

A = rheological parameter

A_o = initial value of A

A_f = final value of A

A_p = projected value of strain rate at zero deviator stress on logarithm strain rate versus deviator stress plot for unit time

$\bar{A}$ = creep index

$\bar{A}_{bo}$ = initial value of $\bar{A}$

$\bar{A}_{bf}$ = final value of $\bar{A}$

B = rheological parameter

B_o = initial value of B

B_f = final value of B

$\bar{B}$ = apparent permeability

$\bar{B}_{bo}$ = initial value of $\bar{B}$

$\bar{B}_{bf}$ = final value of $\bar{B}$

C = rate constant at T° K

C_o = rate constant at T_o° K

C_v = Terzaghi consolidation coefficient

C_1 = the intercept on the $d\epsilon/dt$ axis at $t = 0.1$ min. for the primary stage

C_2 = the intercept on the $d\epsilon/dt$ axis at $t = 0.1$ min. for the secondary stage

C_α = the change in void ratio per $\log_{10}$ cycle of time

d = diameter of particle

D = principal stress difference

DS = degree of settlement

e = void ratio

e_b = time-dependent portion of void ratio at any time

e_{bo} = initial value of the time-dependent portion of void ratio

e_f = final void ratio

e_{bf} = final value of the time-dependent portion of void ratio

e_t = time-independent portion of void ratio at any time

e_{to} = initial value of the time-independent portion of void ratio

e_{tf} = final value of the time-independent portion of void ratio

e_o = initial void ratio

E = activation energy

g = acceleration of gravity

G_s = specific gravity of solids

h = head of fluid phase

h_g = the gravitational head

i = hydraulic gradient

i_t = "apparent" threshold gradient

k = permeability

k_o = initial permeability

k_f = final permeability

k_u = maximum or ultimate permeability

m_1 = slope of the straight line for the primary stage

m_2 = slope of the straight line for the secondary stage

p = equilibrium effective stress

p_b = effective stress in the bottom spring

p_f = final effective stress

p_o = initial effective stress

p_t = effective stress in the top spring

$\bar{r}$ = spatial axis vector

$\bar{r}^s$ = solid axis vector

R = gas constant

$\bar{R}^{sf}$ = resistivity to relative motion of the solid phase and the liquid phase

S = degree of saturation

S_r = residual saturation

t = time

t_1 = unit time

t_f = final time of consolidation

T_s = time factor

T_f = time conversion factor

u = macropore pressure

u_b = micropore pressure

$\bar{v}^f$ = fluid velocity relative to spatial coordinates

$\bar{v}^s$ = solid phase velocity relative to the fixed spatial system

$\bar{v}^\alpha$ = α phase velocity reletive to fixed spatial coordinates

V = bulk volume

V_o = initial bulk volume

z = dimensionless distance

α = rheological parameter

α_f = final value of α

α_o = initial value of α

α_1 = value of the slope of the mid-range linear portion of the logarithm strain rate versus deviator stress plot

γ_w = unit weight of water

ϵ = strain

$\dot{\epsilon}$ = strain rate

ϵ_f = final strain

θ = parameter

θ^α = fraction of volume occupied by the α phase

ρ^α = bulk density of α phase

ρ_a^α = the average point density of phase α

ρ^f = bulk density of fluid phase

ρ^s = bulk density of solid phase

σ_1 = major principal stress

σ_3 = minor principal stress

τ = structural viscosity

ψ^α = the amount of α phase generated

∇ = del operator

Δ = operator denoting an infinitesimal quantity

ϕ = weight of the decomposable part of the milled refuse at time t

ϕ_o = initial weight of the decomposable part of the milled refuse

β = rheological parameter

INTRODUCTION

One of the difficulties associated with the planning and subsequent use of a sanitary landfill is the prediction of its time-settlement behavior. A sanitary landfill is an active mass with a varying degree of saturation, undergoing biological and chemical changes. It has been recognized that the time-settlement behavior of such material is extremely complicated. At present, only limited data on the consolidation behavior of solid waste is available, and laboratory consolidation result of this material is not found in the literature.

In order to gain some insight into the time-settlement behavior of such material, various agencies have maintained settlement records of sanitary landfills for many years. Some agencies have maintained continuous settlement monitoring programs and others have performed short term studies. However, without a general theoretical treatment which incorporates all the essential factors that affect consolidation behavior, the interpretation of the field data is extremely difficult.

Milled refuse landfills, offering a number of advantages over other methods of refuse disposal, are believed likely to come into more widespread use in this country. Because of its homogeneity, milled refuse is potentially amenable to a kind of study and analysis which appears practically hopeless in conventionally handled refuse. The general research project under which this study was conducted has been initiated to establish rational methods of predicting the time-settlement behavior of milled refuse. The information gained will help in optimizing planning and in the subsequent beneficial use of the sanitary landfill using milled refuse.

In the first stage of the project, a mathematical model was developed to represent the time-settlement behavior of milled refuse (Zimmerman, 1972). This model includes the effects of finite strains, biological and chemical activity, time variation of saturation and large creep deformation. The effects of the time variation of material properties, constant and varying partial saturation, and biological activity on the model response have been investigated to yield theoretical time-settlement curves.

The primary objectives of the present study are to compare the theoretical predictions of the previously developed model with laboratory consolidation test results on both raw and aged milled refuse samples and to make necessary modifications and refinements of the theoretical model in light of the available consolidation test results.

Description of the characteristics, decomposition, and structure of milled refuse are given in Chapter II. For complex material such as this, most of the basic assumptions in the Terzaghi theory are not valid. In

Chapter III, various modified consolidation theories and mechanisms responsible for secondary compression are reviewed. A review of the time-settlement model previously developed to simulate the consolidation behavior of milled refuse, as well as the formulation of a modified model, are reported in Chapter IV. A parameter study of a creep model based on structural viscosity and of a creep model based on micropore structure is discussed in Chapter V.

In Chapter VI, description of the apparatus developed for consolidation testing of both raw and laboratory aged milled refuse samples under saturated conditions, and sample preparation, sample aging, and test techniques are reported. Procedures for the determination of model parameters are described in Chapter VII. Chapter VIII discusses the experimental results and the temperature data obtained from the laboratory aging process. Limitations of the model and of the experimental program are discussed in Chapter IX. A simplified method which is convenient for practical use to describe the time-settlement behavior of milled refuse is described in Chapter X. Conclusions of the present study are advanced in Chapter XI, together with recommendations for future investigations.

MILLED REFUSE

Introduction

Because of the growing awareness of the importance of preventing pollution of the environment, the development of new methods for the economic disposal of municipal refuse has become increasingly urgent. It has been customary in the past to deposit refuse on otherwise unused land, and to allow it to compact itself and to decompose slowly; but rising land costs severely inhibit this practice now. Thus prior processing of refuse is now being undertaken by ever larger numbers of authorities.

The concept of refuse shredding or milling, now catching hold in the United States, began in the early 1960's in Europe where it is now seeing increasingly wider use. Basically this process consists of shredding the refuse and mixing it to form a more or less homogeneous mass that can be spread easily, is relatively compact when in place, offers little support to vermin, depending on particle size. In addition to extending the usefulness of landfilling, shredding also may be a useful step in other methods of refuse disposal. With some improvements in the economics of the milling process, the milled refuse landfill is very likely to come into increasingly widespread use in this country.

The milling of refuse is done by one of a number of types of shredder or hammermill. Descriptions of the kinds of equipment in use in the United States are given by Cross et. al. (1971) and others. These devices are designed to reject nonmillable materials, metallic objects for instance, which are separated at the top of the milling chamber and thrown out of the machine through a discharge chute. Tin cans are normally crumpled or shredded. Glass bottles are disintegrated and the glass has the appearance of angular sand with a maximum size of about 1/8 inch. As a result of the milling process, the individual components of refuse such as newspapers and plastic bottles are not recognizable. The putrescible material is finely divided and distributed nearly uniformly throughout the mass, resulting in a material that will decompose faster than the unpulverized material. The general appearance of milled refuse is that of a homogenous mass of dirty, shredded paper.

Because of its relative homogeneity, this material better lends itself to study and analysis than that of the conventional sanitary landfill. Since the primary constituent of both conventional and milled refuse landfills is municipal refuse, it is expected that the study and analysis of milled refuse might give some help in understanding the behavior of the conventional sanitary landfill. However, it must be recognized that, in view of changes in both texture and composition produced by milling, direct application of such work to conventional landfill is not justified.

Characteristics of Milled Refuse

Municipal refuse is a heterogeneous mixture of human discards; its typical composition is exemplified by that of the refuse of the city of Madison, Wisconsin, shown in Table 2-1 (Reinhardt, 1971). The process of milling converts the heterogeneous material into a homogeneous mass of relatively small particle size. Some salient features of milled refuse are:

(1) It is easily transportable and easily handled by automatic devices.

(2) Its volume is reduced by as much as 50% below that in the unprocessed state.

(3) Odor and the possibility of fires are reduced.

(4) It will not support rodents and insects, depending on particle size.

(5) It will support vegetation.

(6) It can be driven on by trucks in all kind of weather.

(7) The problem of blowing paper is virtually eliminated if the refuse is shredded to about 3 inches or less in size.

(8) The activities of thermal, biological, and chemical processes associated with the decomposition of refuse are facilitated.

Table 2-1

Composition of Soild Waste (Wet Basis)
Madison, Wisconsin

	Minimum percent	Maximum percent	Average percent
Food wastes	4.4	28.9	15.3
Garden wastes	0.0	31.1	13.8
Paper products	35.1	53.2	42.4
Plastics, rubber, leather	0.3	3.7	1.8
Textiles	0.1	7.8	1.6
Wood	0.0	2.6	1.1
Metals	5.0	14.5	6.7
Glass, cermics	4.4	17.6	10.1
Rocks, dirt, ashes	0.6	17.6	7.2

The moisture content varies from 30 to 48 percent, with an average of 37 percent

The Gondard mill (Ham, 1971) incorporates a grate through which refuse must pass after being pulverized. Those pieces that can not pass through the grate are either subjected to further milling or are sent up a chimney and out of the mill ballistically by the impact of the hammers. The particle size, the density of the milled refuse, and the capacity of the machine depend on the grate size, i.e. the clear space between bars of the grate. Particle size analyses of milled refuse were made by Reinhardt (1971); the range of particle sizes found is given in Fig. 2-1. As one would expect, the milled refuse is finer when the grate size is smaller. The Tollemache mill (Ham, 1971) has no screen through which pulverized refuse passes, and in this case the hammer pattern is a prime variable in determining the fineness of milling.

Fig. 2-2 shows that for the Gondard mill the comparative densities in the uncompacted condition increase as the grate bar spacing on pulverizer is decreased. However, spacing smaller than 8 inches by 5 inches produces no additional advantage (Hartz, 1972). The compacted milled refuse densities as well as the production capacity of the machine, as obtained from the Madison Demonstration Project (Ham, 1971), are shown in Table 2-2. The density of the milled refuse is seen to be about 50% higher than that of raw refuse.

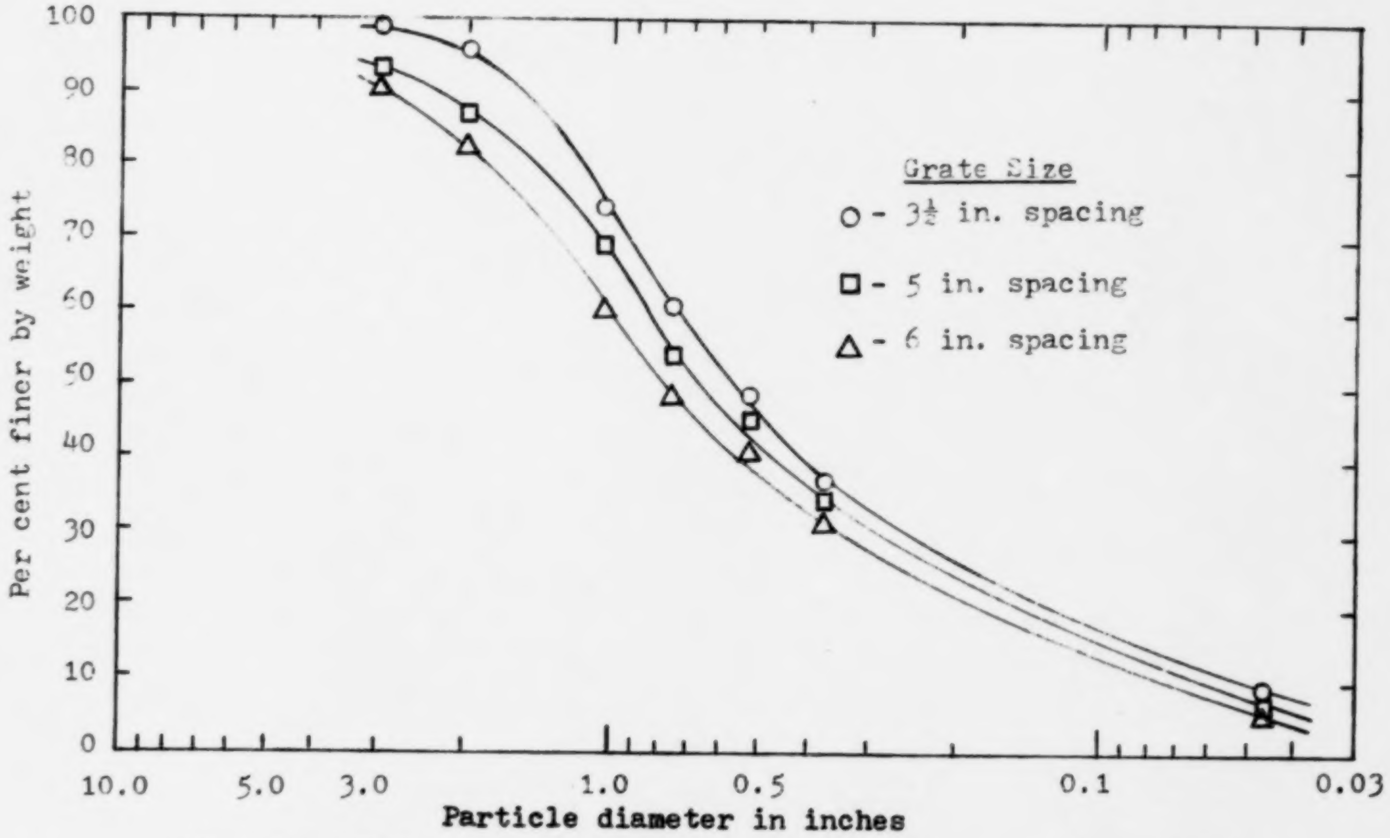

Fig. 2-1. Effect of grate size on the particle size distribution of milled refuse (After Reinhardt, 1971)

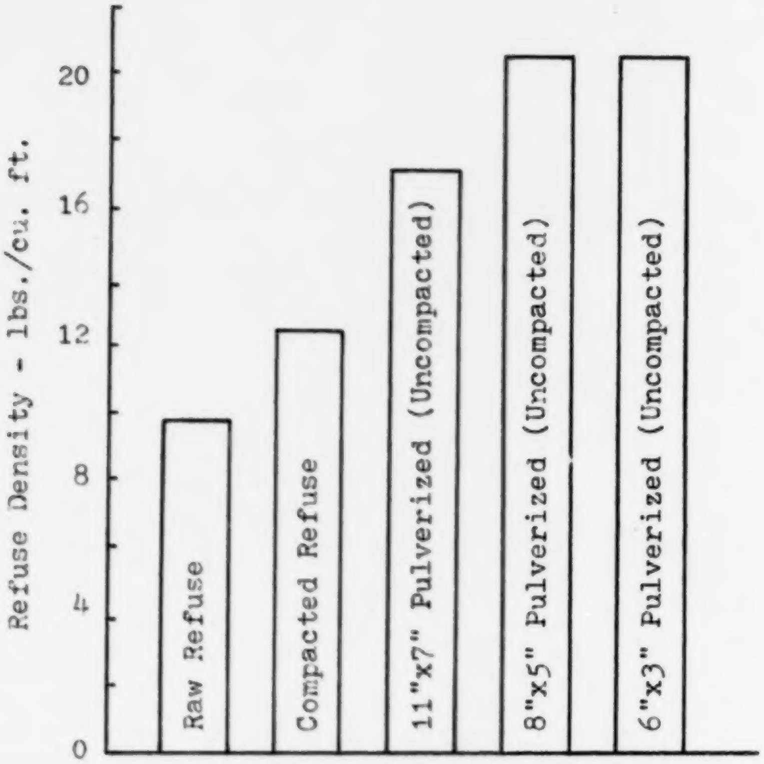

Fig. 2-2. Data from Greater London, England, 1969, showing effect of various grate spacings on pulverized refuse density (After Hartz, 1972)

Table 2-2

Effect of grate size on effective density and machine capacity

Grate size (in.)	Effective density* range (lb/cu. yd)	Machine capacity** (tons/hr.)
3.5	760 to 950	8.4
5.0	1,090	9.0
6.25	810 to 1,130	9.4
raw	440 to 690	---

$$^{*}\text{Effective density} = \frac{\text{weight of refuse}}{\text{vol. of refuse} + \text{vol. of cover soil}}$$

** For Gondard mill with different grate sizes. The machine capacity of the Tollemache mill is 15 tons/hr.

Decomposition of Milled Refuse

Over one-half of the constituents of the milled refuse are composed of cellulose. On a dry weight basis, kraft paper is 97% cellulose, newsprint is about 88% cellulose, and green garbage is about 80% cellulose (Klein, 1971). Since most of the constituents of milled refuse are biodegradable cellulose, it is therefore very likely that the behavior of milled refuse will be similar to that of cellulose under the same conditions, but modified by the presence of materials that are chemically active or will supply nutrients for microbial growth.

According to the organism's source of oxygen and the general temperature range, the biological activities can be described as aerobic or anaerobic processes and as being in the mesophilic (20 - 40 C) or in the thermophilic range (45 - 60 C). When milled refuse is placed in a landfill, the first few feet near the surface will receive sufficient oxygen to maintain aerobic conditions for an extended period of time. Milled refuse has a high proportion of cellulose and lignin, and actinomycetes and fungi are the important organisms in the decomposition of these substance. The maintenance of refuse temperature within the thermophilic range is very important if aerobic processes are to be rapid because these organisms have a temperature range of about 45 - 60 C. Another important variable that influences the aerobic process is the moisture content of the refuse. Theoretically, aerobic decomposition should proceed at any moisture cotent above 30%, and the moisture content of milled refuse is generally within the range of 40 to 60%. Thus, maintaining temperature in the thermophilic range and providing adequate aeration will assure that milled refuse will undergo aerobic decomposition, which is a rather quick process and which produces no methane gas or hydrogen sulphide.

In the actual field case, most of the biological activities will be very slow anaerobic processes, because little gaseous oxygen is present at depth in the landfill mass. Under anaerobic conditions, cellulose materials are decomposed by anaerobic bacteria in the presence of water, yielding as end products methane and carbon dioxide. Several groups of bacteria are involved in the decomposition process. In the first stage, a certain specific group of cellulolytic bacteria, which are capable of using cellulose as a carbon source, are involved (McBee, 1948; McCarty, 1964; Hungate, 1966; Norkrans, 1967). These bacteria hydrolyze cellulose enzymatically to glucose and then to volatile fatty acids and alcohols. Several species of anaerobic facultative bacteria, collectively known as the "acid formers" are able to use glucose as a substrate and produce volatile fatty acids and alcohols. In the second stage, a group of strictly anaerobic bacteria (McCarty, 1964) generally known as "methane formers", are responsible for the breakdown of the volatile fatty acids and alcohols with the production of methane and carbon dioxide. The actual rate of decomposition is difficult to determine. In any system the total production of methane and carbon dioxide is dependent on the distribution and the relative amounts of the different species of microorganisms involved, which, in turn, are dependent on the culture medium and the environmental conditions.

As a result of the biological activities, the behavior of the milled refuse will be influenced in several ways. First, the amount of the solid itself will be reduced. Second, the biological and chemical activities might affect the creep behavior of the remaining material. Third, the gases generated and the decomposition products such as acids and alcohols might change the permeability characteristics of the material. Of course, the importance of such influences depends on the composition of the refuse, the type and amount of the organisms present, and the environmental conditions.

The Structure of Milled Refuse

Because nearly two-thirds of total milled refuse is cellulose, it is, therefore, believed that a close examination of the microstructure of cellulose might give some insight into the behavior of milled refuse. The major constituents of fibrous peat are also composed of cellulose, which is reflected in the fact that when fibrous peat is ashed at high temperatures (800 - 900 C), an ash content as low as 2 per cent has been observed (MacFarlane, 1968). Thus, an analogy between the behavior of milled refuse and peat soils, particularly fibrous peats, can be made.

Chemically, the main constituent of wood and other plant fibers is cellulose. Cellulose is a linear, semicrystalline polysaccharide based on anhydroglucose units linked with 1:4-β-glucosidic bonds. Its empirical formula is $(C_6H_{10}O_5)_n$. The cellulose molecule consists of a large number (i.e. over 1,000) of units of the form

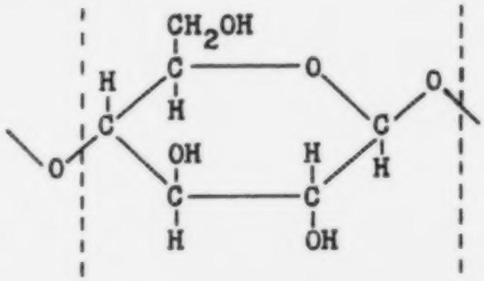

joined end to end in a long flexible molecule (Atkinson, 1958). The fibers are usually native cellulose with a strong longitudinal orientation of the cellulose crystallites. They are, as a rule, tabular or ribbon shaped. The architecture of the fibers exhibits fairly complicated features. The fiber length of paper may range from about 1 mm (beech, straw) to 3-4 mm (spruce, pine) or even centimeters (cotton, hemp). The thickness varies from 10 to 40 μm (Kubāt, 1969). Fig. 2-3 shows a photomicrograph of handsheets made from unbeaten spruce paper pulp. The photograph gives an impression of the

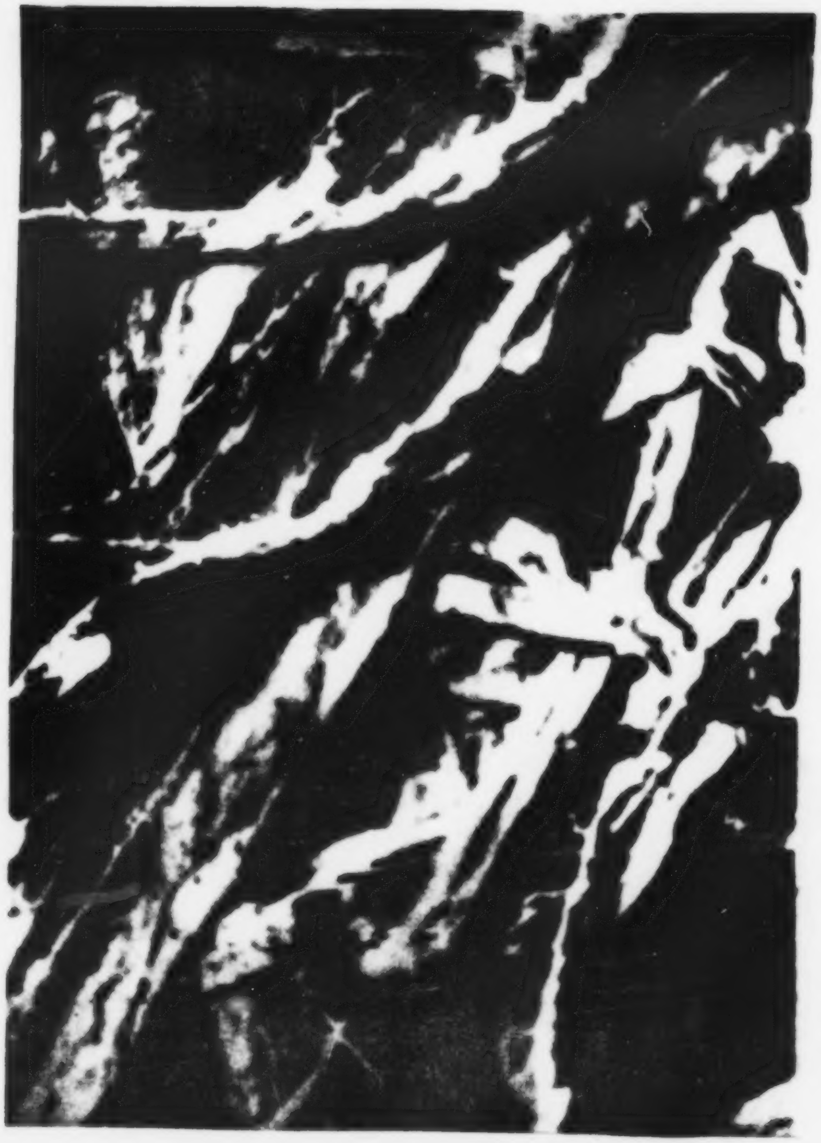

Fig. 2-3. A photomicrograph of handsheets made from bleached unbeaten spruce paper pulp (After Emerton et. al., 1962) (magnification 45x)

two levels of structure of paper, which can be considered as a random agglomerate of fibers containing micropores, interwoven by a network of macropores. This suggests the possibility of a micropore structure being responsible for secondary consolidation effects of such materials.

Only two structural entities are appreciated in gross samples of peat. One is fibrous, the other granular. As very small granules may behave as colloidal particles, it is important to note that peat may be partly colloidal. The three-phase concept of soil applies equally well to peat soils except that for peat the solid phase is not always truly solid but in the microscopic aspect is usually a secondary system of biological entities of cellular structures with contained liquid and/or gas. Fig. 2-4 shows a photomicrograph of a non-woody fine fibrous peat. This photograph implies an arrangement of the primary and secondary elements into a certain structural pattern which, again, shows two levels of structure.

Permeability

Milled refuse is a kind of homogeneous but intricate and complicated material which may comprise not only primary and secondary but also tertiary, and perhaps quaternary, etc., pores. The physical structure and arrangement of the constituents of milled refuse greatly affect the size and continuity of its pores, and hence affect its permeability. Paper constitute a major portion of milled municipal refuse. For

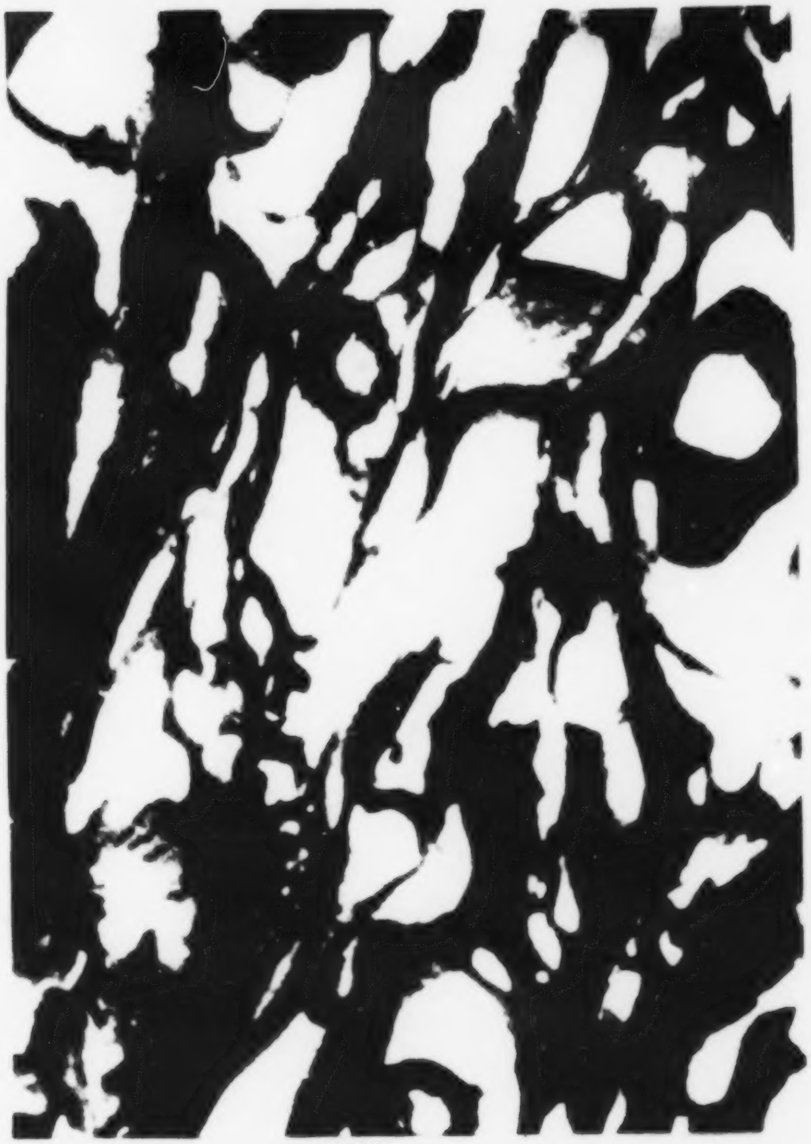

Fig. 2-4. A photomicrograph of a non-woody fine fibrous peat (After MacFarlane, 1968) (magnification 175x)

a mass of shredded papers, one can visualize at least three different levels of pores, i.e. the pores between pieces of paper, the pores between fibers (see Fig. 2-3), and the pores in the cellular structure of the fiber itself (see Fig. 2-5). In the present study only two hypothetical pore levels will be considered, although it is recognized that milled refuse may involve more than two levels. Pores within the fibers will be considered to be micropores, and all large ones will be considered collectively as macropores.

Laboratory permeability tests of fresh milled refuse samples under back pressure, to ensure essentially complete saturation, have been performed by Gupta (1972). These tests showed a bilinear relationship between the logarithm of the coefficient of permeability and the dry density of the refuse, as shown in Fig. 2-6. Andersland et. al. (1972) in a study of the permeability characteristics of papermill sludge, with an organic content of 43 percent, also obtained a very similar relationship between the coefficient of permeability and the solid content of the sludge on a semilog plot. Typical results of the permeability tests of papermill sludge under 60 psi back pressure are shown in Fig. 2-7. Although the permeability were given only for three values of solid content, which are not sufficient by themselves to establish the shape of the curve, these results are consistent with the interpretation of a bilinear log permeability versus density relation.

The results of permeability tests thus tend to substan-

Fig. 2-5. A photomicrograph of fine peat fibers (After Wilson et. al., 1965) (magnification 400x)

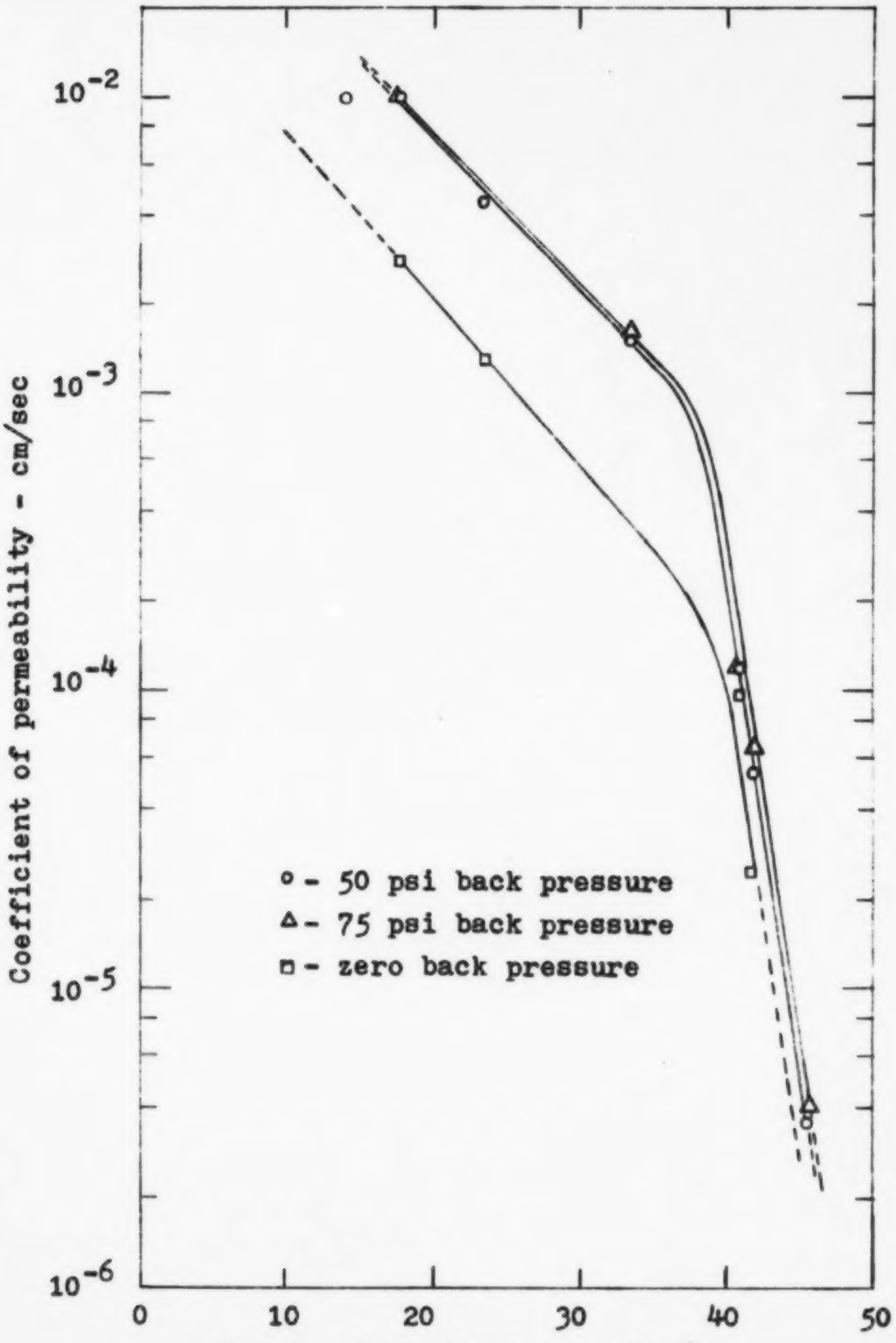

Fig. 2-6. Permeability versus dry density of milled refuse (After Gupta, 1972)

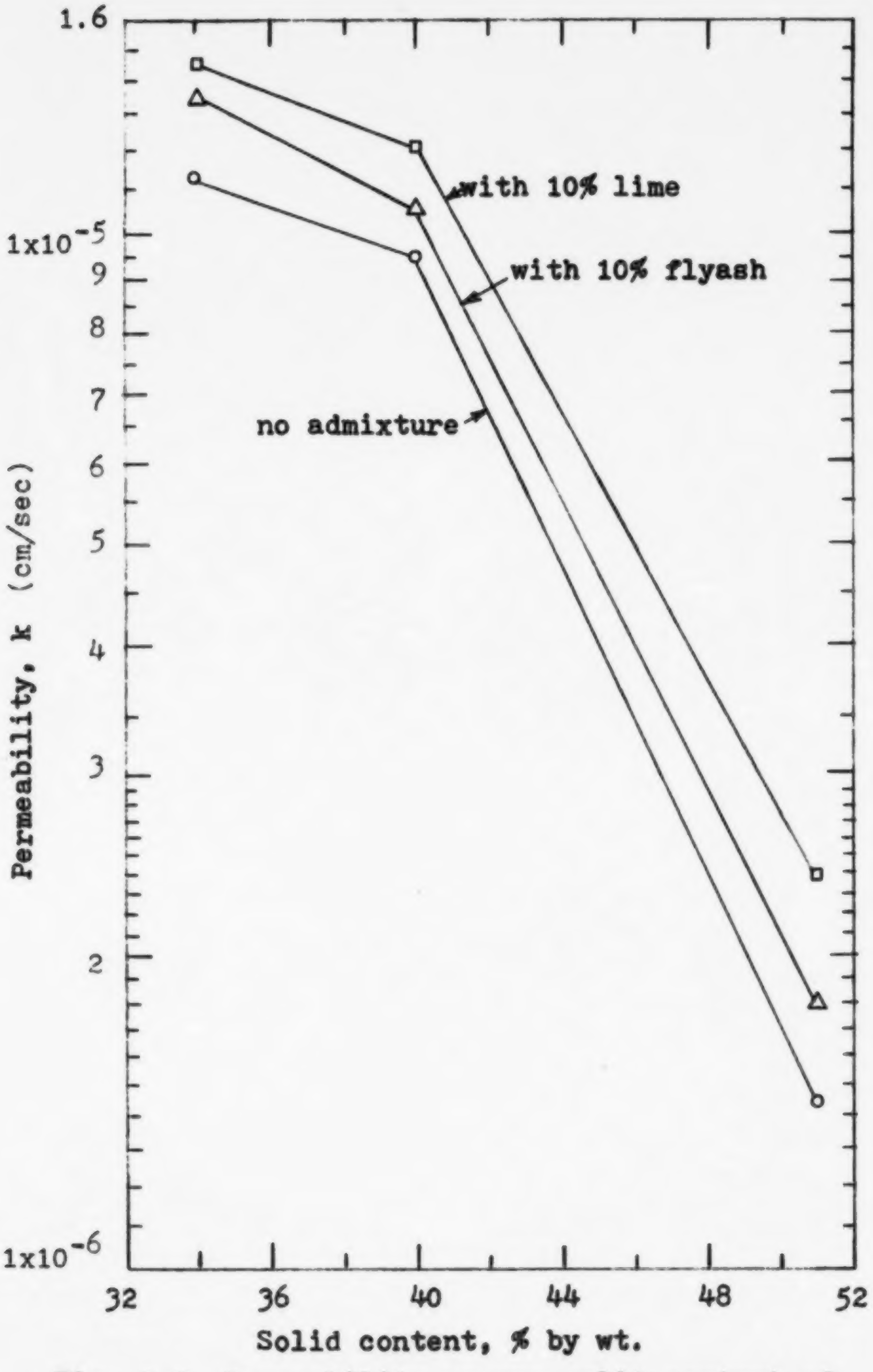

Fig. 2-7. Permeability versus solid content of papermill sludge (After Andersland, 1972)

tiate the concept of multiple levels of structure to model the consolidation behavior of milled refuse and some other materials. The two limbs of the bilinear curve can be interpreted as representing ranges in which fluid flow is dominated by different pore levels. In the range of densities studied, however, it seems probable that the two dominant pore levels both belong to the class considered here as macropores.

CONSOLIDATION THEORY

The theory of consolidation, first developed for clay soil by Terzaghi (1925), deals with the stress-strain-time behavior of a multiphase soil subjected to a statically applied external load. The process of consolidation has been traditionally divided arbitrarily into two stages, i.e. primary and secondary. That part of the time-dependent deformation corresponding to the dissipation of pore pressure is called primary consolidation, while secondary consolidation refers to the continuous deformation after significant pore pressure has been dissipated. The arbitrary division between primary and secondary consolidation is usually taken as the time when the mid-plane pore pressure approaches zero. In fact, consolidation is a continuous process; the secondary consolidation initiates as soon as the soil is subjected to the external load. However, it is still convenient to make a qualitative distinction between the mechanisms that control the deformation rate. During the primary stage, the deformation is controlled by the rate of hydraulic flow, while during the secondary stage, only small excess pore pressure remains and deformation is essentially creep under constant effective stress. In this chapter, various existing consolidation theories will be reviewed with emphasis on the secondary consolidation.

Terzaghi's Theory of Consolidation

The classic theory of consolidation is based on the following constitutive assumptions (Terzaghi, 1943):

(1) The soil is homogeneous and its voids are completely filled with water.

(2) The soil particles and the pore water are incompressible.

(3) Compression of the soil skeleton and the flow of water are one-dimensional.

(4) The fluid flow follows Darcy's law, and the coefficient of permeability is assumed to be constant.

(5) Only small strains and velocities are involved, and the theory is quasi-static.

Following these assumptions, the basic equation of one-dimensional consolidation is:

$$\frac{1}{1+e}\frac{\partial e}{\partial t} = \frac{k}{\gamma_w}\frac{\partial^2 u}{\partial z^2} \qquad (3\text{-}1)$$

where e = void ratio,

k = coefficient of permeability,

γ_w = unit weight of water,

u = excess porewater pressure,

z = depth,

and t = time.

In order to linearize the above equation, Terzaghi made the following two additional assumptions:

(6) The relationship between void ratio and equilibrium effective stress is linear.

$$\frac{de}{dp} = -a_v = \text{constant} \qquad (3\text{-}2)$$

(7) For a particular load increment involving only small strain, the coefficient of consolidation is constant.

Introducing Equation (3-2), one obtains from Equation (3-1),

$$\frac{\partial u}{\partial t} = \frac{k(1+e)}{\gamma_w a_v} \frac{\partial^2 u}{\partial z^2} \qquad (3\text{-}3)$$

$$\frac{\partial u}{\partial t} = c_v \frac{\partial^2 u}{\partial z^2} \qquad (3\text{-}4)$$

where $c_v = \frac{k(1+e)}{\gamma_w a_v}$

= coefficient of consolidation

Although the limitations of one-dimensional consolidation have been appreciated for a long time, it is still the only consolidation theory in general use. The Terzaghi theory is justifiable in many practical applications because: (1) the properties of the soil are usually too ill-defined to warrant a more complex treatment, (2) the mathematics involved in the theory is relatively simple, (3) a large body of experience and nearly all pertinent case histories are linked to conventional theory, and (4) modified procedures, such as those proposed by Skempton and Bjerrum (1957), Schiffman and Gibson (1963), and Lambe (1964, 1967) have often led to improved predictions with the use of conventional theory.

Despite the above facts, there is a body of consistently observed evidence that does not conform to the Terzaghi theory, and which indicates that in many cases the basic assumptions are oversimplified. For instance: (1) foundations resting on clay soils usually settle at higher rates than predicted by the conventional theory (Davis, 1972); (2) when the pore pressure has been dissipated to nearly zero, the settlement does not cease, but a secondary or creep deformation under constant effective stress is generally observed; and (3) the shape of compression-time curves for soils varies markedly with the magnitude of the load increment ratio and may deviate considerably from the form predicted by the Terzaghi theory which is based on the assumption that the compressibility of the soil skeleton is similar to that of a linear spring (Leonards and Altschaeffl, 1964).

Validity of Terzaghi's Assumptions

The validity of the assumptions of Terzaghi theory depends largely on the type of material under consideration. Here the primary interest is placed on very compressible materials such as peat and milled refuse. Laboratory strains as high as 50 percent are common for peat (MacFarlane, 1968) compared to several percent for most clays. Hanrahan (1954) found the permeability of a peat to decrease by a factor of 50,000 during consolidation. Lea (1958) found the coefficient of consolidation to change by a factor of 100. For these materials, the basic assumptions of small strains, constant permeability and constant compressibility in the Terzaghi theory are not valid.

From the assumption of one-dimensional compression, the lateral strains are presumed to be zero. Strict adherence to this assumption would require some conditions not met with in actual field cases, such as uniform distribution of the applied load intensity, the vertical stress increment, and the initial excess pore pressure. The condition of no lateral strains is approximately true only for cases such as in the oedometer and the consolidation of a layer of clay thin with respect to an area of uniform loading. However, in most practical cases, the consolidation process is either two- or three-dimensional.

For the steady-state flow of water through clay, the form of Darcy's law ($v = ki$) has been verified over a wide range of intermediate hydraulic gradients (Hansbo, 1960; Sweatzendruber, 1962; Muskat, 1948). Experiments conducted by Lutz (1959) show a departure from Darcy's law at low hydraulic gradients. The departure from Darcy's law could arise from the existence of a threshold gradient (Miller, 1963; Florin, 1951) which could affect both the magnitude and the rate of consolidation. Whatever the true cause of daparture, one may accept a modified form of Darcy's law for small gradients and study its effect on the consolidation process.

Because of the assumption that the compressibility of the soil skeleton is like that of a linear spring, this theory can not take into account the effects of secondary consolidation and load increment ratio. In order to correctly model such complex materials such as peat or milled refuse, modified assumptions and other factors such as biological and chemical decomposition of the solid skeleton and generation of fluids and gases should be taken into consideration.

Mechanisms of Secondary Consolidation

Current concepts of the mechanisms responsible for secondary consolidation can be classified into three types (Barden, 1969): (1) the Terzaghi-Taylor concept of structural viscosity, (2) Tan's (1964) concept of a cardhouse structure and the jumping of bonds, and (3) the concept of two levels of structure. A brief discussion of these mechanisms will be given in this section.

(1) Terzaghi-Taylor concept of structural viscosity

Terzaghi's hypothesis (1941) states that application of a load increment greater than the grain bond strength causes the soil skeleton to pass from a solid to a lubricated state and a period of consolidation follows. During primary consolidation the total stress is shared by the pressure in the free porewater, the plastic resistance in the highly viscous adsorbed double-layer (film bond), and solid-to-solid contacts between clay particle (grain bond). The film and grain bonds are components of the effective stress. During secondary consolidation the pore pressure is negligible and any pressure increment is shared by the film and the grain bonds. There is a gradual transfer of stress from film to grain bond with an associated period of very slow viscous flow or creep. As clay particles approach one another, the effective viscosity increases (nonlinear behavior) and adjustment proceeds at a decreasing rate. Finally the system reaches equilibrium with all stresses transfered to grain bond, and the soil skeleton once more in the solid state.

Taylor (1942) also considered secondary consolidation to be caused by the remolding or disturbance of the structure induced by primary consolidation. In this hypothesis the film bond of Terzaghi is replaced by a "structural resistance to compression" which is a function of the rate of strain. Taylor felt that the structural viscosity of the clay skeleton, due to the adsorbed layer effects, would possibly exhibit a nonlinearity.

Since the viscous properties of the adsorbed water are not known in detail, the law governing the nonlinear behavior can not be deduced precisely but can only be arrived at intuitively. The simplest empirical form suitable for structural viscosity is Ostward's power law (Wilkinson, 1960). Another obvious empirical choice is the exponential sinh law which has the same general shape.

(2) Tan's concept of the jumping of bonds

In an important series of papers, Tan (1954, 1957a, 1957b, 1957c) developed a theory of consolidation in which the soil is assumed to be visco-elastic. In Tan's concept the jumping may be from one rough spot on a particle to the next, or it may be from one particle to the next. This can be assumed to be analogous to the movement of kinetic units from one equilibrium position to another and therefore can be treated by the rate process theory (Murayama and Shibata, 1964; Mitchell, 1964; Wu, 1966; Berry and Poskitt, 1972). Again the nonlinear viscosity can be expressed by the power law or the exponential sinh law.

(3) The concept of two levels of structure

This mechanism has been proposed for clay by De Jong and Verruijit (1965), Zeevaert (1967), De Jong (1968); for peat soil by Adams (1965) and Wilson et. al. (1965). In a clay soil the micropore structure is provided by the packets or domains which can be looked as compressible "particles". This microstructure is interwoven by a system of coarse channels and macropores. For fibrous peat, there is an open structure with interstices filled with a secondary arrangement of non-woody fine fibrous elements. This offers an excellent example of the micropore mechanism.

In this mechanism the primary stage is the dissipation of pore pressure in the macropores. As stress is transferred to the microstructures, water will start to drain into the macropores, resulting in secondary compression. Since the drainage properties of the micropores are not known in detail, the previously described empirical viscous laws may used to describe them.

It is noted that different mechanisms lead to the same nonlinear physical law. The structure of milled refuse can be considered to be analogous to that of fibrous peat. Considering the structue of milled refuse as discussed in Chapter II, it is believed that the mechanism based on two levels of structure will be most suitable for the description of the creep behavior of such materials.

Modified Theory of Consolidation

A number of modified theories of consolidation have been proposed to account for the departures in observed consolidation behavior from the Terzaghi theory. The major causes of these departures are probably large strains and the effects of these on permeability, compressibility, and viscosity laws. In this section, the modified consolidation theories discussed will be divided arbitrarily into four categories that consider respectively the factors of (1) multi-dimensional compression, (2) validity of Darcy's law, (3) finite strain and variable compressibility and permeability, and (4) nonlinear void ratio- effective stress relationship. It is noted that in many cases one theory may take into account more than one of these factors.

(1) Multi-dimensional compression

Schiffman et. al. (1969) give a detailed discussion of the three-dimensional consolidation theory which is characterized by the Mandel-Cryer effect (Mandel, 1953; Cryer, 1963) that may be manifested as an increase in pore pressure during the early stage of the consolidation after boundary loading has ceased. The mathematics for three-dimensional consolidation theory is much more complicated than that of the Terzaghi theory. Even when the boundary conditions of a problem are highly idealized, analytical solutions are available only for homogeneous, isotropic soils with linear compressibility (Biot, 1935, 1956).

The finite element method of analysis has proven to be an extremely powerful tool to determine the distribution of both stress and strain in many fields of engineering. Recently this method has been used to solve three-dimensional consolidation problems with very general geometry, material properties, and boundary conditions. Sandhu and Wilson (1969) made the first successful attempt in applying the finite element method to consolidation problems by using Gurtin's (1964) variational method resulting in a set of integral equations. Christian and Boehmer (1970) simulate the consolidation process by allowing the solid to undergo deformation with controlled volume change at successive stages. Following Sandhu's approach, Hwang et. al. (1971) use the finite element method to solve plane strain consolidation problems. Ghaboussi and Wilson (1973) investigated the problems of compressible fluid flow in porous media, where the assumption of incompressibility of fluid and solid particle has been relaxed.

From this brief review of the application of finite element methods to three-dimensional consolidation problems, it is noted that all treatments are limited to small strains and linear compressibility of the soil skeleton. Work on extending the consolidation analysis procedure to time-dependent, nonlinear material behavior is still underway When one takes large deformation, and its effect on the permeability, compressibility, and viscosity law, into consideration, the mathematics becomes extremely complicated. This then restricts most of the general theoretical considerations to one-dimensional cases.

(2) Validity of Darcy's law

Several investigators have incorporated modified forms of Darcy's law in consolidation studies. For example, Barden and Berry (1965) proposed the force potential form of Darcy's law, i.e.

$$v_z = \frac{k}{\gamma_w} \frac{\partial u}{\partial z} , \qquad (3\text{-}5)$$

in their consolidation study of normally consolidated clay (Fig. 3-1(d)). Elnaggar (1969) studied the effect of non-Darcian flow on the time rate of consolidation, and proposed the following flow relation:

$$v = k_u \left\{ i - (1-a) i_t \left[1 - \exp(- \frac{\theta i}{i_t}) \right] \right\} , \qquad (3\text{-}6)$$

where k_u = maximum or "ultimate" permeability

i_t = "apparent" threshold gradient

a and θ = parameters to be determined

$0 \leq a \leq 1$

$0 \leq \theta \leq 1$

The above equation reduces to Darcy's law if either $a = 1$ or $\theta = 0$.

The experimental investigation of the effect of the validity of Darcy's law on the time rate of consolidation is extremely difficult. Theoretically the existence of a threshold gradient will affect the magnitude and the time rate of consolidation. In most theoretical treatments, however, Darcy's law is assumed to be valid.

(3) Finite strain and variable permeability and compressibility

A number of investigators have sought to extend the classical theory to take into account the variation of permeability and compressibility during consolidation (McNabb, 1960; Schiffman and Gibson, 1964; Davis and Raymond, 1965; Janbu, 1965; Barden and Berry, 1965). As mentioned before, these factors are likely to be of real importance only if deformation is large, yet these studies have all been based essentially on the small strain theory. Gibson et. al (1967) proposed the first theory in which the limitation of small strain has not been imposed and the variation of soil permeability and compressibility has been taken into account. Aithough Darcy's law is assumed to be valid, it is recast into a form in which the relative velocity of soil skeleton and the pore fluid is related to excess pore pressure gradient. A nonlinear theory has also been given by Poskitt (1969) for study of variable compressibility, permeability, and finite strain (Fig. 3-1(e)). The analytical solution was obtained by means of a perturbation method.

Generally speaking, only special materials, such as partially saturated or highly compressible materials, or those exhibiting exceptional structural effects, such as organic soil, peat, and milled refuse, merit the use of relevant nonlinear theories.

(4) Nonlinear void ratio-effective stress relationship

Merchant (1939) made the first rational attempt to revise the theory of consolidation since its original formulation (Fig. 3-1(b)). As stated by Christie (1964) the model proposed by Merchant is actually equivalent to a Hookean spring in series with a Kelvin body. It is apparent that some of the other theories are mathematically equivalent to Merchant's theory (Ishii, 1951; Gibson and Lo, 1961; Tan, 1957).

Considerable effort has been made to develop rheological models which will closely simulate the secondary consolidation. Theoretically a continuous spectrum of Kelvin bodies (Schiffman et. al., 1964; Saada, 1962; Thompson, 1965; Wahls, 1962) can fit any practical shape of secondary compression curve and with a normal well-conditioned problem only two or three Kelvin bodies should be needed. When a continuous spectrum of Kelvin bodies is used to describe the secondary curve, the problem of determining a considerable number of spring and viscosity parameters arises (Tan, 1964). Usually a multi-parameter linear model is used in attempting to describe the actual nonlinear behavior of the soil skeleton. Thus attempts have been made to improve on this by describing the viscosity element by a nonlinear dashpot. This has a small number of parameters but the solution requires resort to numerical methods.

The linear Kelvin model has only one degree of freedom and is the simplest to describe the secondary consolidation process. Taylor (1942) was the first to use it (Fig. 3-1(c)) and more recently it has been further developed with the use of a nonlinear dashpot by Barden (1965, 1968, 1969), and Poskitt (1971). The rheological models developed by Barden (1965, 1968, 1969) and Poskitt (1971) are shown in (Fig. 3-1(f)), (Fig. 3-1(g)), (Fig. 3-1(i)), and (Fig. 3-1(h)) respectively. For some theories a spring in series has also been added to a Kelvin body to account for the immediate deformation. For a model lacking such a series spring, the resulting consolidation theory can represent as little as one percent of the total settlement for some materials (Poskitt, 1971). Barden (1968) has shown that the immediate compression equivalent to the effect of the series spring can be simulated under certain conditions by a nonlinear dashpot. For some materials, however, spring in series may be important in modelling the early stage of consolidation (Thompson, 1965).

Using the rate process theory to analyze the consolidation of clay, Wu (1966) proposed a model with a Hookean spring and nonlinear dashpot (Fig. 3-1(j)). Poskitt (1971) proposed a more general model with a nonlinear spring and a nonlinear dashpot (Fig. 3-1(k)), but restricted himself to mild nonlinear cases only so that the governing nonlinear equations can be solved analytically. Berry and Poskitt (1972) used the same model to simulate the consolidation of amorphous granular peat with finite strain (Fig. 3-1(l)). The governing equations are highly nonlinear and can only be solved numerically.

All the previous models are developed from either a mechanism based on structural viscosity or one based on the jumping of bonds. Based on the mechanism of two levels of structure, Berry and Poskitt (1972) proposed a double Terzaghi pot with nonlinear spring as an analog for the physical mechanism involved in the primary and secondary consolidation of fibrous peat, which is essentially an open structured material with the interstices filled with a nonwoody material (Fig. 3-1(m)). The flow of water from the lower to the upper compartment, which represents the flow of water from micropores into the macropores, is considered to be non-Newtonian.

Summary

In this chapter, various modified consolidation theories and mechanisms responsible for secondary compression have been reviewed. A summary of rheological models proposed by various investigators to simulate the consolidation process is given in Fig. 3-1. For complex materials such as peats or milled refuse, most of the basic assumptions in the Terzaghi theory are not valid. In order to

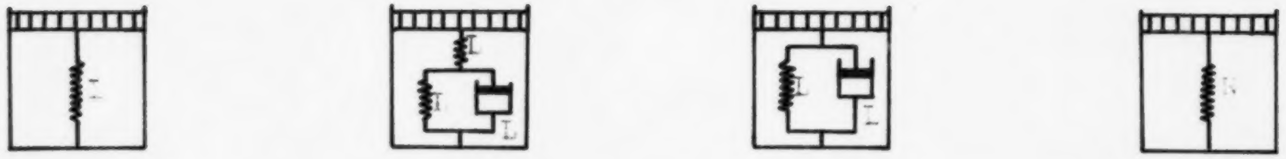

(a) Terzaghi (1925) (b) Taylor & Merchant (1939) (c) Taylor Theory B (1942) (d) Barden & Berry (1965)

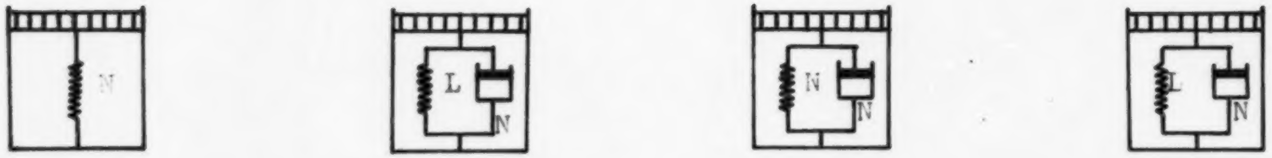

(e) Poskitt (1969) (wild nonlinear) (f) Barden (1965) (g) Barden (1968) (h) Poskitt (1971)

Fig. 3-1. Rheological models (L=Linear, N=Non-linear)

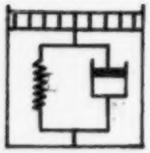

(i) Barder (1969)

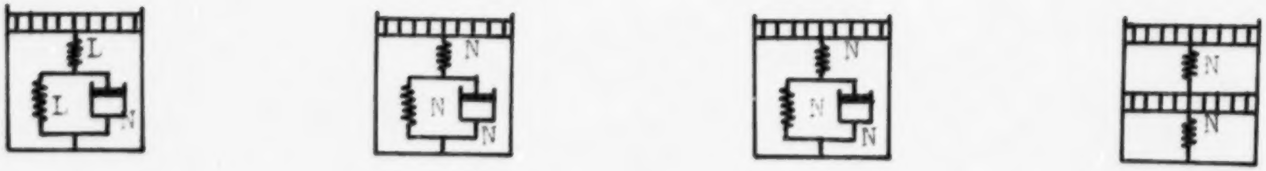

(j) Wu (1966)

(k) Poskitt (1971)
(mild nonlinear)

(l) Berry & Poskitt
(1972)

(m) Berry & Poskitt
(1972)

Fig. 3-1(continued) Rheological models (L=Linear, N=Non-linear) model the time-settlement behavior of such materials, the factors of large deformation, variation of permeability and compressibility, creep, and biological-chemical decomposition of soil skeleton need to be considered. In light of the discussion of the structural aspects of milled refuse given in Chapter II, it appears that the rheological model consisting of a double Terzaghi pot, representing two levels of structure, may be suitable to simulate the consolidation behavior of milled refuse.

CONSOLIDATION MODEL OF MILLED REFUSE

It has been noted that consolidation is a continuous process, in which secondary consolidation is presumed to have started as soon as the external load is applied. In order to define the consolidation problem completely, one has to start with the equation of continuity and then postulate an effective stress-strain-time relationship for the material under consideration. In this chapter, a general equation of continuity based on the theory of mixture will be discussed. A time-settlement model proposed by Zimmerman (1972) to simulate the consolidation behavior of milled refuse will be reviewed. Modifications of this model will be made in light of available laboratory consolidation test data.

Equation of Continuity

In the derivation of Terzaghi's equation of one-dimensional consolidation, the assumption of small strains has been imposed. Gibson et. al. (1967) developed a general equation of continuity without the limitation of small strains. It is, in fact, a combination of the principle of continuity of mass with Darcy's law. The resulting equation is:

$$\frac{(1+e_o)^2}{\gamma_w} \frac{\partial}{\partial z} \left(\frac{k}{1+e} \frac{\partial \underline{u}}{\partial z}\right) = \frac{\partial e}{\partial t} \qquad (4\text{-}1)$$

where e_o is the initial void ratio. Recently, a more general equation of continuity based on the theory of mixture (Truesdell and Toupin, 1960) has found broader applications in the field of soil mechanics (Raats and Klute, 1968a, 1968b, 1969; Sandhu, 1969; Davis, 1972a). The reader interested in the detailed derivation of this equation is referred to Zimmerman (1972) or Raats and Klute (1968a, b). Here, only those elements that are relevant to the present pursuits will be given.

In the continuum theory of mixture, a mixture is considered as a superposition of as many continua as there are constituents. Each constituent is regarded as a continuous medium, for which equations expressing the balance of mass, momentum, etc. may be written. In addition, such balance equations can be written for the entire mixture. A soil is regarded as a mixture of phases; e.g. a saturated soil as a mixture of a solid phase and an aqueous phase; a partially saturated soil as a mixture of a solid phase, an aqueous phase, and a gaseous phase. Two constituents are assumed in the following derivation, i.e. a solid phase s, and a liquid phase f. Any point in the mixture may be simultaneously occupied by both constituents. Also, both constituents are allowed to have their own velocity.

Let $\bar{r}$ denote the position of a point in a rectangular Cartesian coordinate system fixed with respect to an observer, and $\bar{r}^{\alpha}$ represent the coordinates in a material coordinate system for phase α (which stands for s or f in the present case). Some definitions which are useful in this derivation are as follows:

ρ^{α} = the mass of phase α per unit bulk volume.

$\bar{v}^{\alpha}$ = the macroscopic (discharge) velocity of phase α.

ρ_a^{α} = the mass of phase α per unit volume of phase α.

θ^{α} = the fraction of a unit volume of mixture occupied by the phase α.

ψ^{α} = the time rate of generation of mass of α per unit bulk volume.

Following the basic premises of mixture theory, an equation of mass balance for phase f, in which the solid phase is regarded as a reference, can be written as :

$$\rho^s \frac{D(\rho^f/\rho^s)}{D^s t} + \frac{\partial}{\partial \bar{r}^s}\left[\rho^f(\bar{v}^f - \bar{v}^s)\right]\frac{\partial \bar{r}^s}{\partial \bar{r}} - \psi^f + \frac{\rho^f}{\rho^s}\psi^s = 0 \quad (4\text{-}2)$$

If no solid phase is decomposed, Equation 4-2 becomes Zimmerman's (1972) Equation 4-59. In Equation 4-2, ρ^f/ρ^s is the mass of fluid phase f per unit mass of solid phase s, or in the usual case, the moisture content. The term $\partial\bar{r}^s/\partial\bar{r}$ is called the deformation gradient, which serves as a measure of the deformation undergone by the solid phase. "D" represents an operator, the material time derivative, which is defined for a variable θ by the relationship

$$\frac{D\theta}{D^{\alpha}t} = \frac{\partial\theta}{\partial t} + \overline{v}^{\alpha}\nabla\theta. \tag{4-3}$$

Generalized Darcy's Law

In order to evaluate Equation (4-2), the mass flux of f relative to the solid phase s, as well as the deformation gradient, must be known. Ratts and Klute (1968b) developed the needed expression based upon the force balance for phase f. This expression may be written

$$\frac{\rho^f}{\rho^f_a}(\overline{v}^f - \overline{v}^s) = -\frac{\rho^f \rho^f g}{\overline{R}^{sf}\rho^f_a}\frac{\partial\overline{r}^s}{\partial\overline{r}}\left[\frac{\partial(h + h_g)}{\partial\overline{r}^s}\right], \tag{4-4}$$

where $\overline{R}^{sf}$ = resistivity to relative motion of the solid phase and the liquid phase,

h = the head of fluid phase,

h_g = the gravitational head,

and g = the acceleration of gravity.

With the substitution

$$k = \frac{\rho^f \rho^f g}{\overline{R}^{sf}\rho^f_a}, \tag{4-5}$$

Equation (4-4) becomes

$$\frac{\rho^f}{\rho^f_a}(\bar{v}^f - \bar{v}^s) = -k\,\frac{\partial \bar{r}^s}{\partial \bar{r}}\left[\frac{\partial(h + h_g)}{\partial \bar{r}^s}\right] . \qquad (4\text{-}6)$$

Equation (4-6) is the generalized form of Darcy's law that is applicable to saturated porous media that may or may not undergo movements of their solid phases.

General Equation of Pore Pressure Dissipation

Substituting Equation (4-6) into (4-2) yields

$$\rho^s\,\frac{D(\rho^f/\rho^s)}{D^s t} - \frac{\partial}{\partial \bar{r}^s}\left[\rho^f_a\,k\,\frac{\partial \bar{r}_s}{\partial \bar{r}}\,\frac{\partial(h + h_g)}{\partial \bar{r}^s}\right]\frac{\partial \bar{r}^s}{\partial \bar{r}} - \psi^f + \frac{\rho^f}{\rho^s}\psi^s = 0, \qquad (4\text{-}7)$$

which is the generalized form of the differential equation describing primary consolidation. For the special case considered by Terzaghi, the medium is completely saturated with water, which is incompressible, and the amount of deformation of the solid is so small that there is no significant change in the spatial volume occupied by the solids. Then the solid velocity approaches zero and the deformation gradient approaches unity. If the rate of generation of liquid and solid is also zero, Equation (4-7) reduces to

$$\frac{\rho^f}{1+e}\frac{\partial e}{\partial t} = -\nabla(\rho^f\bar{v}^f) \ . \qquad (4\text{-}8)$$

This is equivalent to Terzaghi's equation.

In Equation (4-7), the deformation that the solid phase has undergone is measured by the deformation gradient, and so in order to deal with a transport problem in deformable media one must have information about the deformation gradient. Its measurement appears to be a major difficulty, but is possible in principle. For two and three-dimensional cases, The expression for the deformation gradient is a very complex one; however, for the one-dimensional case, Raats and Klute (1969) give:

$$\frac{\partial\bar{r}^s}{\partial\bar{r}} = \begin{vmatrix} \frac{\partial\bar{r}^s}{\partial\bar{r}_x} & 0 & 0 \\ 0 & 1 & 0 \\ 0 & 0 & 1 \end{vmatrix} = \begin{vmatrix} \frac{\rho^s}{\rho^s_o} & 0 & 0 \\ 0 & 1 & 0 \\ 0 & 0 & 1 \end{vmatrix} \qquad (4\text{-}9)$$

where ρ^s_o is the mass of solid phase per unit bulk volume in the reference configuation at time equals zero. Equation (4-9) expresses that, for this particular deformation, the distance between material particles of the solid phase in the r_x direction and the bulk density are inversely proportional to each other.

The bulk density can be expressed either in term of volume or void ratio:

$$\frac{\partial \bar{r}^s_x}{\partial \bar{r}_x} = \frac{\rho^s}{\rho^s_o} = \frac{V_o}{V} = \frac{1+e_o}{1+e} \, . \qquad (4\text{-}10)$$

If the material is assumed to be homogeneous and at equilibrium prior to the load increase, and if $r_x = x$, one has

$$\rho^s \frac{\partial(\rho^f/\rho^s)}{\partial t} - \frac{\rho^f}{\rho^s_o} \frac{\partial}{\partial x} \left(\frac{k\rho^f_a}{\gamma_w} \frac{\rho^s}{\rho^s_o} \frac{\partial u}{\partial x}\right) - \psi^f + \frac{\rho^f}{\rho^s} \psi^s = 0. \qquad (4\text{-}11)$$

Substituting

$$\rho^s = \frac{G_s \gamma_w}{(1+e)g}$$

$$\rho^f = \frac{Se\gamma_w}{(1+e)g} \qquad (4\text{-}12)$$

$$\rho^f_a = \frac{S\gamma_w}{g}$$

into Equation (4-11) yields

$$\frac{\partial(Se)}{\partial t} = \frac{(1+e_o)^2}{\gamma_w} \frac{\partial}{\partial x} \left(\frac{kS}{1+e} \frac{\partial u}{\partial x}\right) + \frac{(1+e)g}{\gamma_w} \psi^f$$

$$- \frac{(1+e)g}{\gamma_w} \frac{Se}{G_s} \psi^s \qquad (4\text{-}13)$$

where G_s = specific gravity of solids

and S = degree of saturation.

This is the general one-dimensional equation for pore pressure dissipation.

Earlier Consolidation Model For Milled Refuse

In an attempt to simulate the time-settlement behavior of milled refuse, a mathematical model has been proposed by Zimmerman(1972). It consists of a generalized pore pressure dissipation equation (Equation 4-13) and a rate process function which describes the secondary consolidation. The creep function is the same as that in Wu's model (1966) which has the form

$$\frac{d\epsilon}{dt} = \beta \sinh(\alpha\tau) \qquad (4\text{-}14)$$

where $d\epsilon/dt$ is the strain rate, α and β are soil parameters, and τ is the viscous resistance. The method used to solve the two simultaneous equation (4-13 & 4-14) is modified from one proposed by Barden (1965a).

After a critical review of this model, it is evident that, although it is not so described explicitly, the rheological model of the soil skeleton is actually like the one proposed by Barden (1968) with the nonlinear viscosity law (given by Equation 4-14) of the rate process theory (see Figure 3-1). As pointed out by Barden (1969), in many cases, the soil parameters of the creep function, although likely to vary with void ratio, are assumed to be the constant average values applying over an increment of pressure. However, for large load increment or large strain, it might be necessary to introduce the actual variation of the soil parameters during the compression. Because milled refuse in the field has very low initial effective pressures due to its low specific gravity, the load increment values will often be high. In order to deal with large load increment ratios and large strains in milled refuse, it is believed that the creep function should take the variation of soil parameters into account.

To obtain numerical solutions for the model, the pore pressure dissipation equation is expanded and the relationships governing the interdependence of some of the variables are substituted to make it a working form. This equation is then solved simultaneously with Equation (4-14) to give the theoretical prediction of the time-settlement behavior of milled refuse. The relationships governing the variations of void ratio with permeability, compressibility etc. are obtained by fitting the available peat data. It has long been realized that peat is itself a very complex engineering material and has a wide range of composition and characteristics. MacFarlane and Radforth (1965) described two extreme types of peat and stated that all gradations exist between them. At one extreme, amorphous granular peat has a large colloidal fraction. At the other extreme, fibrous peat has an open structure with the interstices filled with a secondary structural arrangement of non-woody fine fibrous elements. Therefore, proposed relationships of permeability versus void ratio, compressibility versus void ratio etc. obtained by fitting available data on peat, without specifying exactly what type of peat it is, will not have much significance in practical application.

As mentioned before, the numerical method used to obtain solutions for the model is modified from one proposed by Barden (1965a). When the variation of soil parameters in the creep function is taken into account, this numerical technique becomes very awkward in application.

More recently, Berry and Poskitt (1972) developed one-dimensional consolidation theories for amorphous granular peat and fibrous peat. The theories take account of finite strain, variation of permeability and compressibility, and the secondary consolidation effects. The model is a combination of Gibson's (1967) equation of continuity for finite strain and an appropriate rate process function which takes the variation of soil parameters into account. Numerical technique for solving the resulting two highly nonlinear partial differential equation was developed by Poskitt (1971). The continuity equation in this model is less general than Equation (4-13), but the creep function adopted is believed to be more appropriate to describe the creep behavior of milled refuse than those do not take the variation of parameters into account. In light of the above discussion, a logical next step is to use the more general pore pressure dissipation Equation (4-13) in combination with Berry's creep models to simulate the consolidation behavior of milled refuse.

Modified Consolidation Model of Milled Refuse

The starting point of the modified model is Equation

(4-13), that is:

$$\frac{\partial(Se)}{\partial t} = \frac{(1+e_o)^2}{\gamma_w} \frac{\partial}{\partial x} \left(\frac{kS}{1+e} \frac{\partial u}{\partial x}\right) + \frac{(1+e)g}{\gamma_w} \psi^f - \frac{(1+e)g}{\gamma_w} \frac{Se}{G_s} \psi^s . \quad (4\text{-}13)$$

In the modified model some of the usual assumption of the consolidation theory will be made i.e. that the material is homogeneous and is fully saturated with an incompressible pore fluid. The solid particles are incompressible but some of them are decomposable because of the biological and chemical activities. It is assumed that the decomposition process can be represented by a uniformly distributed sink or source. One-dimensional compression and fluid flow, and the validity of Darcy's law are also assumed.

Based on the previous discussion, a rheological model comprising a double Terzaghi pot Figure 4-1(a) is used as an analog for the physical mechanism involved in the primary and secondary consolidation of milled refuse. In this model the top spring represents the macro compressibility of the milled refuse skeleton, and the bottom spring simulates the micro compressibility of the porous skeleton structure. The top and bottom porous pistons represent the average permeability of the macrovoids and microvoids respectively. To account for the nonlinear compressibility of the material, the springs are considered to be nonlinear. For a detailed description of this model, the reader is referred to Berry and Poskitt (1972).

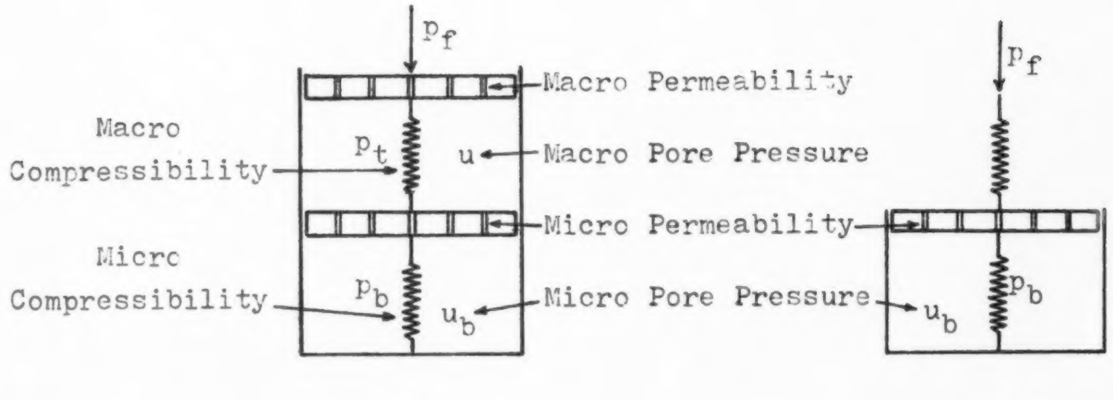
p_f
Macro Permeability
Macro Compressibility
p_t
u
Macro Pore Pressure
Micro Permeability
Micro Compressibility
p_b
u_b
Micro Pore Pressure
p_f
p_b
u_b

(a) (b)

Fig. 4-1. Rheological model based on the micropore mechanism

Let e_t and e_b represent the time-independent part (top spring) and time-dependent part (bottom spring) of the compression, respectively. Suffixes o and f refer to the initial and final values of quantities to which they are attached. Then e_{to} would represent the initial void ratio of the top spring and e_{bf} would represent the final void ratio of the bottom spring. Let e_o be the total void ratio; then

$$e_o = e_{to} + e_{bo} \; .$$

At anytime after the start of consolidation,

$$e = e_t + e_b \; .$$

Permeability tests with back pressure on saturated raw milled refuse indicate that the void ratio and log permeability have a bilinear relationship (Gupta, 1972). For the variation of the range of void ratio to be considered herein, the linear e versus log k law will be used, i.e.

$$k = k_o \left(\frac{k_f}{k_o} \right)^{\frac{e_o - e}{e_o - e_f}}$$

To account for nonlinear compressibility of the material, the widely accepted linear void ratio log effective stress law is assumed for e, e_t, and e_b. Thus,

$$p = p_o\left(\frac{p_f}{p_o}\right)^{\frac{e_o-e}{e_o-e_f}} , \qquad (4\text{-}16a)$$

$$p_t = p_o\left(\frac{p_f}{p_o}\right)^{\frac{e_{to}-e_t}{e_{to}-e_{tf}}} , \qquad (4\text{-}16b)$$

$$p_b = p_o\left(\frac{p_f}{p_o}\right)^{\frac{e_{bo}-e_b}{e_{bo}-e_{bf}}} . \qquad (4\text{-}16c)$$

The effects of the fluid generation term ψ^f, and the degree of saturation, S, on the consolidation behavior of milled refuse will be considered in more detail later. These terms will be omitted in the following derivation. If the decomposition of milled refuse is assumed to follow the law

$$\phi = \phi_o \exp(-Ct) , \qquad (4\text{-}17)$$

where ϕ = weight of the decomposable part of the milled refuse at time t,

ϕ_o = initial weight of the decomposable part of the milled refuse,

C = rate constant,

and t = time,

then Equation (4-13) reduces to

$$\frac{(1+e_o)^2}{\gamma_w} \frac{\partial}{\partial x}\left(\frac{k}{1+e} \frac{\partial u}{\partial x}\right) - \frac{e\phi_o C}{\gamma_w G_s} \exp(-Ct) = \frac{\partial e}{\partial t} . \qquad (4\text{-}18)$$

From the principle of effective stress,

$$u = p_f - p_t = p_f - p_o\left(\frac{p_f}{p_o}\right)^{\frac{e_{to}-e_t}{e_{to}-e_{tf}}} \qquad (4\text{-}19)$$

Substituting (4-15) and (4-19) into (4-18) gives

$$\frac{e_o-e_f}{e_{to}-e_{tf}} \, \frac{k_o(1+e_o)^2}{\gamma_w a_{vo}} \, \frac{\partial}{\partial x}\left[\frac{\left(\frac{k_f}{k_o}\right)^{\frac{e_o-e}{e_o-e_f}} \left(\frac{p_f}{p_o}\right)^{\frac{e_{to}-e_t}{e_{to}-e_{tf}}}}{1+e} \, \frac{\partial e_t}{\partial x}\right]$$

$$+ \frac{e\phi_o C}{\gamma_w G_s} \exp(-Ct) = -\frac{\partial e}{\partial t} \qquad (4\text{-}20)$$

where a_{vo} equals $c_c/(2.3p_o)$.

When the macropore pressure approaches zero, the compression becomes entirely time-dependent. The creep behavior of the material is governed by the average rate of flow of pore water from the microvoids to the macrovoids. Unfortunately, the exact form of the law governing this pore water flow is not known. It is necessary to develop the law purely on the basis of physical intuition. Barden and Berry (1967) pointed out that for material in which secondary compression results from volume change within the micropore structure it would appear that the rate process function proposed by Murayama and Shibata (1964) best accounts for the secondary compression of such material. Thus, the Murayama and Shibata law, which has the following form, will be used to describe the creep behavior of the material:

$$\frac{d\epsilon}{dt} = A(e_b)\Delta p \sinh\left(\frac{B(e_b)u_b}{\Delta p}\right). \qquad (4\text{-}21)$$

In terms of void ratio, Equation (4-21) is

$$\frac{1}{1+e_o}\frac{de_b}{dt} = -A(e_b)\Delta p \sinh\left(\frac{B(e_b)u_b}{\Delta p}\right) . \qquad (4\text{-}22)$$

$A(e_b)$ and $B(e_b)$ are material parameters which depend on the current value of the void ratio. Δp is the load increment and u_b is the equivalent average micropore pressure. The actual variation of parameters A and B with void ratio is not known. A linear form of the variation of the parameters of the rate process function with void ratio has been used by Poskitt (1971). For the mathematical convonience, linear e_b-log A and e_b-log B relationships will be assumed here. Thus

$$A = A_o\left(\frac{A_f}{A_o}\right)^{\frac{e_{bo}-e_b}{e_{bo}-e_{bf}}} , \qquad (4\text{-}23a)$$

and

$$B = B_o\left(\frac{B_f}{B_o}\right)^{\frac{e_{bo}-e_b}{e_{bo}-e_{bf}}} . \qquad (4\text{-}23b)$$

It is evident from Fig. 4-1b that the vertical equilibrium of the bottom spring gives

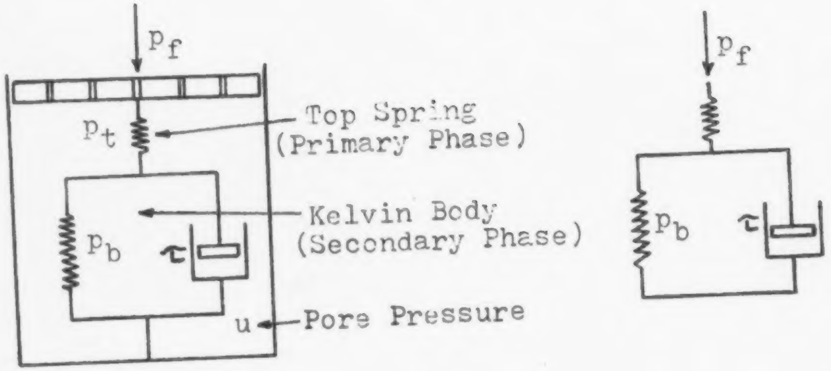
p_f
p_t
Top Spring
(Primary Phase)
Kelvin Body
(Secondary Phase)
p_b
τ
u
Pore Pressure
p_f
p_b
τ

(a)

(b)

Fig. 4-2. Rheological model based on the structural viscosity

$$u_b - u = p_t - p_b = p_o\left[\left(\frac{p_f}{p_o}\right)^{\frac{e_{to}-e_t}{e_{to}-e_{tf}}} - \left(\frac{p_f}{p_o}\right)^{\frac{e_{bo}-e_b}{e_{bo}-e_{bf}}}\right]. \qquad (4\text{-}24)$$

Substituting Equation (4-23) and (4-24) into (4-22) yields

$$\frac{\partial e_b}{\partial t} = -A_o p_o (1+e_o)\left(\frac{p_f}{p_o} - 1\right)\left(\frac{A_f}{A_o}\right)^{\frac{e_{bo}-e_b}{e_{bo}-e_{bf}}} \sinh\left\{\frac{B_o\left(\frac{B_f}{B_o}\right)^{\frac{e_{bo}-e_b}{e_{bo}-e_{bf}}}}{\left(\frac{p_f}{p_o} - 1\right)}\right.$$

$$\left.\left[\left(\frac{p_f}{p_o}\right)^{\frac{e_{to}-e_t}{e_{to}-e_{tf}}} - \left(\frac{p_f}{p_o}\right)^{\frac{e_{bo}-e_b}{e_{bo}-e_{bf}}}\right]\right\}. \qquad (4\text{-}25)$$

Equation (4-20) and (4-25) completely define the consolidation process of the milled refuse except the effect of biological and chemical decomposition. They are highly nonlinear but can be solved by a numerical method modified from one proposed by Poskitt (1971).

Another rheological model which has received a wide range of experimental support is shown in Fig. 4-2a. By the consideration of the principle of effective stress, an equation which has exactly the same form as Equation (4-20) can be obtained. The equation governing the time-dependent compression is obtained by considering the vertical equilibrium of the model shown in Fig. 4-2b. Viscous resistance of the nonlinear dashpot is given by

$$\tau = p_t - p_b \, . \qquad (4\text{-}26)$$

A rate process function which was originally proposed by Wu (1964) has been used to describe the viscous behavior of the nonlinear dashpot. For the finite strain case, it has the form

$$\frac{1}{1+e_o} \frac{de_b}{dt} = -\beta(e_b) \sinh(\alpha(e_b)\tau), \qquad (4\text{-}27)$$

where α and β are parameters that describe material properties. Wu (1966) stated that β remains sensibly constant over a wide range of effective stress and α decreases with increase in effective stress. Assuming linear e_b-log p, e_b-log relationships and constant β, and substituting Equation (4-26) into (4-27), one has

$$\frac{de_b}{dt} = -\beta(1+e_o) \sinh\left\{ \alpha_o p_o \left(\frac{\alpha_f}{\alpha_o}\right)^{\frac{e_{bo}-e_b}{e_{bo}-e_{bf}}} \left[\left(\frac{p_f}{p_o}\right)^{\frac{e_{to}-e_t}{e_{to}-e_{tf}}} - \left(\frac{p_f}{p_o}\right)^{\frac{e_{bo}-e_b}{e_{bo}-e_{bf}}} \right] \right\}. \qquad (4\text{-}28)$$

Equation (4-20) together with Equation (4-28) offer alternative model for describing the time-settlement behavior of the milled refuse.

Summary

A close review of Zimmerman's model shows that the rheological model of the solid skeleton is equivalent to a Kelvin body with a nonlinear spring in series with a nonlinear dashpot, which is described by $d\epsilon/dt = \beta \sinh \alpha \tau$. The parameters α and β of the rate process relation are assumed to be constant. The numerical method used to obtain solutions is modified from one proposed by Barden. When one takes the variation of the material parameters with void ratio into account, this numerical method becomes complicated. Two possible consolidation models for milled refuse obtained by combining the general pore pressure dissipation equation with an appropriate creep function have been formulated. Similar formulations of this kind can also be found in the works of Poskitt (1971), and Berry and Poskitt (1972). These two creep models will be closely examined in the next chapter in order to determine which model will give a better description of the creep behavior of milled refuse.

Chapter V

CREEP MODELS

There are three modes of compressive deformation commonly treated in soil mechanics theories : (1) hydrostatic compression defined by the stress condition that the principal stresses are all equal, which in the case of isotropic media results in volumn change only; (2) one-dimensional compression, which is defined by the strain condition of complete lateral confinement with strain exclusively in the vertical direction, and (3) triaxial compression, in which all principal stresses and strains may be different (Burmister, 1959). A normal material is least compressible in hydrostatic compression and is more compressible in one-dimensional compression. In triaxial compression, shearing deformations finally predominate, failure in shear results, and there is a limited compressive strength. Creep phenomena can occur in all three of these deformation modes in clays and many other materials, but may not be of comparable magnitude in all three. Tests by Taylor (1942) and Fang (1956) show substantially reduced secondary compression during triaxial consolidation as compared with one-dimensional tests.

With the radial displacements of the sample being zero, the study of creep phenomena by oedometer tests is limited to the stress states corresponding to this displacement condition. In triaxial tests the radial stresses on the periphery of the sample can be controlled and arbitrarily chosen. Thus, triaxial tests enable a better observation and more thorough study of creep phenomena. However, the first study of the influence of creep on consolidation (Taylor and Merchant, 1940) was applied to the oedometer test, which is designed as an idealization of the type of compression seen in the field. Oedometer tests still provide the main experimental basis for practical computation of settlements and consolidation.

In this chapter, theoretical solutions of two creep models, based on structural viscosity and micropore structure respectively, will be discussed. This is undertaken because (1) the behavior of the material near the drainage boundary is given by the basic creep equation of the solid skeleton, as the pore pressure here becomes zero soon after the external load is applied; (2) ultimately it is necessary to curve fit the secondary compression tails of the void ratio versus time curves to these solutions in order to evaluate the rheological parameters of the material. It is also hoped that the parameter study of the creep models will provide more information on their behavior which will help in choosing the best model to describe the consolidation creep behavior of milled refuse.

Parameter Study of Creep Model Based On Structural Viscosity

In this case, the basic equation governing the consolidation creep of the solid skeleton is obtained directly from Equation (4-28) by setting $u = 0$. Equation (4-28) then reduces to the ordinary differential equation

$$\frac{de_b}{dt} = -\beta(1+e_o)\sinh\left\{\alpha_o p_o \left(\frac{\alpha_f}{\alpha_o}\right)^{\frac{e_{bo}-e_b}{e_{bo}-e_{bf}}} \left[\frac{p_f}{p_o} - \left(\frac{p_f}{p_o}\right)^{\frac{e_{bo}-e_b}{e_{bo}-e_{bf}}}\right]\right\} . \quad (5\text{-}1)$$

An examination of this equation shows it to be expressed in terms of the three parameters: (1) the ratio of the slope of the e_b - log p curve to the slope of the e_b - logα curve, (2) the stress ratio, p_f/p_o, and (3) the value of $\alpha_o p_o$. Numerical solutions of the above creep equation can be obtained by procedures described in Appendix A (Chen). These solutions, for special case in which $(\alpha_f/\alpha_o)(p_f/p_o)^{0.5} = 1$, are shown plotted in Figs. (D-1) to (D-5). With C_α defined as the change in void ratio per $\log_{10}$ cycle of time, degree of settlement defined as $(e_{bo} - e_b)/(e_{bo} - e_{bf})$, and time factor defined as $\beta(1+e_o)t/(e_{bo} - e_{bf})$, these curves show that for a given value of $\alpha_o p_o$ and a given value of p_f/p_o, C_α remains sensibly constant with time. For a given value of $\alpha_o p_o$, C_α decreases with increasing values of p_f/p_o. Figs. (D-6) to (D-8) show that for a given value of p_f/p_o, C_α decreases with increasing values of $\alpha_o p_o$.

Secondary compression is usually defined as that part of time-dependent compression which occurs after the excess pore pressure has been substantially dissipated. Thus Figs. (D-1) to (D-5) show that for a given $\alpha_o p_o$, a smaller amount of secondary compression occurs during the primary stage under small Δp. Also Figs. (D-6) to (D-8) predict that for a given p_f/p_o, the larger the value of $\alpha_o p_o$, the greater the amount of secondary compression that occur during the primary stage. It is to be noted that some of the numerical solution for large values of p_f/p_o have not been given, because escessive computing time would be required to obtain such solutions.

In Fig. (D-9) to Fig. (D-13) the numerical solutions to Equation (5-1) for the case $(\alpha_f/\alpha_o)(p_f/p_o)=1$ are given. Here, $(\alpha_f/\alpha_o)(p_f/p_o)=1$ implies that the slope of the e_b-log p curve is equal to the slope of the e_b-log curve. From these curves it may be seen that for a fixed value of $\alpha_o p_o$ and a fixed value of p_f/p_o, C_α remains approximately constant with time. These curves also predict that for a constant $\alpha_o p_o$, small Δp results in a smaller amount of secondary compression during the primary stage. From Fig. (D-14) to Fig. (D-16), it is apparent that for a constant value of p_f/p_o. the larger the value of $\alpha_o p_o$, the greater the amount of secondary compression that occurs in the primary stage.

Numerical solutions to Equation (5-1) for the special case in which $(\alpha_f/\alpha_o)(p_f/p_o)=1$ are shown plotted in Fig. (D-17) to Fig. (D-21). These curves also predict a smaller amount of secondary compression during the primary stage under small Δp when the value of $\alpha_o p_o$ remains constant. For a constant value of p_f/p_o, Fig. (D-22) to Fig. (D-24) show the larger the value of $\alpha_o p_o$, the greater the amount of secondary compression during the primary stage. The main difference from the previous cases is that for a constant value of p_f/p_o and $\alpha_o p_o$, C_α now increases with increasing time.

The influence of the ratio of the slope of the e_b-log p curve to the slope of the e_b-log α curve on the behavior of the model is shown in Fig. (D-25) to Fig. (D-27). From these curves it may be seen that for a constant value of $\alpha_o p_o$ and p_f/p_o, the larger the value of this ratio, the smaller the amount of secondary compression during the primary stage. Also when this ratio becomes larger, C_α then increases with increasing time.

The main feature of this model is that for a constant value of $\alpha_o p_o$ it predicts a smaller proportion of secondary compression during the primary stage under a small Δp. This model also predicts an initial creep rate that increases expoentially with Δp. Thus a soil element near the drain will undergo a very rapid decrease in permeability with increasing p_f/p_o. The pore pressure is therefore not able to dissipate quickly. Because the magnitude of p_f/p_o dominates the rate of pore pressure dissipation, the use of a simple scaling law applies. As pointed out by Barden and Berry (1967), for clay soils, in which the creep mechanism is one of viscous shear failure at particle contact points, a large amount of experimental evidence would appear to support the prediction of this model.

Parameter Study of The Creep Model Based On Micropore Structure

In this case, the basic deformation-time relationship governing the creep behavior of the solid skeleton is obtained directly from Equation (4-20) by setting u = 0. Equation (4-20) then reduces to the ordinary differential equation

$$\frac{de_b}{dt} = -A_o p_o (1+e_o)\left(\frac{p_f}{p_o} -1\right)\left(\frac{A_f}{A_o}\right)^{\frac{e_{bo}-e_b}{e_{bo}-e_{bf}}} \sinh\left\{ \frac{B_o \left(\frac{B_f}{B_o}\right)^{\frac{e_{bo}-e_b}{e_{bo}-e_{bf}}}}{\left(\frac{p_f}{p_o} -1\right)} \left[\left(\frac{p_f}{p_o}\right) - \left(\frac{p_f}{p_o}\right)^{\frac{e_{bo}-e_b}{e_{bo}-e_{bf}}}\right]\right\} . \qquad (5\text{-}2)$$

In the previous parameter study, it has been shown that it is the variation in α which has the most significant effect on the behavior of the model. It might be expected that in the present case it will be the variation in B which will have the dominant influence. With the assumption that the ratio of the slope of the e_b- log p curve to the slope of the e_b- log A curve is equal to unit, the numerical solutions to Equation (5-2) for the cases in which (B_f/B_o)x $(p_f/p_o)^{0.5}=1$, $(B_f/B_o)(p_f/p_o)=1$, and $(B_f/B_o)(p_f/p_o)^2=1$ have been plotted in Figs. (D-28) to (D-66). These curves indicate that for a constant value of B_o, the amount of secondary compression during the primary stage is nearly independent of the value of p_f/p_o.

Figs. (D-67) to (D-75) predict that for a constant value of p_f/p_o, the lager the value of B_o the greater the amount of secondary compression during the primary stage. The difference in the amount of secondary compression during the primary stage for different values of B_o is not so significant as compared to that predicted by the creep model based on structural viscosity. The influence of the ratio of the slope of the e_b-log P curve to the slope of the e_b-log B curve on the creep behavior of the model is shown in Figs. (D-76) to (D-78) for the case in which $p_f/p_o=4$. From these curves it might be shown that different values of this ratio result in almost the same amount of secondary compression during the primary stage. However, for higher values of this ratio, C_α begins to increase with increasing time.

A characteristic feature of this model is that the value of C_α increases with increasing time, especially under large values of p_f/p_o. It also predicts that for a constant value of B_o, the proportion of secondary consolidation occuring during the primary stage is nearly constant with varying values of p_f/p_o. This has been observed on both remolded and undisturbed samples of fibrous peats by Barden and Berry (1968). This model also predicts that the initial creep rate is a linear function of Δp. Thus the soil elements near the drain do not undergo such a rapid decrease in permeability with increasing p_f/p_o as do those in the creep model based on structural viscosity. The pore pressure is therefore able to dissipate more quickly. As the magnitude of p_f/p_o does not dominate the dissipation rate, the use of a simple scaling law no longer applies. It has been shown (Barden and Berry, 1967) that for fibrous peats in which secondary compression results from the dissipation of micropore water it appears that this model best describes the response.

Summary

The creep model based on structural viscosity predicts a smaller proportion of secondary compression during the primary stage under small Δp. This has been shown to be a relevant model for clay soils in which the secondary compression has been suggested as the result of slow viscous displacement at the soil particle contacts. Another creep model based on the micropore structure predicts an almost constant proportion of secondary compression during the primary stage under different values of p_f/p_0. For fibrous peat in which the secondary compression has been suggested as the result of the volume decrease within the microstructures, this model has been shown to be more relevant.

The structure of milled refuse is very similar to that of fibrous peat. Also the secondary compression tails from the laboratory consolidation tests on milled refuse samples tend to fit the theoretical solution of the creep model based on micropore structure better. For these reasons, the creep model based on the micropore structure will be adopted in this study to simulate the consolidation creep behavior of milled refuse. Typical theoretical solutions of these two creep models are shown in Fig. (5-1) and (5-2) respectively.

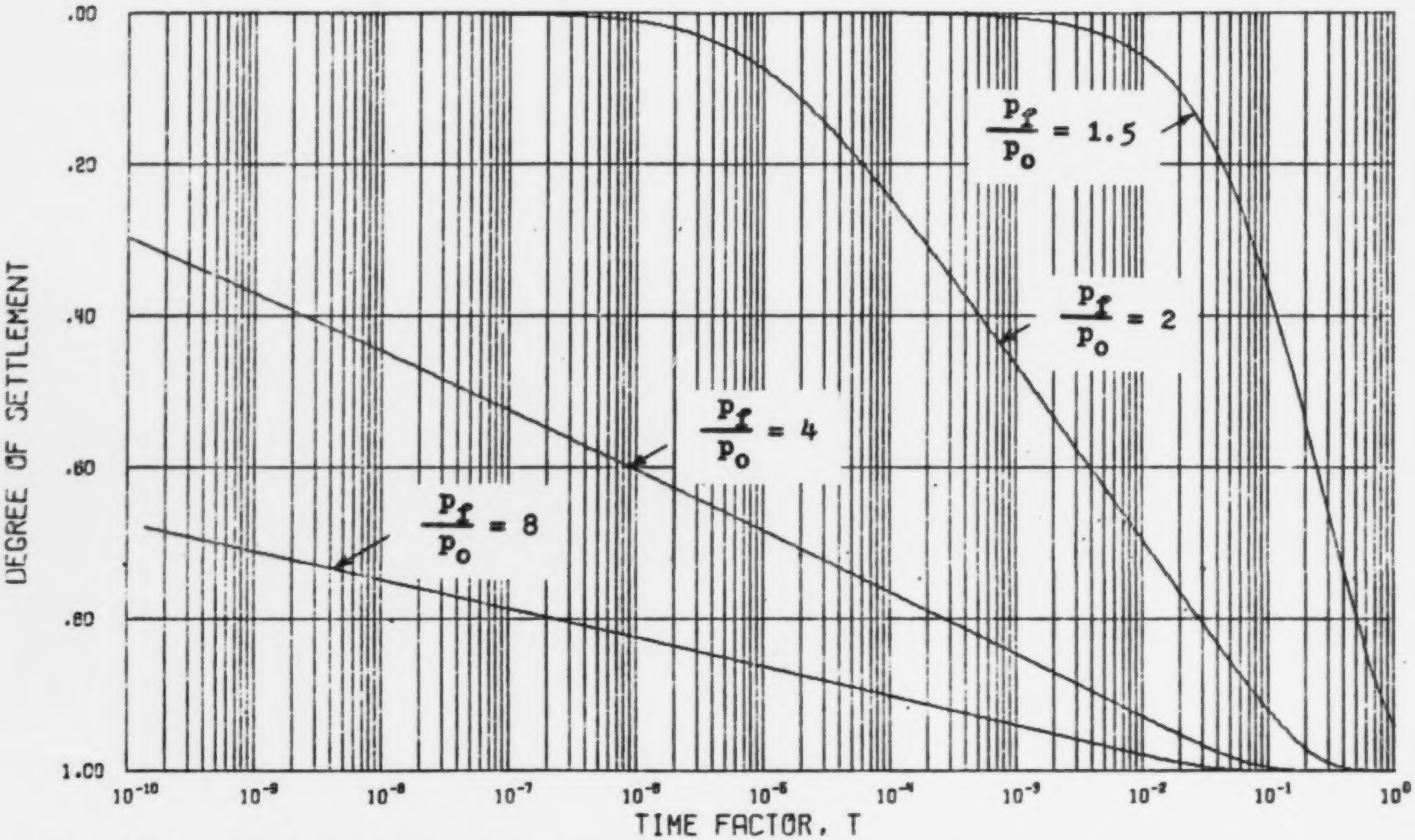

Fig. 5-1. Settlement vs. time factor of the creep model based on structural viscosity for various values of stress increment: $\alpha_o p_o = 10$, $(p_f/p_o)(\alpha_f/\alpha_o)^{0.5} = 1$

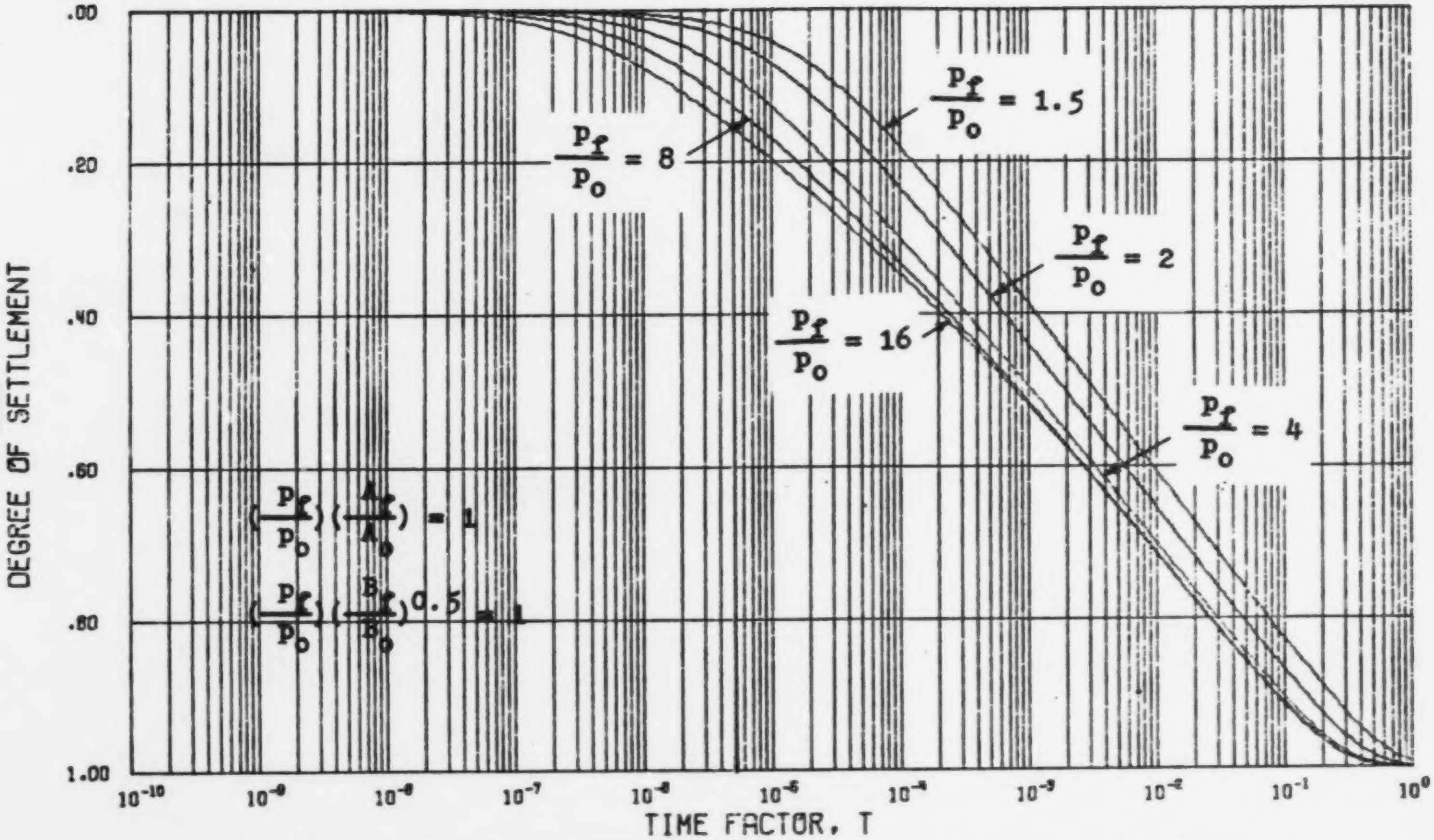

Fig. 5-2. Settlement vs. time factor of the creep model based on micropore structure for various values of p_f/p_o; $B_o = 10$

CONSOLIDATION TESTS OF MILLED REFUSE

Other than the present study, no data on the consolidation behavior of solid waste are presently available, and laboratory consolidation testing of refuse is not found in the literature. Various agencies have made considerable effort to maintain settlement records of solid waste disposal sites by the installation of either settlement plates or settlement monuments at the sanitary landfills. Using a hose settlement device, a continuous profile of settlement along a PVC line buried under a landfill site has been obtained by Zoino (1971). Without a general consolidation theory developed for such complex material as milled refuse, the interpretation of such data is extremely difficult.

The present study is intended to help in providing an understanding of the settlement process in the milled refuse landfill, and it includes both theoretical and experimental study of the consolidation of milled refuse. In this chapter, a consolidometer developed for consolidation testing of both raw and laboratory aged milled refuse samples under fully saturated conditions will be described. Descriptions of sample preparation, sample aging, and test techniques will also be given.

Consolidometer For Milled Refuse

(1) Development of Consolidometer

The first consolidation cell for soil testing was used by Frontard in 1910 (Skempton, 1960). A sample 2 in. thick and 14 in. in diameter was placed in a metal container with a perforated base and was loaded by means of a piston. In 1919, The Swedish Geotechnical Commission used a consolidometer in which a clay sample was contained within a cylinder closed at the base and loaded by means of a stiff plunger through a layer of sand. Terzaghi in 1919 devised an oedometer which was actually a single drainage cell, to demonstrate the principle of effective stress. The sample was approximately ¼ in. thick and 3 in. in diameter. The presently widely used oedometer, which has the essential test arrangement and size of sample chosen by Terzaghi, is generally known as the Casagrande oedometer.

In order to reproduce in-situ neutral pressure, a new type of consolidometer and loading unit was developed by Lowe et. al. (1964). A major feature of this apparatus was the provision for the Casagrande oedometer to be mounted within a pressure chamber so as to allow the application of back pressure. Rowe and Barden (1966) developed a consolidometer in which the total stress was applied by means of hydraulic pressure acting across a convoluted rubber jack. The arrangement improved control of the drainage conditions, allowing the separation of the instant loading from the commencement of drainage and permitting the measurement of initial pore pressure. Back pressure could also be easily applied.

The consolidometer developed in the present study is designed to provide for backpressure on the test specimen and for the control of drainage and measurement of pore pressure at the base of the specimen. This device is in some respects similar to that described by Lowe et. al. (1964).

(2) The Consolidation Cell

The assembly of the basic cell is similar to that of a standard triaxial cell. The dimensions of the cell itself are designed to accommodate a sample of 6.75 in. diameter and 5 in. height and to allow ample space for some special accessories for holding and loading the sample. Details are given in Fig. 6-1. The principal components are the base, the pressure chamber, and the cover.

The base is machined from a single aluminum plate. Provision for pressure connections and pore pressure measurement is made through an outlet in the base. A porous stone made of coarse silica sand cemented with epoxy resin is set into the top surface of the base and a system of drainage grooves ½ in. wide and 1/8 in. in depth are provided under the porous stone. The base and the cover are fitted to the pressure chamber with O-rings as seals. Three ½ in. steel tie bars spaced at 120° are sufficient to tighten the assembly.

For the pressure chamber, a transparent plexiglas cylinder is used, which facilitates the setting up of the test. As a safety precaution this cylinder is reinforced with an outer aluminum protection mesh. The cylinder used has an 8.25 in. outside diameter and ½ in. wall thickness and is

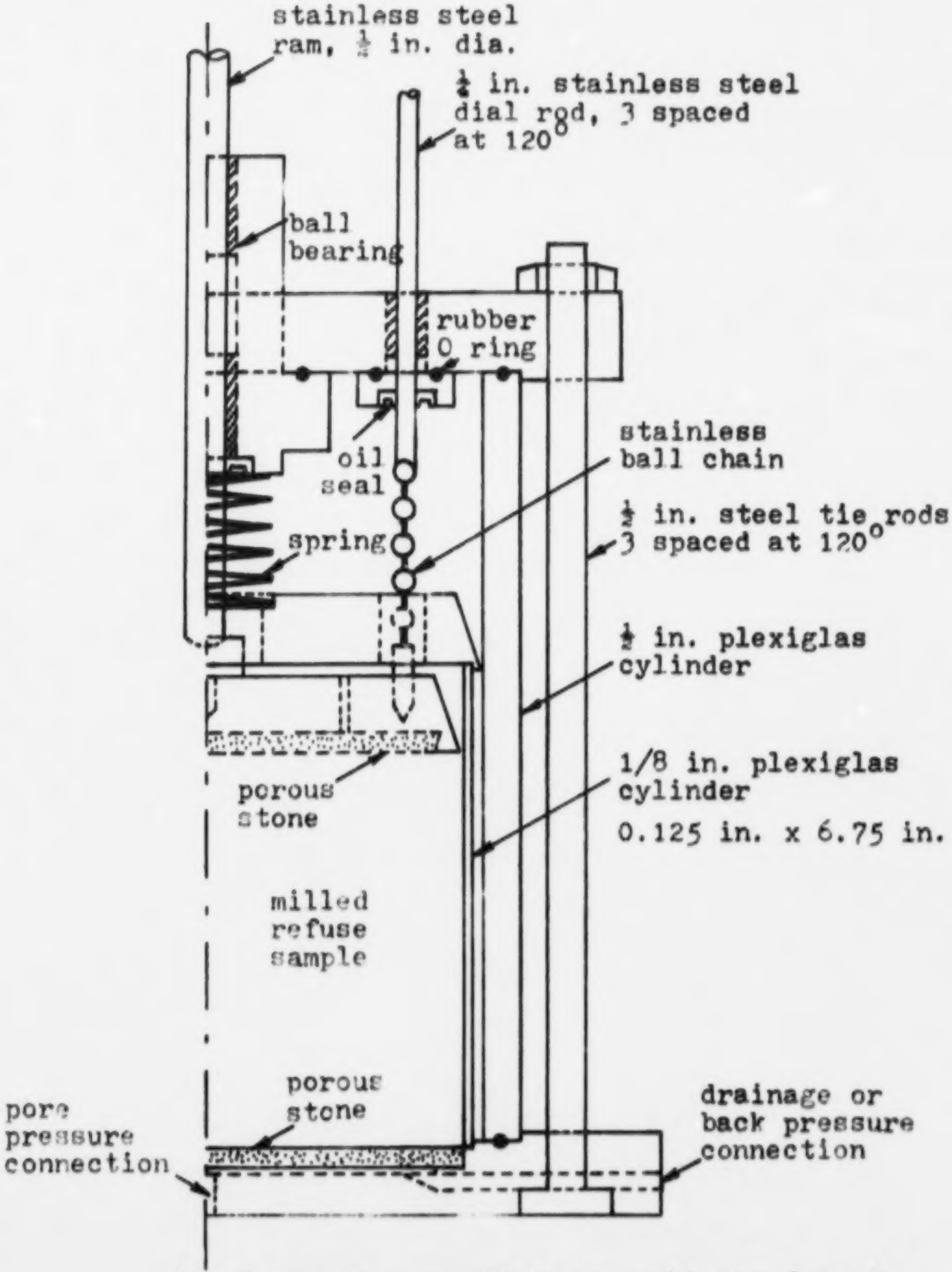
stainless steel ram, ½ in. dia.
¼ in. stainless steel dial rod, 3 spaced at 120°
ball bearing
rubber O ring
oil seal
stainless ball chain
½ in. steel tie rods 3 spaced at 120°
spring
½ in. plexiglas cylinder
1/8 in. plexiglas cylinder
0.125 in. x 6.75 in.
porous stone
milled refuse sample
porous stone
pore pressure connection
drainage or back pressure connection

Fig. 6-1. The consolidation cell for 6.75-in diameter samples

designed for pressure up to 150 psi. The sample holder is a plexiglas cylinder with an inside diameter of 6.75 in. and wall thickness of 0.125 in., and is sealed to the base at the time the test is set up by silicone rubber. A rigid aluminum plate is put on the top of the sample holder to hold it in place. Spring force is exerted on this plate to help prevent leakage at the sealed bottom of the sample holder. Thus, the drainage condition at the bottom of the sample can be controlled by a valve at the outlet. A rigid loading plate, with drainage grooves and a porous stone, transfers the load to the sample from the loading ram. Free drainage is provided from the top of the sample to the outer chamber.

The vertical settlement of the loading plate is measured at three points spaced at 120° by means of three stainless steel spindles of ½ in. diameter attached through stainless steel ball chains to the loading plate and passing out through the spring-loaded holding plate and the top of the chamber to suitable dial gauges. This arrangement makes tolerable a small degree of tilt of the loading plate.

The top is also machined from a single aluminum plate. The holes for the dial spindles in the top contain ball bearings and oil seals which grip the spindles tightly enough to prevent leakage but not so tightly that friction has significant effects on the settlement reading or the load on the sample. The loading ram used is a ½ in. ground stainless steel shaft running through two ball bearings and an oil seal and lubricated with silicone grease. Both the top and the base are provided with pressure connections so that the predetermined back pressure can be applied gradually in small increments.

(3) Loading And Back Pressure System

The experimental set-up used in this study is shown in Fig. 6-2a, b, c. A stainless steel pneumatic cylinder with a capacity of 250 psi and a 3 in. stroke is used for applying the load. A pressure regulator is used for controlling and maintaining constant pressure. Pressure for the regulator is supplied from a large volume, high pressure storage tank containing compressed air. A minor problem of the pneumatic pressure system from the soil testing point of view is the variation in pressure due to temperature changes. However, with careful and patient adjustments, this system has been used successfully in this study. Back pressure is supplied from an air reservoir with a physical volume of about 2.6 ft^3. The air passes through the controlling valve and acts on the water supply to the cell and is itself supplied by a central compressed-air system. A minor problem encountered in this system was pressure variation due either to changes in temperature after sealing off the reservoir and/or to the solubility of air in water. The variation in temperature changes can also be overcome by careful and patient adjustments of the pressure. The solution of air in water can be minimized by closing the valves to the back pressure reservoir after the predetermined back pressure has been applied. Back pressure then applies through the burette which has a much

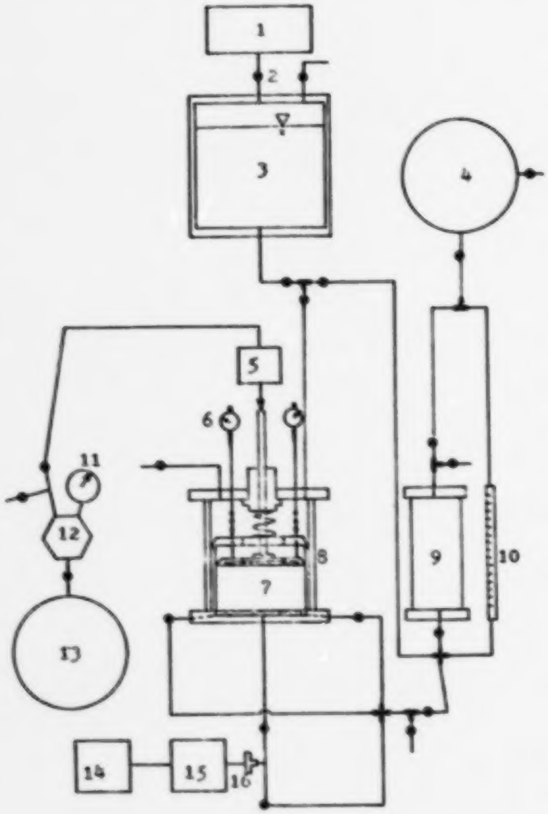

1. Vacuum or pressure
2. Valve
3. De-aired water reservoir
4. Back pressure tank
5. Air cylinder
6. Dial gauge
7. Milled refuse sample
8. Consolidation test chamber
9. Back pressure reservoir
10. Burette
11. Pressure gauge
12. Pressure regulator
13. Compressed-air source
14. Strip chart recorder
15. Power supply
16. Electric transducer

Fig. 6-2a. Schematical overall experimental set-up

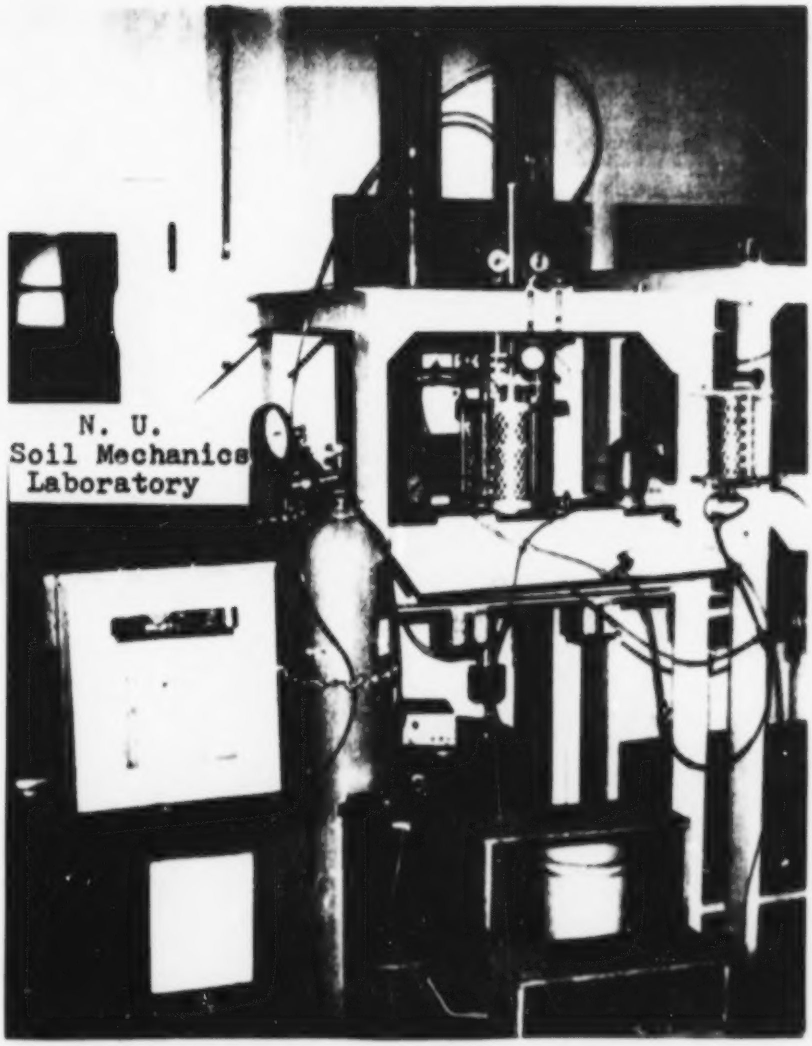
N. U.
Soil Mechanics
Laboratory

Fig. 6-2b. Overall experimental set-up

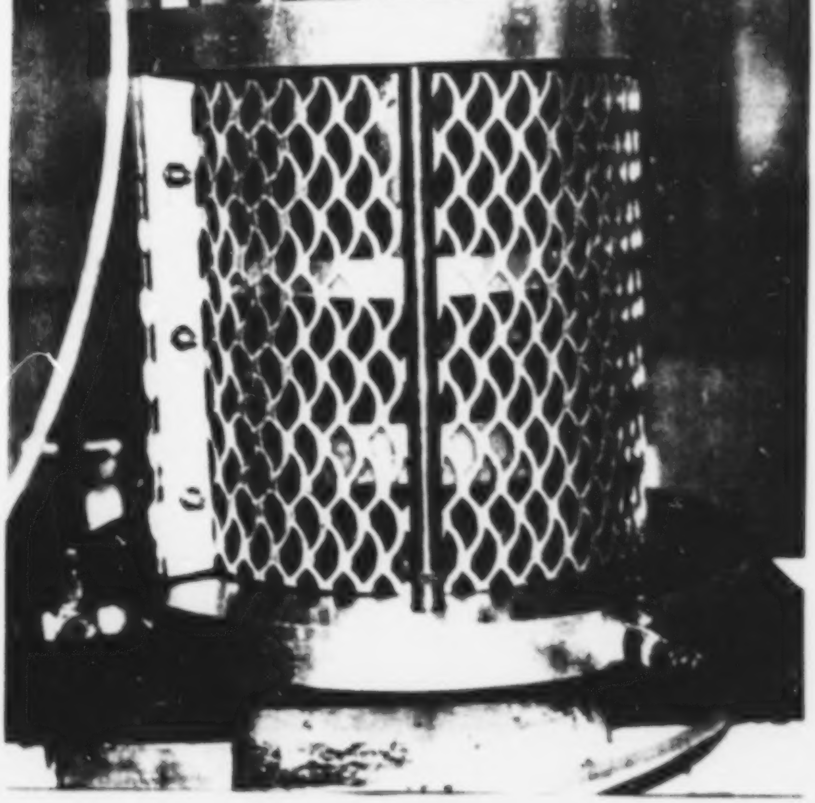

Fig. 6-2c. Consolidation test cell

smaller diameter than that of the back pressure reservoir; the solution of air in the water is thus greatly reduced.

(4) Pore Pressure Measurement

Taylor (1942) was probably the first to measure pore pressure in the consolidation test. He used a null balancing system to measure pressure at the bottom of the sample. Following the same technique, Aldrich (1951) used a needle inserted at the midplane of the sample. Norwegian Geotechnical Institute equipment with manual and automatic pressure balancing has been used by various investigators (Rowe, 1959; Leonards and Girault, 1961). The more advanced electric pressure transducer was introduced by Whitman et. al.(1961).

In this study, a small-displacement absolute pressure transducer, which uses two semiconductor strain gauges to measure the deflection of a diaphragm at its center, was used with a power supply and a strip chart recorder. The transducer has a rated pressure of 100 psi. A differential pressure transducer if available would offer greater convenience in laboratory tests conducted under back pressure. However, the absolute pressure transducer was adapted by incorporating in the readout circuitry an adjustable bias signal and adjustable scale factor, so that the pressure in excess of the back pressure could utilize the whole range of the recorder.

The principal disadvantage of the present arrangement of pore pressure measurement is that the drainage commences directly when a differential pressure is applied (Rowe, 1965). For a completely saturated sample, theoretically, the excess pore pressure at some distance from the drain should reach its peak valve as soon as the load increment is instantaneously applied and its peak can, in principle, be observed. Since it takes finite time, during which pore pressure dissipation occurs, to apply a load increment, the theoretical peak of the excess pore pressure is missed in the experimental curve obtained in this study.

Preparation of Samples

The milled refuse used in this study was obtained from the refuse reduction plant at Madison, Wisconsin. This material was first throughly mixed upon arrival and then placed in airtight plastic bags which were stored until use in a cool room with a temperature of 2 C. Shredded tin cans, pieces of woods, and the like, were removed. The moisture content of Madison's milled refuse has been reported to vary from 30 to 48 percent, with an average of 37 percent (Reinhart, 1971). The average moisture content of the freshly collected milled refuse used for this study was 36 percent.

Samples were prepared by compacting the milled refuse in a plexiglas cylinder of 8.25 in. diameter and ½ in. wall thickness. The consolidation test would later be done in a cylinder of the same diameter. To reduce wall friction, the inside was coated with silicone grease. A ½ in. thick porous stone and a 1/8 in. perforated plexiglas plate were used at the bottom. Proportional amounts of milled refuse were used to prepare samples of different height with the same void ratio. The compacting load was applied by a 60,000 pound capacity Universal Testing Machine. Compaction loads varying from 4,000 pounds to 6,000 pounds were used to achieve the desired densities. The sample was allowed to rebound freely and then another 1/8 in. perforated plexiglas plate was placed on the top of the sample. Because of the potential for swelling (swelling pressures of about 600 lbs/sq. ft. have been found for the milled refuse with a dry density of 48.2 lbs/cu. ft., Gupta, 1972), two 3/4x1x1/8 in. aluminum channels were used to tighten and reinforce the perforated plexiglas plates. The sample was then submerged in water. Samples to be aged in the laboratory were prepared in the same way except they were seeded with activated sludge.

Aging of Samples

Samples were aged in an insulated chamber with temperature maintained at 125 F by a thermostat. Heating was provided by long-life electric light bulbs, shielded to keep the interior of the chamber in darkness. The samples were irrigated regularly to maintain moisture content.

In order to monitor the temperature of the sample during the laboratory aging process, the individual samples were instrumented with electronic temperature sensors (thermistors). Thermistors are semi-conductors of ceramic material with a high negative temperature coefficient of resistance, and they are manufactured in various useful forms. Thermistor beads are made by forming small ellipsoids of thermistor material on two fine parallel wires about .01 in. apart; the thermistor probes used in this study contained thermistor beads in the tips of solid glass rods of 1/8 in. diameter and 2 in. length. These were calibrated prior to installation. A typical temperature vs. resistance calibration curve is shown in Fig. 6-3. The resistance of the installed thermistors was monitored regularly during the process of aging, and temperatures of samples were obtained from the calibration curves.

The principal disadvantage of the glass thermistors turned out to be that they were easily broken or cracked under very small disturbances. Despite the fact that special care was taken in installing the thermistors and handling the aged samples, only four out of the twenty installed thermistors functioned properly. The rest when examined were seen to be either broken or cracked and the temperature readings were either abnormal or unstable. The temperature data will be presented and analyzed in Chapter VIII.

Testing Procedures

Because only tests under saturated conditions were included in the laboratory testing plan, each sample was treated prior to testing to make it as fully saturated as possible. The freshly prepared or laboratory aged sample was submerged in a sealed container, which was filled with de-aired water, and was subjected to a vacuum of approximately 30 ft. of water for about 15 hours. It was then removed

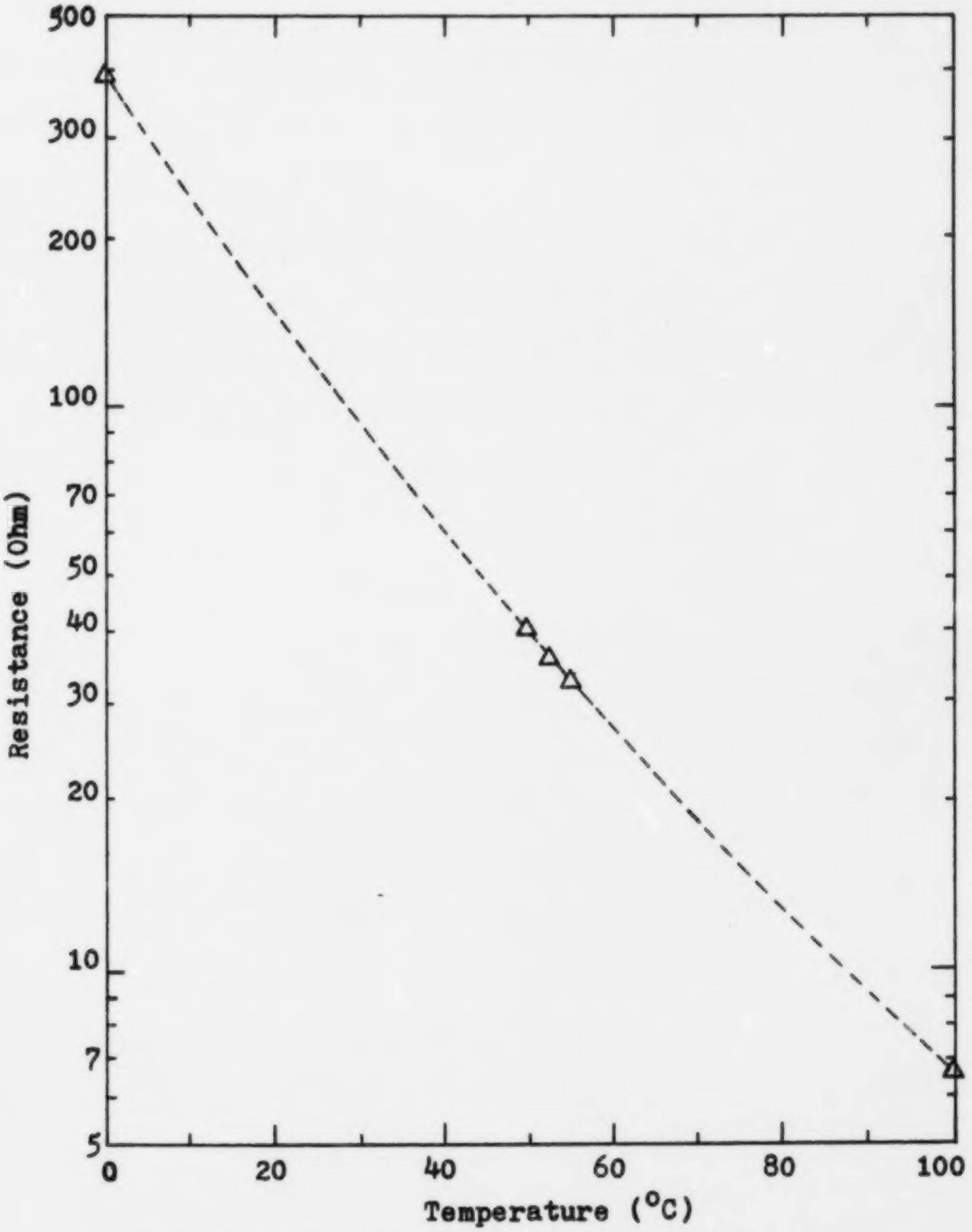

Fig. 6-3. Typical relationship of thermistor resistance to its temperature

from the container and extruded from the sample holder to another of the same diameter, which was also coated with silicone grease to reduce the side friction. The sample holder was then sealed to the bottom plate of the consolidation cell with silicone rubber cement. The top plate, the pressure chamber, and the bottom plate were then assembled and sealed with O-ring seals and silicone grease.

To fill the system with de-aired water, the de-aired water reservoir, the consolidation cell, and the back pressure reservoir were opened to the atmosphere. This allowed the de-aired water to flow slowly downward from the reservoir to the system under gravity. After the system was filled, it was flushed with more de-aired water under pressure to remove entrapped air. The bleed valve of the transducer was also open to the atmosphere in order to remove any trapped air bubbles in the connecting tube.

When a back pressure is applied to the system, the loading ram can be blown out of the consolidation cell due to the action of the cell pressure; therefore, a counterbalancing force is required to balance the upward force on the ram. The predetermined back pressure, which is applied both to the drainage and supply reservoir, and the counterbalancing force were applied proportionally in small increments at intervals of about ten minutes. After the predetermined pressure had been reached, the system was allowed to adjust under full back pressure and counterbalancing force for a period of approximately 24 hours.

Following the period of adjustment, the sample was subjected to a seating load of 1 psi for a period of about 24 hours to make sure that the loading plate and the sample were in good contact. The loading sequence was then commenced. In some tests, the pore pressure at the base of the specimen, and its variation with time, was recorded on a strip chart recorder (Fig. 6-2).

Compressive deformations were observed on three dial gauges with .001 in. divisions located 120° apart, so that any tilt of the loading plate could be accounted for. The dial readings began at 0.1 minute and were taken at smaller time intervals than those of the conventional consolidation test. Whenever possible, each load increment was maintained until the trend of the secondary compression was well defined before another load increment is applied. The value of the load increment was not constant but was varied from test to test in order to study its effect on the consolidation process.

Since the consolidation tests were intended to be conducted under fully saturated conditions, it was a matter of some interest to have some idea about the degree of saturation of the sample after its 24 hours of adjustment under full back pressure. A burette connected in series to the back pressure reservoir was used to measure the fluctuation of the air-water interface due to the proportionally applied back pressure and the counterbalancing force on the loading ram. Two such tests were performed during the early stages of the test program. The burette readings of the first application of back pressure for sample R3-4-1 are given in column (1) of Table 6-1. The burette readings of the same sample for the release and re-application of back pressure after a period of about 24 hours adjustment under full back pressure are shown in column (2) and (3) in Table 6-1 respectively. Similar data for sample A4-4-1 are given in Table 6-2. These almost exactly equal burette readings indicate that the sample had a constant degree of saturation under a back pressure of 75 psi and a 24 hour period of adjustment under such back pressure. Also, permeability test data obtained by introducing 75 psi back pressure in the test system indicated that nearly complete saturation was obtained (Gupta, 1972). It is, therefore, believed that as a result of such effort, a satisfactory degree of saturation has been achieved.

Summary

An apparatus for the consolidation test of milled refuse is described in which a back pressure of up to 100 psi can be applied to insure the saturation of the sample. Procedures for sample preparation and operation of the consolidometer are also given. Laboratory aging of samples was conducted in an insulated chamber which was maintained at a constant temperature of about 125 F. Electric temperature sensors were installed in the samples to monitor the temperature during the process of aging. A sample was found to be satisfactorily saturated under a back pressure of 75 psi and a period of adjustment under such pressure for about 24 hours.

Table 6-1

Burette readings for sample R3-4-1

back pressure (psi)	(1)	(2)	(3)
1.5	7.76	7.72	7.72
10.0	7.55	7.44	7.47
20.0	7.45	7.30	7.30
30.0	7.35	7.20	7.21
40.0	7.18	7.15	7.15
50.0	7.13	7.10	7.11
60.0	7.09	7.07	7.07
70.0	7.07	7.05	7.05
75.0	7.05	7.03	7.03

Table 6-2

Burette readings for sample A4-4-1

back pressure (psi)	(1)	(2)	(3)
1.5	7.59	7.50	7.50
10.0	7.51	7.46	7.48
20.0	7.46	7.42	7.44
30.0	7.40	7.39	7.40
40.0	7.38	7.36	7.37
50.0	7.35	7.33	7.34
60.0	7.32	7.31	7.31
70.0	7.30	7.30	7.30
75.0	7.29	7.29	7.29

DETERMINATION OF MODEL PARAMETERS

As pointed out in a previous chapter, the governing differential equations for consolidation of milled refuse are highly nonlinear and are not amenable to analytical solution. Numerical solutions to such equations are possible but they lend themself less readily to physical interpretation and to treatment of the problem of determining physical constants through the analysis of test data. Indeed, the great number of physical parameters to be determined by appropriate physical tests and the mathematical difficulties in applying the fundamental solutions to practical technical problems are the major problems in applying nonlinear models to simulate the effective stress-strain-time relation of a soil.

The procedures for the determination of rheological parameters from the laboratory time-settlement curves will be given in this chapter. For convenience these procedures are broken down into the following steps, each of which is illustrated by reference to the laboratory consolidation test data for sample R3-4-1, given in Fig. 7-1.

(1) Before any analysis can be performed, the ultimate void ratio e_f must first be determined. For practical engineering purposes it can be assumed arbitrarily that after say $t_f = 300$ years all significant consolidation of the material has been completed. If the void ratio versus log time curve tends to merge into a linear asymptote at the end of a rea-

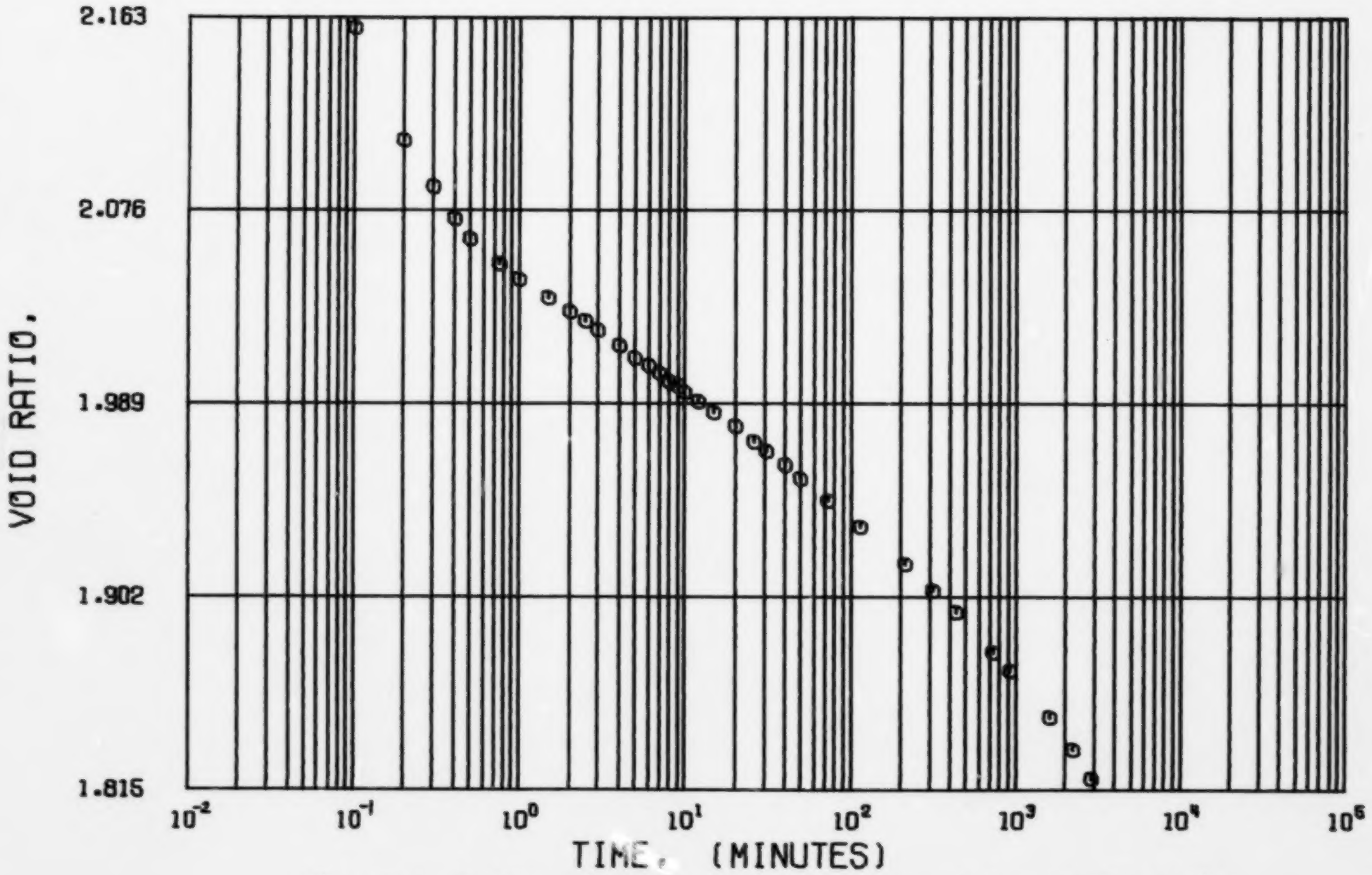

Fig. 7-1. Void ratio versus log time record for sample R3-4-1

sonably long period of time, then the ultimate void ratio can be estimated by extrapolating the secondary consolidation tail of the curve and e_f may be taken at t_f= 300 years. For the present case, the slope of the void ratio versus log time curve increases with increasing time. The ultimate void ratio e_f obtained by extrapolating the secondary tail to t_f= 300 years will be unreliable.

It has been observed that at large t the slope of the curve of strain versus log strain rate approaches a constant . A typical plot of this relation for the same sample is shown in Fig. 7-2. A similar relation has also been observed for the curve of the plot of log strain rate versus log time. This relation is shown in Fig. 7-3. By extrapolating the straight line portion at large time (Fig. 7-3), one obtains a strain rate of 2.0 x 10^{-10}/minute for the final consolidation time taken arbitrarily as 300 years. From Fig. 7-2, one can find that the ultimate strain corresponding to this strain is 2.855 x 10^{-1} (In both cases, the extrapolation goes beyond the margins of the figure as shown.) The corresponding ultimate equilibrium void ratio, e_f, is 1.402, which is readily available from the definition of a strain, that is

$$\epsilon_f = \frac{e_o - e_f}{1 + e_o} . \qquad (7\text{-}1)$$

(2) The next step is to fit the secondary compression tail to the basic creep curves shown in Figs. D-28 to D-66

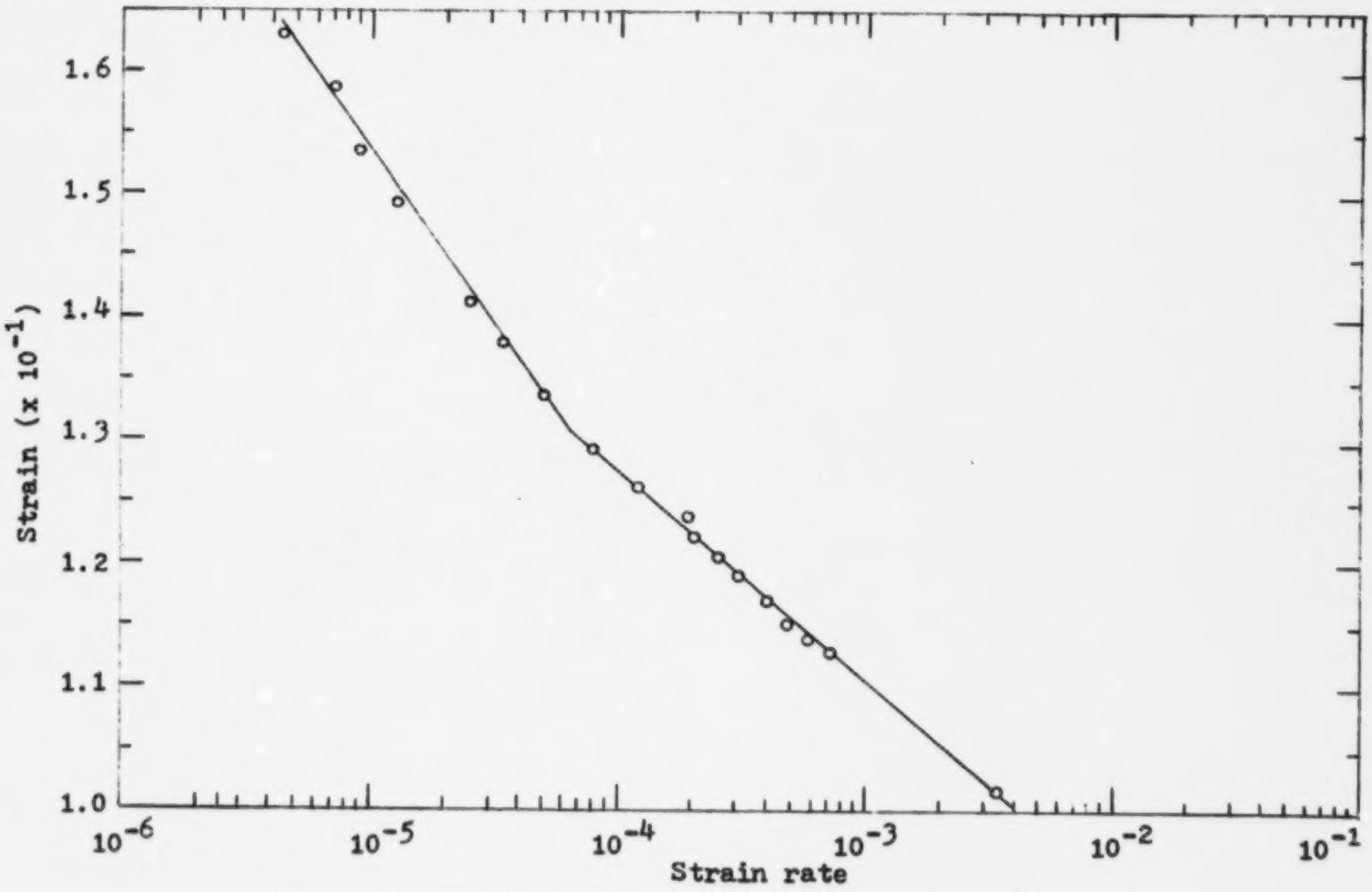

Fig. 7-2. Strain versus log strain rate of sample R3-4-1

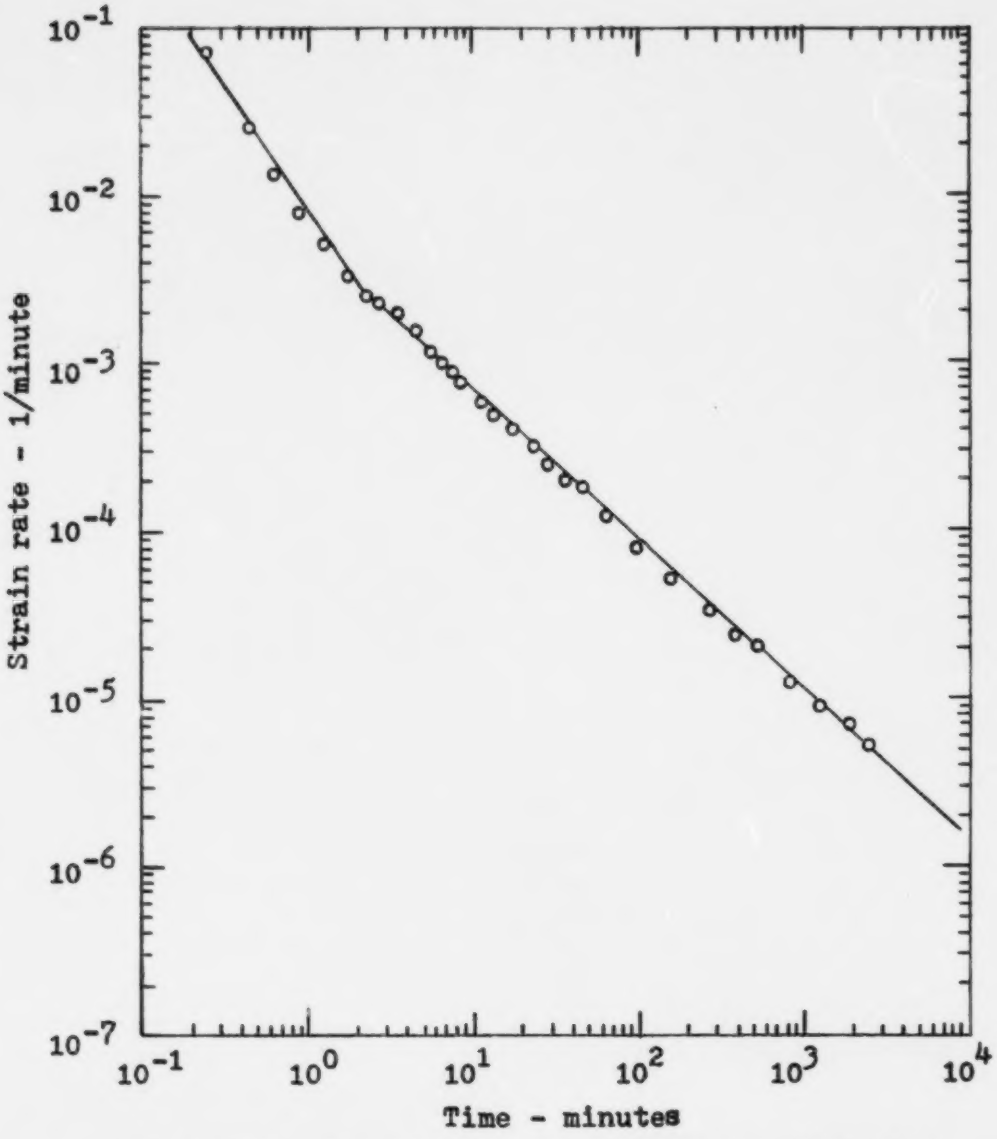

Fig. 7-3. Log strain rate versus log time plot of sample R3-4-1

in Chapter V. As explained earlier, the initial void ratio e_o can be conceptually divided for convenience of computation into two parts, e_{to} and e_{bo}, which are associated with the primary and secondary (creep) consolidation processes, respectively. The final void rate e_f is similarly divided. The pore pressure measurement during the test indicated that for this particular sample the excess pore pressure approached approximately zero at time equal to about one minute, corresponding to a void ratio of 2.045. It is very probable that some portion of the secondary compression had already been completed during the primary stage of consolidation. Thus the void ratio 2.045 actually represents the sum of e_{tf} and e_b where e_b is the void ratio associated with the secondary consolidation at t = 1 minute. One then has to calculate the sum of e_{tf} and e_{bo} so as to obtain the quantity $e_{bo}-e_{bf}$. In order to obtain $e_{tf}+e_{bo}$, the following procedure is adopted.

The portion of the time-compression curve (Fig. 7-1) after t = 1 minute is completely in the secondary compression stage. In addition to the point at t = 1 minute, four approximately equally spaced points are taken from the secondary compression tail. These are:

t = 7 min., void ratio = 2.002
t = 40 min., void ratio = 1.961
t = 216 min., void ratio = 1.917
t = 2900 min., void ratio = 1.820

The theoretical basic creep curves are shown in plots of degree of settlement versus time factor, which are defined respectively as:

$$\text{degree of settlement (DS)} = \frac{e_{bo}-e_b}{e_{bo}-e_{bf}} \qquad (7\text{-}2)$$

and $$\text{time factor } (T_s) = \frac{A_o p_o (1+e_o)t}{e_{bo}-e_{bf}} \qquad (7\text{-}3)$$

A close examination of these plots reveals that the final strains are reached at essentially the same time factor value, about unity, that is

$$T_s = \frac{A_o p_o (1+e_o)t}{e_{bo}-e_{bf}} = 1. \qquad (7\text{-}4)$$

Substituting t_f= 300 years into Equation 7-4, one can calaulate A_o from the following equation:

$$A_o = \frac{e_{bo}-e_{bf}}{300 p_o (1+e_o)} . \qquad (7\text{-}5)$$

The value of time factor, T_s, corresponding to the actual time of one minute then can be calculated as:

$$T_{s(1min)} = \frac{e_{bo}-e_{bf}}{300 p_o (1+e_o)} \times \frac{p_o (1+e_o)\ 1}{(e_{bo}-e_{bf})\ 525600} = 6.34\times10^{-9}.$$

If one converts the actual time to values of the time factor, following the above procedure, these four points become:

$T_s = 4.44 \times 10^{-8}$, void ratio = 2.002

$T_s = 2.54 \times 10^{-7}$, void ratio = 1.961

$T_s = 1.37 \times 10^{-6}$, void ratio = 1.917

$T_s = 1.84 \times 10^{-5}$, void ratio = 1.820

For instance, consider the fit of these points to the $p_f/p_o=4$ basic creep curve shown in Fig. D-34 of Chapter V; in which $B_o=16$, $(A_f/A_o) \times (P_f/P_o)^{1.0}= 1$, and $(B_f/B_o) \times (P_f/P_o)^{0.5} = 1$. The degree of settlement (DS) corresponding to $T_s= 6.34\times10^{-9}$ (or t = 1 minute) equals 0.0505. Let $EX = e_{tf}+e_{bo}$; then EX should satisfy the following relation:

$$\frac{EX-2.045}{EX-1.402} = 0.0505 \ . \tag{7-6}$$

Thus EX is found to be 2.079. The degree of settlement for these four points then can be calculated from Equation 7-2. The results are shown as follows:

$T_s = 4.44 \times 10^{-8}$, DS = 0.11351

$T_s = 2.54 \times 10^{-7}$, DS = 0.17382

$T_s = 1.37 \times 10^{-6}$, DS = 0.23992

$T_s = 1.84 \times 10^{-5}$, DS = 0.38251

These points are plotted against the curves of Fig D-34 to see how well they fit the corresponding basic creep line. Similar calculations are performed for 33 other possible cases using the computer and the results are shown in Table 7-1. The closest agreement between the experimental creep line and the theoretical curves is obtained for the case of $B_o= 18$, $(A_f/A_o) \times (P_f/P_o) = 1$, $(B_f/B_o) \times (P_f/P_o) = 1$, and

TABLE 7-1

CURVE-FITTING DATA FOR SAMPLE R3-4-1

```
DNI=    .50    BO= 10.0     DS=     0.00000     EX=     2.04500
T=      4.44000E-08     DS=     .06687
T=      2.54000E-07     DS=     .13064
T=      1.37000E-06     DS=     .19907
T=      1.84000E-05     DS=     .34992

DNI=    .50    BO= 11.0     DS=     0.00000     EX=     2.04500
T=      4.44000E-08     DS=     .06687
T=      2.54000E-07     DS=     .13064
T=      1.37000E-06     DS=     .19907
T=      1.84000E-05     DS=     .34992

DNI=    .50    BO= 12.0     DS=     0.00000     EX=     2.04500
T=      4.44000E-08     DS=     .06687
T=      2.54000E-07     DS=     .13064
T=      1.37000E-06     DS=     .19907
T=      1.84000E-05     DS=     .34992

DNI=    .50    BO= 13.0     DS=     0.00000     EX=     2.04500
T=      4.44000E-08     DS=     .06687
T=      2.54000E-07     DS=     .13064
T=      1.37000E-06     DS=     .19907
T=      1.84000E-05     DS=     .34992

DNI=    .50    BO= 14.0     DS=      .01050     EX=     2.05182
T=      4.44000E-08     DS=     .07667
T=      2.54000E-07     DS=     .13977
T=      1.37000E-06     DS=     .20748
T=      1.84000E-05     DS=     .35675

DNI=    .50    BO= 15.0     DS=      .02320     EX=     2.06027
T=      4.44000E-08     DS=     .08852
T=      2.54000E-07     DS=     .15081
T=      1.37000E-06     DS=     .21765
T=      1.84000E-05     DS=     .36530

DNI=    .50    BO= 16.0     DS=      .05050     EX=     2.07920
T=      4.44000E-08     DS=     .11400
T=      2.54000E-07     DS=     .17454
T=      1.37000E-06     DS=     .23951
T=      1.84000E-05     DS=     .38275
```

TABLE 7-1 (CONTINUE)

CURVE-FITTING DATA FOR SAMPLE R3-4-1

```
DNI=   .50    BO= 17.0    DS=     .08420    EX=    2.10412
T=     4.44000E-08      DS=     .14544
T=     2.54000E-07      DS=     .20384
T=     1.37000E-06      DS=     .26651
T=     1.84000E-05      DS=     .40466

DNI=   .50    BO= 18.0    DS=     .12420    EX=    2.13619
T=     4.44000E-08      DS=     .18277
T=     2.54000E-07      DS=     .23861
T=     1.37000E-06      DS=     .29854
T=     1.84000E-05      DS=     .43066

DNI=   .50    BO= 19.0    DS=     .16420    EX=    2.17132
T=     4.44000E-08      DS=     .22009
T=     2.54000E-07      DS=     .27339
T=     1.37000E-06      DS=     .33058
T=     1.84000E-05      DS=     .45667

DNI=   .50    BO= 20.0    DS=     .20000    EX=    2.20575
T=     4.44000E-08      DS=     .25350
T=     2.54000E-07      DS=     .30451
T=     1.37000E-06      DS=     .35925
T=     1.84000E-05      DS=     .47994

DNI=  1.00    BO= 10.0    DS=    0.00000    EX=    2.04500
T=     4.44000E-08      DS=     .06687
T=     2.54000E-07      DS=     .13064
T=     1.37000E-06      DS=     .19907
T=     1.84000E-05      DS=     .34992

DNI=  1.00    BO= 11.0    DS=    0.00000    EX=    2.04500
T=     4.44000E-08      DS=     .06687
T=     2.54000E-07      DS=     .13064
T=     1.37000E-06      DS=     .19907
T=     1.84000E-05      DS=     .34992

DNI=  1.00    BO= 12.0    DS=    0.00000    EX=    2.04500
T=     4.44000E-08      DS=     .06687
T=     2.54000E-07      DS=     .13064
T=     1.37000E-06      DS=     .19907
T=     1.84000E-05      DS=     .34992
```

TABLE 7-1 (CONTINUE)

CURVE-FITTING DATA FOR SAMPLE R3-4-1

```
DNI= 1.00    BO= 13.0    DS=    0.00000    EX=    2.04500
T=      4.44000E-08     DS=    .06687
T=      2.54000E-07     DS=    .13064
T=      1.37000E-06     DS=    .19907
T=      1.84000E-05     DS=    .34992

DNI= 1.00    BO= 14.0    DS=     .00950    EX=    2.05117
T=      4.44000E-08     DS=    .07574
T=      2.54000E-07     DS=    .13890
T=      1.37000E-06     DS=    .20668
T=      1.84000E-05     DS=    .35610

DNI= 1.00    BO= 15.0    DS=     .02110    EX=    2.05886
T=      4.44000E-08     DS=    .08655
T=      2.54000E-07     DS=    .14898
T=      1.37000E-06     DS=    .21597
T=      1.84000E-05     DS=    .36364

DNI= 1.00    BO= 16.0    DS=     .04210    EX=    2.07326
T=      4.44000E-08     DS=    .10616
T=      2.54000E-07     DS=    .16724
T=      1.37000E-06     DS=    .23279
T=      1.84000E-05     DS=    .37729

DNI= 1.00    BO= 17.0    DS=     .06630    EX=    2.09066
T=      4.44000E-08     DS=    .12874
T=      2.54000E-07     DS=    .18828
T=      1.37000E-06     DS=    .25217
T=      1.84000E-05     DS=    .39302

DNI= 1.00    BO= 18.0    DS=     .09370    EX=    2.11148
T=      4.44000E-08     DS=    .15431
T=      2.54000E-07     DS=    .21210
T=      1.37000E-06     DS=    .27411
T=      1.84000E-05     DS=    .41083

DNI= 1.00    BO= 19.0    DS=     .11580    EX=    2.12921
T=      4.44000E-08     DS=    .17493
T=      2.54000E-07     DS=    .23131
T=      1.37000E-06     DS=    .29181
T=      1.84000E-05     DS=    .42520
```

TABLE 7-1 (CONTINUE)

CURVE-FITTING DATA FOR SAMPLE R3-4-1

```
DNI= 1.00    BO= 20.0    DS=     .14210    EX=    2.15150
T=     4.44000E-08     DS=     .19947
T=     2.54000E-07     DS=     .25417
T=     1.37000E-06     DS=     .31258
T=     1.84000E-05     DS=     .44230

DNI= 2.00    BO= 10.0    DS=    0.00000    EX=    2.04500
T=     4.44000E-08     DS=     .06687
T=     2.54000E-07     DS=     .13064
T=     1.37000E-06     DS=     .19907
T=     1.84000E-05     DS=     .34992

DNI= 2.00    BO= 11.0    DS=    0.00000    EX=    2.04500
T=     4.44000E-08     DS=     .06687
T=     2.54000E-07     DS=     .13064
T=     1.37000E-06     DS=     .19907
T=     1.84000E-05     DS=     .34992

DNI= 2.00    BO= 12.0    DS=    0.00000    EX=    2.04500
T=     4.44000E-08     DS=     .06687
T=     2.54000E-07     DS=     .13064
T=     1.37000E-06     DS=     .19907
T=     1.84000E-05     DS=     .34992

DNI= 2.00    BO= 13.0    DS=    0.00000    EX=    2.04500
T=     4.44000E-08     DS=     .06687
T=     2.54000E-07     DS=     .13064
T=     1.37000E-06     DS=     .19907
T=     1.84000E-05     DS=     .34992

DNI= 2.00    BO= 14.0    DS=     .01530    EX=    2.05499
T=     4.44000E-08     DS=     .08115
T=     2.54000E-07     DS=     .14394
T=     1.37000E-06     DS=     .21132
T=     1.84000E-05     DS=     .35987

DNI= 2.00    BO= 15.0    DS=     .02000    EX=    2.05812
T=     4.44000E-08     DS=     .08554
T=     2.54000E-07     DS=     .14802
T=     1.37000E-06     DS=     .21509
T=     1.84000E-05     DS=     .36292
```

```
                         TABLE 7-1 (CONTINUE)

                 CURVE-FITTING DATA FOR SAMPLE  R3-4-1

DNI= 2.00     BO= 16.0    DS=      .03160    EX=     2.06598
T=        4.44000E-08    DS=     .09636
T=        2.54000E-07    DS=     .15811
T=        1.37000E-06    DS=     .22438
T=        1.84000E-05    DS=     .37046

DNI= 2.00     BO= 17.0    DS=      .04740    EX=     2.07699
T=        4.44000E-08    DS=     .11110
T=        2.54000E-07    DS=     .17185
T=        1.37000E-06    DS=     .23703
T=        1.84000E-05    DS=     .38074

DNI= 2.00     BO= 18.0    DS=      .05260    EX=     2.08070
T=        4.44000E-08    DS=     .11596
T=        2.54000E-07    DS=     .17637
T=        1.37000E-06    DS=     .24120
T=        1.84000E-05    DS=     .38412

DNI= 2.00     BO= 19.0    DS=      .08210    EX=     2.10251
T=        4.44000E-08    DS=     .14348
T=        2.54000E-07    DS=     .20201
T=        1.37000E-06    DS=     .26482
T=        1.84000E-05    DS=     .40329

DNI= 2.00     BO= 20.0    DS=      .10530    EX=     2.12068
T=        4.44000E-08    DS=     .16513
T=        2.54000E-07    DS=     .22219
T=        1.37000E-06    DS=     .28341
T=        1.84000E-05    DS=     .41839
```

$EX = 2.111$.

(3) Subtracting $e_f = e_{tf} + e_{bf} = 1.402$ from $EX = e_{tf} + e_{bo} = 2.111$, one has $e_{bo} - e_{bf} = 0.709$. By substituting this value, one obtains from Equation 7-5, the result A_o equals 4.861×10^{-6}. From the relations $(A_f/A_o) \times (P_f/P_o) = 1$, $(B_f/B_o) \times (P_f/P_o) = 1$, and $P_f/P_o = 4$, the values of A_f/A_o and B_f/B_o can be calculated and both are found to be equal to 0.25.

In order to obtain the theoretical solution, two more physical constants, i.e., a_{vo} and k_f/k_o have to be determined. As defined previously, a_{vo} is the initial value of the tangent to the basic equilibrium e - p curve and k_f/k_o is the ratio of the coefficients of permeability corresponding to e_f and e_o. In the previous derivation of the general consolidation equations, a widely accepted linear e-log p law is assumed to be applicable. From the definition of $a_{vo} = C_c/2.3p_o$, where $C_c = (e_o - e_f)/(\log p_f - \log p_o)$,

$$a_{vo} = \frac{2.377 - 1.402}{2.3 \times 1 \times \log 4} = 0.705$$

The value of k_f/k_o can be obtained from an experimental coefficient of permeability versus void ratio relation such as that shown in Chapter II. Unfortunately, permeability test data on aged refuse samples are presently not available. For mathematical simplicity a linear e-log k relationship on a semilog plot shown in Fig. 7-4 is assumed to be applicable to the range of strains encountered in this study. This relationship was obtained by curve-fitting the theoretical pore pressure dissipation curve to the experimental one for sample R3-4-1. From Fig. 7-4, then, $k_f/k_o = 50/260 = 0.1923$. The standard procedure used in soil mechanics (Lambe, 1954) is adopted to determine the specific gravity and water content of milled refuse.

Theoretical solutions to the governing consolidation equations will be obtained by using physical parameters determined from the procedures described in this chapter. Analysis and comparison of the theoretical solutions and the laboratory test data will be given in the next chapter.

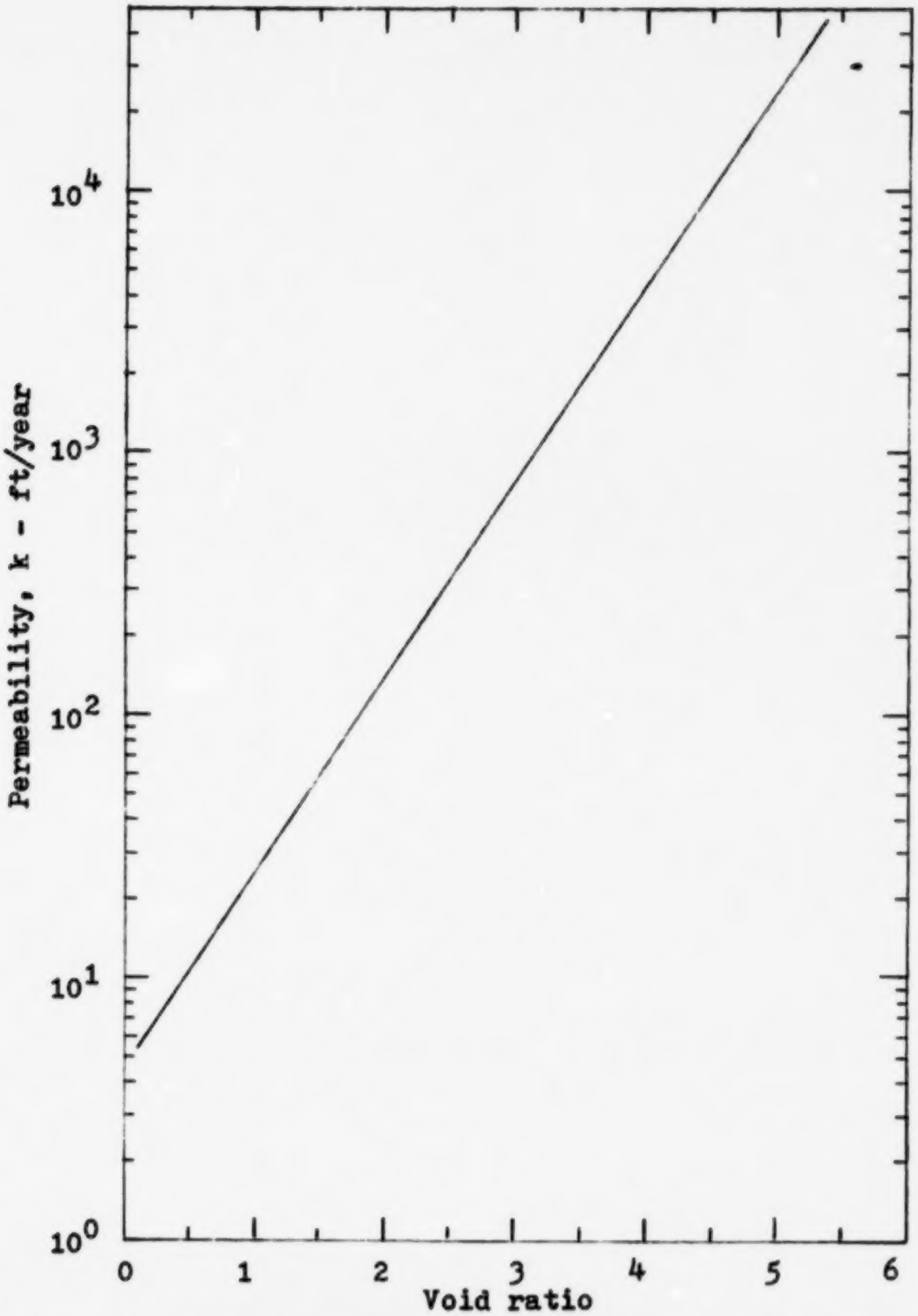

Fig. 7-4. Permeability versus void ratio used in the present study

EXPERIMENTAL RESULTS

Laboratory consolidation tests were conducted on both raw (freshly prepared) and laboratory aged milled refuse samples in order to assess the adequacy of the mathematical model. These experimental results will be presented and discussed in this chapter. The temperature data obtained from the laboratory aging of milled refuse samples, the determination of the rate constant for the decomposition of milled refuse, and various assumptions involved in this determination will also be discussed in this chapter. The numerical procedures for the solution of the two partial differential equations governing the consolidation process of milled refuse are given in Appendix A.

Experimental Program

Four raw and eleven laboratory aged milled refuse samples, with aging periods of from nine to twelve months, were tested in the consolidometer developed in this research project. The material tested, the experimental apparatus, and its associated test procedures have been fully described in Chapter VI. The thickness of samples varied from 2 inches to 4 inches. Because of the low specific gravity of milled refuse (about 1.7), the initial effective pressure in natural milled refuse landfills is usually very low. Therefore, relatively high ratios of the final effective pressure to the initial effective pressure (p_f/p_o), varying from two to sixteen, were used in the consolidation tests. The following convention is used in referring to tests: The type and thickness of sample will be given first, followed by the value of p_f/p_o, and finally by the number of the pressure increment. The letter R and A refer to raw and aged refuse sample respectively. Thus, R2-2-1 refers to a 2 in. thick raw refuse sample, with $p_f/p_o=2$, under the first pressure increment (i.e. from 1 psi to 2 psi).

Temperature Data From Laboratory Aged Milled Refuse Samples

Chemical and biological reactions of refuse decomposition are mostly exothermic. As the constituents decompose, heat, some of which is retained by the overlying refuse, is generated. This build-up of heat results in a temperature rise which leads to increases in chemical and biological activities. Temperature variations of refuse during decomposition can thus serve as an indication of the extent of the chemical and biological activity within the refuse. Field temperature data of experimental refuse cells have been collected by many investigators (Merz, 1968; Reinhardt, 1971). Fig. 8-1 shows a typical curve of the variation of the field temperature of the refuse cell versus time. In most cases, the temperature variations of the refuse cell are overshadowed by the seasonal variation of the air temperature.

In the present study, laboratory aging of milled refuse

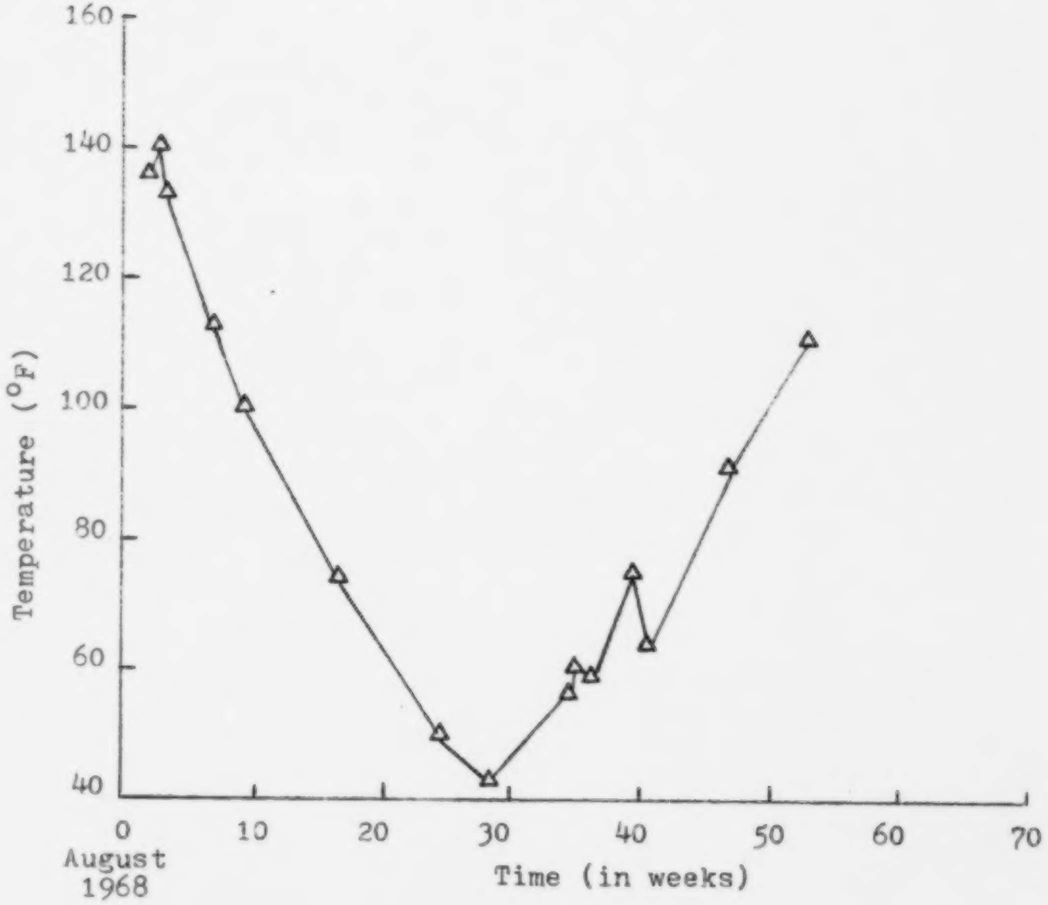

Fig. 8-1. Milled refuse cell temperature vs. time (Field data, Merz, 1968)

samples was conducted in an insulated box with temperature maintained at 125 F. The aging box and the aging process have been described in Chapter VI. It is believed that the temperature difference between the refuse sample and the aging box is of more significance than the absolute temperature to indicate the degree of the chemical and biological activities of the refuse. The variation of this temperature difference versus time for some of the collected laboratory temperature data thus are plotted in Figs. 8-2 to 8-5. All of the samples reached their peak temperature difference within 30 to 50 days after the start of the laboratory aging process. After this time, the temperature difference dropped off gradually, indicating that the decomposition of the refuse proceeded at gradually decreasing rate.

The Rate Constant Of Milled Refuse Decomposition

The kinetics of the milled refuse decomposition process is very complicated and has not received extensive attention. The rate of decomposition of refuse is dependent on the distribution and relative amount of different species of microorganisms involved, the amount and distribution of critical nutrients, the pretreatment of refuse, such as shredding and/or compaction, and environmental conditions. The actual rate is difficult to determine and has not been established. In order to obtain some information about rates of decomposition, a series of digestion tests of milled refuse have been conducted under anaerobic conditions and at very high

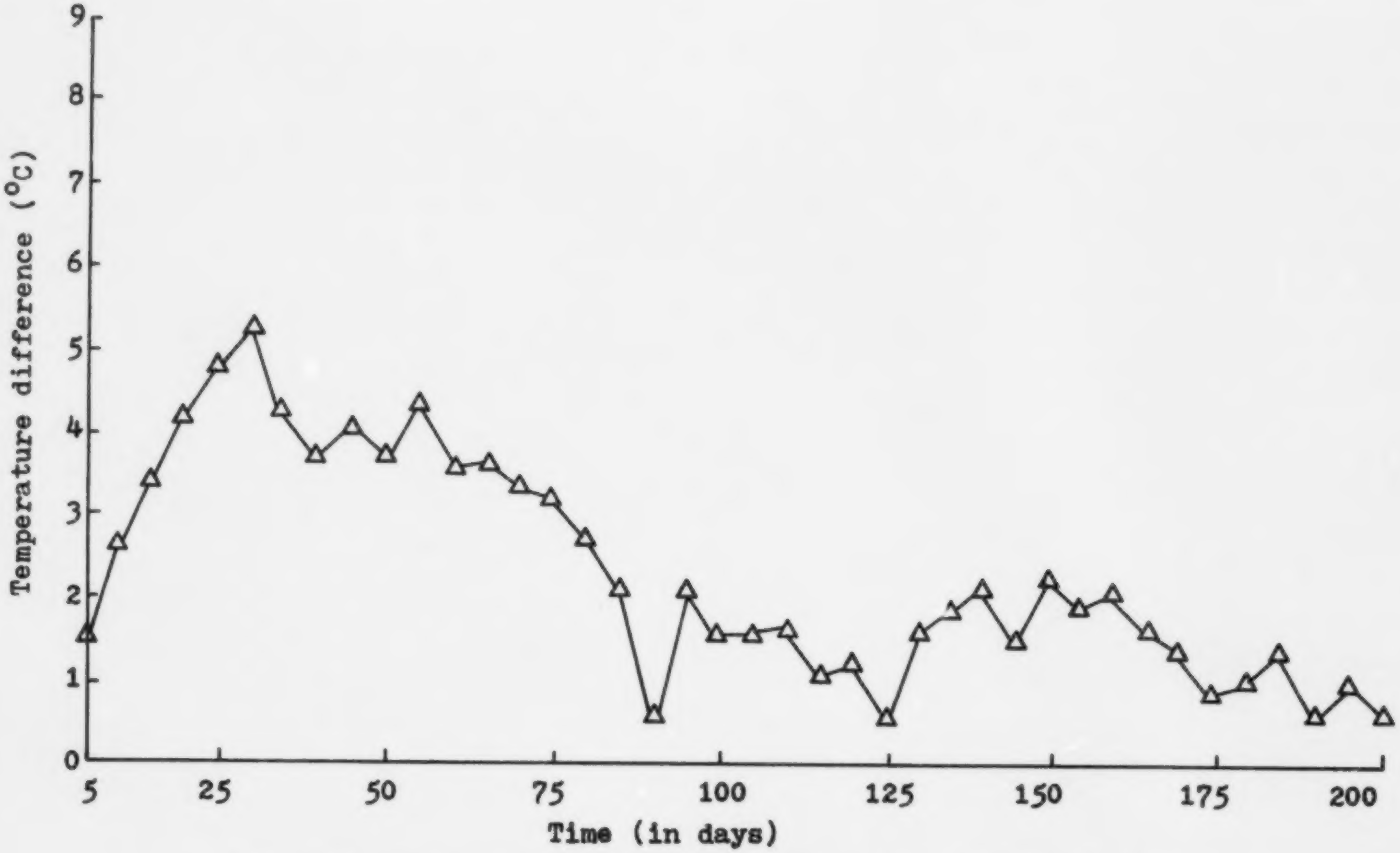

Fig. 8-2. Temperature difference vs. time for sample A2-2-1

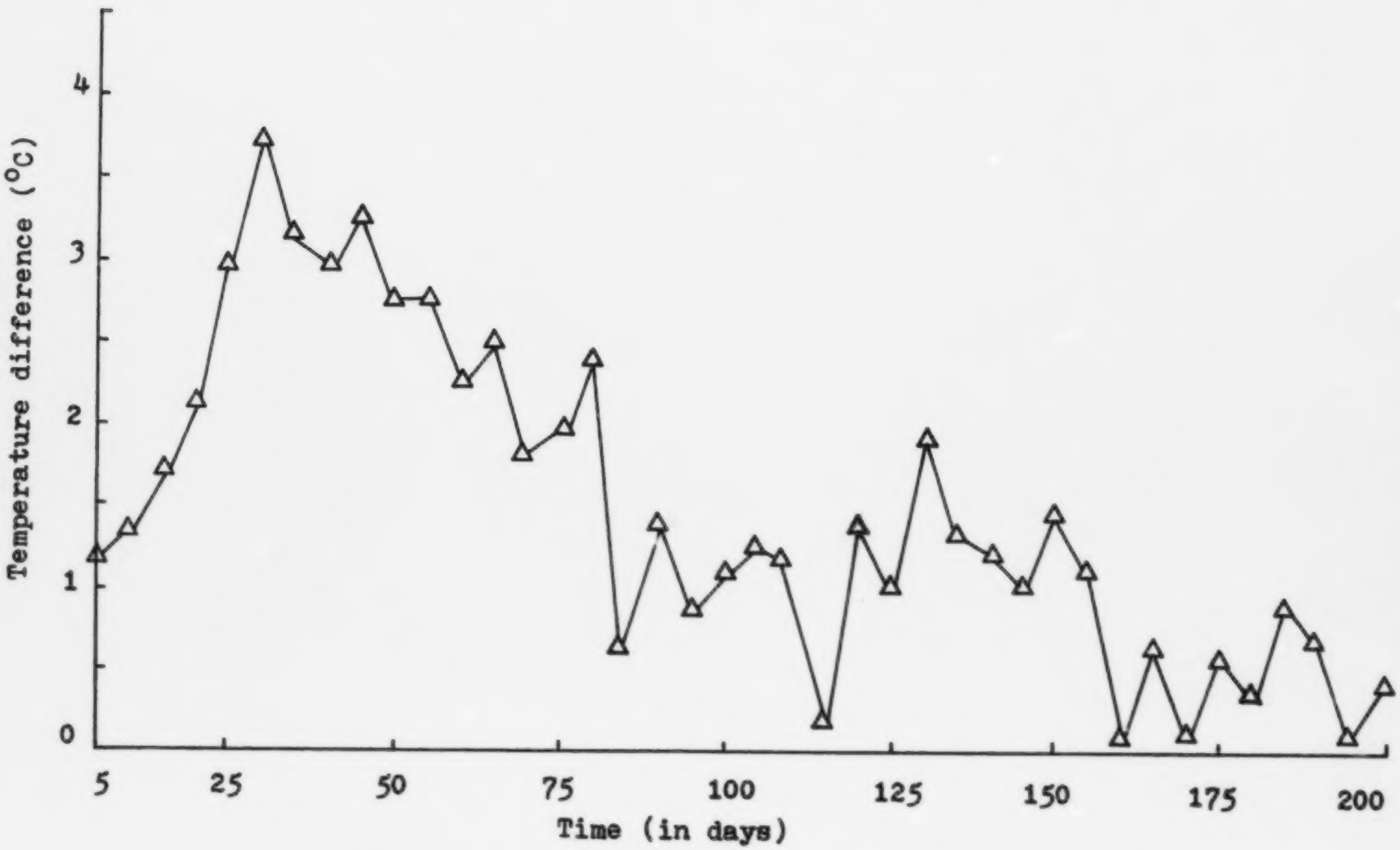

Fig. 8-3. Temperature difference vs. time for sample A3-2-1

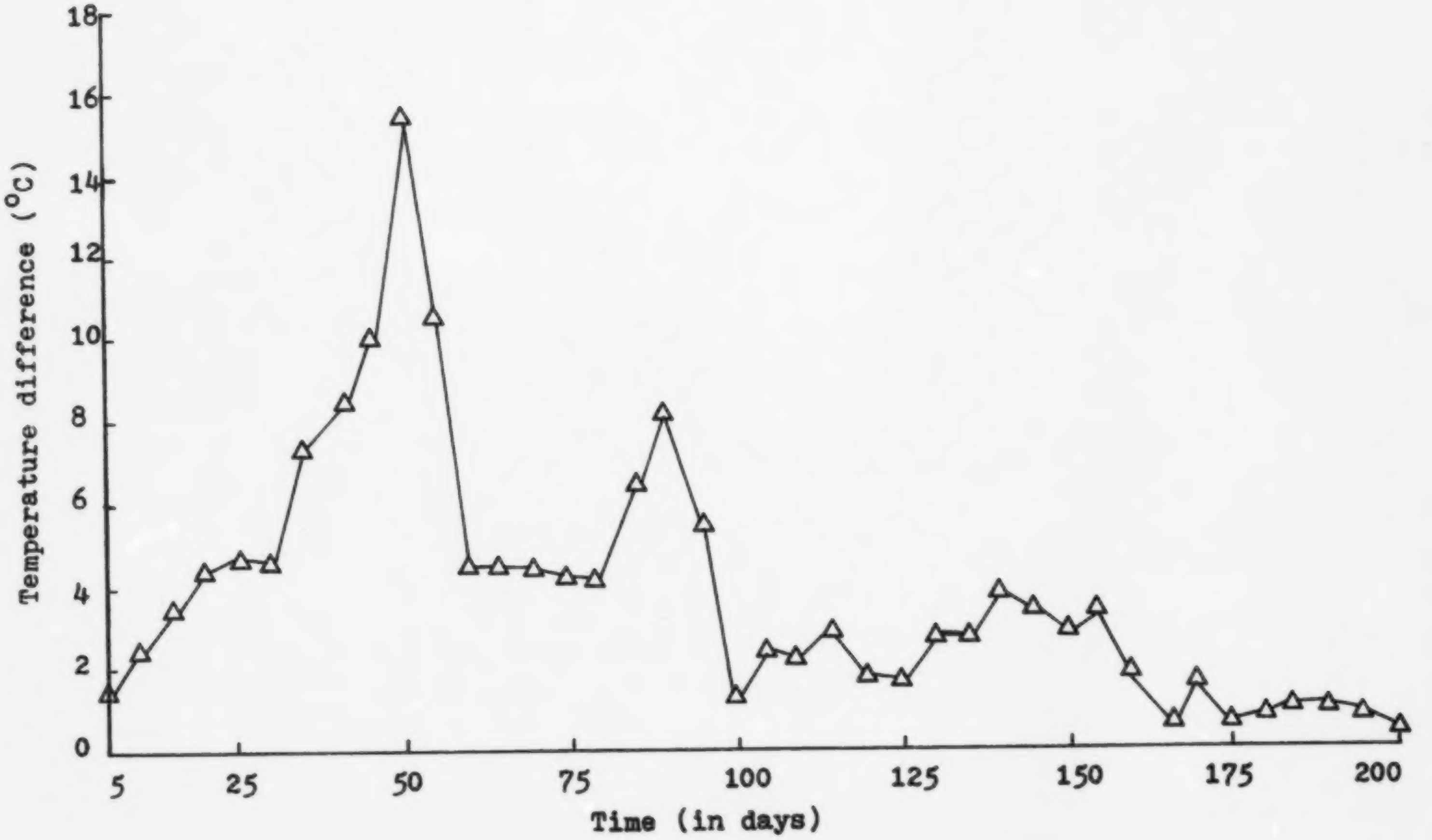

Fig. 8-4. Temperature difference vs. time for sample A3-4-1

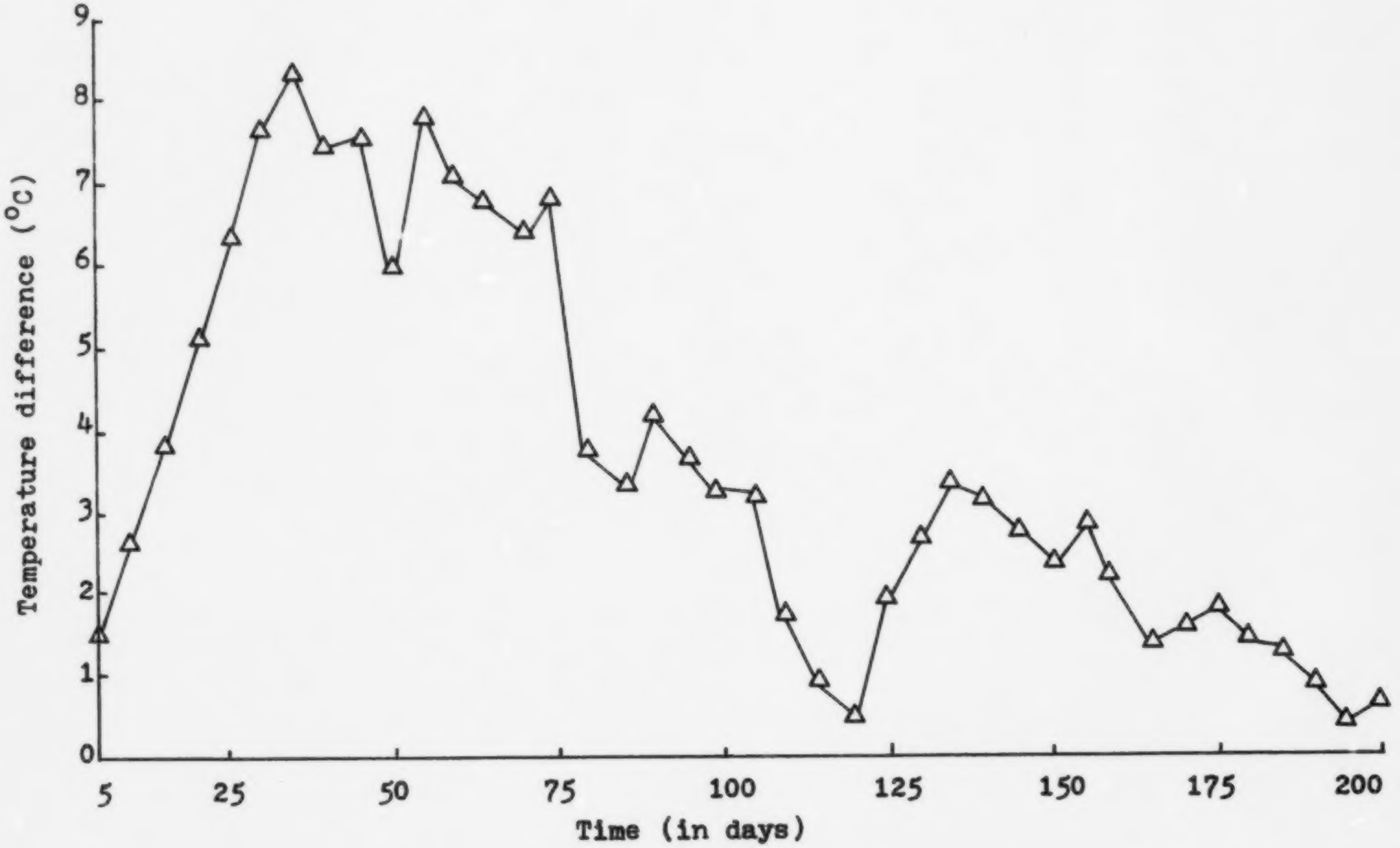

Fig. 8-5. Temperature difference vs. time for sample A4-2-1

moisture contents. These experimental data as well as information obtained from the literature have been studied and analyzed by Chakraverty (1973). Rates of decomposition of cellulose and cellulosic materials have been calculated for different digestion processes and are summarized in Table 8-1.

Although the exact rate of decomposition of milled refuse is not known, it is unlikely that it is constant. Chakraverty (1973) assumes a logarithmic decay relationship (Equation 4-17) to describe the process of milled refuse decomposition. The same relationship will also be assumed herein. The calculated rate constants have been normalized to 37 C according to the following relation (Fair, 1968):

$$\frac{C}{C_o} = \exp\left(\frac{E}{R}\,\frac{T-T_o}{TT_o}\right) \qquad (8\text{-}1)$$

where C = Rate constant at T^o K;

C_o = Rate constant at T_o^o K;

E = Activation energy in cal./gm.-mole-^{o}K (4900 between 20 C and 37 C, and 3000 between 37 C and 55 C);

R = Gas constant = 1.99 cal./gm.-mole-^{o}K

In the above calculation, the rate of decomposition is assumed to be constant with depth. The rate constants for carbon reduction listed in Table 8-1 are calculated under the assumption that carbon reduction is due to the loss by

Table 8-1. Rate constant for digestion of cellulose and cellulosic materials (After Chakraverty, 1973)

Process	Culture	References	Temp.	Rate Constant, day^{-1} at 37° C, for reduction of		
				Volatile solids	Cellulose	Carbon
Stirred-Continuous Digesters, Anaerobic	Mixed Sewage sludge	Chan, 1972 Golueke, 1971	37	0.007 to 0.014		
Batch-Digesters Anaerobic	Mixed, Rumen fluid	Stranks, 1956	40		0.59	
	Pure strain	McBee, 1948	55		0.875 to 1.012	
	Mixed, Rice soil	Acharya, 1935	35 to 40		0.0094	0.0005
	Mixed, varied	Zimmerman, 1972	20 to 55	0.00105 to 0.00216		0.0006 to 0.0017
Activated Sludge Aerobic	Mixed	Polkowski, 1962	20		1.475 to 1.967	
Compositing Aerobic	Mixed	Schulze, 1960	26 to 63	0.065		
Sanitary Landfill	Mixed	SWQCB, Calif. 1965	16 to 37			3.3×10^{-5}

gasification only. Some carbon reduction may also occur due to the loss of intermediate products such as volatile acids and/or alcohols; however, it has been assumed that such losses are negligible. Thus, the carbon reduction rates represent the rate constants for the complete decomposition of cellulosic materials. The rate constants for volatile solids reduction and cellulose reduction shown in Table 8-1 are of a similar magnitude because in all the digestion tests the material digested consisted of approximately 70% cellulose on a dry weight basis. Therefore, these constants are the rate constants for cellulose hydrolysis, which is the first stage decomposition of cellulose.

As mentioned in Chapter II, in the first stage of anaerobic decomposition, cellulose is hydrolyzed enzymatically to glucose and then to volatile fatty acids and alcohols by a certain group of cellulolytic bacteria. In the second stage of decomposition, the volatile fatty acids and alcohols are broken down to methane and carbon dioxide by a group of strictly anaerobic bacteria which are generally known as the "methane formers". The settlement behavior of milled refuse involves the rearrangement of the solids and expulsion of macropore and/or micropore fluids from the mass. Intermediate products of refuse decomposition such as volatile fatty acids and alcohols can be squeezed out of the mass during the consolidation process. It is, therefore, appropriate to adopt rate constants of the first stage of cellulose decomposition such as volatile solids reduction or cellulose reduction rate constants in the time-settlement model of milled refuse. The rate constant used in this study is .01497 /year.

Test Results

A total of 23 consolidation tests were conducted on raw and laboratory aged refuse samples. A typical e versus log t plot obtained from the consolidation test (sample A3-8-1) is shown in Fig. 8-6. The rheological parameters for the samples tested can be obtained by applying the procedures outlined in Chapter VII; the results are summarized in Table 8-2. The theoretical predictions for the model behavior were then obtained by using these parameters as input data for the computer program COMBINE which solves the two governing nonlinear consolidation equations. For the detailed input data used for each sample, the reader is referred to Appendix C (Chen). The pore pressure at the base of the sample was measured in some tests to provide an independent check on the adequacy of model and a check on the determination of the end of the primary consolidation.

The experimental and theoretical void ratio versus log time curves for raw refuse samples with different values of p_f/p_o are shown in Figs. 8-7 to 8-12. Similar curves for 2 in., 3 in., and 4 in. laboratory aged refuse samples are shown in Figs. 8-13 to 8-18, Figs. 8-19 to 8-24, and Figs. 8-25 to 8-29 respectively. A close examination of these curves indicates that good agreement between theoretical predictions and experimental results for time greater than 10 minutes is

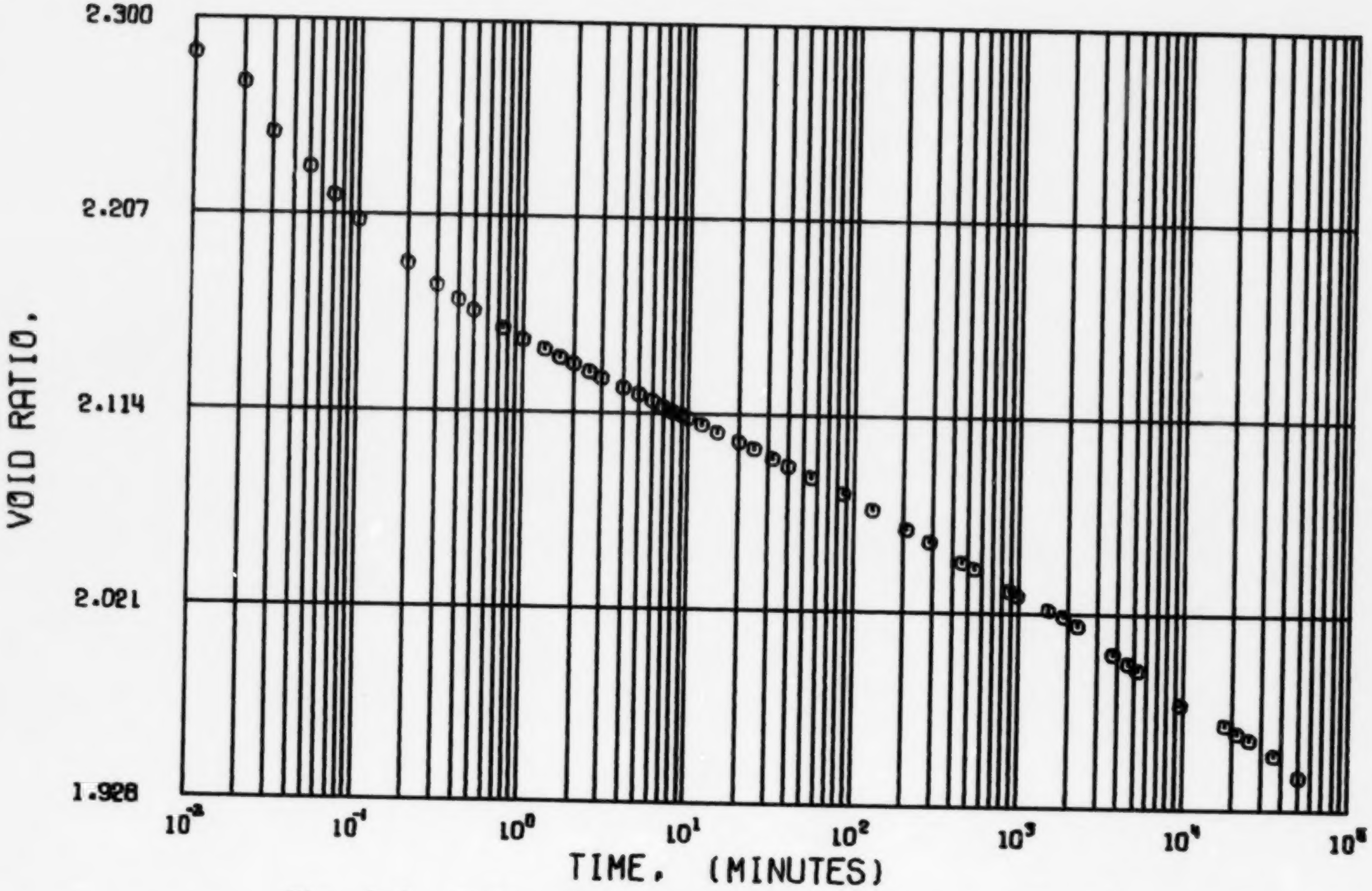

Fig. 8-6. Void ratio vs. log time plot for sample A3-8-1

Table 8-2

Values of rheological parameters

Sample	e_o	H_o(ft)	A_o(ft^2/lb-yr)	B_o	$\frac{e_{bo} - e_{bf}}{e_o - e_f}$	A_f/A_o	B_f/B_o	k_f/k_o	Period of lab. aging (days)
A2-2-1	2.585	.142	1.577×10^{-6}	15.0	.739	.500	.250	.566	275
A2-2-2	2.433	.136	8.433×10^{-7}	16.0	.715	.500	.500	.550	275
A2-4-1	2.498	.140	2.130×10^{-6}	13.0	.633	.250	.250	.450	310
A2-4-2	2.228	.129	5.994×10^{-7}	15.0	.462	.250	.500	.286	310
A2-8-1	2.495	.138	2.771×10^{-6}	12.0	.470	.125	.354	.212	326
A2-16-1	2.035	.129	3.292×10^{-6}	15.0	.389	.063	.250	.150	370
A3-2-1	2.543	.216	1.758×10^{-6}	15.0	.859	.500	.250	.578	286
A3-2-2	2.437	.208	8.509×10^{-7}	14.0	.893	.500	.250	.610	286
A3-4-1	2.808	.230	1.021×10^{-6}	16.0	.442	.250	.500	.518	316
A3-4-2	2.521	.213	6.036×10^{-7}	20.0	.475	.250	.500	.265	316
A3-8-1	2.533	.216	2.525×10^{-6}	15.0	.506	.125	.354	.276	331
A3-16-1	2.668	.223	2.710×10^{-6}	15.0	.316	.063	.250	.107	374

Table 8-2 (continued)

Values of rheological parameters

Sample	e_o	H_o(ft)	A_o(ft^2/lb-yr)	B_o	$\frac{e_{bo} - e_{bf}}{e_o - e_f}$	A_f/A_o	B_f/B_o	k_f/k_o	Period of lab. aging (days)
A4-2-1	2.799	.305	1.431×10^{-6}	15.0	.636	.500	.707	.222	300
A4-2-2	2.585	.289	6.481×10^{-7}	20.0	.796	.500	.500	.645	300
A4-4-1	2.652	.292	1.672×10^{-6}	15.0	.564	.250	.250	.452	321
A4-4-2	2.374	.270	8.219×10^{-6}	16.0	.585	.250	.250	.242	321
A4-8-1	2.241	.263	4.469×10^{-6}	20.0	.630	.125	.125	.181	366
R3-2-1	2.511	.224	2.437×10^{-6}	15.0	.800	.500	.250	.250	---
R3-2-2	2.340	.213	1.961×10^{-6}	15.0	.814	.500	.250	.296	---
R3-4-1	2.377	.216	4.861×10^{-6}	18.0	.727	.250	.250	.192	---
R3-4-2	1.820	.180	1.463×10^{-6}	18.0	.682	.250	.250	.165	---
R3-8-1	2.435	.219	4.725×10^{-6}	16.0	.608	.125	.354	.141	---
R3-16-1	2.485	.223	4.812×10^{-6}	16.0	.492	.063	.250	.078	---

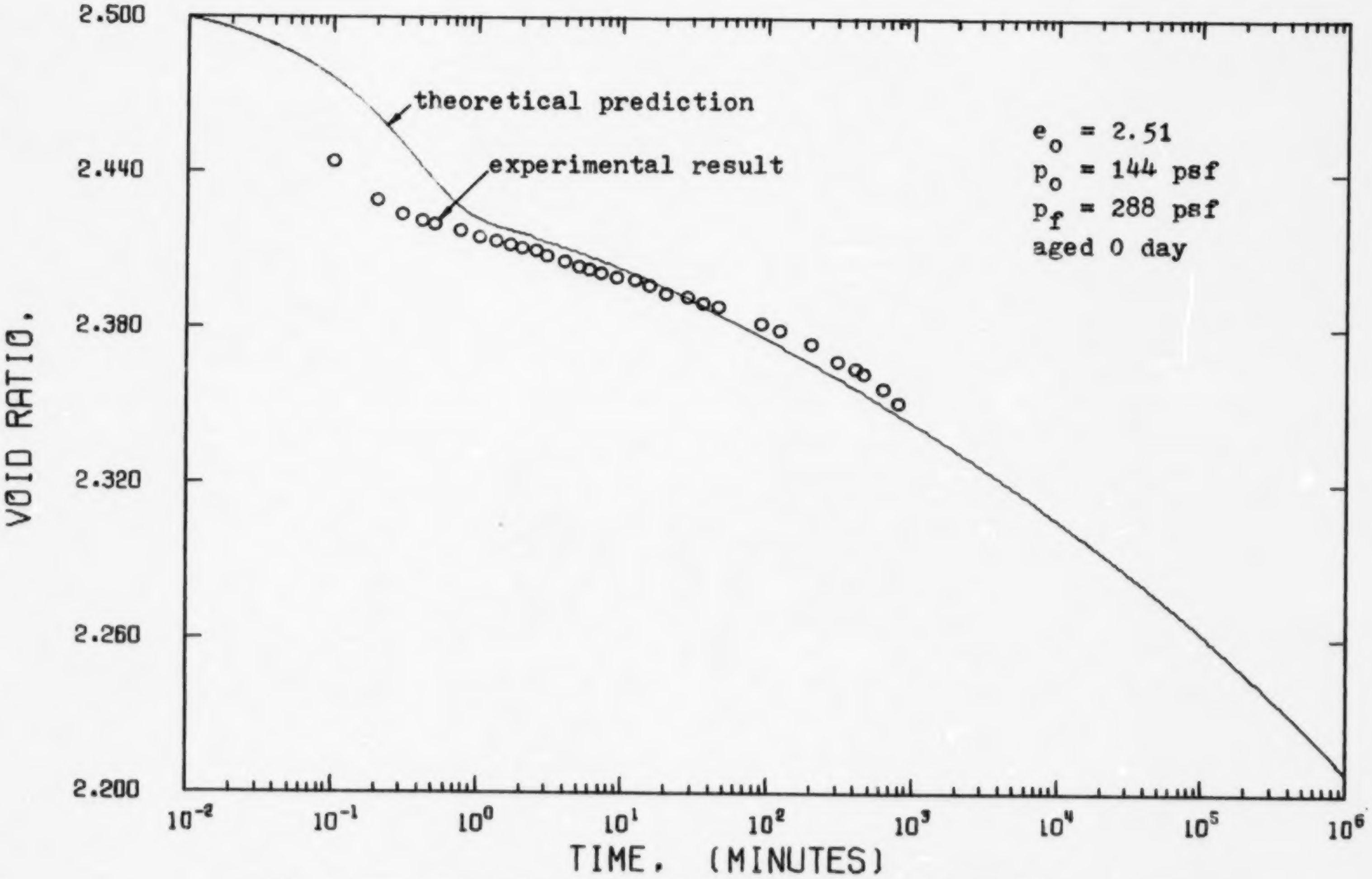

Fig. 8-7. Experimental and theoretical void ratio vs. log time curve for sample R3-2-1

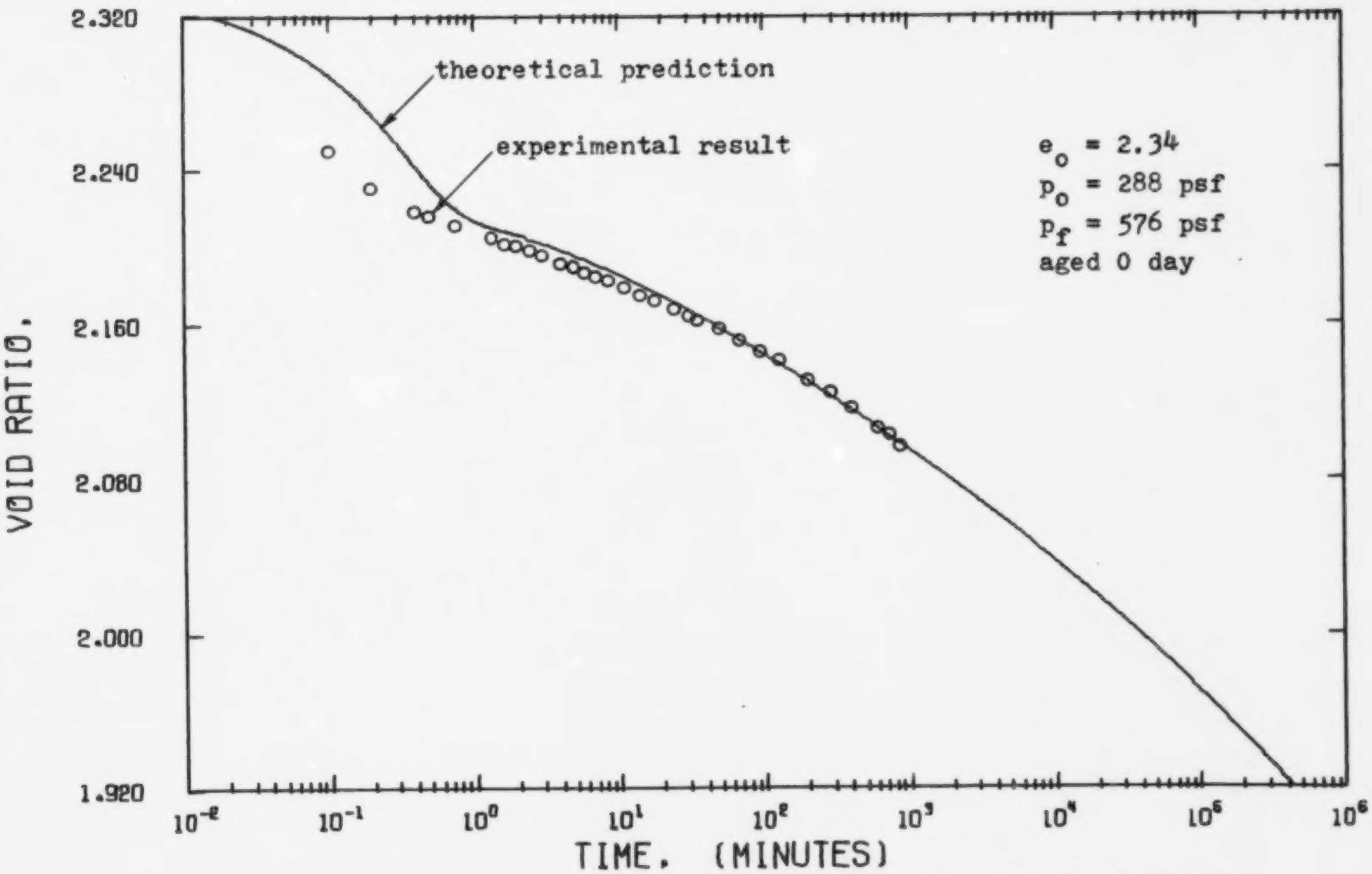

Fig. 8-8. Experimental and theoretical void ratio vs. log time curve for sample R3-2-2

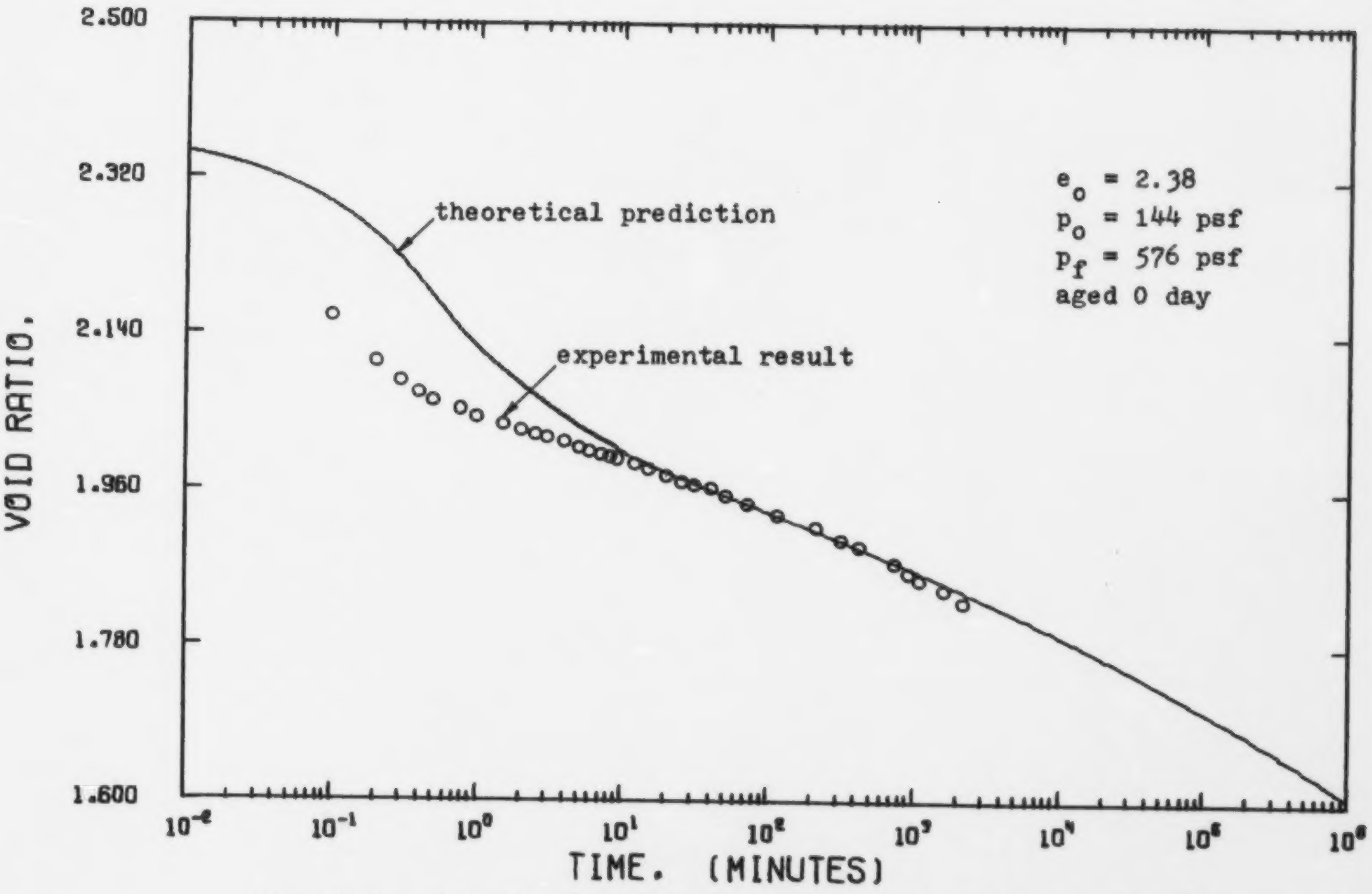

Fig. 8-9. Experimental and theoretical void ratio vs. log time curve for sample R3-4-1

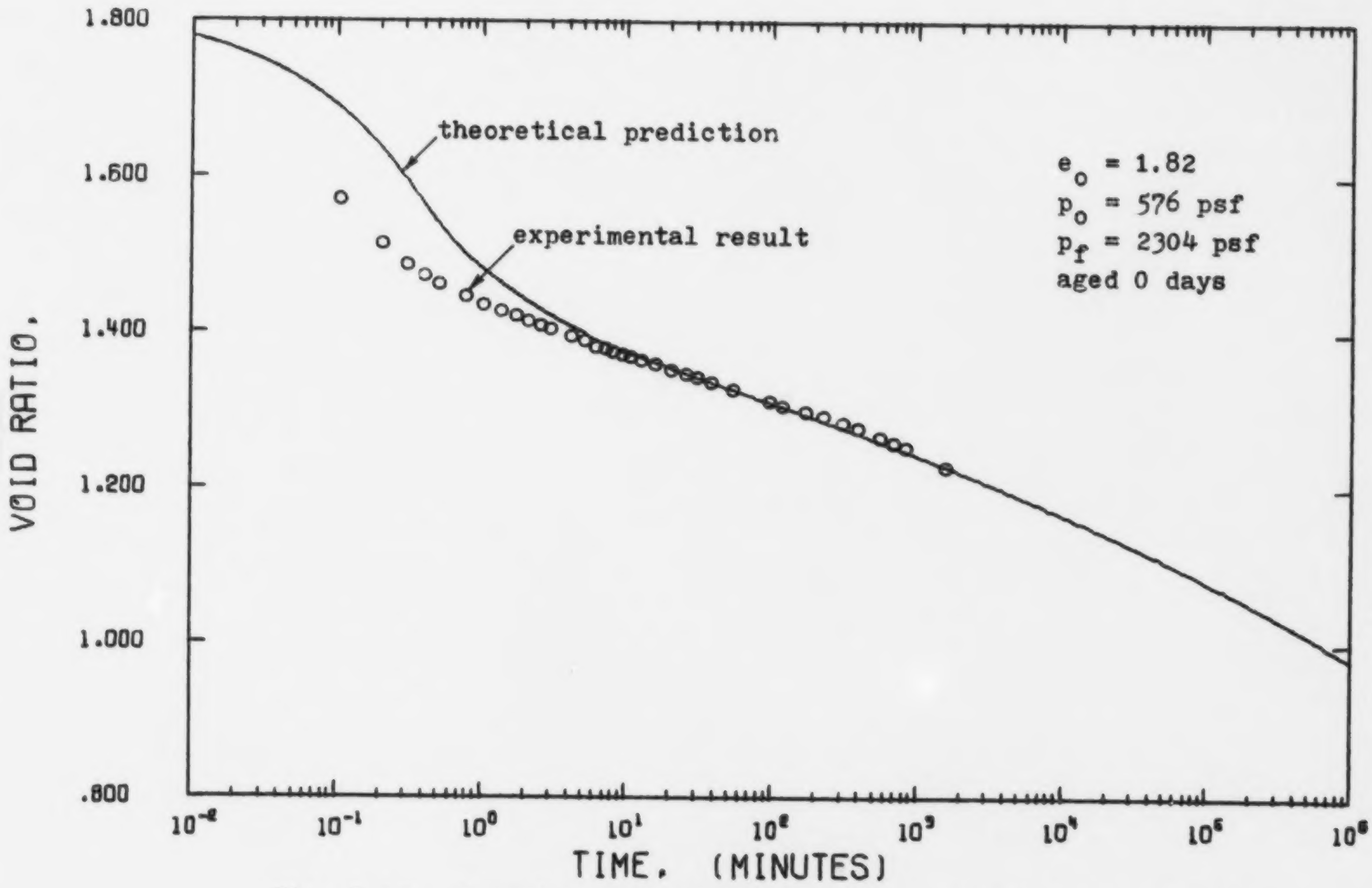

Fig. 8-10. Experimental and theoretical void ratio vs. log time curve for sample R3-4-2

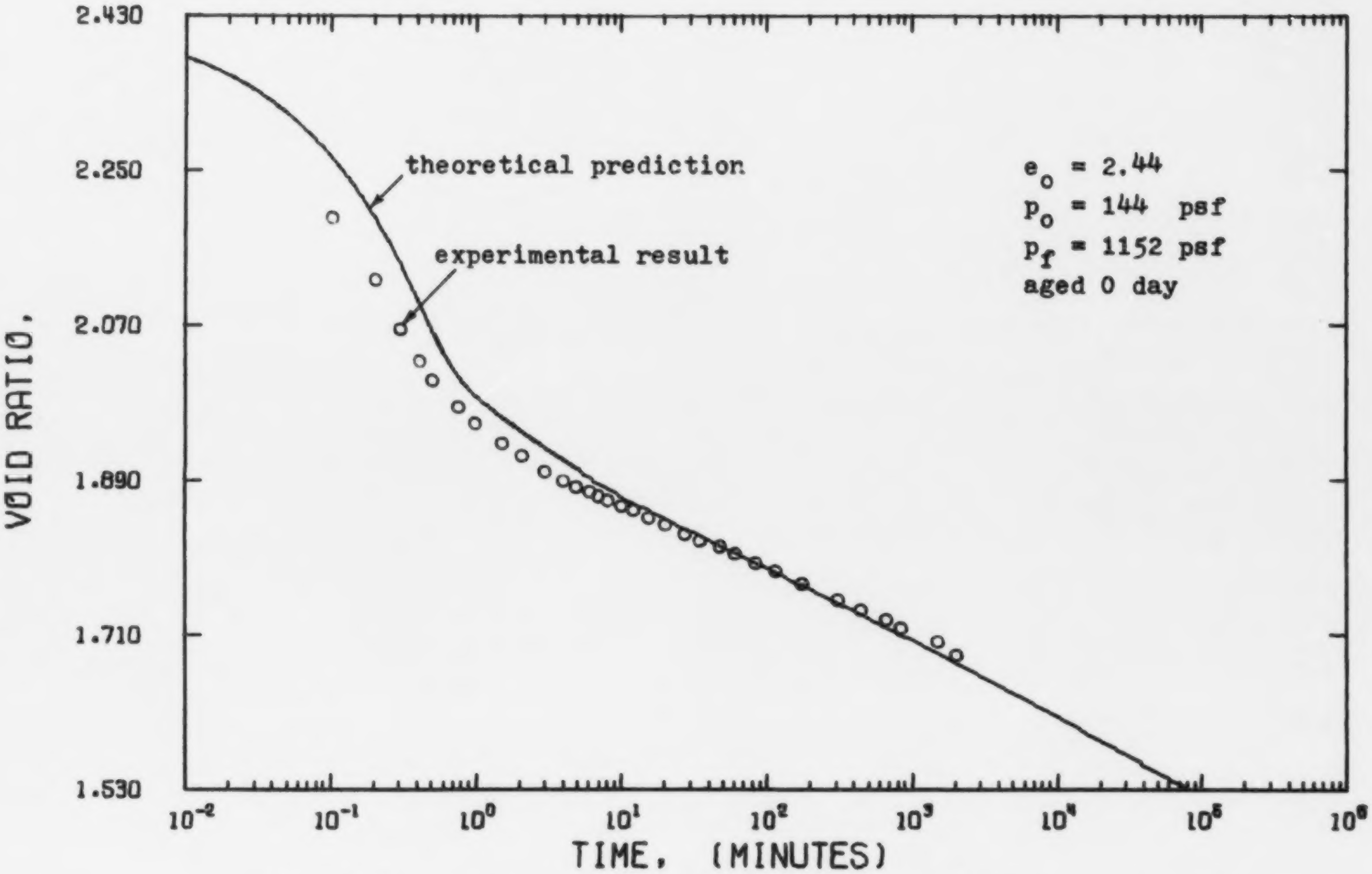

Fig. 8-11. Experimental and theoretical void ratio vs. log time curve for sample R3-8-1

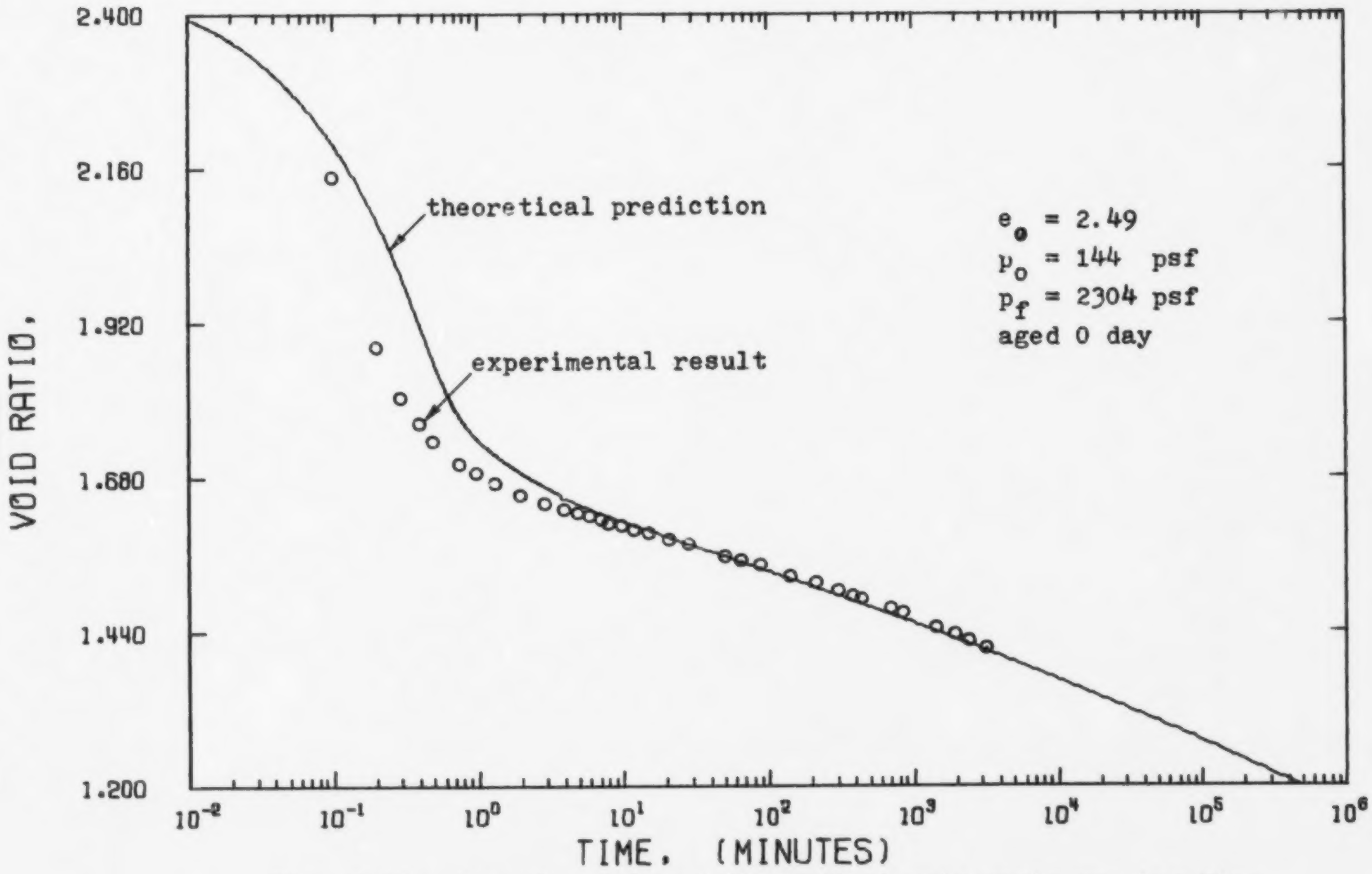

Fig. 8-12. Experimental and theoretical void ratio vs. log time curve for sample R3-16-1

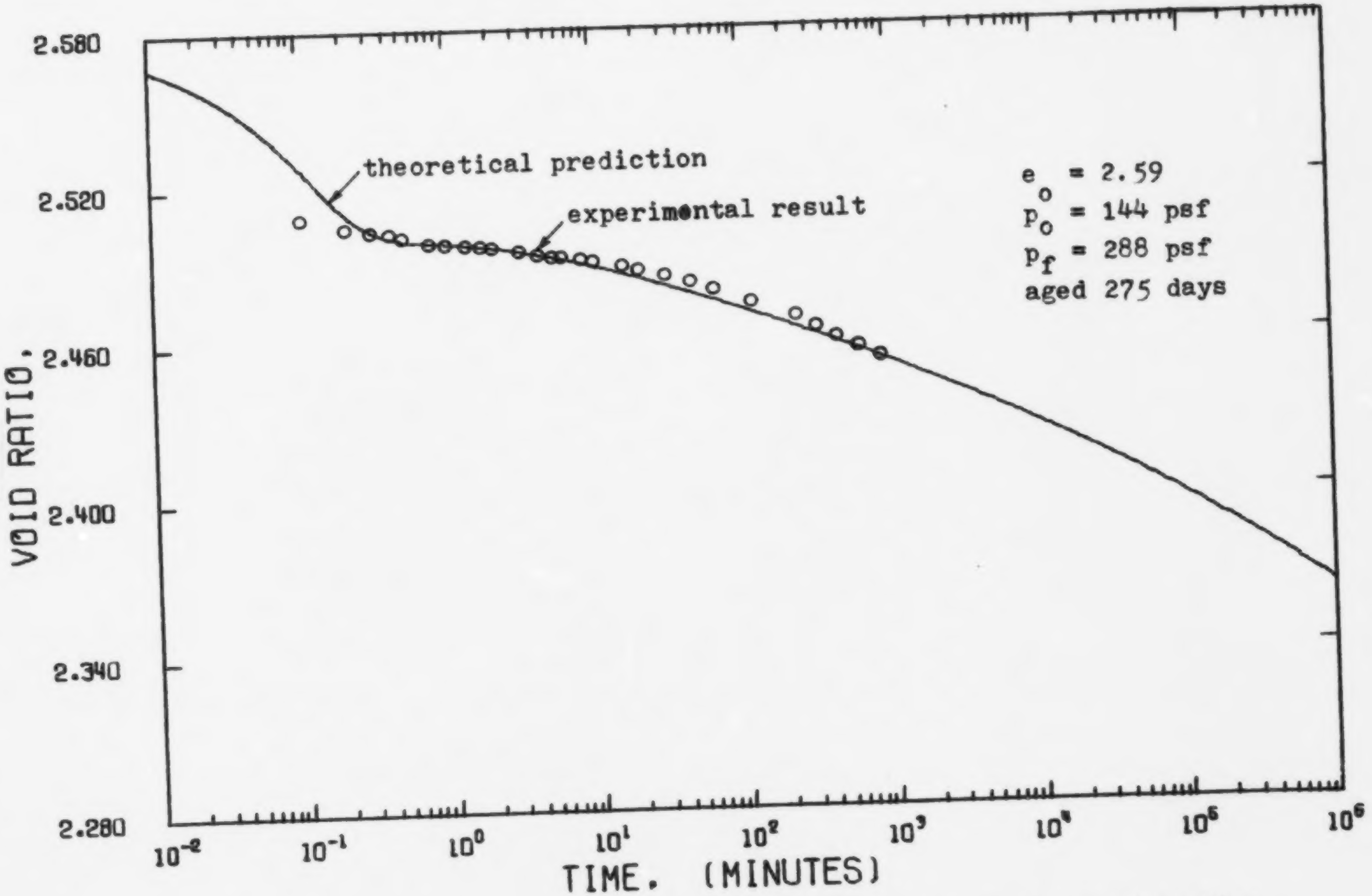

Fig. 8-13. Experimental and theoretical void ratio vs. log time curve for sample A2-2-1

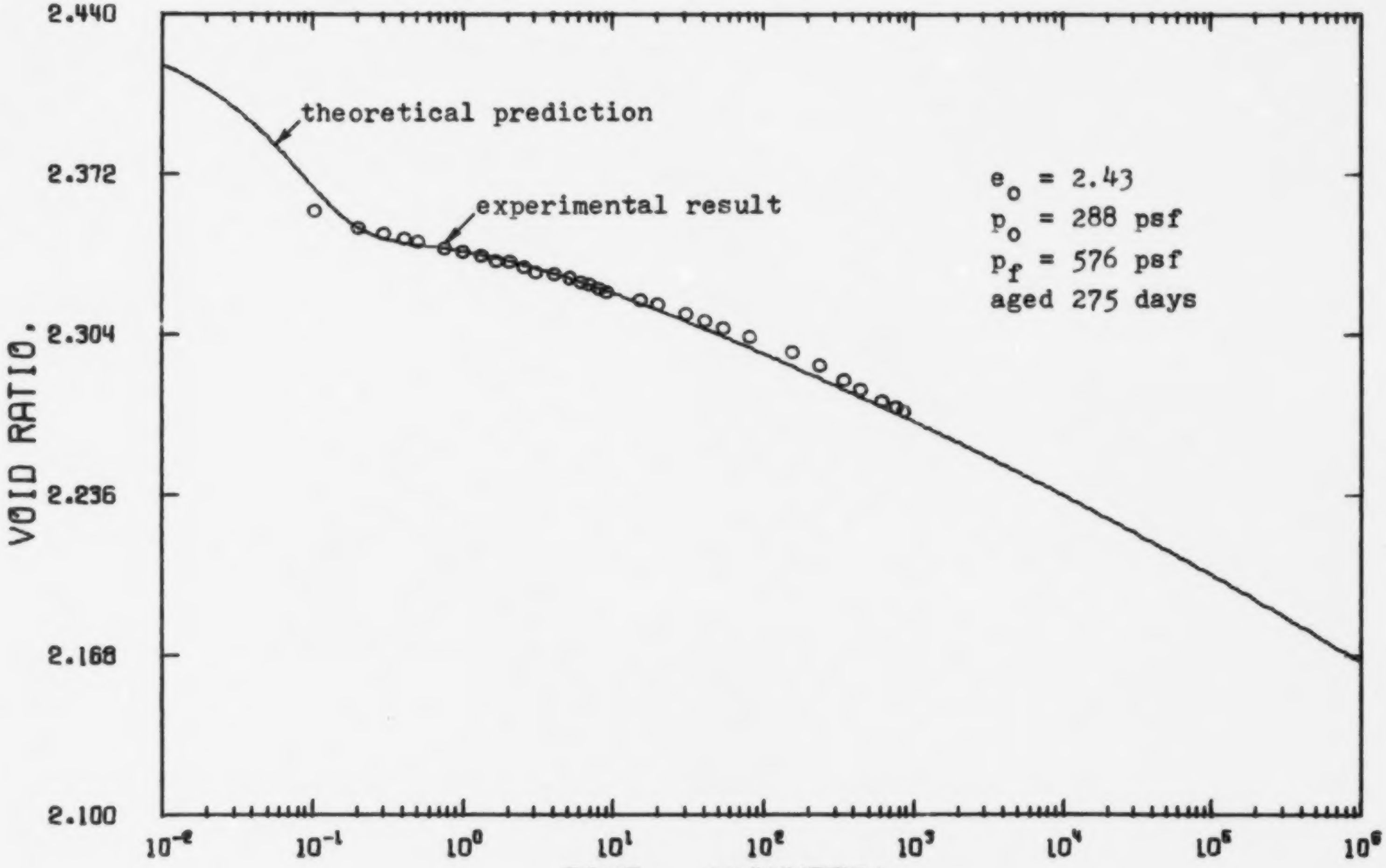

Fig. 8-14. Experimental and theoretical void ratio vs. log time curve for sample A2-2-2

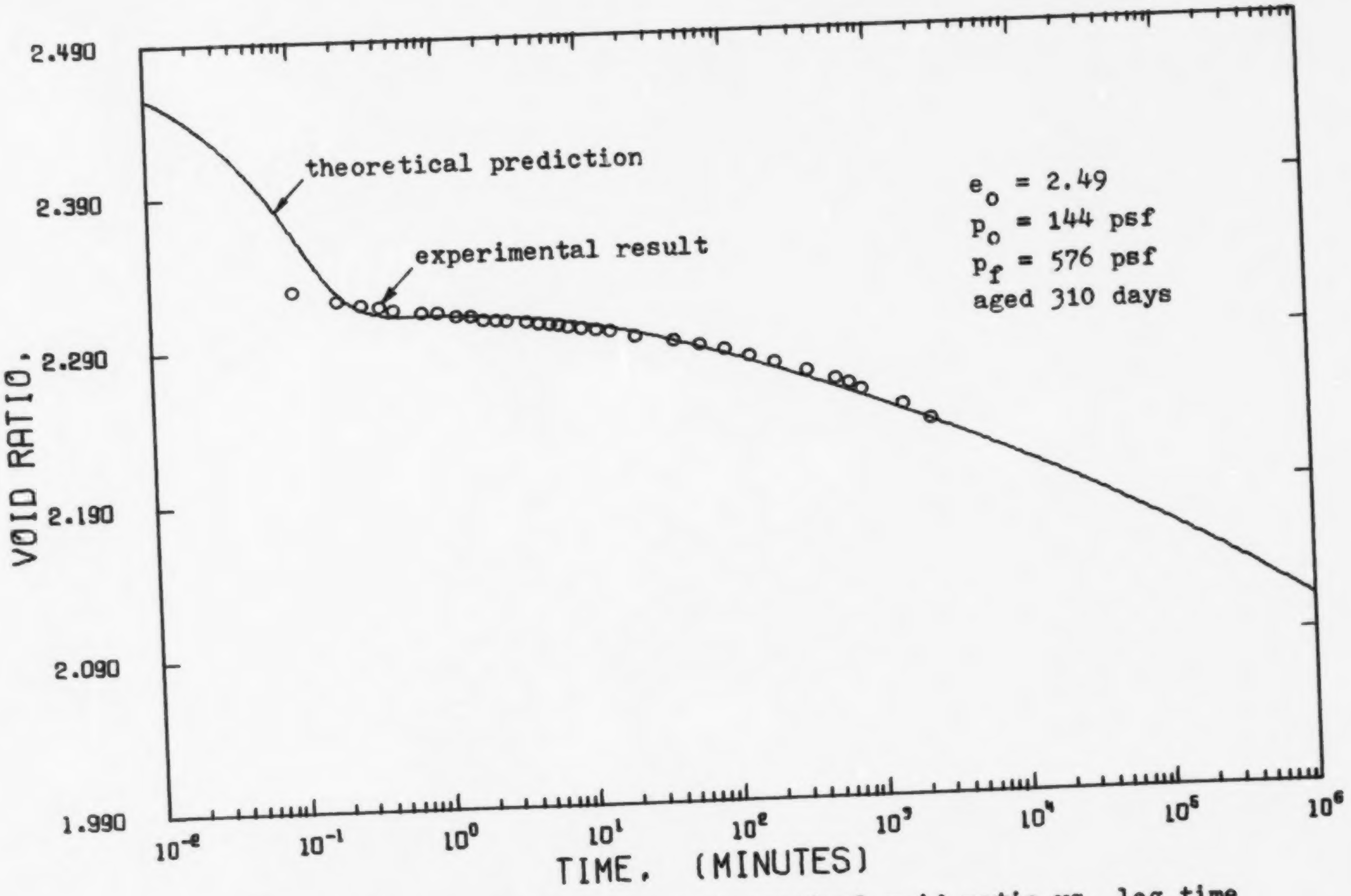

Fig. 8-15. Experimental and theoretical void ratio vs. log time curve for sample A2-4-1

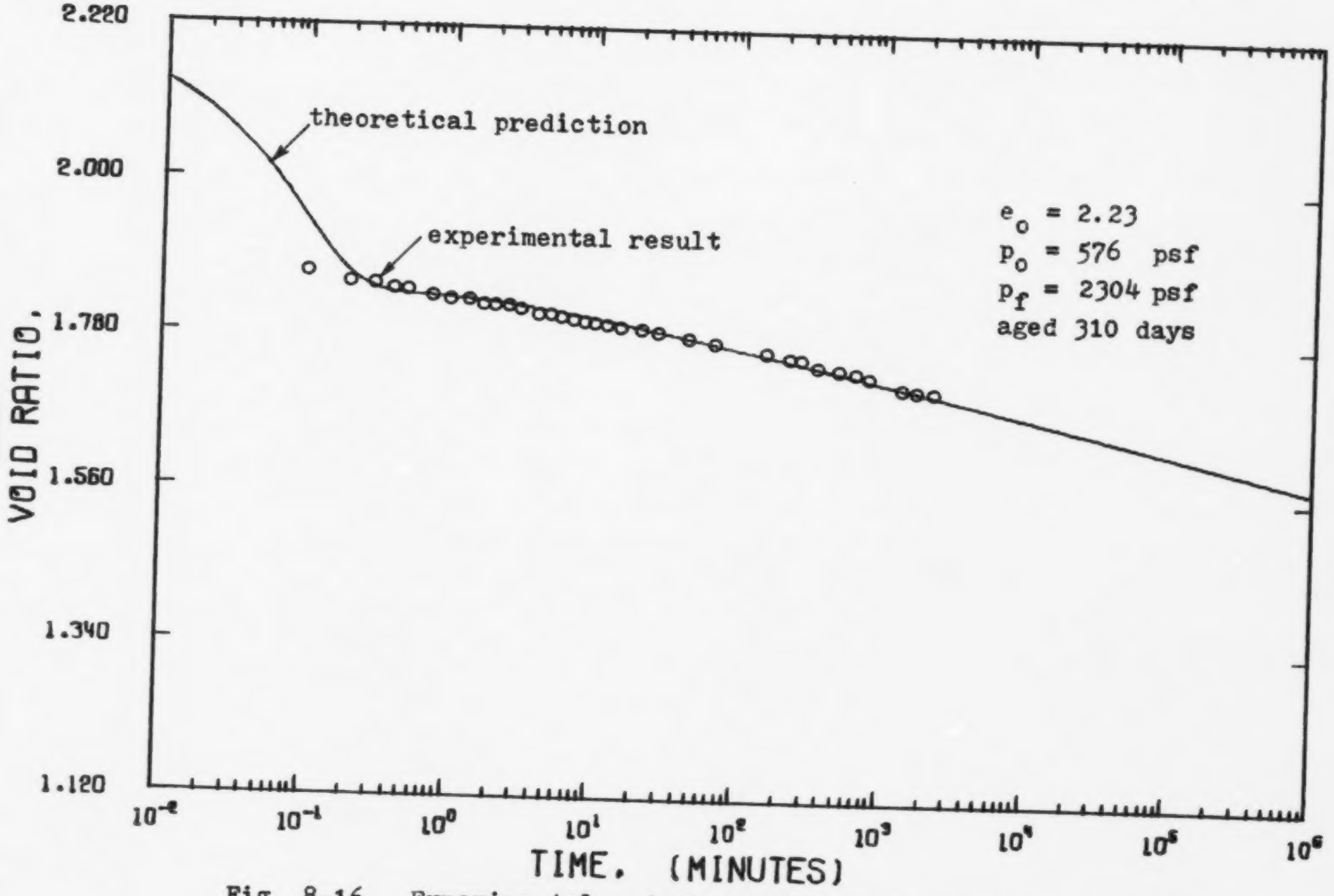

Fig. 8-16. Experimental and theoretical void ratio vs. log time curve for sample A2-4-2

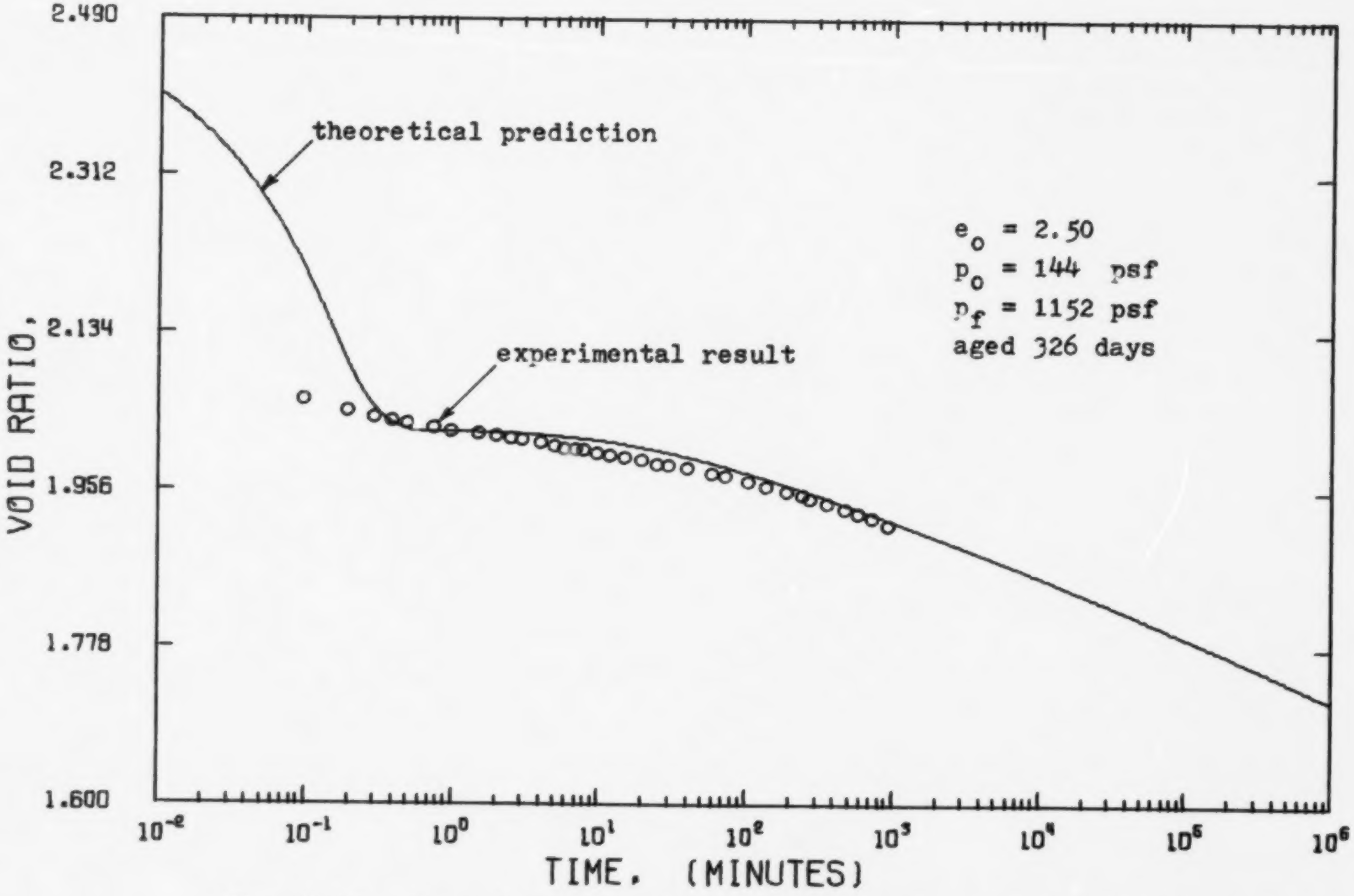

Fig. 8-17. Experimental and theoretical void ratio vs. log time curve for sample A2-8-1

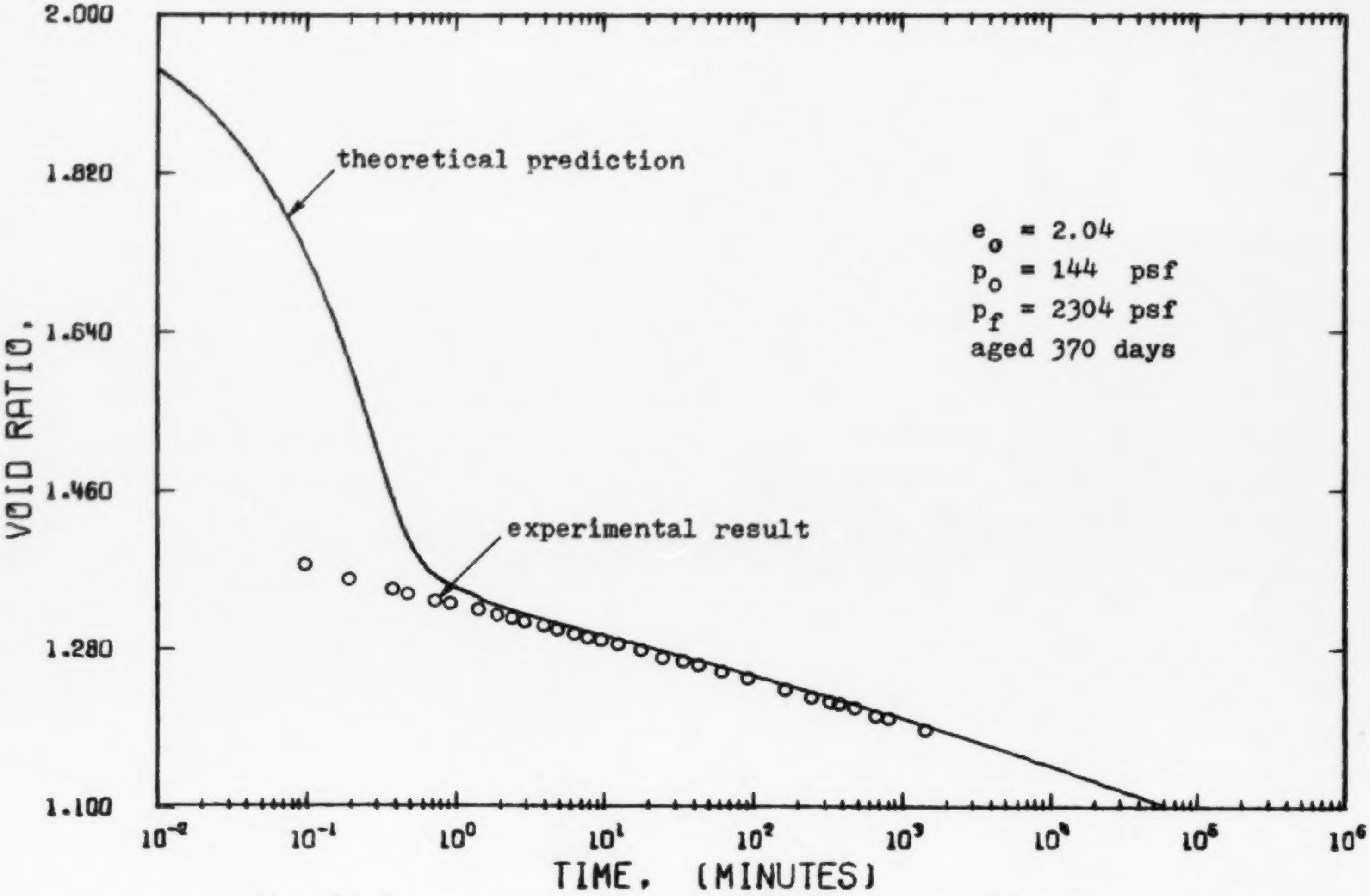

Fig. 8-18. Experimental and theoretical void ratio vs. log time curve for sample A2-16-1

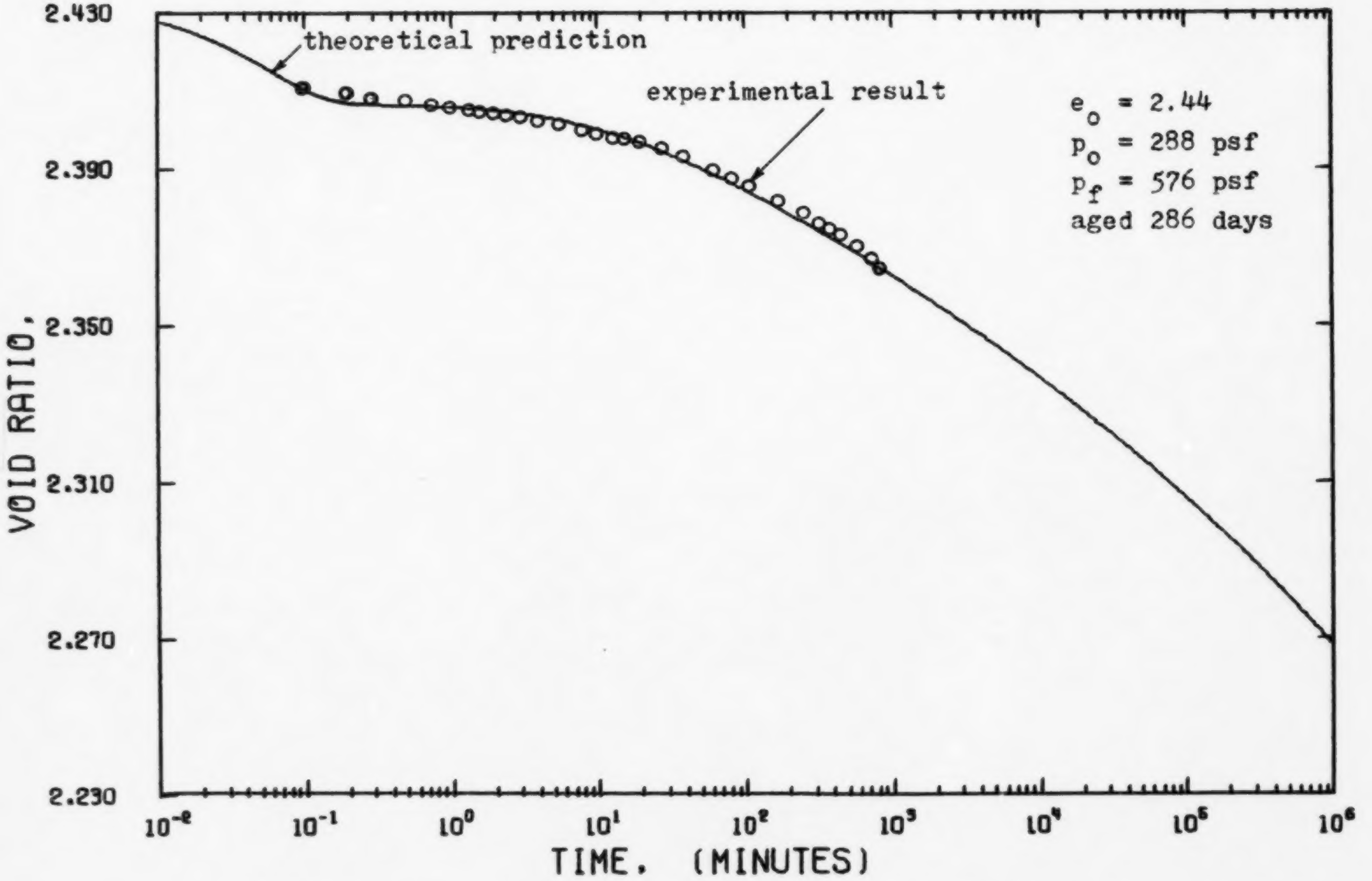

Fig. 8-20. Experimental and theoretical void ratio vs. log time curve for sample A3-2-2

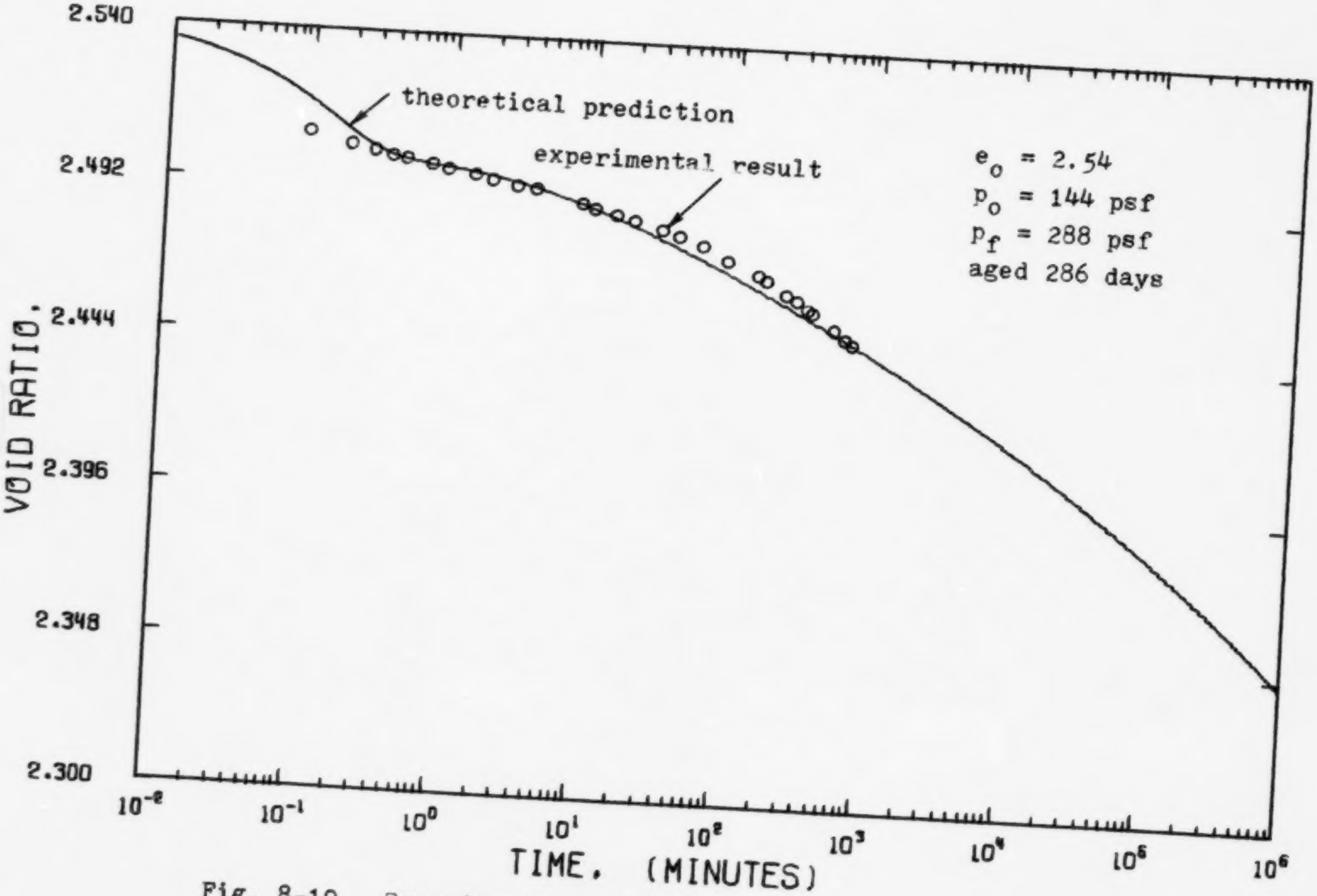

Fig. 8-19. Experimental and theoretical void ratio vs. log time curve for sample A3-2-1

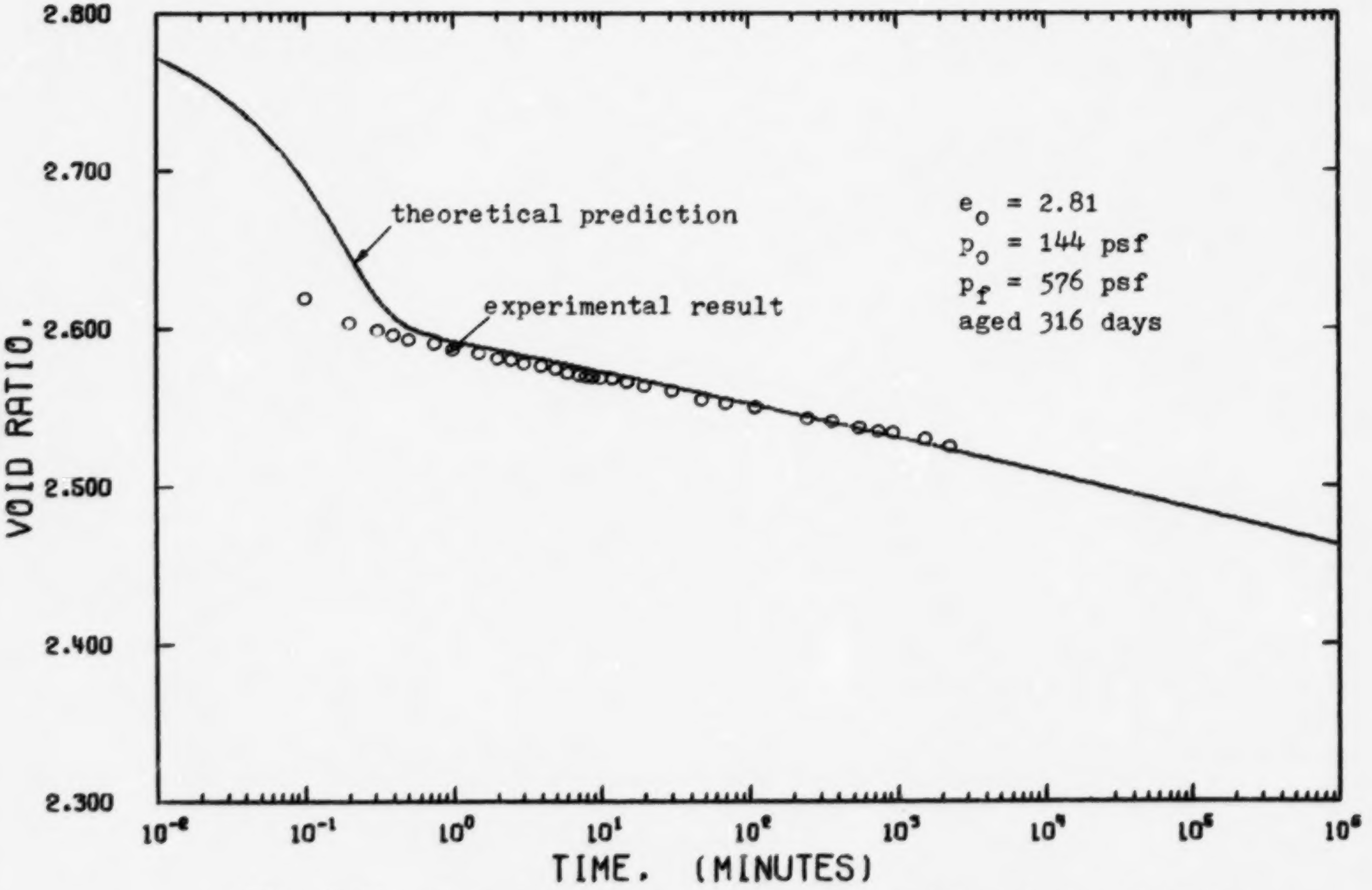

Fig. 8-21. Experimental and theoretical void ratio vs. log time curve for sample A3-4-1

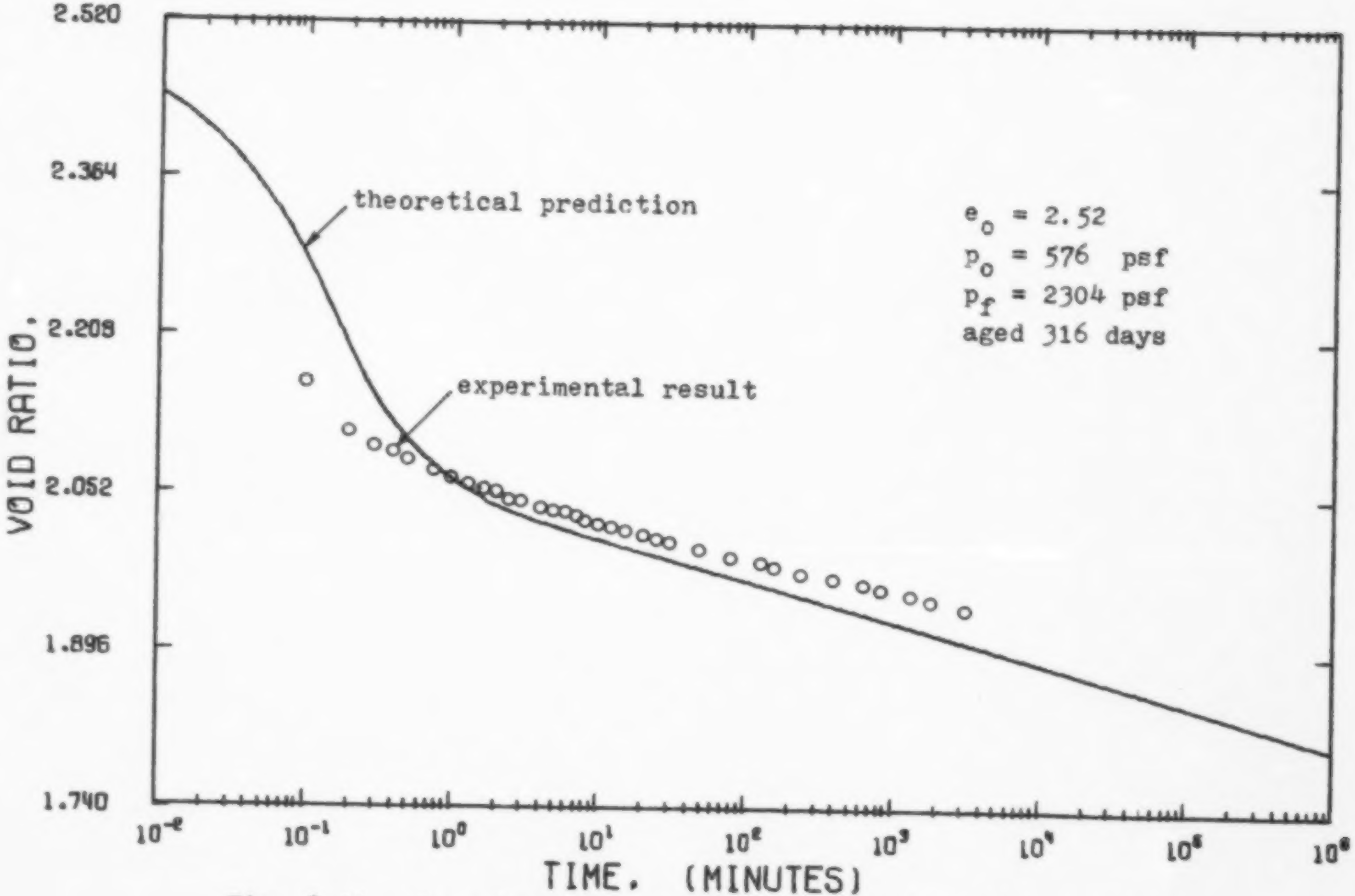

Fig. 8-22. Experimental and theoretical void ratio vs. log time curve for sample A3-4-2

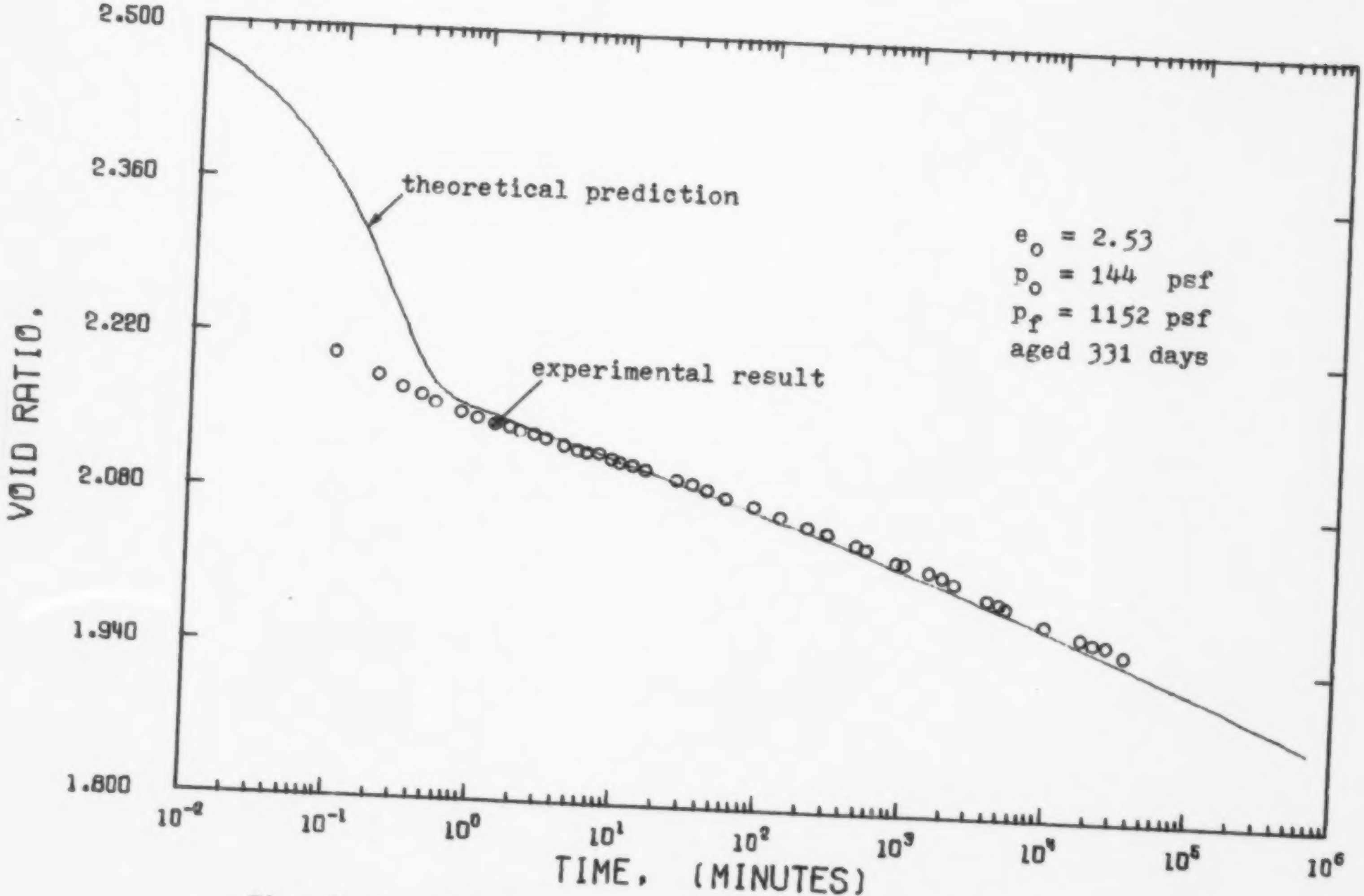

Fig. 8-23. Experimental and theoretical void ratio vs. log time curve for sample A3-8-1

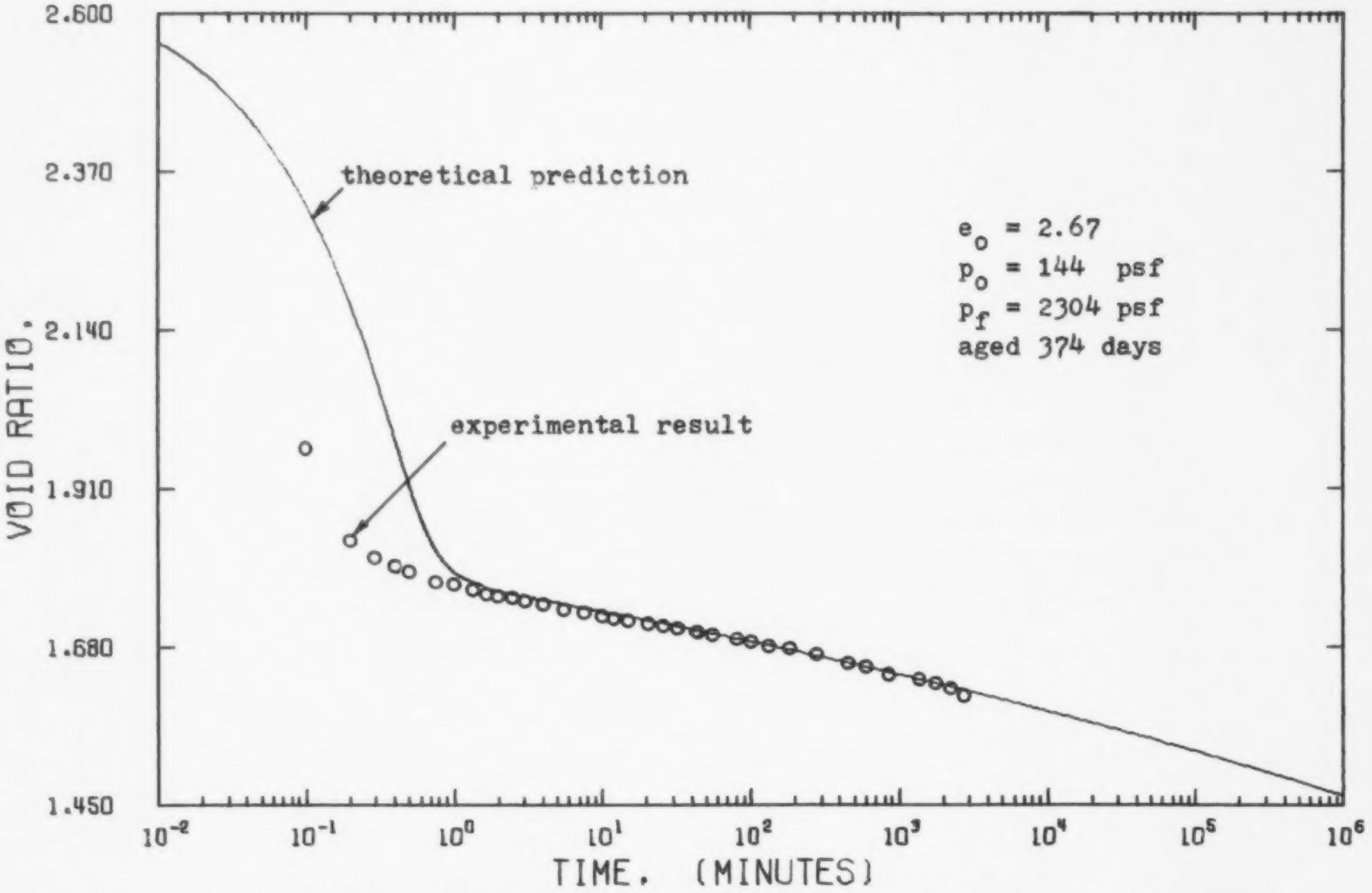

Fig. 8-24. Experimental and theoretical void ratio vs. log time curve for sample A3-16-1

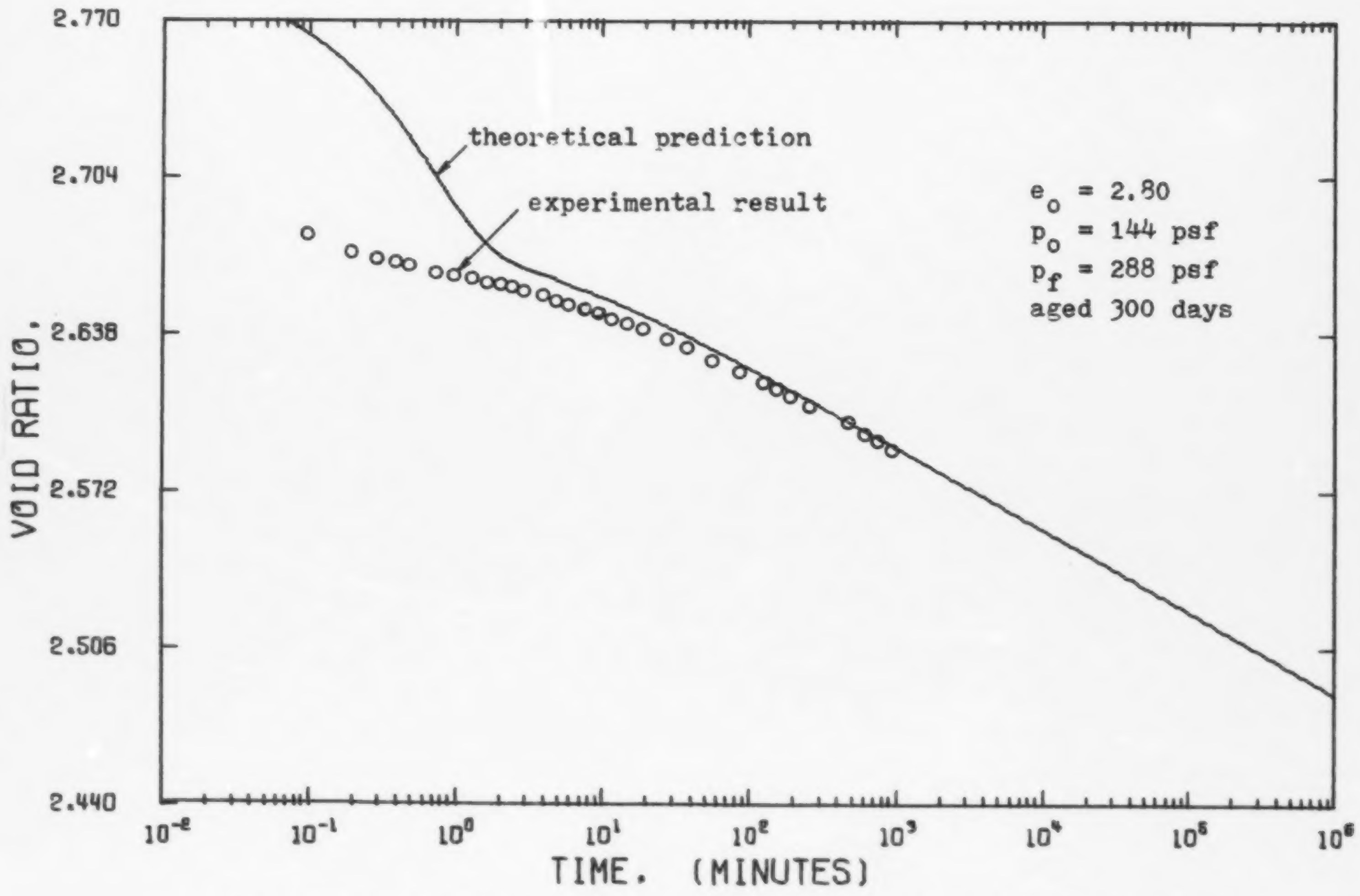

Fig. 8-25. Experimental and theoretical void ratio vs. log time curve for sample A4-2-1

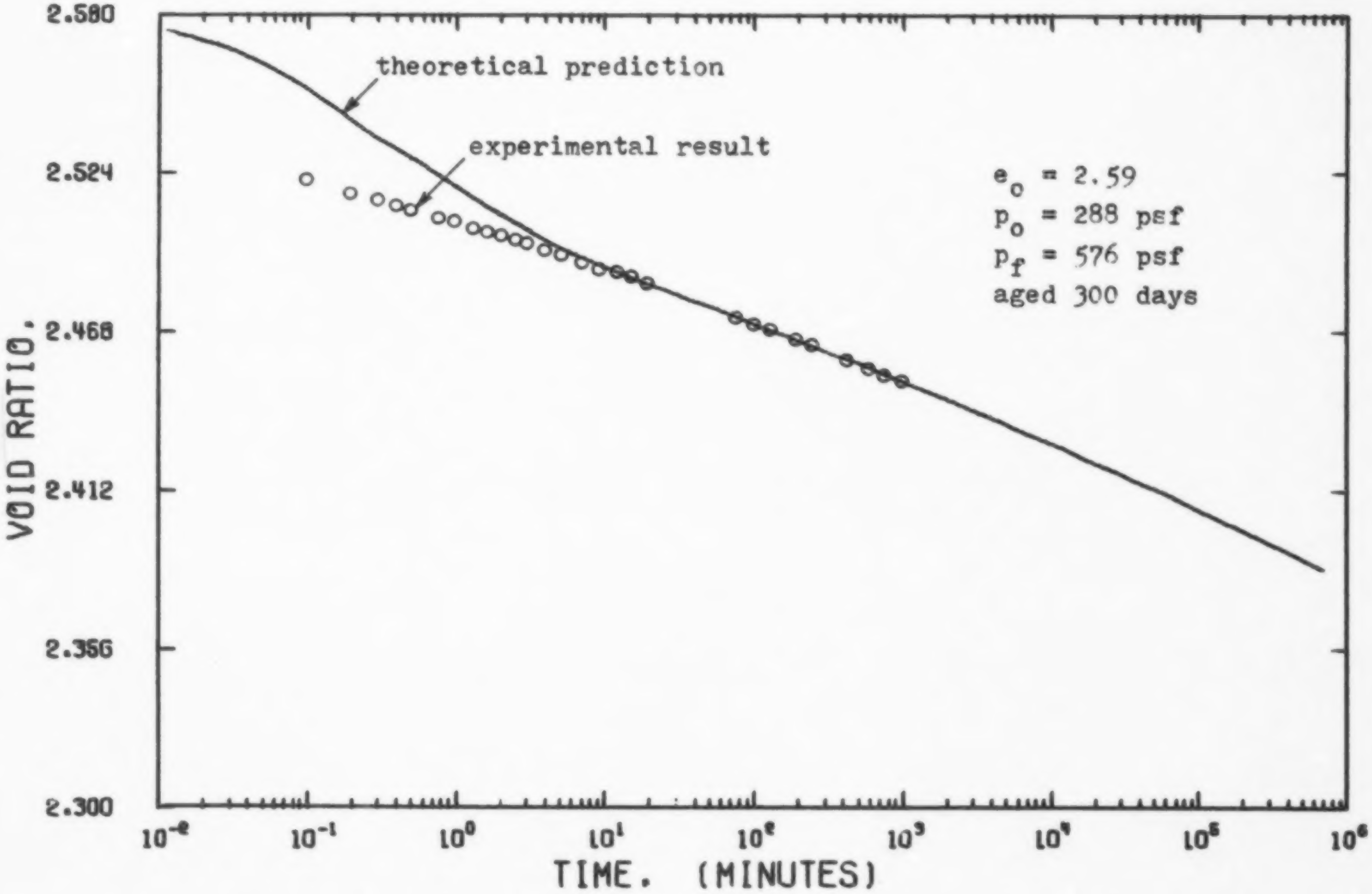

Fig. 8-26. Experimental and theoretical void ratio vs. log time curve for sample A4-2-2

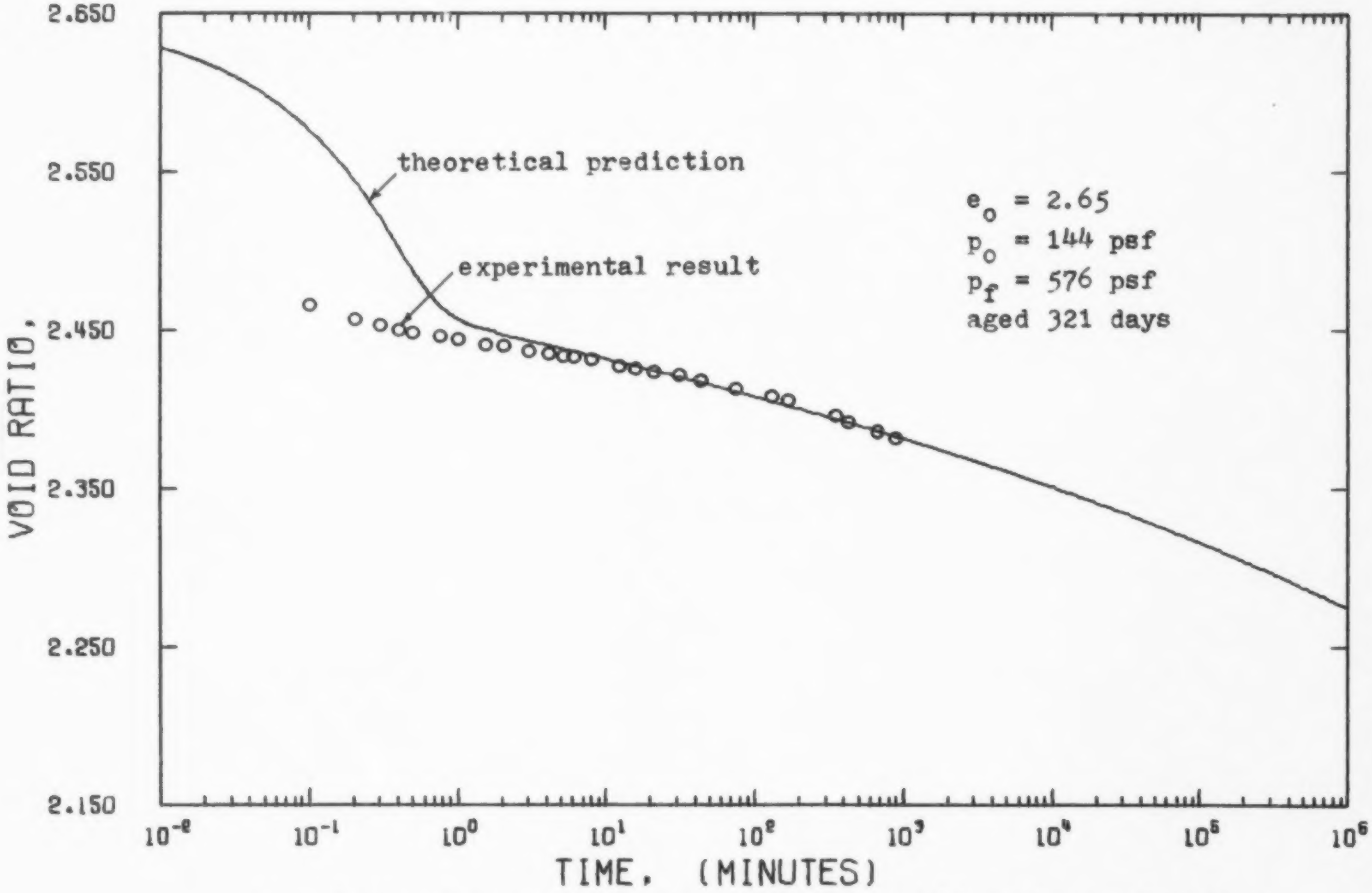

Fig. 8-27. Experimental and theoretical void ratio vs. log time curve for sample A4-4-1

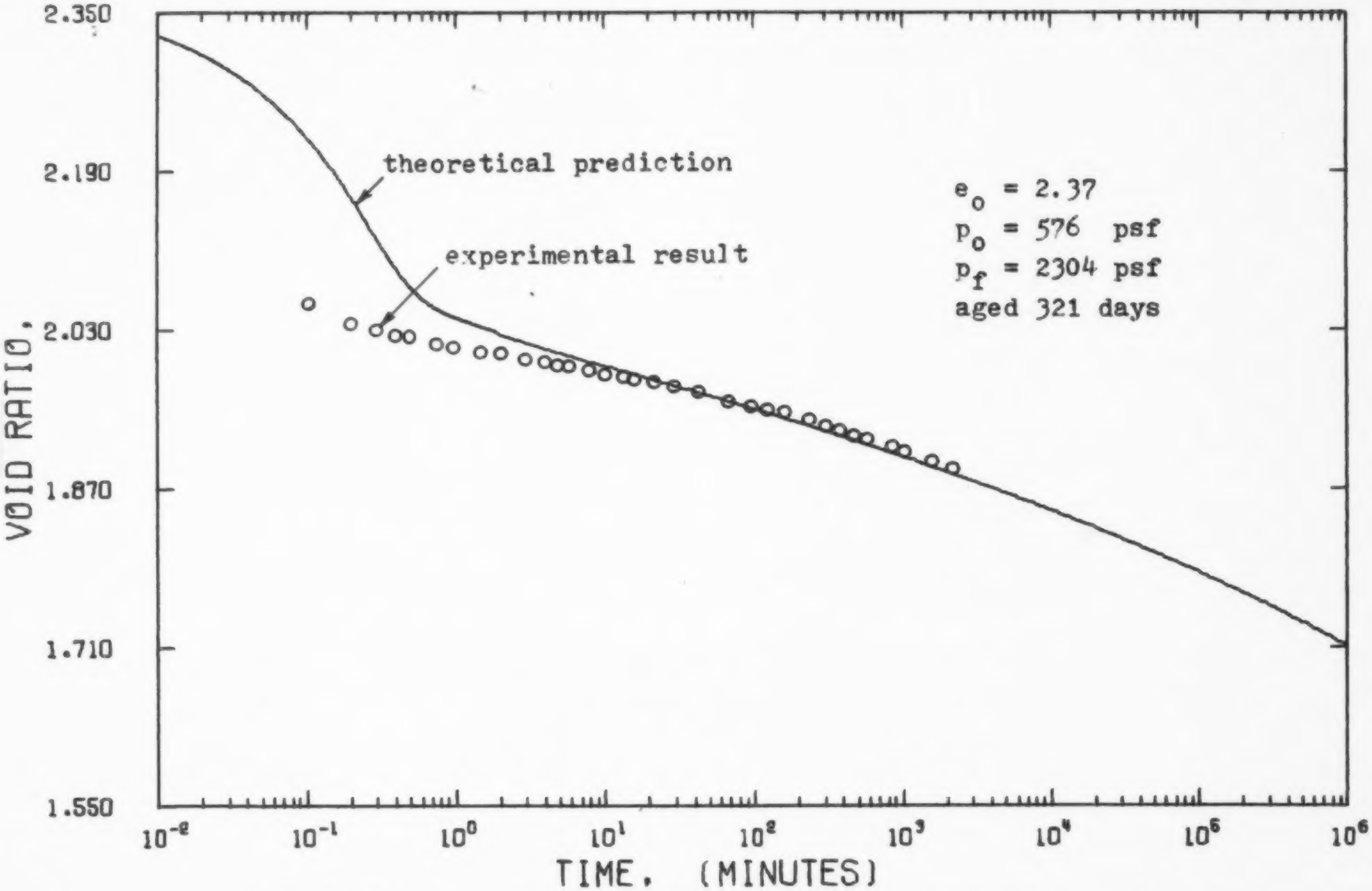

Fig. 8-28. Experimental and theoretical void ratio vs. log time curve for sample A4-4-2

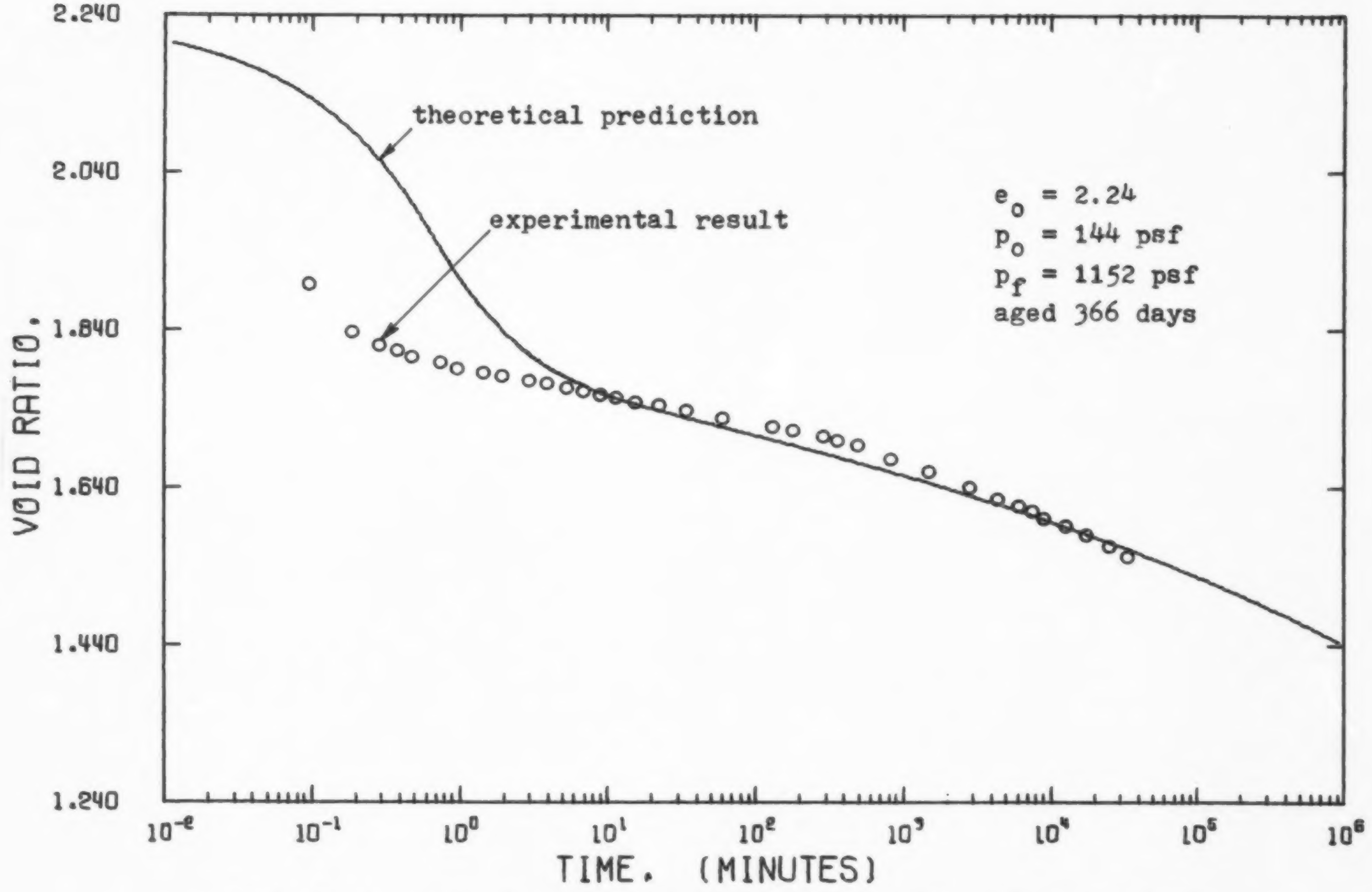

Fig. 8-29. Experimental and theoretical void ratio vs. log time curve for sample A4-8-1

obtained for all samples but one (A3-4-2) which shows considerable discrepency which is attributed to some unexplained experimental errors. The first 10 minutes in the laboratory scale is equivalent to two weeks for a field refuse fill of 10 feet thickness. The encouraging agreement between the theoretical and experimental curves is therefore believed to indicate that the theoretical model describes the consolidation well for times that are of engineering significance, because in the actual field problems the portion of consolidation in which agreement is poor would be finished before the construction is completed.

A set of typical curves showing the theoretical prediction and observed pore pressure dissipation (in this case for sample A3-8-1) is shown in Fig. 8-30. The two curves agree quite well in the time indicated for the end of primary consolidation (about one minute). In most of the tests, the time for pore pressure dissipation was found to be in the vicinity of one minute. However, as pointed out in Chapter VI, because a finite time is required for the application of the load increment, the peak excess pore pressure is missed in the experimental curve. In addition, agreement between the theoretical prediction and experimental curves is adversely affected by lack of information on the permeability of aged refuse, which requires that a hypothetical void ratio versus log permeability be used.

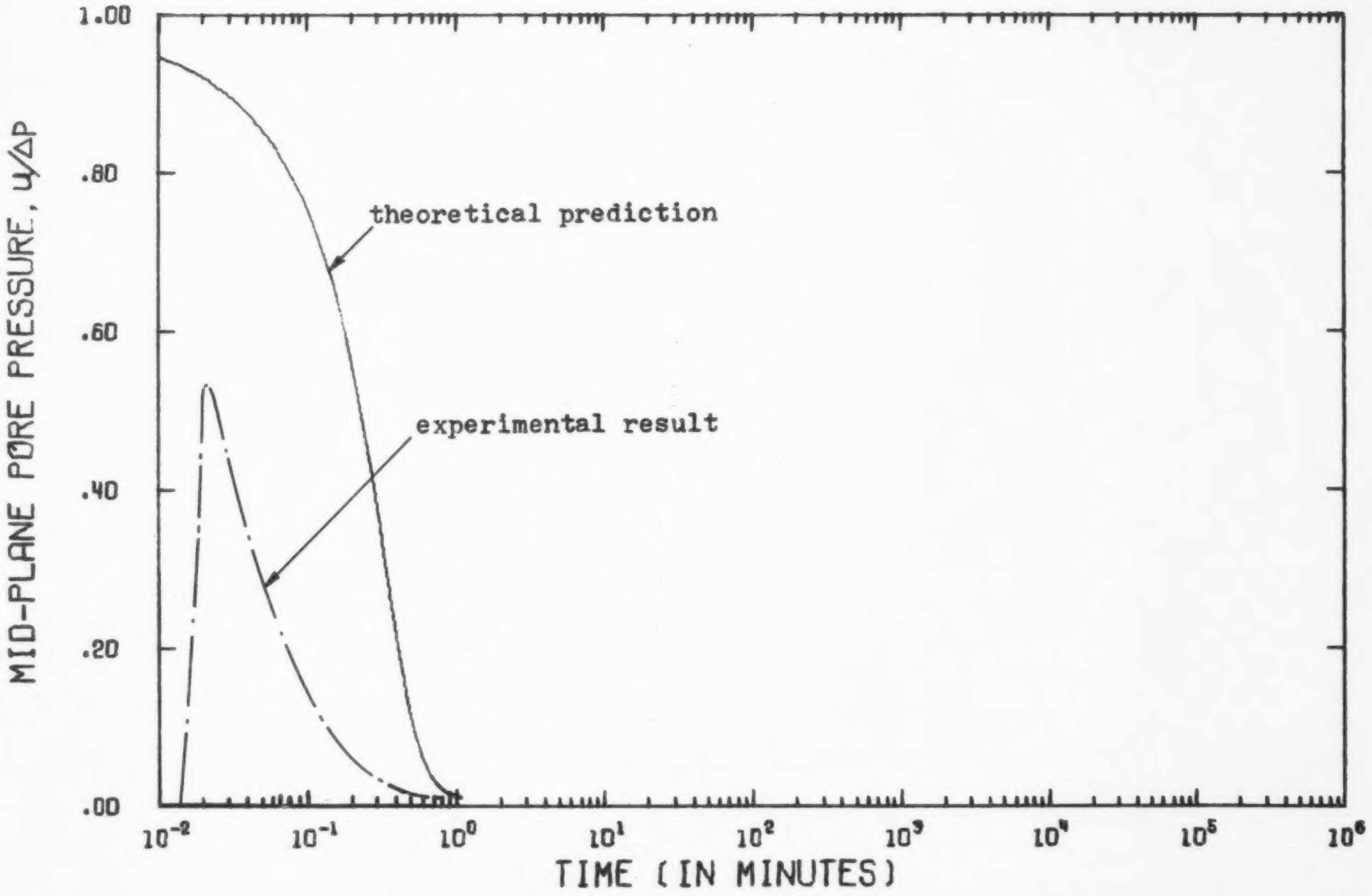

Fig. 8-30. Experimental and theoretical pore pressure dissipation curve for sample A3-8-1

Discussion of Test Results

(1) Effect of the load increment ratio on the shape of the time-deformation curve

It is known that the shape of the time-deformation curve can vary over a wide range depending on such factors as the load increment ratio, type of soil, and stress history. Fig. 8-31 shows the influence of the load increment ratio on the shape of the settlement versus log time curve for clay soil. Leonards and Girault (1961) observe that for large load increment ratios, settlement versus log time curve is obtained which, with the exception of secondary compression, is characterized by the Terzaghi theory (Type I curve). For small load increment ratios, a Type III curve is obtained, while for intermediate load increment ratios a transition curve (Type II) is obtained. Wu et. al. (1966) used the rate process theory to provide a physical explanation of the diverse types of time-deformation behavior of clay soils.

It has been observed in this study that milled refuse can also have diverse types of time-deformation curves, depending on the value of the load increment ratio. The consolidation model for milled refuse proposed herein can predict a wide range of time-deformation curve shapes if appropriate model parameters are given. In this investigation, these parameters are determined from the experimental

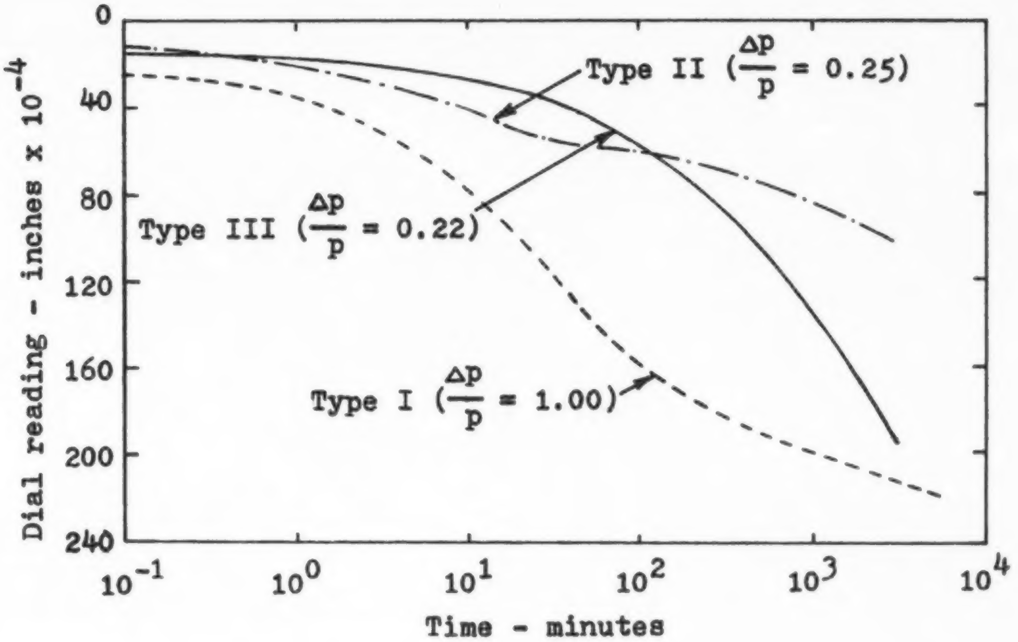

Fig. 8-31. Effect of load increment on shape of settlement versus time curves, undisturbed Mexico City clay (After Leonards et. al., 1961)

time-deformation curve. Typical curves showing the effect of the load increment ratio on consolidation behavior of raw and laboratory aged milled refuse samples are shown in Figs. 8-32 and 8-33 respectively. Because of the high load increment ratios used, only Type I and Type II curves are observed.

(2) Effect of load increment ratio on relative amount of secondary compression

It is known that for clay and many other other materials, a large amount of secondary compression per unit of total compression is associated with small load increment ratios. The experimental time-deformation curves of both raw and laboratory aged milled refuse samples have also been found to show the same behavior. Typical experimental results for raw and aged milled refuse samples under different values of load increment ratio p_f/p_o are shown in Figs. 8-34 and 8-35 in the form of strain versus log time plots. Here, N is defined as the ratio of the amount of secondary compression to the amount of total compression for some particular value of p_f/p_o. As one would expect, the value of N is larger when p_f/p_o is smaller.

(3) Effect of aging and load increment ratio on consolidation behavior

In the development of the time-settlement model for

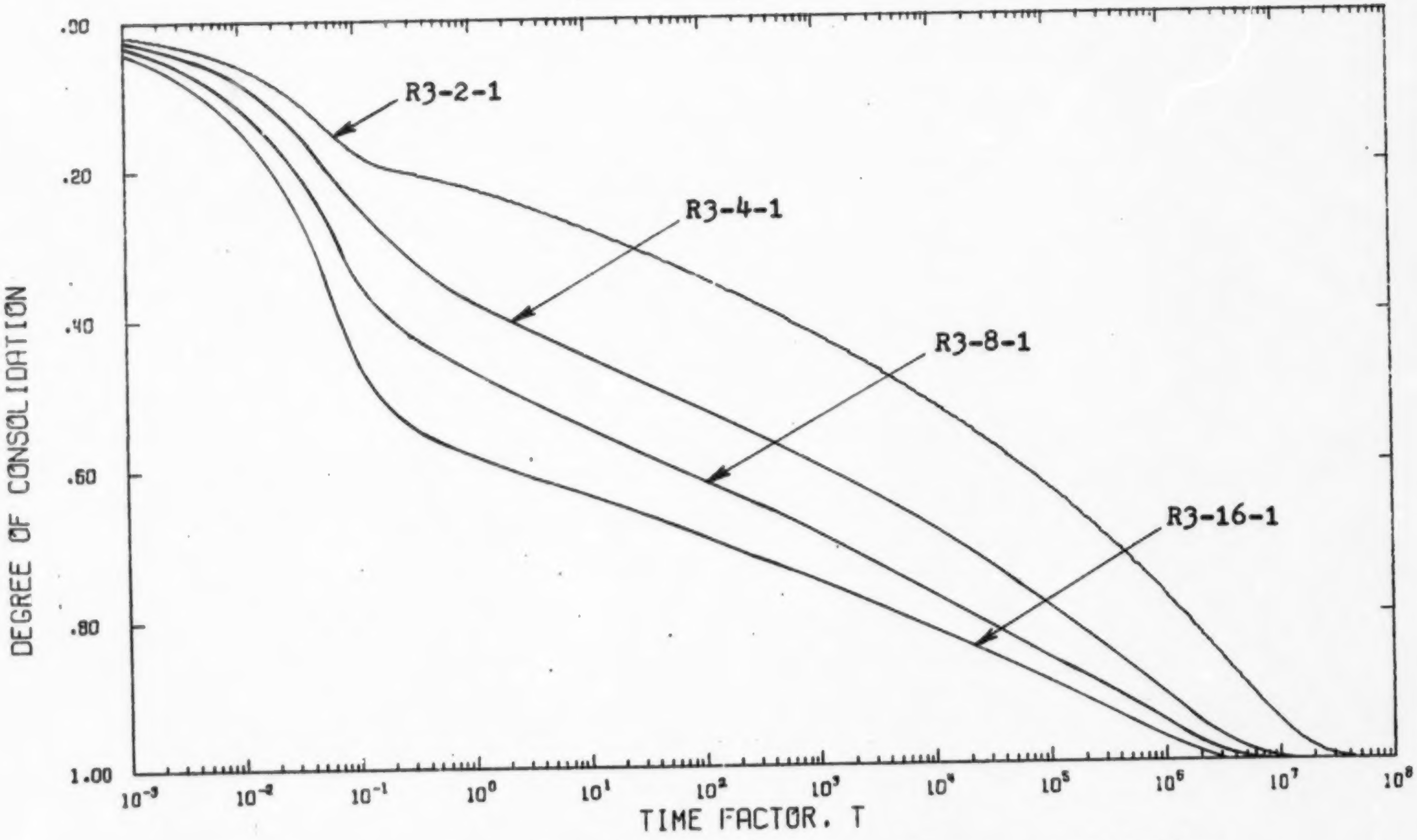

Fig. 8-32. Effect of load increment ratio on consolidation behavior of raw milled refuse samples

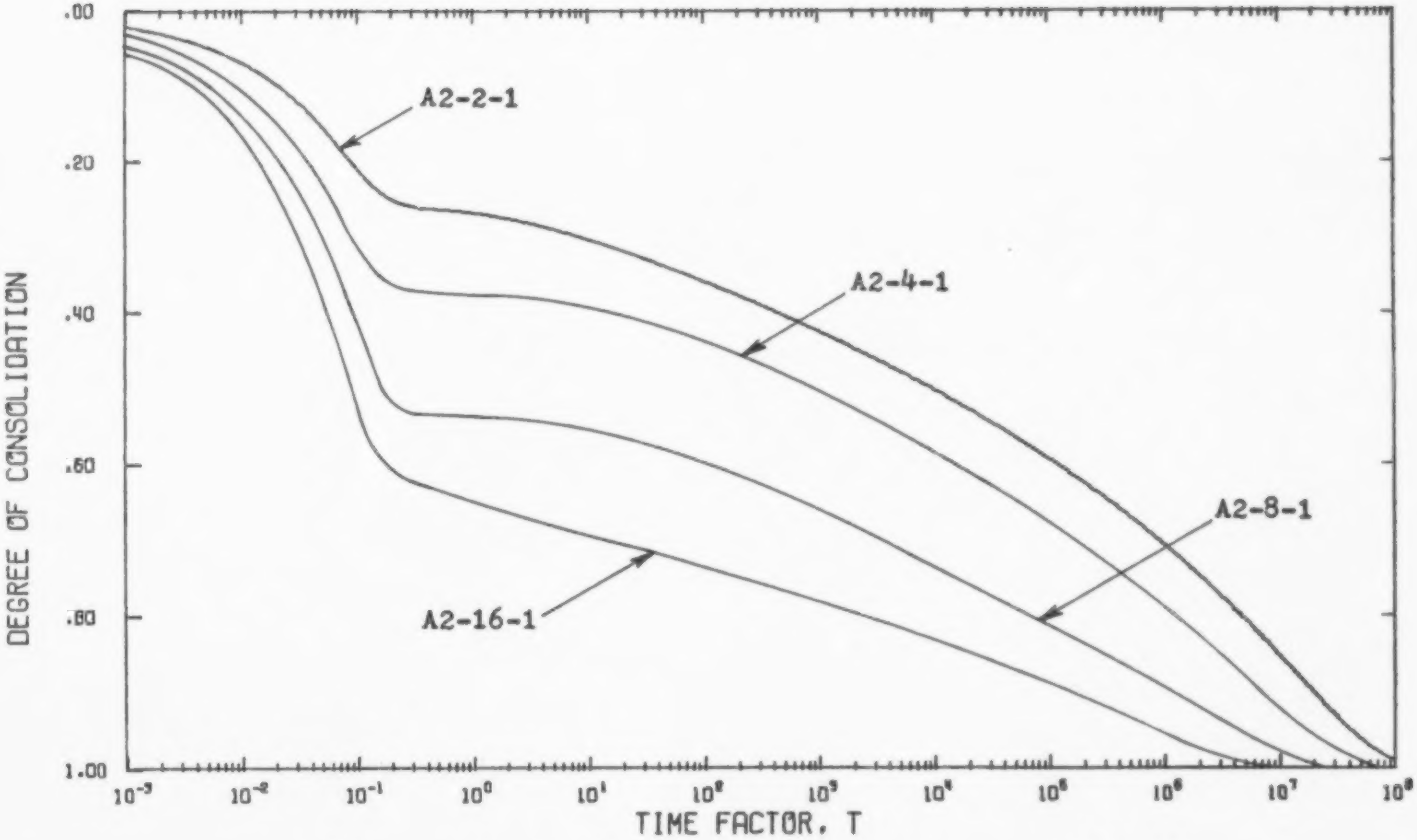

Fig. 8-33. Effect of load increment ratio on consolidation behavior of aged milled refuse samples

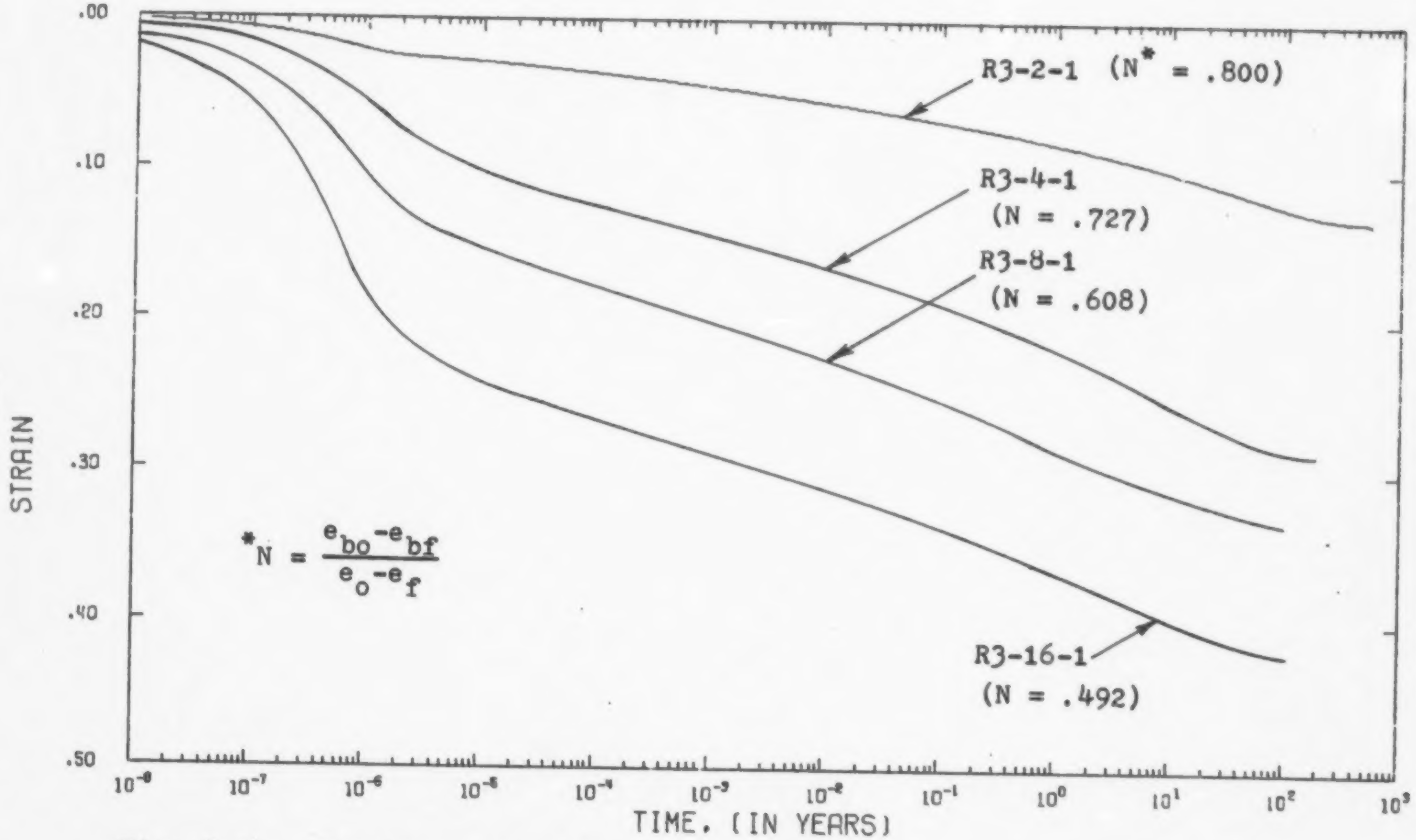

Fig. 8-34. Strain vs. log time curves for various value of p_f/p_o, sample R3

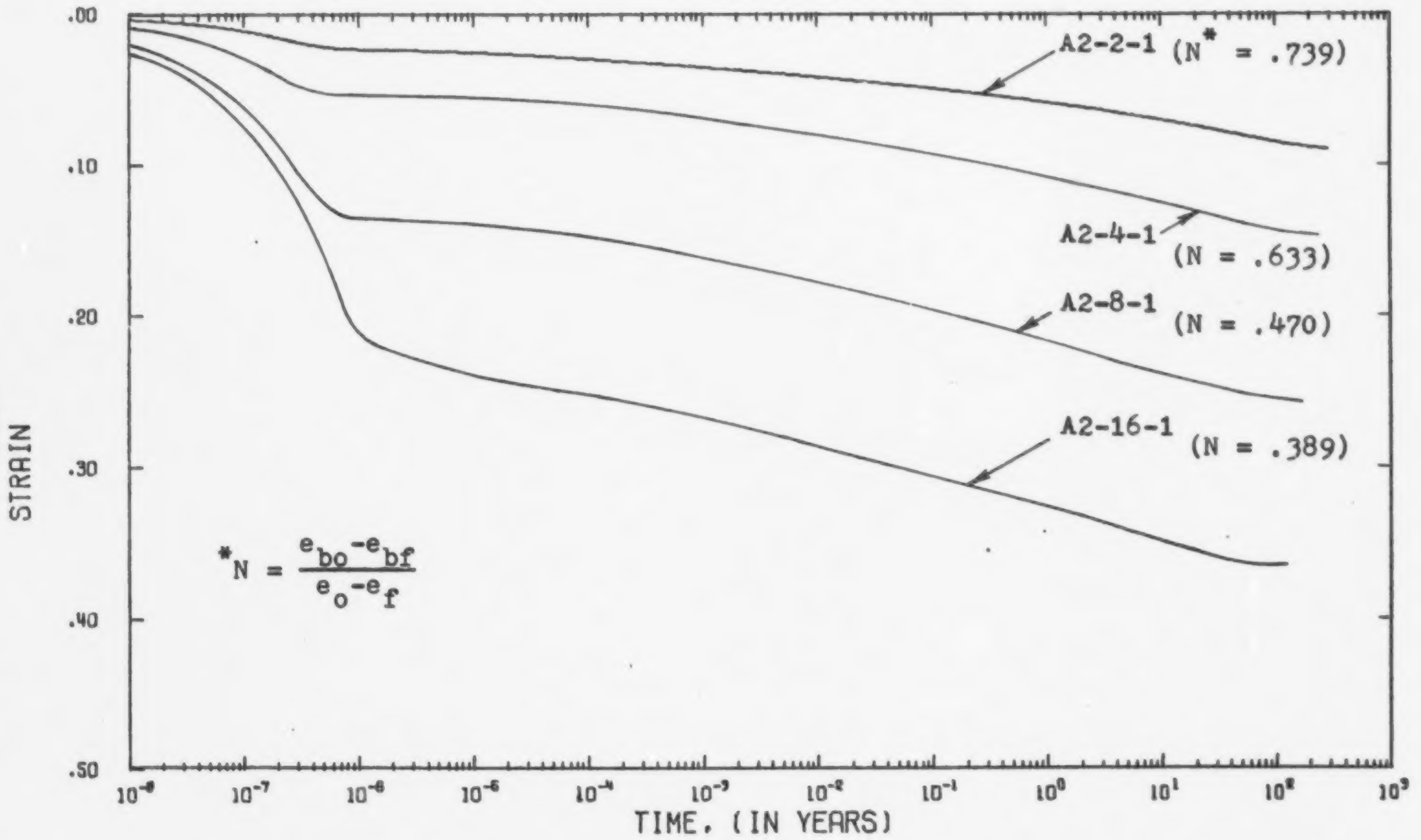

Fig. 8-35. Strain vs. log time curves for various value of p_f/p_o; sample A2

milled refuse, it has been assumed that the secondary consolidation results from the very slow dissipation of pore pressure from the micropores by drainage into the macropores. It is also assumed that the law governing the pore water flow from the micropores into the macropores is in accordance with the theory of rate process. Mitchell et. al. (1968) demonstrated that the rate process theory does in fact provide a reasonable physical basis for the creep flow of soils. In other previous works using rheological models the validity of the rate process theory has been assumed a priori in the formulation of the model. It has been pointed out by Glasstone et. al. (1941) that the theory of absolute reaction rate is not merely a theory of the kinetics of chemical reactions, but that it is one that can, in principle, be applied to any process involving a rearrangement of matter, that is to say, to any "rate process". The rate process theory has been applied successfully to describe the phenomenon of viscosity (Eyring, 1936; Taylor, 1938) and the problem of diffusion in solution (Eyring, 1936; Ewell and Eyring, 1937). Since the dissipation of pore pressure in the micropores is a flow problem which, in turn, is a rate process, it seems raesonable to suppose that the rate process theory can be applied to the consolidation creep behavior of both raw and aged milled refuse.

The general creep equation (Equation 4-25) for milled refuse takes the following form:

$$\frac{d\epsilon_b}{dt} = \Delta p A_o \left(\frac{A_f}{A_o}\right)^{\frac{e_{bo}-e_b}{e_{bo}-e_{bf}}} \sinh \left\{ B_o \left(\frac{B_f}{B_o}\right)^{\frac{e_{bo}-e_b}{e_{bo}-e_{bf}}} \frac{u}{\Delta p} \right\} \qquad (8\text{-}1)$$

In order to study the effect of aging and p_f/p_o on the creep behavior of milled refuse, it is preferable to have a simpler form of Equation 8-1, which can be obtained by writing

$$\overline{A} = \Delta p A_o \left(\frac{A_f}{A_o}\right)^{\frac{e_{bo}-e_b}{e_{bo}-e_{bf}}} \qquad (8\text{-}2a)$$

$$\text{and} \quad \overline{B} = B_o \left(\frac{B_f}{B_o}\right)^{\frac{e_{bo}-e_b}{e_{bo}-e_{bf}}} . \qquad (8\text{-}2b)$$

Substituting Equations 8-2a and 8-2b into Equation 8-1 yields

$$\frac{d\epsilon_b}{dt} = \overline{A} \sinh \left(\overline{B} \frac{u}{\Delta p}\right) . \qquad (8\text{-}3)$$

In the above equation, $\overline{A}$ is a coefficient which is proportional to the rate of consolidation creep. Therefore, it may be appropriately termed the creep index. $\overline{B}$ represents the ratio of micropore discharge velocity to the excess micropore pressure, and may be termed the apparent permeability. For a material with a pseudoplastic nonlinearity, the apparent permeability, $\overline{B}$, falls progressively with decreasing excess micropore pressure and the flow curve has horizontal tangent only at a very low value of excess micropore pressure.

It has been pointed out in Chapter IV that the creep parameters $\overline{A}$ and $\overline{B}$ are not constants and are likely to vary with void ratio during an increment of pressure. However, the precise variation of $\overline{A}$ and $\overline{B}$ with void ratio is not known. A linear variation of void ratio with these creep parameters has been assumed by Poskitt (1971), while a linear variation of void ratio with the logarithm of these creep parameters has been used by Berry and Poskitt (1972). For mathematical convenience, the linear form of the e_b versus log $\overline{A}$ and e_b versus log $\overline{B}$ relationships have been used in the present study. Ozaydin (1974) showed a linear relationship in the plot of void ratio versus log k_2 (which is equivalent to $\overline{B}$ for the present case) in the study of the creep response of kaolin clay. Although the k_2 were given only for two values of void ratio, which are not sufficient to establish the linear relationship, these results are consistent with the assumed linear e_b versus log k_2 relation.

Let $\overline{A}_{bo}$, $\overline{A}_{bf}$ and $\overline{B}_{bo}$, $\overline{B}_{bf}$ represent the initial and final values of $\overline{A}$ and $\overline{B}$ respectively; then

$$A_{bo} = A_o \Delta p \ , \qquad (8\text{-}4a)$$

$$A_{bf} = A_f \Delta p \ , \qquad (8\text{-}4b)$$

$$B_{bo} = B_o \ , \qquad (8\text{-}4c)$$

and

$$B_{bf} = B_f \ . \qquad (8\text{-}4c)$$

These parameters can be calculated for each sample tested by using the data listed in Table 8-2. The results are summarized in Table 8-3. Although considerable effort has been made to obtain the same initial void ratio for all the samples tested, it can be observed from Table 8-2 that some variations in the initial void ratio do exist, especially for the aged samples. Therefore, the test results are comparable only for those samples which have the same initial void ratio. Despite the slight variation in the initial void ratio, it can be observed from Figs. 8-36 and 8-37 that the initial and final value of $\overline{A}$ increse with increasing p_f/p_o, thus indicating that the sample will have a larger strain rate under larger p_f/p_o. Due to the variation in the initial void ratio in the samples tested, the effect of p_f/p_o on the initial and final values of $\overline{B}$ is not so obvious. However, for those samples

Table 8-3

Values of creep index and apparent permeability

Sample	$\overline{A}_{bo}$	$\overline{A}_{bf}$	$\overline{B}_{bo}$	$\overline{B}_{bf}$
A2-2-1	2.271×10^{-4}	1.136×10^{-4}	15.0	3.75
A2-2-2	2.429×10^{-4}	1.215×10^{-4}	16.0	8.00
A2-4-1	9.202×10^{-4}	2.301×10^{-4}	13.0	3.25
A2-4-2	3.435×10^{-4}	8.633×10^{-4}	15.0	7.50
A2-8-1	2.793×10^{-3}	3.491×10^{-4}	12.0	4.25
A2-16-1	7.111×10^{-3}	4.480×10^{-4}	15.0	3.75
A3-2-1	2.532×10^{-4}	1.266×10^{-4}	15.0	3.75
A3-2-2	2.451×10^{-4}	1.226×10^{-4}	14.0	3.50
A3-4-1	4.411×10^{-4}	1.103×10^{-4}	16.0	8.00
A3-4-2	3.477×10^{-4}	8.693×10^{-5}	20.0	10.00
A3-8-1	2.545×10^{-3}	3.181×10^{-4}	15.0	5.31
A3-16-1	5.854×10^{-3}	3.688×10^{-4}	15.0	3.75

Table 8-3 (continued)

Values of creep index and apparent permeability

Sample	$\overline{A}_{bo}$	$\overline{A}_{bf}$	$\overline{B}_{bo}$	$\overline{B}_{bf}$
A4-2-1	$2.061\text{x}10^{-4}$	$1.031\text{x}10^{-4}$	15.0	10.61
A4-2-2	$1.867\text{x}10^{-4}$	$9.335\text{x}10^{-5}$	20.0	10.00
A4-4-1	$7.223\text{x}10^{-4}$	$1.806\text{x}10^{-4}$	15.0	3.75
A4-4-2	$4.734\text{x}10^{-3}$	$1.184\text{x}10^{-3}$	16.0	4.00
A4-8-1	$4.505\text{x}10^{-3}$	$5.613\text{x}10^{-3}$	20.0	2.50
R3-2-1	$3.509\text{x}10^{-4}$	$1.755\text{x}10^{-4}$	15.0	3.75
R3-2-2	$5.648\text{x}10^{-4}$	$2.824\text{x}10^{-4}$	15.0	3.75
R3-4-1	$2.100\text{x}10^{-3}$	$5.250\text{x}10^{-4}$	18.0	4.50
R3-4-2	$8.427\text{x}10^{-4}$	$2.107\text{x}10^{-4}$	18.0	4.50
R3-8-1	$4.763\text{x}10^{-3}$	$5.954\text{x}10^{-4}$	16.0	5.66
R3-16-1	$1.039\text{x}10^{-2}$	$6.546\text{x}10^{-4}$	16.0	4.00

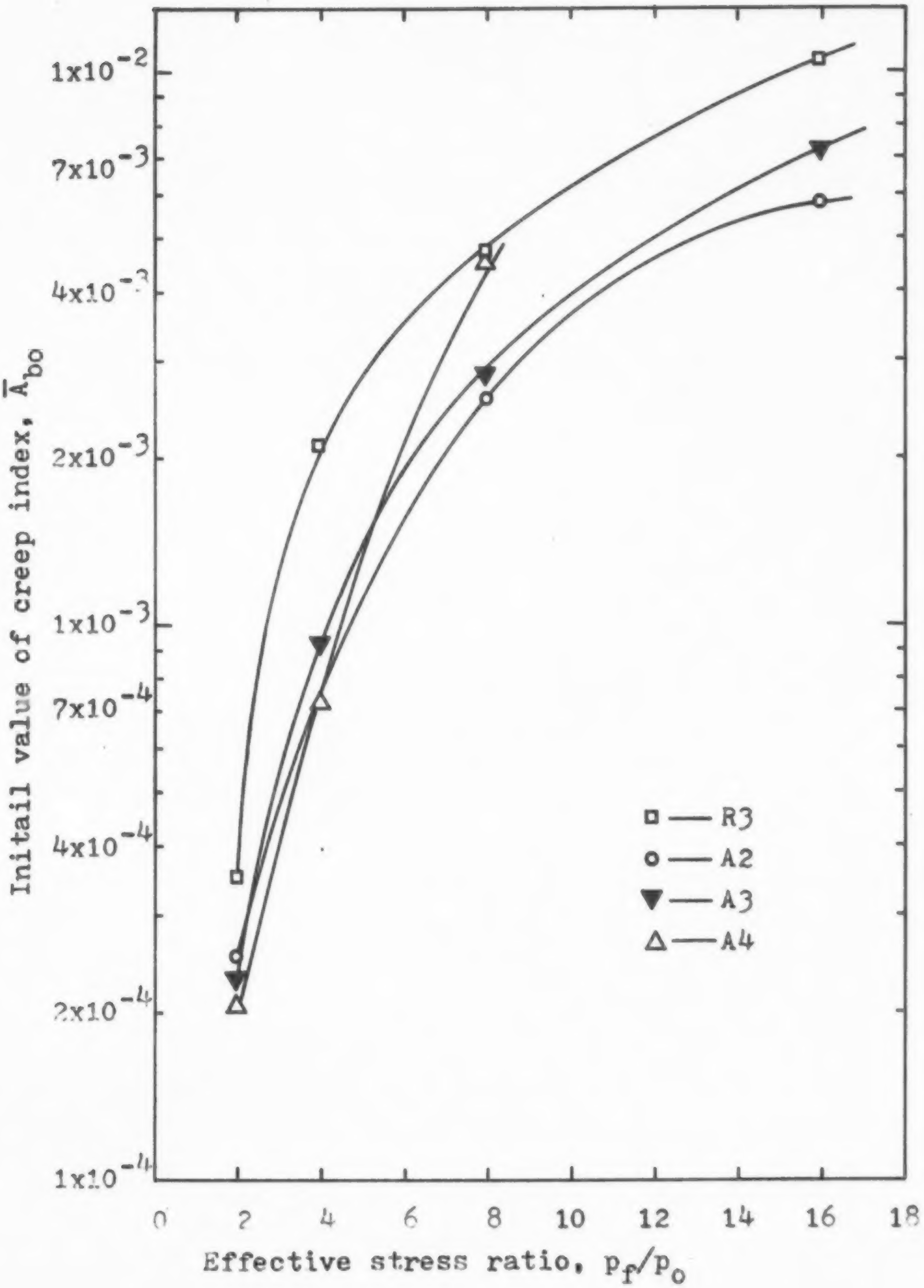

Fig. 8-36. Influence of effective stress ratio on the initial value of creep index

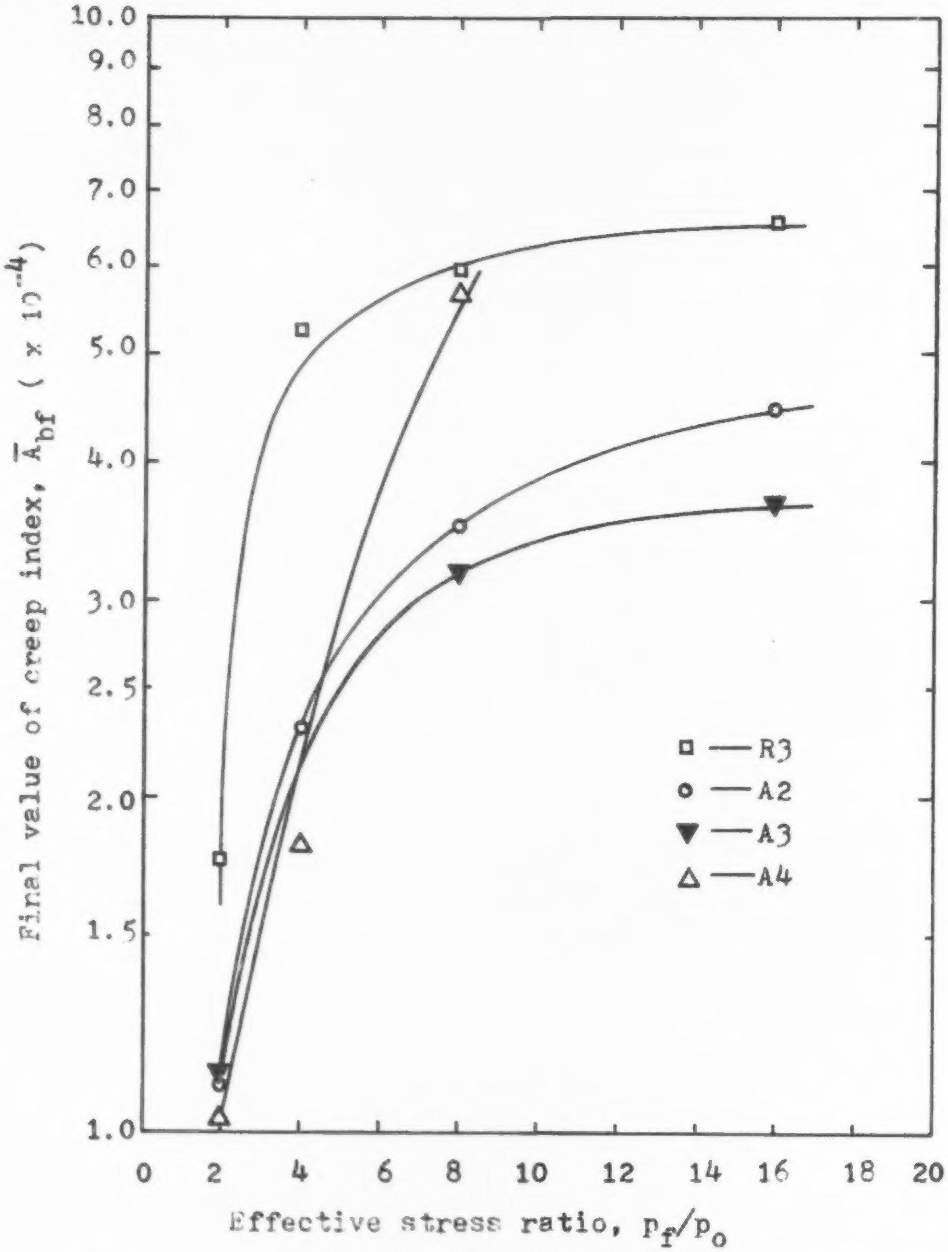

Fig. 8-37. Influence of effective stress ratio on the final value of creep index

that have the same initial void ratio, the test results do indicate that the larger values of $\overline{B}_{bo}$ and $\overline{B}_{bf}$ are associated with larger p_f/p_o. Typical experimental results for raw and laboratory aged milled refuse samples that substantiate the above statements are shown in Figs. 8-38 to 8-40.

There is not enough test data to establish the relationship between the period of aging and the variation in the creep parameters. However, the samples tested can be divided qualitatively into raw and aged samples because these aged samples reached their peak temperature difference at about the same period (30 to 50 days) and had the same aging period (270 to 374 days). For samples that had the same initial void ratio and under same load increment ratio, the aged samples have larger values of $\overline{A}$ and $\overline{B}$ than the raw samples, thus indicating that the aged samples are more susceptible to creep deformation. Some typical experimental results are shown in Fig. 8-41. As one would expect, the strain rate is larger for the aged sample than for the raw sample.

(4) Effect of the rate of decomposition of solid on the consolidation behavior of milled refuse

As a result of the decomposition of milled refuse, the amount of solid itself will be decreased. It has been assumed that such a process can be represented by a uniformly distri-

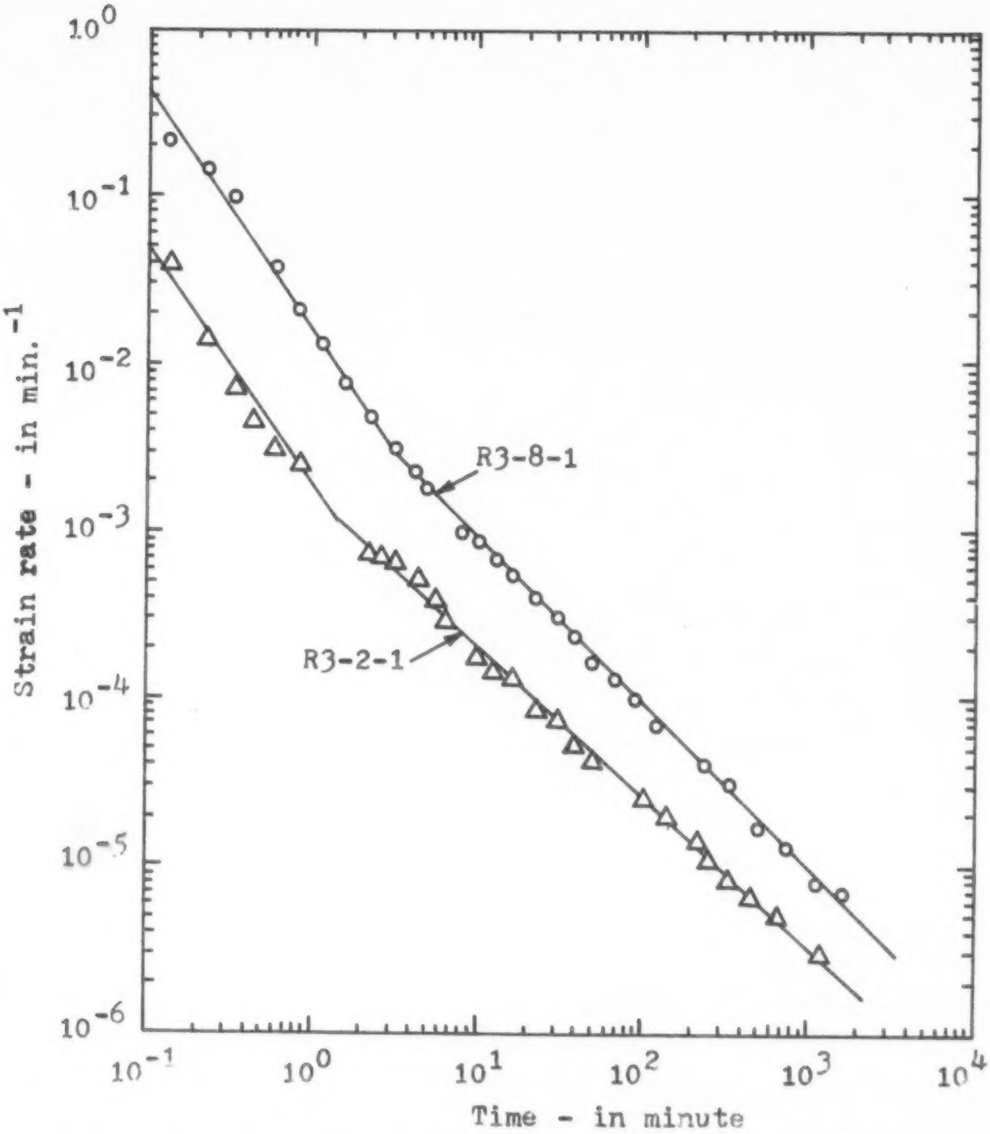

Fig. 8-38. **Influence of effective stress ratio on strain rate for R3 samples**

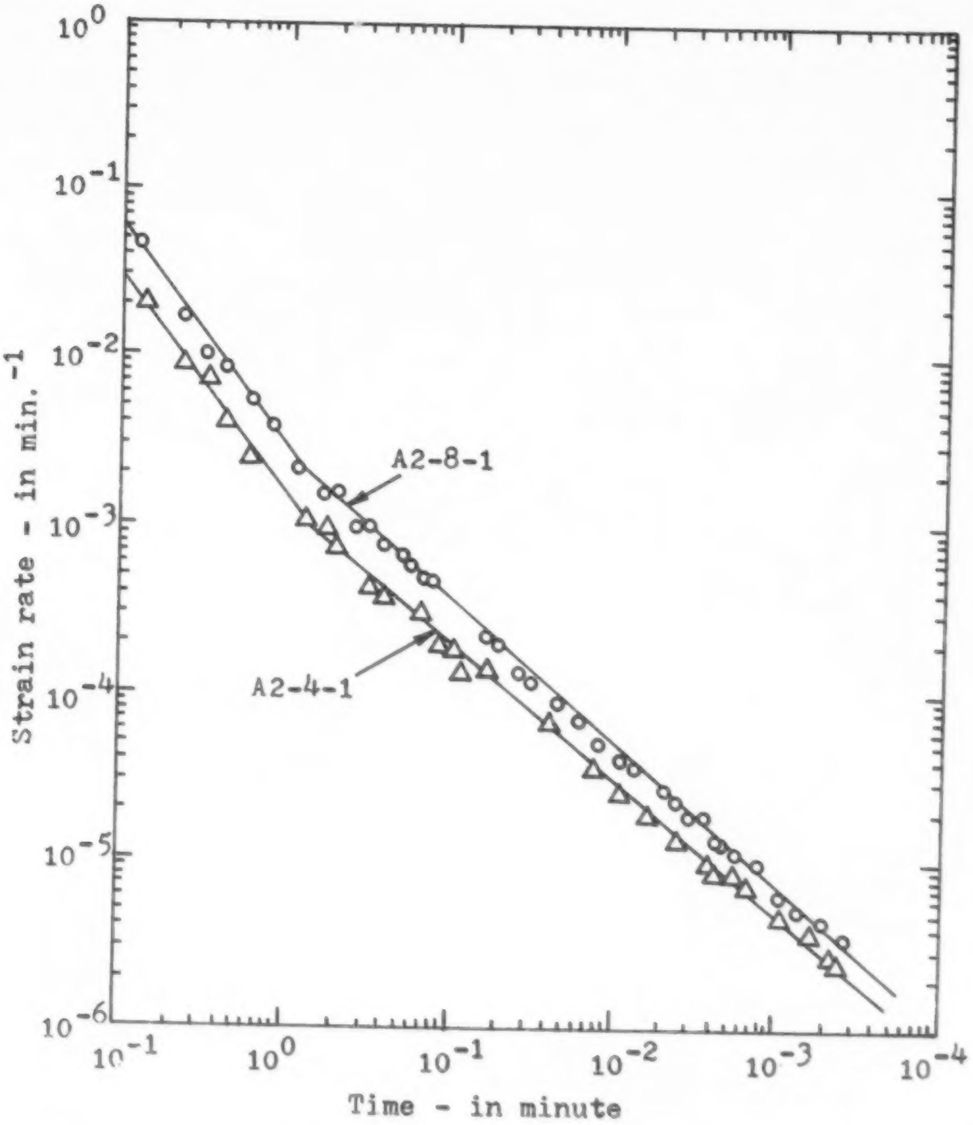

Fig. 8-39. Influence of effective stress ratio on strain rate for A2 samples

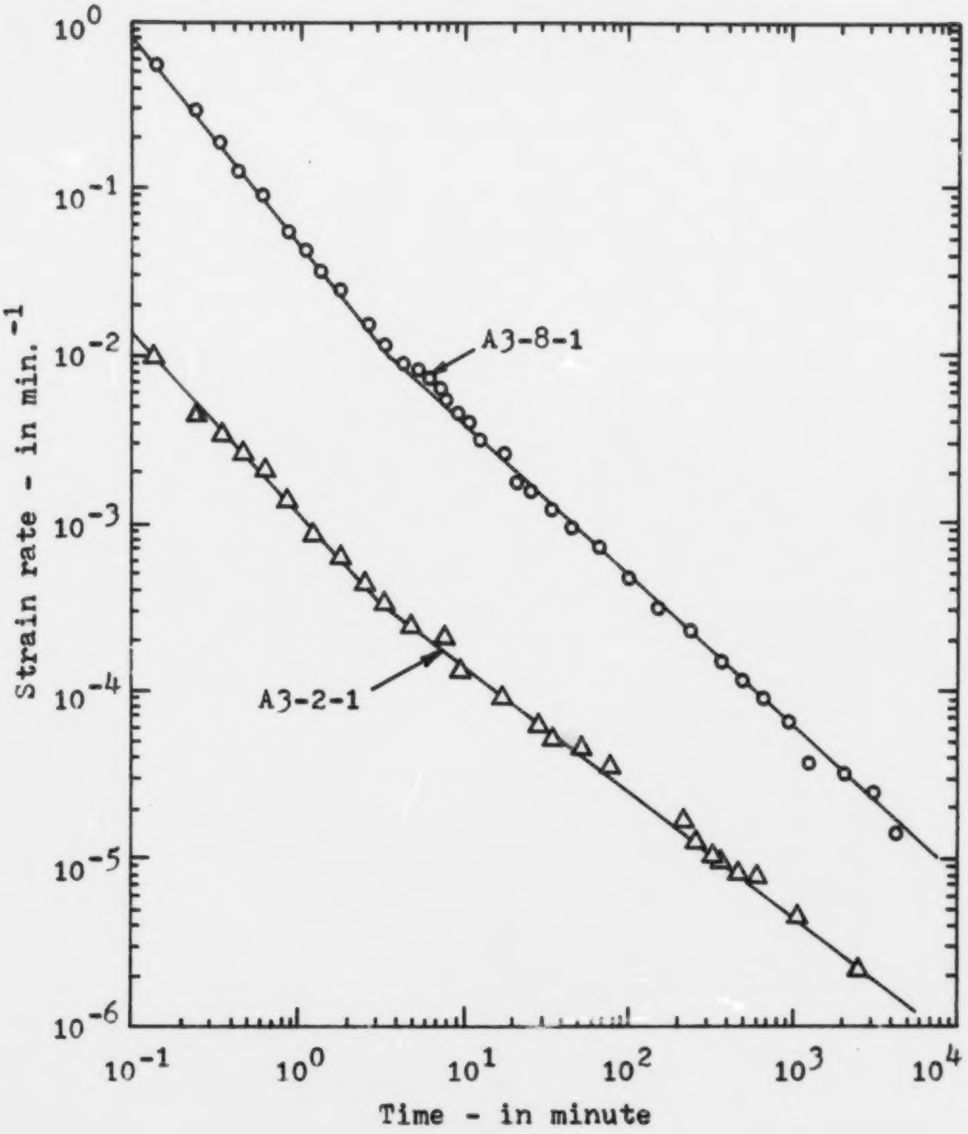

Fig. 8-40. Influence of effective stress ratio on strain rate for A3 samples

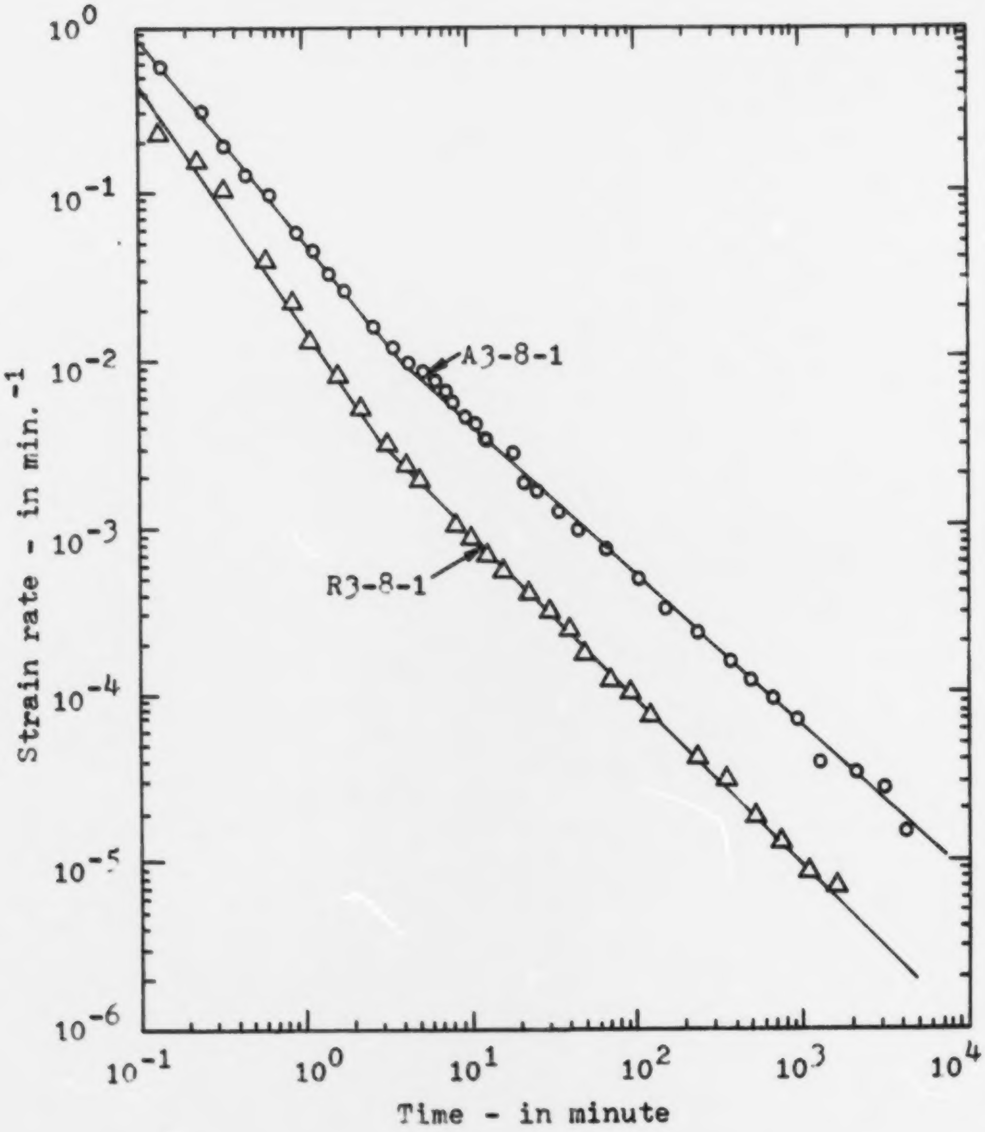

Fig. 8-41. Influence of sample aging on the strain rate

buted sink or source. In order to investigate the influence of the rate of decomposition of solid on the consolidation behavior of milled refuse, a wide range of rate constants has been used. The lower limit of this range is 0.012 /year, which is the carbon reduction rate reported for a sanitary landfill in California (State Water Control Board, State of California, 1965). The upper limit is 0.788 /year which is the rate constant of cellulose reduction obtained from the anaerobic digestion test reported by Chakraverty (1973). These limits represent the extents of rate constants of solid decomposition under comparable conditions reported in the literature. The effect of the rate of decomposition of solid on the consolidation behavior of milled refuse has been investigated by solving the governing partial differential equations by using different values of rate constant. Under the assumptions of fully saturated conditions and a negligible amount of liquid generation, which require that all gases generated go into the solution, it has been observed that the consolidation behavior of milled refuse is insensitive to the value of the rate constant within the range of 0.012 to 0.788 /year, if other factors are kept constant.

Summary

The temperature data obtained from the laboratory aging of milled refuse show that the samples reached their peak temperature within 30 to 50 days after the start of the aging process. The temperature then decreased gradually, indicating that the rate of decomposition of the refuse was decreasing.

Laboratory consolidation test were conducted on raw and laboratory aged milled refuse samples to assess the proposed time-settlement model for milled refuse. The agreement between the experimental results and theoretical curves is seen to be resonably close. Within the limits of the theoretical and experimental studies reported herein, the following conclusions can be advanced:

1. Depending on the value of the load increment ratio, the milled refuse can have diverse types of time-deformation curve.

2. For both raw and laboratory aged milled refuse, a larger amount of secondary compression per unit of total compression is associated with a smaller load increment ratio.

3. For both raw and laboratory aged milled refuse, a larger consolidation creep rate is associated with a larger load increment ratio.

4. Aged milled refuse samples are more susceptible to consolidation creep deformation than the raw milled refuse samples.

5. Under the conditions of full saturation of the sample and negligible amount of liquid generation, and assuming other factors are kept constant, the consolidation

behavior of milled refuse is insensitive to the value of the rate constant of solid decomposition for the range between 0.012 and 0.788 /year.

APPLICABILITY OF THE MODEL

In this chapter the influence on the time-settlement behavior of the degree of saturation and the generation of liquids and gases resulting from decomposition will be described. Limitations and applications of the model and limitations of the experimental program will be discussed.

Effect of The Degree of Saturation

The differential equation of pore pressure dissipation for saturated materials is derived from Darcy's law and the continuity equations for both the solid and liquid phases of the material. An unsaturated material is usually regarded as a three-phase system, i.e., as a mixture of solid phase and two fluid phases f and g, an aqueous **phase** and a gaseous phase. In order to obtain a general pore pressure dissipation equation for such materials, the continuity equation for gaseous phase of the three-phase system must also be considered. This must take into account the compressibility of the gas and its solubility in water. The governing equation resulting from such considerations is usually extremely complicated (Florin, 1961). Because of the complexity of the governing equation, Barden (1965a) subdivided the consolidation process of unsaturated clay into a number of less general treatment, each being relevant to a particular range of degree of saturation.

In the general one-dimensional equation of pore pressure dissipation used in the present study, i.e.

$$\frac{\partial(Se)}{\partial t} = \frac{(1+e_o)^2}{\gamma_w} \frac{\partial}{\partial x}\left(\frac{kS}{1+e} \frac{u}{x}\right) + \frac{(1+e)g}{\gamma_w}\psi^f - \frac{(1+e)g}{\gamma_w} \frac{Se}{G_s}\psi^s, \quad (4\text{-}13)$$

the effect of saturation has been taken into account. Under the assumptions that the degree of saturation is constant with depth and the transmissibility (which is the general coefficient for both saturated and unsaturated flow) is a function of void ratio and degree of saturation, Zimmerman (1972) expanded Equation 4-13 and studied the theoretical effect of degree of saturation on the pore pressure dissipation of milled refuse under load. It was found that if the degree of saturation is below residual saturation (the saturation at which the transmissibility becomes zero and only gas will flow), the rate of settlement will be controlled by the creep behavior of the material under consideration. For cases in which the saturation is greater than the residual value, the pore pressure dissipation is delayed because the presence of gas will reduce the fluid transmissibility of the material. As consolidation proceeds, the excess pore pressure is reduced and the volume of gas will expand. It was also found that this expansion of gas will reduce the transmissibility of the material, thus increasing the pore pressure dissipation time. However, the time-settlement behavior of milled refuse is insensitive to the value of the degree of saturation because primary consolidation of this material lasts only a very short period of time.

No information on the influence of the degree of saturation on the creep behavior of milled refuse is available. However, it is assumed that if the degree of saturation is greater than the residual value, the creep behavior of milled refuse will be insensitive to the saturation value.

Effect of The Generation of Gases And Liquids

When relatively unstable milled refuse is placed in a landfill, decomposition of the organic matter will occur because of chemical and/or biological activities. Oxygen is needed for the respiration of the microorganisms responsible for the decomposition of organic matter. Until the initial gaseous oxygen is consumed, the active organisms will be aerobic with water and carbon dioxide being the primary end products. For the majority of the time, the decomposition process will be anaerobic. In the absence of gaseous oxygen, aerobic organisms succumb. Anaerobic or facultatively anaerobic organisms switch to the oxygen of the organic matter instead. The mechanism of anaerobic fermentation involves two steps: the breakdown of organic matter by anaerobic organisms to organic acids, and the subsequent breakdown of these organic acids to methane and carbon dioxide.

Qualitatively speaking, phase changes accompanying chemical and/or biological activities consist of conversion of solid into liquid and gas. The possibility of these phase changes is recognized by the introduction of the mass generation terms, ψ^{α}, in the left hand side of Equation 4-13. It has been assumed that such a process can be represented as a uniformly distributed sink or source. If the mass generation is important then a constitutive assumption for its space and time dependence is needed. The selection of a particular constitutive expression for the mass generation term is usually determined by physical reasonability and by mathematical convenience. The fact that mass is conserved, i.e., is neither destroyed nor created, requires that

$$\Sigma \, \psi^{\alpha} = 0. \qquad (9\text{-}1)$$

The constitutive assumptions for the mass generation term, ψ^{α}, must satisfy Equation 9-1.

It has been shown in Chapter VIII that the consolidation behavior of milled refuse is relatively insensitive to the decrease of the amount of the solid itself. In terms of volume, the gases generated are much greater than the changes in the liquid and solid phases, and it is expected that the volume change in both the solid and liquid phases is negligable. Another effect of these phase changes is that the physical structure of solid will be affected. This has been shown by the experimental results which indicate that the aged milled refuse samples are more susceptible to creep deformation than the raw samples.

Although considerable effort has been made to collect gas generation data from various solid waste disposal sites, the exact nature of gas production is not known. Assuming a constant rate of gas generation, Zimmerman (1972) studied the influence of bio-chemical gas production during consolidation on the time-settlement behavior of milled refuse. Fig. 9-1 shows that with various constant rates of gas production, the response time of milled refuse is greater with a higher rate of gas generation. The possibility of absorption of gas is realized by introducing the negative

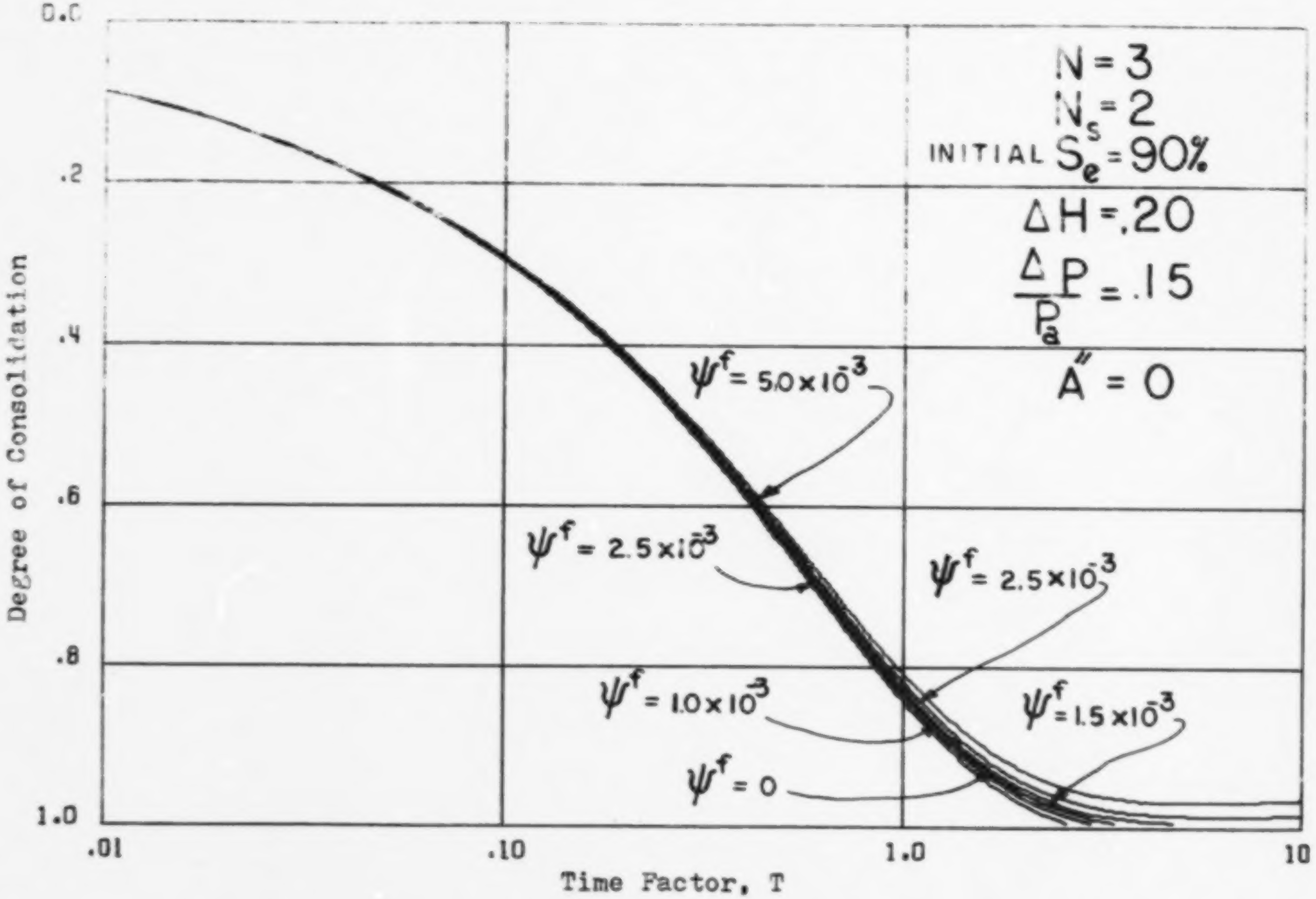

Fig. 9-1. Time-settlement curves showing the effect of biological and/or chemical activity (After Zimmerman, 1972)

rate of gas generation. As would be expected, the negative rate of gas generation tends to speed the consolidation.

The effect of gas generation on the effective saturation of milled refuse is shown in Fig. 9-2. It can be observed that the effective saturation decreases with an increasing rate of gas generation. Therefore, the consolidation duration increases as does the rate of gas production. On the other hand, if absorption of gas take place the effective saturation decreases initially but then increases, and the duration of consolidation will be less than if no absorption occurs.

Limitations of The Model And The Test Program

The physical laws, i.e. e - log p, e - log k, and the creep law, used in Equations 4-20 and 4-25 are currently believed to be the best available for describing the time-settlement behavior of milled refuse. However, it should be recognized that some or all of them may have to be modified or replaced as more experimental evidence becomes available. The assumption that the rate process function is an acceptable creep law for milled refuse implies that the consolidation creep of milled refuse is an activated process. Thus if identical samples are subjected to creep tests under the same stress intensity but at different temperatures, then there should be a linear variation of ln $(\dot{\epsilon}/T)$ with $1/T$, the curve having a slope of $-E/R$

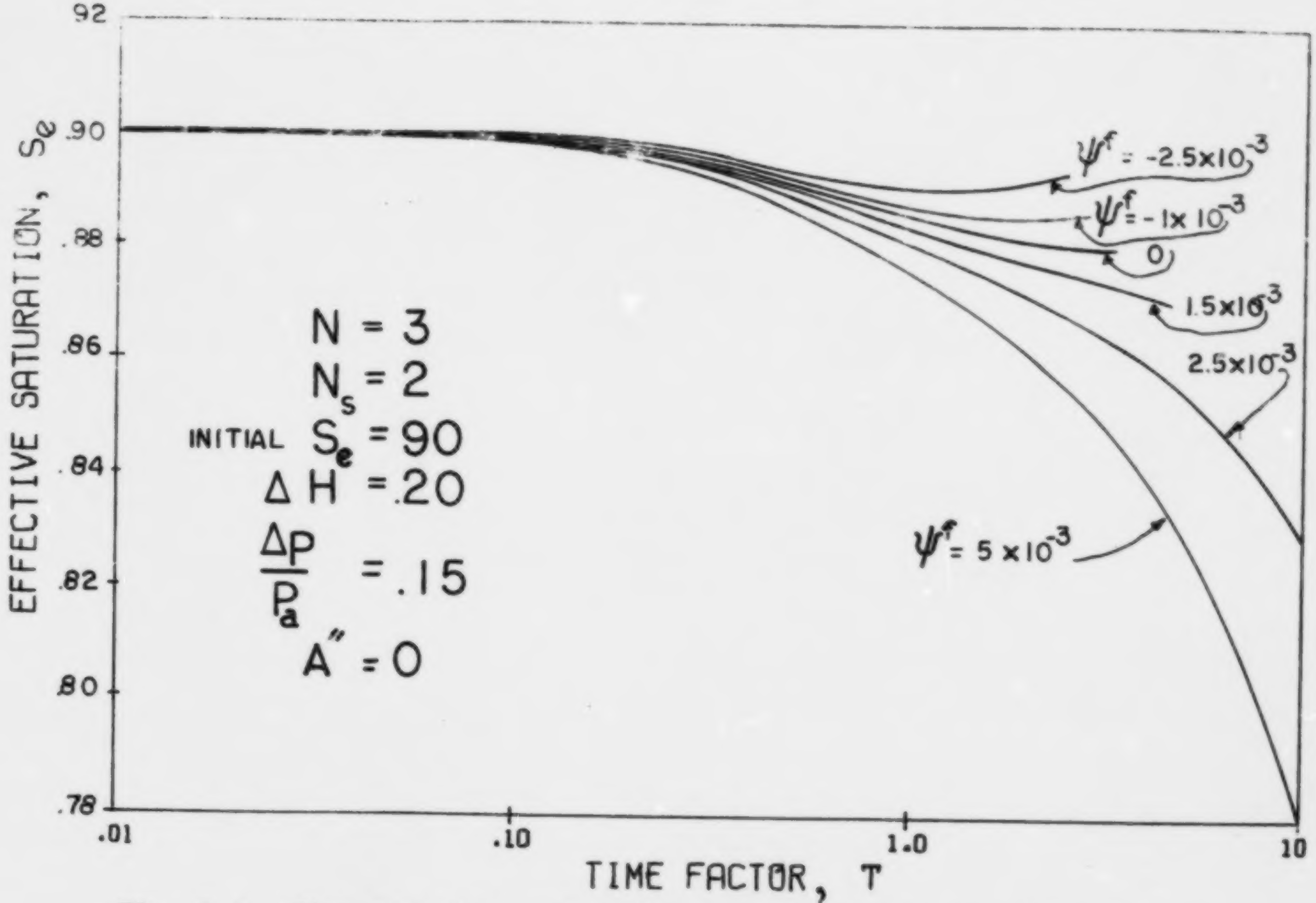

Fig. 9-2. Time-effective saturation curves showing the effect of the biological and/or chemical activity (After Zimmerman, 1972)

(Mitchell, 1968). Here, T is the absolute temperature, E is experimental activation energy, and R is the universal gas constant. Although no experimental results are presently available to support the postulate that the consolidation creep of milled refuse can be treated as a thermally activated process, it is expected that the strain rate will increases with increasing temperature. Therefore, the creep equation and its solutions presented in this study cannot generally be applied to problems in which considerable temperature variation is involved.

In the present study, only laboratory tests on thin samples with short drainage paths have been considered. In order to extrapolate the laboratory tests to the field scale, one has to consider sample thickness much larger than that in the laboratory. The sample thickness can easily be taken into account if one works in terms of time factor instead of actual time. Fig. 9-3 shows the strain versus log time plot for sample R3-16-1. For the same value of p_f/p_o and of the rheological parameters, but different sample thickness, the primary consolidation for thin and thick samples merge onto the same basic creep line. This mode of behavior was first postulated by Taylor (1942). One has to take the effect of sample thickness into account when considering the time-settlement behavior of milled refuse at the field scale. The effect is that for a thick sample a much greater proportion of secondary compression take place during the

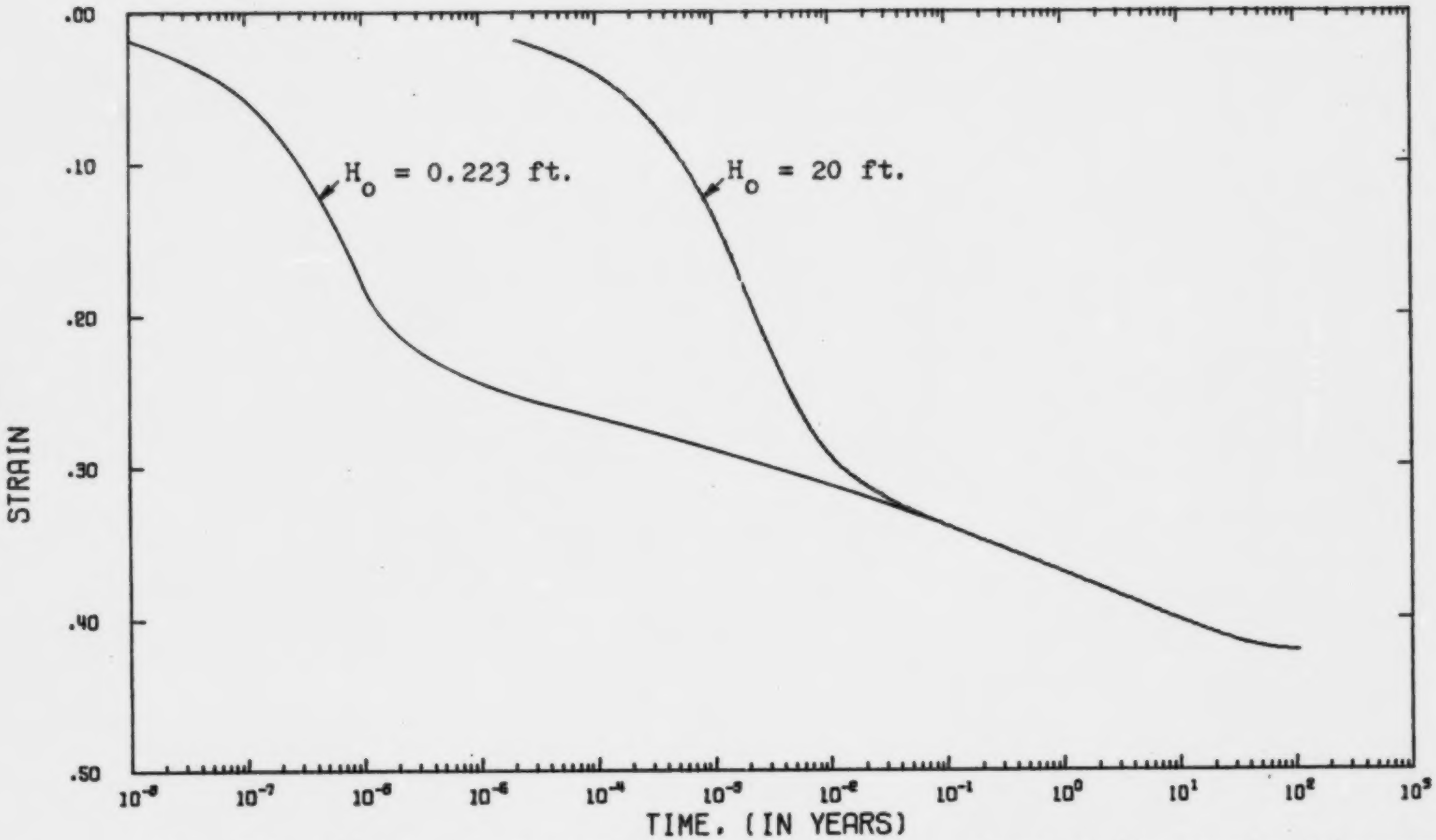

Fig. 9-3. Strain vs. log time plot showing the effect of the sample thickness

primary stage than for a thin sample. It is possible that all quantatively significant secondary compression can occur during the primary stage if the sample is extremely thick.

The effect of the degree of saturation and the rate of generation of gases on the consolidation creep behavior of milled refuse is not known. It has been assumed that if the degree of saturation of the refuse is greater than the residual value then the consolidation creep behavior of milled refuse is insensitive to its saturation value. Milled refuse in the solid waste disposal sites is usually not fully saturated. From the discussion given in the previous section, it is expected that the actual response time for the pore pressure at the field scale will be larger than that predicted by the model.

The laboratory aged samples tested in this study were aged in an insulated chamber with temperature maintained at 125 ± 1 F by thermostat. The details of the sample aging have been described in Chapter VI. Although the laboratory aging condition is quite different from the field environmental conditions. It is believed that the study and analysis of laboratory aged samples are qualitatively applicable to field problems. However, it should be noted that the direct verification of the application of such work to actual field problems has not been done.

Practical Applications

This section includes an illustration of practical applications of the theoretical model to predict the time-settlement behavior of a hypothetical milled refuse landfill with a thickness of 20 ft. and with drainage permitted at the top only. Before attempting to predict its time-settlement behavior, it is necessary to obtain undisturbed samples at the center of the landfill and test these samples according to the procedures outlined in Chapter VI. It is assumed that the effective vertical pressure on the undisturbed sample is increased from 144 psf to 2304 psf as a result of the external applied load. The consolidation test result along with the characteristics of the undisturbed sample are shown in Fig. 8-12.

To evaluate the rheological parameters of the sample, it is necessary to fit the secondary compression curve to the basic creep lines presented in Appendix D. The rheological parameters for the sample tested can be obtained by applying the procedures outlined in Chapter VII; the results are shown in Appendix C (sample R3-16-1)(Chen). The theoretical prediction of the time-settlement behavior of the hypothetical refuse landfill is then obtained by using these parameters as input data for the computer program COMBINE which solves the two governing nonlinear consolidation equations. The only quantity which is different is the thickness of the landfill, which is 20 ft. now instead of 0.223 ft. The theoretical result is shown as the strain versus log time plot in Fig. 9-3. The time for pore pressure dissipation is found to be in the vicinity of one week and the time required to reach 40 percent strain is about one year.

Summary

Theoretical study indicates that for milled refuse with a saturation greater than the residual value, the response time of pore pressure dissipation increases with decreasing degree of saturation. A positive rate of gas generation tends to increase the time required for settlement while a negative rate (absorption of gas) tends to speed consolidation. It has been observed that the creep equation and its solutions proposed herein can not generally be applicable to problems in which considerable variation of temperature is involved. This is because the fact that the rate process function has been assumed in the formulation implies that the consolidation creep behavior of milled refuse is an activated process.

SIMPLIFIED METHOD OF ANALYSIS

Some of the earlier proposed simplified creep expressions for clay and peat are described in this chapter. A simplified method which is convenient for practical use to predict the time-settlement behavior of milled refuse will also be described.

Simplified Creep Expressions

In an attempt to describe the rates of one-dimensional consolidation for peats, Wilson (1965) proposed a simple relation

$$\frac{de}{dt} = C_k t^{m_k} \tag{10-1}$$

where C_k and m_k are experimental parameters obtained from the log (de/dt) versus log time plot. This relation was developed from the K_o effective stress ratio associated with the oedometer.

It has been observed that the three most important factors affecting the consolidation characteristics of peat are sample thickness (H), stress intensity (p), and initial void ratio (e_o). Other factors such as temperature and atmospheric pressure also have an effect but a lesser one.

In order to evaluate the individual effect of sample height (H), stress intensity (p), and initial void ratio (e_o) on the consolidation characteristics of peat, Wilson conducted three series of tests with each of the three parameters individually varied. Only one load increment was applied to each sample in all the tests. The results are shown in Fig. 10-1 in a log (de/dt) - log t plot.

Fig. 10-1 shows that when the test results are presented in this form, two tangents to a short arc are produced. This indicates that after some time has elapsed following loading, a significant change in the rates of consolidation occurs. The initial tangent is analogous to the primary consolidation and the final tangent is analogous to the secondary consolidation. The rates of consolidation in both the primary and the secondary stages are affected by the sample height (H) and the stress intensity (p). The initial void ratio (e_o) affects the rates of consolidation to some extent in the primary stage but has negligible effect on the secondary stage. It is apparent that the consolidation characteristics of peat can be described in analytical terms by the use of Equation 10-1.

The relationship shown in Fig. 10-1 indicates that the consolidation characteristics of peat can also be described by graphical means. It is possible to construct nomographs to determine the void ratio of peat during the tests. Fig. 10-2 shows such a nomograph which is constructed on the

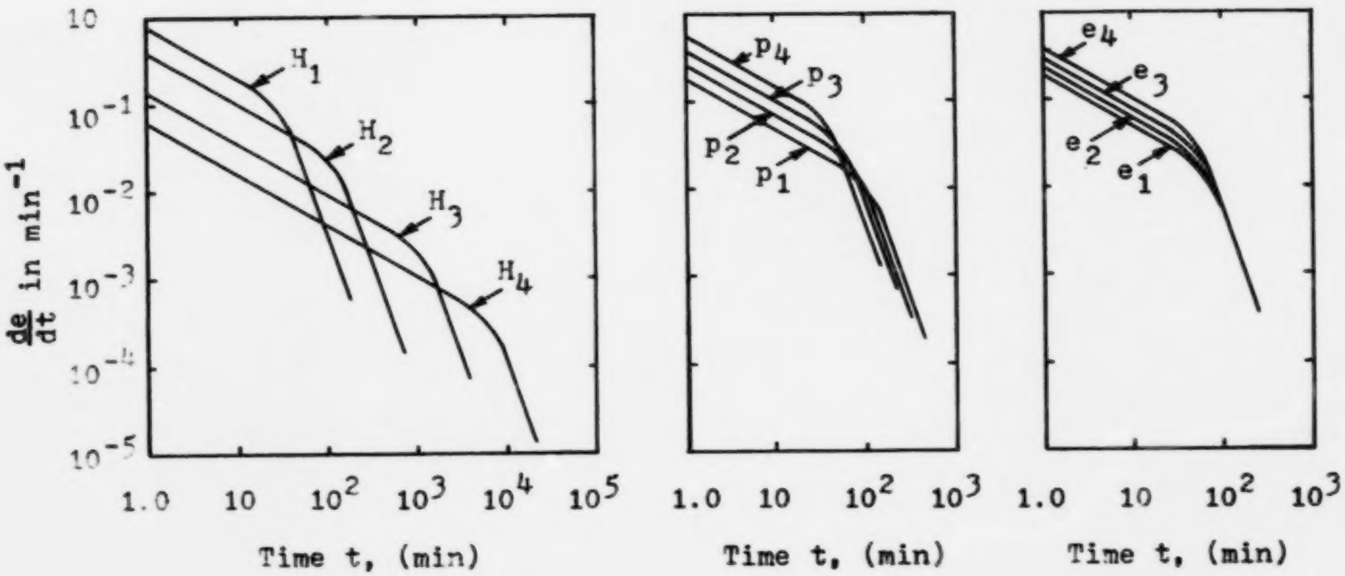

Fig. 10-1. Log (de/dt) versus log time graphs for individual variations of H, p, and e_o (After Wilson, 1965)

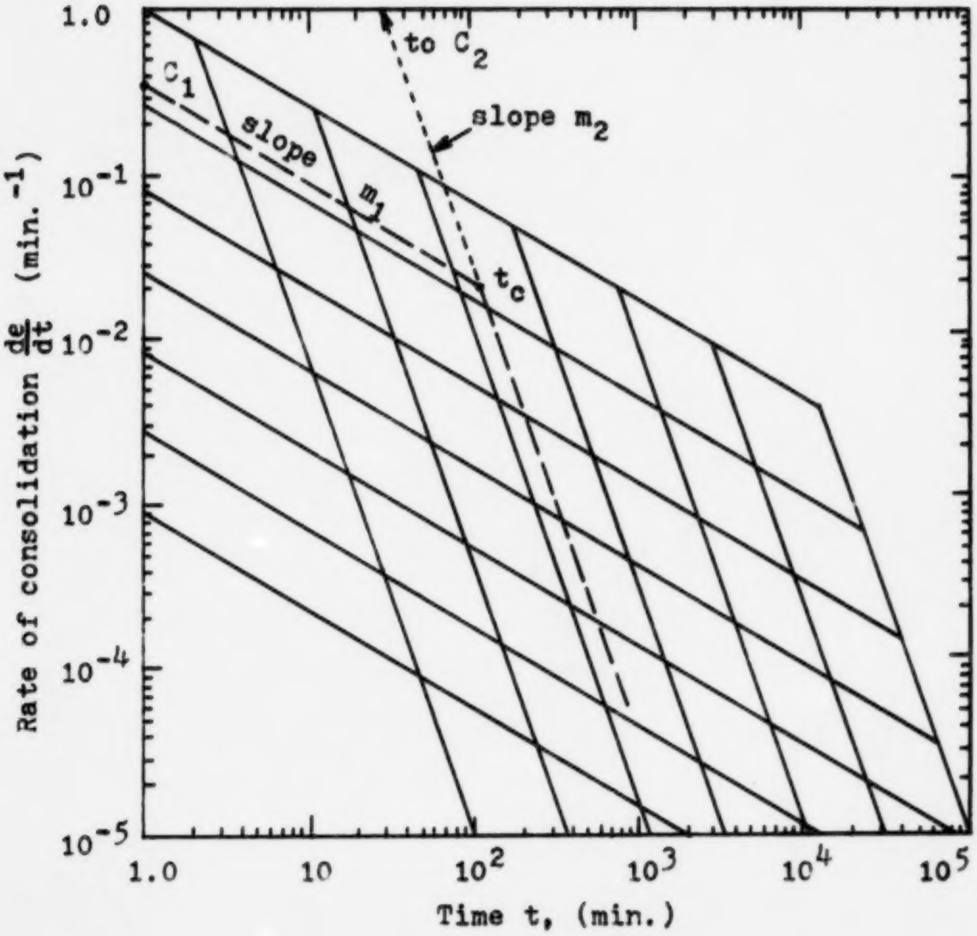

Fig. 10-2. Nomograph for settlement predictions (After Wilson, 1965)

log (de/dt) - log t axes in a manner similar to Fig. 10-1. Since the slopes of the primary and secondary stages of consolidation remain essentially constant for variations of any one of the three parameters (H, p, and e_o), two series of lines can be drawn to represent these tangents. For a sample of a particular height, the value of C_1 (the rate of consolidation when t = 1 minute for the present case) and t_c (the time to the significant change in the rate of consolidation) can be obtained. From the nomograph (Fig. 10-2) the dotted line that relates the rate of consolidation to the elapsed time from loading for this particular sample can be determined. This nomograph has been drawn to show the influence of sample height (H) on rates of consolidation (de/dt) with constant values of stress intensity (p) and initial void ratio (e_o). Similar nomographs can be drawn to show the influence of stress intensity and initial void ratio on rates of consolidation with other parameters held constant.

Singh (1968) proposed for clay soils a stress-strain-time function of the form

$$\dot{\epsilon} = Ae^{\alpha D}\left(\frac{t_1}{t}\right)^{m_n} \qquad (10\text{-}2)$$

where A = projected value of strain rate, at zero
deviator stress, on the plot of the

logarithm of strain rate at unit time versus deviator stress;

α = the slope of the mid-range linear portion of the curve of logarithm of strain rate versus deviator stress;

D = maximum principal stress difference, $(\sigma_1 - \sigma_3)$,

t_1 = unit time;

t = any time; and

m_n = slope of the straight line fitted to the plot of logarithm of strain rate versus logarithm of time.

The same basic form of relationship is applicable for the first application of shear stress irrespective of whether the clays are undisturbed or remolded, wet or dry, normally consolidated or overconsolidated, tested drained or undrained. The superposition technique can be used to describe the creep behavior of clay for a succession of load increments. Equation 10-2 can account for both linear and nonlinear relationships between strain and logarithm of time and is, therefore, more general than Equation 10-1.

Simplified Method

It has been observed that for both raw and laboratory aged milled refuse a bilinear relationship is a good approximation of the logarithm of strain versus logarithm of time plot. One set of typical results is shown in Fig. 10-3 for sample R3-4-1. This shows that after some time, t_c, has elapsed following loading, a significant change in the rates of consolidation occurs. The straight line with slope m_1 represents the primary stage and the one with slope m_2 represents the secondary stage. These straight lines can be represented mathematically by the same general relationship proposed by Wilson. The primary and secondary stages can, therefore, be expressed by

$$\log\left(\frac{d\epsilon}{dt}\right) = \log t^{m_1} + \log C_1 \quad \text{or} \quad \frac{d\epsilon}{dt} = C_1 t^{m_1} \qquad (10\text{-}3)$$

$$\log\left(\frac{d\epsilon}{dt}\right) = \log t^{m_2} + \log C_2 \quad \text{or} \quad \frac{d\epsilon}{dt} = C_2 t^{m_2} \qquad (10\text{-}4)$$

where m_1, C_1 and m_2, C_2 are the slope of the straight line and the intercept on the $(d\epsilon/dt)$ axis, when $t = 0.1$ minute, for the primary and secondary stage respectively. The total change in strain for any time interval can then be obtained by integrating Equations 10-3 and 10-4.

The parameters m_1, C_1, m_2, C_2, and t_c for the samples tested can be obtained by applying the procedures outlined in the above paragraph; the results are summarized in Table 10-1. The time to significant change in the rate of consolidation, t_c, which is arbitrarily taken as an indication of the termination of the primary stage of consolidation,

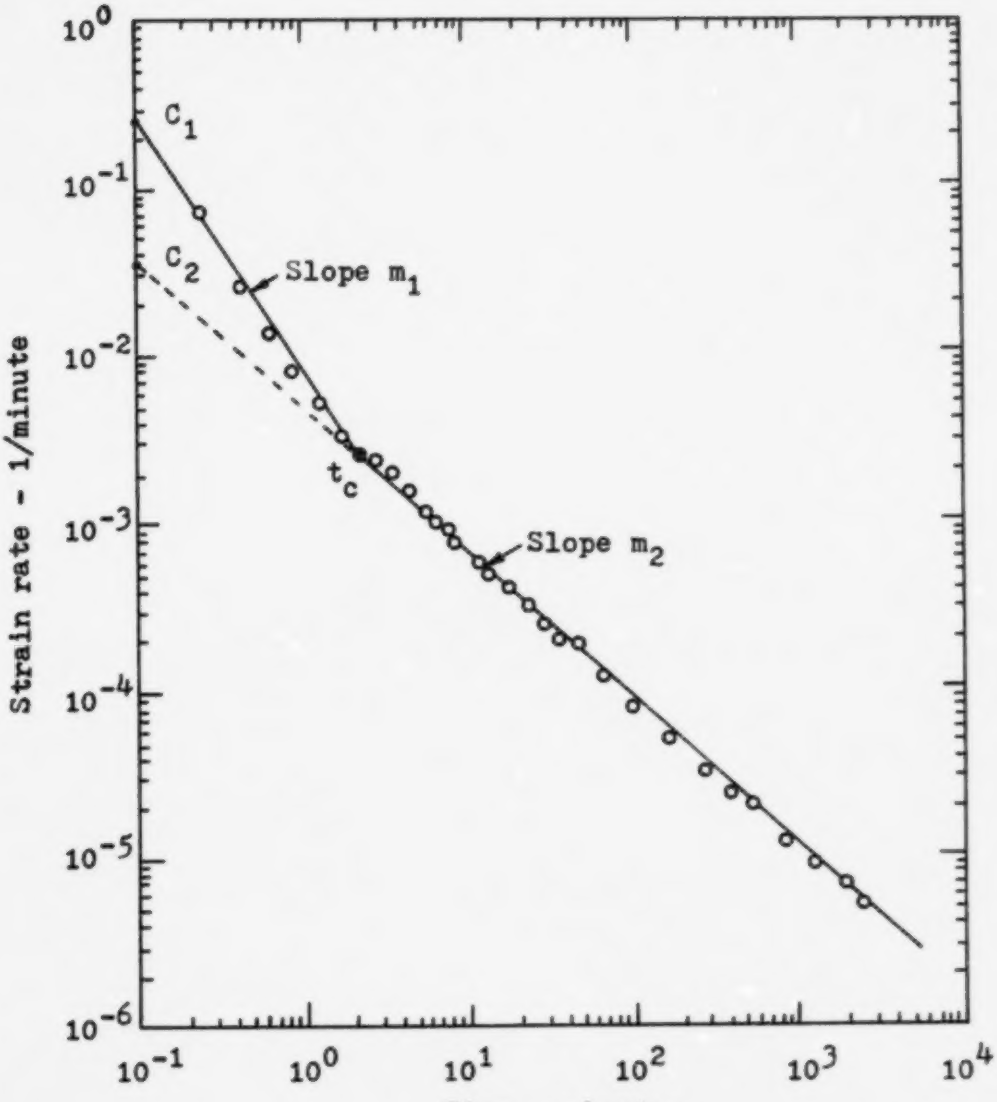

Fig. 10-3. Log strain rate versus log time plot of sample R3-4-1

varies from 1.1 to 3.0 minutes. This shows encouraging agreement with the experimental pore pressure dissipation time of about one minute. Although a bilinear relationship is a good representation of the logarithm of strain rate versus logarithm of time plot for both peats and milled refuse, it can be observed from Fig. 10-1 and Table 10-1 that for peats m_2 is greater than m_1 while for both raw and aged milled refuse samples m_2 is always smaller than m_1. This is believed to be due to the more rapid change in permeability of milled refuse, even under constant load, than that of peat. Although the secondary stage of consolidation can be approximated reasonably well by a linear relationship between logarithm of strain rate and logarithm of time that extends indefinitely, it should be realized that consolidation must ultimately cease.

As pointed out in Chapter VIII, in spite of considerable effort made to obtain the same initial test conditions for all samples tested, some variations in the initial void ratio and sample height do exist, especially for the aged samples. Therefore, the test results can be analyzed by the simplified method only for those samples which have comparable test conditions. Figs. 8-38 to 8-40 shown in Chapter VIII can be used to show the influence of the stress intensity on rates of consolidation with values of sample height and initial void ratio held constant. Although these figures have been given only for two different values

Table 10-1

Values of parameters for simplified method

Sample	C_1	C_2	m_1	m_2	t_c (min.)	e_o	H_o (ft)
A2-2-1	$1.6\text{x}10^{-1}$	$2.8\text{x}10^{-2}$	-1.256	-0.713	2.5	2.858	0.142
A2-2-2	$3.0\text{x}10^{-1}$	$1.0\text{x}10^{-1}$	-1.212	-0.824	1.5	2.433	0.136
A2-4-1	$3.0\text{x}10^{-2}$	$5.7\text{x}10^{-3}$	-1.401	-0.767	1.5	2.498	0.140
A2-4-2	$5.4\text{x}10^{-2}$	$2.8\text{x}10^{-2}$	-1.170	-0.932	1.4	2.228	0.129
A2-8-1	$5.7\text{x}10^{-2}$	$1.6\text{x}10^{-2}$	-1.326	-0.838	1.5	2.495	0.138
A2-16-1	$7.7\text{x}10^{-2}$	$4.6\text{x}10^{-2}$	-1.401	-0.948	1.2	2.035	0.129
A3-2-1	$1.5\text{x}10^{-2}$	$4.9\text{x}10^{-3}$	-1.129	-0.767	2.0	2.543	0.216
A3-2-2	$6.0\text{x}10^{-3}$	$3.0\text{x}10^{-3}$	-1.000	-0.726	1.2	2.437	0.208
A3-4-1	$5.0\text{x}10^{-2}$	$1.7\text{x}10^{-2}$	-1.375	-0.982	1.8	2.808	0.230
A3-4-2	$2.0\text{x}10^{-1}$	$5.0\text{x}10^{-2}$	-1.481	-1.017	1.9	2.521	0.213
A3-8-1	$8.0\text{x}10^{-1}$	$2.8\text{x}10^{-1}$	-1.212	-0.916	3.0	2.533	0.216
A3-16-1	$3.0\text{x}10^{-1}$	$4.0\text{x}10^{-2}$	-1.630	-0.965	1.9	2.668	0.223

Table 10-1 (continued)

Values of parameters for simplified method

Sample	C_1	C_2	m_1	m_2	t_c (min.)	e_o	H_o (ft)
A4-2-1	$2.4 x 10^{-2}$	$1.0 x 10^{-2}$	-1.234	-0.884	1.1	2.799	0.305
A4-2-2	$1.8 x 10^{-2}$	$1.4 x 10^{-2}$	-1.035	-0.916	1.2	2.585	0.289
A4-4-1	$3.8 x 10^{-2}$	$1.0 x 10^{-2}$	-1.350	-0.838	1.7	2.652	0.292
A4-4-2	$9.0 x 10^{-2}$	$2.0 x 10^{-2}$	-1.401	-0.853	1.8	2.374	0.270
A4-8-1	$3.0 x 10^{-1}$	$3.2 x 10^{-2}$	-1.802	-0.916	1.2	2.241	0.263
R3-2-1	$4.0 x 10^{-2}$	$1.0 x 10^{-2}$	-1.375	-0.884	1.5	2.511	0.224
R3-2-2	$8.0 x 10^{-2}$	$2.2 x 10^{-2}$	-1.326	-0.838	1.8	2.340	0.213
R3-4-1	$2.5 x 10^{-1}$	$3.8 x 10^{-2}$	-1.538	-0.884	1.7	2.377	0.216
R3-4-2	$3.5 x 10^{-1}$	$8.0 x 10^{-2}$	-1.481	-0.965	1.8	1.820	0.180
R3-8-1	$4.3 x 10^{-1}$	$9.5 x 10^{-2}$	-1.481	-1.000	2.0	2.435	0.219
R3-16-1	$1.2 x 10^{0}$	$7.5 x 10^{-2}$	-1.802	-0.982	2.8	2.485	0.223

of stress intensity, which is not sufficient to establish the comparable relationship, these results are consistent with the relationship outlined in the simplified method. Further research is necessary to verify this and to enable field problems to be analyzed.

Summary

The interpretation of the rheological parameters in the general model is difficult because only limited amounts of consolidation test data on milled refuse are currently available. A simplified method which has been proposed to describe the behavior of peat under load can also be used to describe the consolidation behavior of milled refuse. This method is simple mathematically but involves also five experimental parameters.

SUMMARY, CONCLUSIONS, AND RECOMMENDATIONS

Summary

The research program under which this study was conducted was initiated primarily to develop a means of predicting the time-settlement behavior of a sanitary landfill of milled refuse. In the first stage of the research program, a mathematical model was developed to simulate the time-settlement behavior of milled refuse with the effects of finite deformations, large creep strains, and biological and chemical decomposition of the material being taken into account. The study reported herein consists of the experimental study of the time-settlement behavior of both raw and laboratory aged milled refuse and the modification and refinement of the previously proposed mathematical model.

Because nearly two-thirds of the total milled refuse is cellulose, consideration was given to the micro-structure of cellulose in order to gain some insight into the behavior of milled refuse. This suggests the possibility of a micropore structure being responsible for secondary consolidation effects of such material. Various modifications of the Terzaghi theory of one-dimensional consolidation have been reviewed and the rheological models proposed by various investigators to simulate the consolidation process have been examined. Current concepts of the mechanisms responsible for secondary consolidation have also been discussed. A general equation of continuity based on the theory of mixture, which has found broad applications in the field of soil mechanics, has been described. The time-settlement model proposed by Zimmerman (1972) to simulate the consolidation behavior of milled refuse has been critically reviewed and modified in light of the available laboratory consolidation test data. Parameter studies of two creep models based on structural viscosity and micropore structure have provided information on their behavior which is helpful in choosing the best model to describe the consolidation creep behavior of milled refuse.

The experimental portion of the study consisted of the development of a consolidometer for the consolidation testing of both raw and laboratory aged milled refuse samples under fully saturated conditions. Aging of samples was conducted in an insulated chamber with temperature maintained at 125 F. A total of 23 consolidation tests were conducted on raw and aged refuse samples. Procedures were developed for the determination of rheological parameters from laboratory time-settlement curves, and the agreement between experimental results and theoretical predictions was found to be reasonably close. Limitations of the model and of the experimental program have also been discussed. Finally, a simplified method which is convenient for practical use to predict the time-settlement behavior of milled refuse has been described.

Conclusions

Based on the studies reported herein, the following conclusions can be advanced:

1. Although it was not so described explicitly, a close review of Zimmerman's model shows that the rheological model of the solid skeleton is equivalent to a Kelvin body with a nonlinear spring in series with a nonlinear dashpot, which is described by $d\epsilon/dt = \beta \sinh \alpha\tau$. The parameters α and β of the rate process relation are assumed to be constant. Therefore, for large load increments or large strains this model fails to take into account the actual variation of rheological parameters during the compression.
2. Based on the information derived from the consideration of the micro-structure of cellulose, the permeability characteristics of milled refuse, and the model parameter study, it is found that the creep model based on micropore structure is most relevant to describe the consolidation creep behavior of milled refuse.
3. The general equation of continuity based on the theory of mixture and the creep equation based on the micropore structure give a good and complete

description of the consolidation process of milled refuse.

4. Depending on the value of the load increment ratio, the milled refuse can have diverse types of time-deformation curves.

5. For both raw and laboratory aged milled refuse, a larger amount of secondary compression per unit of total compression is associated with a smaller load increment ratio.

6. For both raw and laboratory aged milled refuse, a larger consolidation creep rate is associated with a larger load increment ratio.

7. Aged milled refuse samples are more susceptible to consolidation creep deformation than raw milled refuse samples.

8. Under the conditions of full saturation of the sample and negligible amounts of liquid generation, and assuming other factors are kept constant, the consolidation behavior of milled refuse is insensitive to the value of the rate constant of solid decomposition for the range between 0.012 and 0.778 /year.

9. The creep equation and its solutions proposed herein are applicable only to problems in which considerable variation of temperature is not involved. This is because the fact that the rate process function has been assumed in the formulation implies that the

consolidation creep behavior of milled refuse is an activated process.

10. The model proposed herein indicates that for the same value of the load increment ratio and of the rheological parameters, but different sample thickness, the primary consolidation for thin and thick samples merge onto the same basic creep line. Thus, for a thick sample a much greater proportion of secondary compression takes place during the primary stage than for a thin sample.

11. A bilinear relationship is a good representation of the logarithm of strain rate versus logarithm of time for both raw and laboratory aged milled refuse. Thus, it is possible to construct nomograms to predict the time-settlement behavior of milled refuse under load. Further research is needed to verify this and to enable field problems to be analyzed.

Recommendations

The theoretical model proposed herein consists not only the effects of large deformation and its influence on the permeability, compressibility, and creep laws but also the effects of the biological and chemical decomposition of the material with accompanying gas and liquid generation. The present study is limited to the cases where the sample is fully saturated and the volume changes in both the liquid phase and solid phase are negligible. The possibility of phase changes is recognized by the introduction of the mass generation term, ψ^{α}, in the governing differential equation. Therefore, a general investigation of the time-settlement behavior of milled refuse must include the constitutive assumption for the space and time dependence of the mass generation terms. The fact that the mass is neither created nor destroyed requires that $\Sigma\psi^{\alpha} = 0$. More comprehenisve studies should be conducted to derive the amount and rate of decomposition of milled refuse in the landfill conditions.

The interpretation of the rheological parameters in the theoretical model is difficult because only a limited amount of consolidation test data on milled refuse is available at the present time. A research program for further study should include an investigation of the influence of decomposition on the permeability characteristics and creep behavior of milled refuse. A more complete experimental program is needed to verify the physical laws assumed in the model, the applicability of the simplified method of analysis, and to enable field problems to be analyzed. A program of field tests of milled refuse landfill is recommended so as to verify the model and the material properties in situ.

REFERENCE

Abbott, M. B., "The One-dimensional Consolidation of Multi-layered Soils," Geotechnique, Vol. 10, No. 4, December 1960, pp. 151-165.

Abbott, M. B., and De Leeuw, E. H., "On the Nonlinear Consolidation of Multi-layered Soils," LGM-Modedelingen, Vol. 10, No. 3, 1966, pp. 57-83.

Acharya, C. N., "Studies in the Anaerobic Decomposition of Plant Materials, IV," Biochem. J., Vol. 29, 1935, pp. 1459-1467.

Adams, J. I., "The Engineering Behavior of a Canadian Muskeg," Proceedings, 6th International Conference on Soil Mechanics and Foundation Engineering, Vol. 1, Canada, 1965, pp. 3-7.

Aldrich, H. P., "Analysis of Foundation Stresses and Settlement At The Hayden Library," Sc.D. Thesis, M.I.T., 1951.

Andersland, O. B., and Laza, R. W., "Permeability of High Ash Papermill Sludge," Journal of the Sanitary Engineering Division, ASCE, Vol. 98, No. SA6, December, 1972, pp. 927-936.

Atkinson, E. B., "The Rheology of Cellulose Derivatives," in Rheology - Theory and Application, Vol. 2, Edited By Eirich, F. R., Academic Press Inc., New York, 1958, pp. 478-492.

Barden, L., and Berry, P. L., "Consolidation of Normally Consolidated Clay," Journal of the Soil Mechanics and Foundations Division, ASCE, Vol. 95, No. SM5, September, 1965, pp. 15-35.

Barden, L., and Berry, P. L., Discussion on "The Analysis of Consolidation By Rate Process Theory," (By Wu et. al., November 1966) Journal of The Soil Mechanics and Foundations Division, ASCE, Vol. 93, No. SM5, September, 1967, pp. 340-344.

Barden, L., "Primary and Secondary Consolidation of Clay and Peat," Geotechnique, Vol. 18, No. 1, March, 1968, pp. 1-24.

Barden, L., "Time Dependent Deformation of Normally Consolidated Clays and Peats," Journal of the Soil Mechanics and Foundations Division, ASCE, Vol. 90, No. SM1, January, 1969, pp. 1-31.

Berry, P. L., and Poskitt, T. J., "The Consolidation of Peats," Geotechnique, Vol. 22, No. 1, March, 1972, pp. 27-52.

Biot, M. A., "Le Problem de la Consolidation des Matieres Argileuses sous une Charge," Annaies de la Societe de Bruxelles, Series B-55, 1935, pp. 110-113.

Biot, M. A., "General Solution of the Equation of Elasticity and Consolidation for a Porous Material," Transaction, Journal of Applied Mechanics, ASME, Vol. 78, 1956, pp. 91-96.

Burmister, D. M., "Strain Rate Behavior of Clay and Organic Soils," Symposium on Time Rates of Loading in Soil Testing, ASTM, (Issued as separation publication, ASTM, STP. No. 254) 1959, pp. 88-105.

Chan, D. B., and Pearson, E. A., "Comprehensive Study of Solid Waste Management - Hydrolysis Rate of Cellulose in Anaerobic Fermentation," Sanitary Engineering Research Laboratory, SERL Report No. 70-3, College of Engineering and School of Public Health, University of California, Berkeley, 1970.

Chen, W. H., Franklin, A. G., and Quon, J. E., "Consolidation of Milled Refuse", Volume 2 - Appendix, M.S. Thesis, Dept. of Civil Engineering, Northwestern University, 1972.

Christian, J. T., and Boehmer, J. W., "Plane Strain Consolidation by Finite Elements," Journal of the Soil Mechanics and Foundations Division, ASCE, Vol. 96, No. SM4, July, 1970, pp. 1435-1457.

Christie, I. F., "A re-appraisal of Merchant's Contribution to the Theory of Consolidation," Geotechnique, Vol. 14, No. 4, December, 1964, pp. 309-320.

Crandall, S. H., "Engineering Analysis, A Survey of Numerical Procedures," New York McGraw-Hill, 1956.

Cross, J. A., and Franklin, W. E., "Market Opportunity for Shredders in Solid Waste Management," MRI Report (Final Report), MRI Project 350 8-D, Midway Research Institute, 1971.

Cryer, C. W., "A Comparison of the Three-dimensional Consolidation Theories of Biot and Terzaghi," Quarterly Journal of Mechanics and Applied Mathematics, Vol. 16, 1963, pp. 401-412.

Davis, E. H., and Raymond, G. P., "A nonlinear Theory of Consolidation," Geotechnique, Vol. 15, No. 2, 1965, pp. 161-173.

Davis, E. H., and Poulos, H. G., "Rate of Settlement Under Two- and Three-dimensional Conditions," Geotechnique, Vol. 22, No. 1, 1972, pp. 95-114.

Davis, R. O., "Numerical Approximation of One-dimensional Consolidation," International Journal for Numerical Methods in Engineering, Vol. 4, 1972, pp. 279-287.

De Jong, J., and Verruijit, A., "Primary and Secondary Consolidation of a Spherical Clay Sample," Proceedings, 6th International Conference on Soil Mechanics and Foundation Engineering, Vol. 1, Canada, 1965, pp. 254-258.

De Jong, J., "Consolidation Models Consisting of an Assembly of Viscous Elements or a Cavity Channel Network," Geotechnique, London, Vol. 18, No. 2, June, 1968, pp. 172-194.

Elnaggar, A. A., "Effect of Non-Darcian Flow on the Time Rate of Consolidation," Ph.D. Dissertation, Department of Civil Engineering, Northwestern University, 1970.

Emerton, E. W., Page, D. H., and Hale, W. H., "Formation and Structure of Paper," (F. Bolam, ed.) Tech. Sect. B. P. & B.M.A., London, 1962, pp. 53-62.

Eyring, H., "Viscosity, Plasticity, and Diffusion as Examples of Absolute Reaction Rates," Journal of Chemical Physics, Vol. 4, 1936, pp. 283-291.

Ewell, R. H., "The Reaction-rate Theory of Viscosity and Some of Its Applications," Journal of Applied Physics, Vol. 9, 1938, pp. 252-269.

Fair, G. M., Geyer, J. C., and Okun, D. A., "Water and Wastewater Engineering, Vol. 2," John Wiley and Sons, Inc., New York, 1968.

Fang, H. Y., "Three-dimensional Consolidation Characteristics of Clays," M.S. Thesis, Department of Civil Engineering, Purdue University, 1956.

Florin, V. A., "Consolidation of Earth Media and Seepage Under Conditions of Variable Porosity and Consideration of the Influence of Bond Water," Izvestiya, Academic of Science, Section of Tech. Science, USSR, No. 11, 1951, pp. 1625-1649.

Ghaboussi, J., and Wilson, E. L., "Flow of Compressible Fluid in Porous Media," International Journal of Numerical Methods in Engineering, Vol. 5, 1973, pp. 419-442.

Gibson, R. E., and Lumb, P., "Numerical Solution of Some Problems in the Consolidation of Clay," Proceedings, Institute of Civil Engineers, Vol. 2, 1953, pp. 182-198.

Gibson, R. E., and Lo, K. Y., "A Theory of Consolidation for Soils Exhibiting Secondary Compression," Acta Polytechnica Scandinavia, 296/1961, Ci 10, (Reprint by Norwegian Geotechnical Institute) 1961.

Gibson, R. E., England, G. L., and Hussey, M. J. L., "The Theory of One-dimensional Consolidation of Saturated Clays," Geotechnique, Vol. 17, No. 3, September, 1967, pp. 261-273.

Glasstone, S., Laidler, K. J., and Eyring, H., "The Theory of Rate Processes," McGraw-Hill Book Company, Inc., New York, 1941.

Golueke, G. G., and McGauhey, P. H., "Comprehensive Studies of Solid Waste Management," First, Second, and Third Reports, EPA Research Grant No. EC-00260, University of California, 1971.

Gupta, S., "Some Engineering Properties of Milled Refuse," M. S. Thesis, Department of Civil Engineering, Northwestern University, 1972.

Gurtin, M., "Variational Principles for Linear Elastodynamics," Arch. Rat. Mech. and Anal. Vol. 16, 1964, pp. 34-50.

Ham, R. K., Porter, W. K., and Reinhardt, J. J., "Refuse Milling for Landfill Disposal, Part One," Public Works, December, Vol. 102, 1971, pp. 42-47.

Ham, R. K., Porter, W. K., and Reinhardt, J. J., "Refuse Milling for Lnadfill Disposal, Part Two," Public Works, January, Vol. 103, 1972, pp. 70-72.

Ham, R. K., Porter, W. K., and Reinhardt, J. J., "Refuse Milling for Landfill Disposal, Part Three," Public Works, February, Vol. 103, 1972, pp. 49-54.

Hanrahan, E. T., "An Investigation of Some Physical Properties of Peat," Geotechnique, Vol. 4, No. 3, 1954, pp. 108-123.

Hansbo, S., "Consolidation of Clay With Special Reference to Influence of Vertical Sand Drains," Proceedings, Swedish Geotechnical Institute, Stockholm, Sweden, No. 18, 1960.

Hartz, K. E., "A Landfill Technique for Pulverized Refuse," Public Works, Vol. 103, 1972, pp. 102-103.

Hungate, R. E., "The Rumen and Its Microbes," Academic Press, New York, 1966.

Hwang, C. T., and Morgenstern, N. R., "On the Solution of Plane Strain Consolidation Problems by Finite Element Methods," Canadian Geotechnical Journal, Vol. 18, 1971, pp. 109-118.

Ishii, Y., General Discussion, Symposium on Consolidation Testing of Soils, ASTM, STP, No. 126, 1951, pp. 103-109.

Janbu, N., "Consolidation of Clay Layers Based on Non-linear Stress-strain," Proceedings, 6th International Conference on Soil Mechanics and Foundation Engineering, Canada, Vol 2, 1965, pp. 83-87.

Klein, S. A., "Anaerobic Digestion of Solid Waste," Compost Science-Journal of Waste Recycling, Vol. 13, 1971, pp. 6-11.

Kubat, J., "Rheology of Paper," in Rheology-theory and applications, Vol. 5, Edited by Eirich, F. R., Academic Press Inc. New York, 1969.

Lambe, T. W., "Soil Testing for Engineers," John Wiley & Sons, Inc., New York, 1954.

Lambe, T. W., "Methods of Estimating Settlement," Journal of the Soil Mechanics and Foundations Division, ASCE, Vol. 90, No. SM5, September, 1964, pp. 43-67.

Lambe, T. W., "Stress Path Method," Journal of the Soil Mechanics and Foundations Division, ASCE, Vol. 93, No. SM6, November, 1967, pp. 309-331.

Lea, N. D., "Note on the Mechanical Properties of Peats," Proceedings, 4th Muskeg Research Conference, National Research Council, Ottawa, Canada, 1958, pp. 53-57.

Leonards, G. A., and Altschaffl, A. G., "Compressibility of Clays," Journal of the Soil Mechanics and Foundations Division, ASCE, Vol. 90, No. SM5, September, 1964, pp. 133-156.

Lowe, J., Zaccheo, P. F., and Feldman, H. S., "Consolidation Testing With Back Pressure," Journal of the Soil Mechanics and Foundations Division, ASCE, Vol. 90, No. SM5, September, 1964, pp. 69-86.

Ludwig, H. F., and Black, R. J., "Report on the Solid Waste Problem," Journal of the Sanitary Engineering Division, ASCE, Vol. 94, No. SA2, April, 1968, pp. 355-370.

Lutz, J. F., and Kemper, W. D., "Intrinsic Permeability of Clay As Affected by Clay Water Interaction," Soil Science, Vol. 88, 1959, pp. 90-93.

MacFarlane, I. C., and Radforth, N. W., "A Study of the Physical Behavior of Peat Derivatives Under Compression," Proceedings, 10th Muskeg Research Conference, National Research Council, Ottawa, Canada, 1965, pp. 159-164.

MacFarlane, I. C., "Muskeg Engineering Handbook," University of Toronto Press, 1968.

Malina Jr., J. F., and Morgan, W., "Refuse Reclamation, and Recycle," Journal of the Sanitary Engineering Division, ASCE, Vol. 98, No. SA6, December, 1972, pp. 819-831.

Mancel, J., "Consolidation des sols (Etude Mathematique)," Geotechnique, Vol. 3, No. 1, September, 1953, pp. 287-299.

McBee, R. H., "The Culture and Physiology of a Thermophilic Cellulose-fermenting Bacterium," Journal of Microbiology, Vol. 5, 1948, pp. 653-663.

McCarty, P. L., "Anaerobic Waste Treatment Fundamental, I. Chemistry and Microbiology," Public Works, Vol. 95, 1964, pp. 107-112.

McGauhey, P. H., "Recycling Versus Waste of Resources," Waste Age, Vol. 1, No. 1, 1970.

McNabb, A., "A Mathematical Treatment of One-dimensional Soil Consolidation," Quarterly Journal of Applied Mathematics, Vol. 27, No. 4, 1960, pp. 337-347.

Merchant, W., "Some Theoretical Consideration on the One-dimensional Consolidation of Clay," M.S. Thesis, M.I.T., 1939.

Merz, R. C., and Stone, R., "Quantitative Study of Gas Produced by Decomposing Refuse," Public Works, Vol. 99, 1968, pp. 86-88.

Miller, R. J., and Low, P. F., "Threshold Gradient for Water Flow in Clay System," Proceedings, Soil Science of America, Vol. 27, No. 6, 1963, pp. 605-609.

Mitchell, J. K., "Shearing Resistence of Soils As A Rate Process," Journal of the Soil Mechanics and Foundations Division, ASCE, Vol. 90, No. SM1, Janyary, 1964, pp. 29-61.

Mitchell, J. K., and Campanella, R. G., "Soil Creep as A Rate Process," Journal of the Soil Mechanics and Foundations Division, ASCE, Vol. 94, No. SM1, January, 1968. pp. 231-253.

Murayama, S., and Shibata, T., "Flow and Stress Relaxation of Clays," IUTAM, Symposium Rheology and Soil Mechanics, Grenoble, France, 1964, pp. 99-129.

Musket, M., "The Flow of Homogeneous Fluids Through Porous Media," Ann Arbor, Michigan, 1946.

Norkrans, B., "Cellulose and Cellulolysis," Advanced Applied Microbiology, Vol. 5, 1967, pp. 91-130.

Ozaydin, I. K., "A Micro-mechanistic Analysis for Creep Response of Kaolin Clay," Ph.D. Dissertation, Department of Civil Engineering, Northwestern University, 1974.

Polkowski, L. B., "Biological Utilization of Cellulose," Proceedings, 17th Industrial Waste Conference, Engineering Bulletin of Purdue University, Extension Service No. 112, 1962, pp. 566-582.

Poskitt, T. J., "The Consolidation of Saturated Clays With Variable Permeability and Compressibility," Geotechnique, Vol. 19, No. 4, 1969, pp. 478-494.

Poskitt, T. J., "The Numerical Solution of Nonlinear Consolidation Problems," International Journal for Numerical Methods in Engineering, Vol. 3, 1971, pp. 5-11.

Poskitt, T. J., and Birdsall, R. O., "A Theoretical and Experimental Investigation of Mildly Nonlinear Consolidation Behavior in Saturated Soil," Canadian Geotechnical Journal, Vol. 8, 1971, pp. 182-216.

State Water Quality Control Board, State of California, Publication No. 31, The Resource Agent, "In-situ Investigation of Movement of Gases Produced from Decomposing Refuse," 1965.

Raats, P. A. C., and Klute, A., "Transport in Soils - The Balance of Mass," Soil Science Society of America, Proceedings, Vol. 32, 1968a, pp. 161-166.

Raats, P. A. C., and Klute, A., "Transport in Soils - the Balance of Momentum," Soil Science Society of America, Proceedings, Vol. 32, 1968b, pp. 452-456.

Raats, P. A. C., and Klute, A., "One-dimensional, Simultaneous Motion of the Aqueous and the Solid Phase of Saturated and Partial Saturated Porous Media," Soil Science, Vol. 107, No. 5, 1969, pp. 329-333.

Reinhardt, J., "A Report on the Demonstration of Gondard Grinding Mill for Pulverizing Refuse and Landfilling Refuse Without Daily Cover," Department of Health, Education and Welfare, Grant No. S-D01-ul-00004, By the City of Madison and University of Wisconsin, 1971.

Rowe, P. W., Discussion on "Consolidation Testing With Back Pressure," By Lowe et. al., September, 1964, Journal of the Soil Mechanics and Foundations Division, ASCE, Vol. 91, No. SM3, March, 1965. pp. 153-153.

Rowe, P. W., and Barden, L., "A New Consolidation Cell," Geotechnique, Vol. 16, No. 2, June, 1966, pp. 162-170.

Rowe, P. W., "Measurement of the Coefficient of Consolidation of Lacustrine Clay," Geotechnique, Vol. 9, No. 3, September, 1959, pp. 107-118.

Saada, A. S., "A Rheological Analysis of Shear and Consolidation of Saturated Clays," Highway Research Board Bulletin, Vol. 342, 1962, pp. 52-65.

Sandhu, R. S., and Wilson, E. L., "Finite-element Analysis of Seepage in Elastic Media," Journal of the Engineering Mechanics Division, ASCE, Vol. 95, No. EM3, June, 1969, pp. 641-653.

Schiffman, R. L., and Gibson, R. E., "Consolidation of Nonhomogeneous Clay Layers," Journal of the Soil Mechanics and Foundations Division, ASCE, Vol. 95, No. SM5, January, 1964, pp. 1-30.

Schiffman, R. L., Ladd, C. C., and Chen, A. T., "The Secondary Consolidation of Clay," IUTAM, Symposium Rheology and Soil Mechanics, Grenoble, France, 1964, pp. 273-304.

Schiffman, R. L., Chen, A. T., and Jordan, J. C., "An Analysis of Consolidation Theories," Journal of the Soil Mechanics and Foundations Division, ASCE, Vol. 95, No. SM1, January, 1969, pp. 285-311.

Schulze, K. L., "Rate of Oxygen Consumption and Respiration Quotients During the Anaerobic Decomposition of Synthetic Garbage," Compost Science, Vol. 1, 1960, pp. 36-40.

Singh, A., and Mitchell, J. K., "A General Stress-Strain-time Function for Soils," Journal of the Soil Mechanics and Foundations Division, ASCE, Vol. 94, No. SM1, January, 1968, pp. 21-46.

Skempton, A. W., and Bjerrum, L., " A Contribution to the Settlement Analysis of Foundation on Clay," Geotechnique, Vol. 7, No. 4, 1957, pp. 168-178.

Skempton, A. W., "Significance of Terzaghi's Concept of Effective Stress," Published in From Theory to Practice in Soil Mechanics, John Wiley & Sons, 1960, pp. 42-53.

Strank, D. W., "Microbiological Utilization of Cellulose and Wood," Canadian Journal of Microbiology, Vol. 2, 1965.

Swartzendruber, D., "Midification of Darcy's Law for the Flow of Water in Soils," Soil Science, Vol. 93, 1962, pp. 81-92.

Tan, T. K., "Onderzoekingen Over de Rheologische van Klei," Thesis, University of Delft, Holland, 1954.

Tan, T. K., "Three-Dimensional Theory on the Consolidation and Flow of Clay Layers," Scientia Sinica, Vol. 6, No. 1, 1957a.

Tan, T. K., Contribution to Discussion, Proceedings, 4th International Conference on Soil Mechanics and Foundation Engineering, Vol. 3, 1957b, pp. 87-88, 110-111, 140-141, 154, and 278-279.

Tan, T. K., "Secondary Time Effect and Consolidation of Clays," Academia Sinica, Institute of Civil Engineering and Architecture, Harbin, China, 1957c.

Tan. T. K., "Determination of Rheological Parameters and the Hardening Coefficients of Clays," Symposium, IUTAM, Rheology and Soil Mechanics, Grenoble, France, 1964, pp. 256-272.

Taylor, D. W., and Merchant, W., "A Theory of Clay Consolidation Accounting for Secondary Compression," Journal of Mathematics and Physics, Vol. 19, No. 3, 1940, pp. 167-185.

Taylor, D. W., "Research on the Consolidation of Clays," Serial 82, M.I.T. Publications, Cambridge, Mass, 1942.

Taylor, H. S., "The Temperature Variation of Diffusion Processes," Journal of Chemical Physics, Vol. 6, 1938, pp. 331-334.

Terzaghi, K., Erdbaumechanick auf Bodenfisikalische Grundlage, Leipzig, Deiticke, 1925.

Terzaghi, K., "Undisturbed Clay Samples and Undisturbed Clays," Journal of Boston Society of Civil Engineers, Vol. 28, No. 3, 1941, pp. 211-231.

Terzaghi, K., "Theoretical Soil Mechanics," McGraw-Hill Book Company, Inc., New York, 1943.

Thompson, W. J., "Some Deformation Characteristics of A Saturated Remoulded Silty Clay," Proceedings, 6th Inter. Conf. On Soil Mechanics and Foundation Engineering, Vol. 1, Canada, 1965, pp. 373-376.

Truesdell, C., and Poupin, R. A., "The Classic Field Theories," Handbuch der Physik, Vol. 3, Springer Verlag, Berlin, 1960, pp. 226-793.

Wahls, H. E., "Analysis of Primary and Secondary Consolidation," Journal of the Soil Mechanics and Foundations Div., ASCE, Vol. 88, No. SM6, December, 1962, pp. 207-231.

Whitman, R. V., Richardson, A. M., and Healy, K. A., "Time-Lags In Pore Pressure Measurements," Proceedings, 5th International Conference on Soil Mechanics and Foundation Engineering, Vol. 1, Paris, France, 1961, pp. 407-411.

Wilkinson, W. L., "Non-Newtonian Fluids," Pergamon Press, 1962.

Wilson, N. E., Radforth, N. W., MacFarlane, I. C., and Lo, M. B., "The Rates of Consolidation For Peats," Proceedings, 6th International Conference on Soil Mechanics and Foundation Engineering, Vol. 1, Canada, 1965, pp. 407-411.

Wu, T. H., Resendiz, D., and Neukirchner, R. J., "The Analysis of Consolidation by Rate Process Theory," Journal of the Soil Mechanics and Foundations Division, ASCE, Vol. 92, No. SM6, November, 1966, pp. 229-248.

Zeevaert, L., "Consolidation Theory for Materials Showing Intergranular Viscosity," Proceedings, 3rd Pan American Conference, Soil Mechanics and Foundation Engineering, Vol. 1, Caracas, Venezuela, 1967, pp. 89-110.

Zimmerman, R. E., "Mathematical Model for Solid Waste Settlement," Ph.D. Dissertation, Department of Civil Engineering, Northwestern University, 1972.

Zoino, W. S., "Settlement of Rubbish Fill, Yellow Freight System Facility - Boston," Paper Presented at Boston Society of Civil Engineers, Geotechnical Forum on Problems of Construction on Rubbish Fill and Peat, Boston, Mass., 1971.

Appendix A

THE NUMERICAL SOLUTION OF THE GOVERNING NONLINEAR PARTIAL DIFFERENTIAL EQUATIONS

The numerical method used to solve the two simultaneous partial differential equations is modified from one developed by Poskitt (1971). The equations to be solved are:

$$\frac{e_o-e_f}{e_{to}-e_{tf}}\,\frac{k_o(1+e_o)^2}{\gamma_w a_{vo}}\,\frac{\partial}{\partial x}\left[\left(\frac{k_f}{k_o}\right)^{\frac{e_o-e}{e_o-e_f}}\left(\frac{p_f}{p_o}\right)^{\frac{e_{to}-e_t}{e_{to}-e_{tf}}}\,\frac{\partial e_t}{\partial x}\right]$$

$$+\frac{e\phi_o C}{\gamma_w G_s}\exp(-Ct) = -\frac{\partial e}{\partial t} \qquad (4\text{-}20)$$

and

$$A_o p_o(1+e_o)\left(\frac{p_f}{p_o}\right)^{\frac{e_{bo}-e_b}{e_{bo}-e_{bf}}}\left\{\sinh\frac{B_o\left(\frac{B_f}{B_o}\right)^{\frac{e_{bo}-e_b}{e_{bo}-e_{bf}}}}{\left(\frac{p_f}{p_o}-1\right)}\left[\left(\frac{p_f}{p_o}\right)^{\frac{e_{to}-e_t}{e_{to}-e_{tf}}}\right.\right.$$

$$\left.\left.-\left(\frac{p_f}{p_o}\right)^{\frac{e_{bo}-e_b}{e_{bo}-e_{bf}}}\right]\right\} = -\frac{\partial e_b}{\partial t}\ . \qquad (4\text{-}25)$$

The definition of strain has been given in Equation 7-1, i.e.

$$\varepsilon_t = \frac{e_{to} - e_t}{1+e_o} \text{, and } \varepsilon_{bf} = \frac{e_{bo} - e_{bf}}{1+e_o} . \tag{7-1}$$

Instead of working in terms of actual strain it is convenient to work in terms of relative strain, defined by

$$W = \frac{\varepsilon_t}{\varepsilon_{tf}} , \qquad V = \frac{\varepsilon_b}{\varepsilon_{bf}} . \tag{A-1}$$

Also define

$$R = \frac{k_o(1+e_o)}{\gamma_w a_{vo} H_o^2 A_o F_o} , \quad T = \frac{k_o(1+e_o)t}{\gamma_w a_{vo} H_o} = T_f \cdot t$$

$$z = \frac{x}{H_o} \text{ , and } N = \frac{\varepsilon_{bf}}{\varepsilon_f} . \tag{A-2}$$

Equations 4-20 and 4-25 can be expressed in the following concise form:

$$\frac{\partial V}{\partial T} = Q \tag{A-3}$$

and $$\frac{\partial W}{\partial T} = F, \tag{A-4}$$

with the use of

$$P = \frac{1}{(1-N)} \frac{\left(\frac{k_f}{k_o}\right)^{(1-N)W+NV} \left(\frac{p_f}{p_o}\right)^{W}}{1-\varepsilon_f((1-N)W+NV)} , \tag{A-5a}$$

$$Q = \frac{(\frac{p_f}{p_o} - 1)}{R_{bf}} (\frac{A_f}{A_o})^V \sinh\left\{ \frac{B_o}{(\frac{p_f}{p_o} - 1)} (\frac{B_f}{B_o})^V \left[(\frac{p_f}{p_o})^W - (\frac{p_f}{p_o})^V \right] \right\}, \qquad \text{(A-5b)}$$

$$F = \frac{\partial}{\partial z}(P\frac{\partial W}{\partial z}) - \frac{N}{1-N} Q + P_h , \qquad \text{(A-5c)}$$

$$P_h = \left[(\frac{e_o}{1+e_o}) - \varepsilon_f((1-N)W+NV) \right] \frac{\phi_o}{G_s \gamma_w \varepsilon_{tf}} \exp(-C\frac{T}{T_f}). \qquad \text{(A-5d)}$$

For the standard case of an oedometer sample contained between an impermeable surface at one end and a freely drained surface at the other end, the boundary conditions for W and V are shown in Figs. A-1a and A-1b. The time-space grid used for the study is shown in Fig. A-2. The z axis is taken with its origin at the impervious boundary.

Several numerical methods, both implicit (Abbott, 1960, 1961) and explicit (Gibson, 1953) can be used to obtain solutions to Equations A-3 and A-4. Here, a general form of the implicit method (Crandall, 1956) will be used for approximating the time derivatives. Equations A-3 and A-4 can be written in finite difference form

$$W_{i,k+1} = W_{i,k} + 0.5\,\Delta T F_{i,k} + 0.5\,\Delta T F_{i,k+1} , \qquad \text{(A-6)}$$

$$V_{i,k+1} = V_{i,k} + 0.5\,\Delta T Q_{i,k} + 0.5\,\Delta T Q_{i,k+1} ; \qquad \text{(A-7)}$$

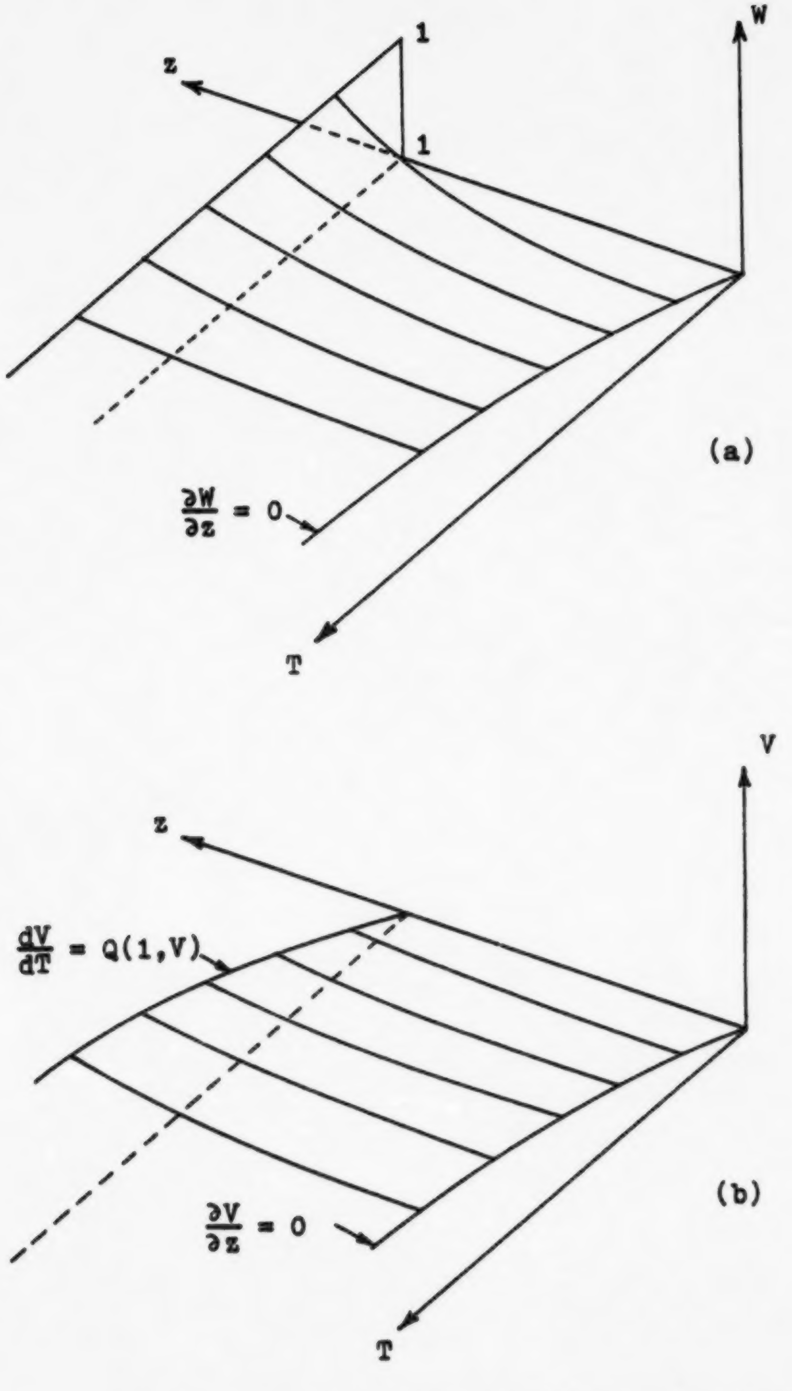
W
z
1
1
$\frac{\partial W}{\partial z} = 0$
T
(a)
V
z
$\frac{dV}{dT} = Q(1,V)$
$\frac{\partial V}{\partial z} = 0$
(b)
T

Fig. A-1. Boundary conditions for W and V

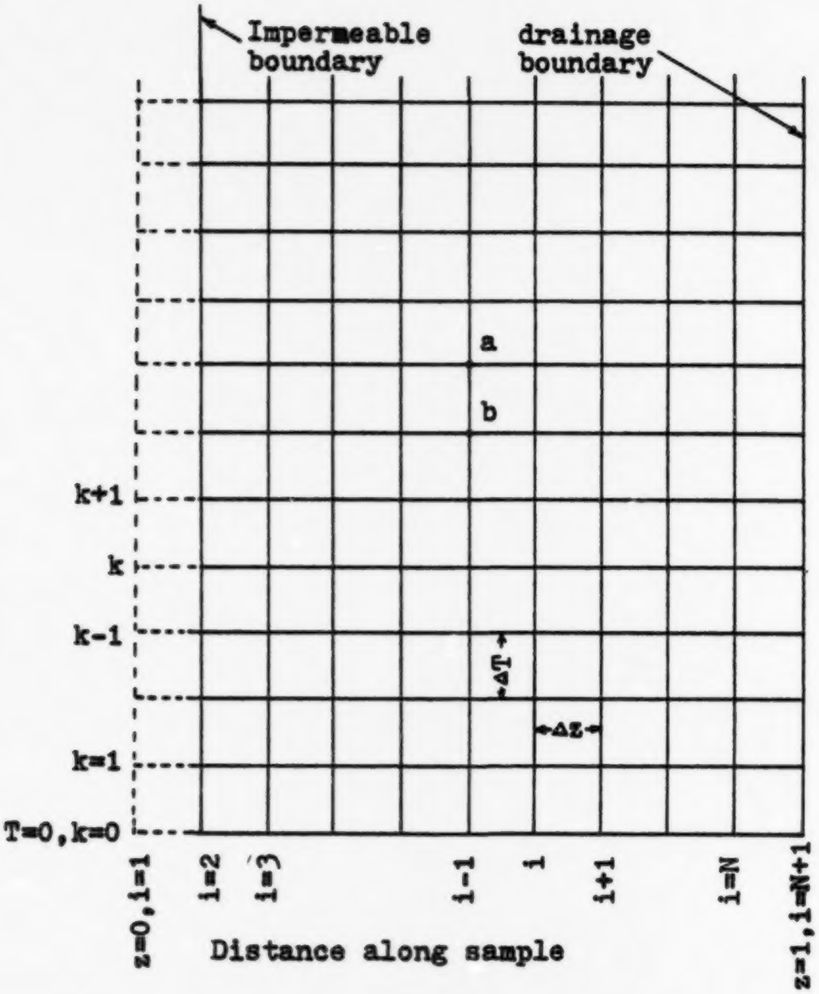
Impermeable boundary
drainage boundary
a
b
k+1
k
k-1
k=1
T=0,k=0
ΔT
ΔZ
z=0,i=1
i=2
i=3
i-1
i
i+1
i=N
z=1,i=N+1
Distance along sample

Fig. A-2. Time-space grid

i = 1 to N.

The function F, which is given by Equation A-5, may be approximated by the following finite difference form:

$$F_{i,k} = \frac{(P_{i+1,k} - P_{i-1,k})(W_{i+1,k} - W_{i-1,k})}{4\,\Delta z^2} +$$

$$\frac{P_{i,k}(W_{i+1,k} - 2W_{i,k} + W_{i-1,k})}{\Delta z^2}$$

$$- \frac{N}{1-N} Q_{i,k} + P_{h(i,k)}. \qquad \text{(A-8)}$$

At the two ends of the sample, the boundary equations are given by

$$\frac{\partial W}{\partial z} = 0 \quad \text{and} \quad \frac{\partial V}{\partial z} = 0, \qquad \text{(A-9)}$$

which requires that

$$W_{0,k} = W_{2,k} \; ; \; W_{0,k+1} = W_{2,k+1} \qquad \text{(A-10)}$$

$$V_{0,k} = V_{2,k} \; ; \; V_{0,k+1} = V_{2,k+1} \; . \qquad \text{(A-11)}$$

Similar equations to Equations A-6 and A-7 are available for all the points i = 2 to N along the z aixs of the sample. A total of 2N nonlinear algebraic equations is thus available, from which the values of $W_{i,k+1}$ and $V_{i,k+1}$ can be found by iteration methods.

The initial estimates of the values of $W_{i,k+1}$ and $V_{i,k+1}$ are obtained by means of the explicit method:

$$W^{o}_{i,k+1} = W_{i,k} + \Delta TF_{i,k} , \qquad (A-12)$$

$$V^{o}_{i,k+1} = V_{i,k} + \Delta TQ_{i,k} , \qquad (A-13)$$

$$i = 1 \text{ to } N .$$

The following recurrence formulae are used to generate the r+1th iteration from the rth:

$$W^{r+1}_{i,k+1} = W_{i,k} + 0.5\,\Delta TF^{r}_{i,k} + 0.5\,\Delta TF^{r}_{i,k+1} , \qquad (A-14)$$

$$V^{r+1}_{i,k+1} = V_{i,k} + 0.5\,\Delta TQ_{i,k} + 0.5\,\Delta TQ^{r}_{i,k+1} . \qquad (A-15)$$

This iteration process is considered to be convergent if, within ten iterations, the absolute values of the difference between successive iterations for each variable is less than 0.0001. The iteration process sometimes does not converge because the time increment is too large. The time increment is then halved and another attempt is made to advance the solution. The program is stopped if the iteration process fails to converge after the time increment has been halved more than six times.

Both the boundary condition for V at the drain and the equation governing the secondary stage are given by

$$\frac{dV}{dT} = Q(1,V) \ . \tag{A-16}$$

A numerical solution for Equation A-16 may be obtained by use of a Taylor series. If only the first two terms of such a series are used, one has

$$\frac{\Delta V}{\Delta T} = \frac{dV}{dT} + \frac{\Delta T}{2}\,\frac{d^2V}{dT^2}$$

$$= Q(1,V)\left[1 + 0.5\,\Delta T\frac{dQ(1,V)}{dV}\right]. \tag{A-17}$$

Suppose the solution is known up to a time T; then the solution at time T + ΔT can be obtained by using the recurrence formula

$$V_{T+\Delta T} = V_T + \Delta T Q(1,V_T)\left[1 + 0.5\,\Delta T\,\frac{dQ(1,V_T)}{dV}\right]. \tag{A-18}$$

The field equations of consolidation as formulated in this study involve integration in the time domain. Conventionally this has been based on linear interpolation. The fact that in the consolidation process the variation of state variables in time is logarithmic has motivated the use of a logarithmic interpolation function in the time solution of the governing equations. The use of a logarithmic time increment, which is more representative of the actual consolidation process, significantly reduces the required computing time.

Appendix B

LISTING OF COMPUTER PROGRAM AND FLOW CHART

```
      PROGRAM COMBINE (INPUT,OUTPUT, TAPE 99, TAPE60=INPUT,PUNCH)
C************************************************************************
C*                                                                      *
C*    THIS PROGRAM IS FOR THE SIMULTANEOUS SOLUTION OF TWO NONLINEAR    *
C*      PARTIAL DIFFERENTIAL EQUATIONS GOVERNING THE PRIMARY AND        *
C*      SECONDARY CONSOLIDATION BEHAVIOR OF MILLED REFUSE.              *
C*      THE NUMERICAL TECHNIQUE  IS MODIFIED FROM ONE DEVELOPED BY      *
C*      PROFESSOR T. J. POSKITT OF MANCHEST UNIVERSITY (1971).          *
C*      THIS PROGRAM WAS CODED IN STANDARD FORTRAN IV FOR CDC 6400      *
C*      COMPUTER.                                                       *
C*                                                                      *
C*  THE INPUT DATA IS AS FOLLOWS------------                            *
C*                                                                      *
C*    FIRST GROUP  OF DATA-----------FORMAT(8F10.5)                     *
C*      CK--------INITIAL VALUE OF PERMEABILITY IN FT/YEAR.             *
C*      EO--------INITIAL VOID RATIO.                                   *
C*      RW--------UNIT WEIGHT OF WATER.                                 *
C*      HO--------INITIAL HEIGHT OF SAMPLE.                             *
C*      AO--------INITIAL VALUE OF CREEP PARAMETER A.                   *
C*      BO--------INITIAL VALUE OF CREEP PARAMETER B.                   *
C*      PO--------INITIAL VALUE  OF EFFECTIVE STRESS.                   *
C*      ETCF------INITIAL TIME-DEPENDENT VOID RATIO MINUS FINAL TIME-   *
C*                DEPENDENT VOID RATIO.                                 *
C*      EOF-------INITIAL VOID RATIO MINUS FINAL VOID RATIO.            *
C*      PP--------FINAL EFFECTIVE STRESS / INITIAL EFFECTIVE STRESS.    *
C*      AA--------FINAL A / INITIAL A.                                  *
C*      BB--------FINAL B / INITIAL B.                                  *
C*      AKK-------FINAL PERMEABILITY OVER INITIAL PERMEABILITY.         *
C*      RVG-------INITIAL VOLUME OF DECOMPOSABLE SOLID OF MILLED REFUSE. *
C*      EK--------RATE CONSTANT OF THE DECOMPOSITION (IN 1/YEAR).       *
C*                                                                      *
C*    SECOND GROUP OF DATA-----------FORMAT (I10,2F10.5)                *
C*      IT--------NO. OF ITERATIONS.                                    *
C*      DELX------INTERVAL IN X-DIRECTION.                              *
C*      TIMEF-----FINAL TIME FOR THE USE OF LOG TIME INCREMENT.         *
C*      TTIMEF----FINAL TIME OF CONSOLIDATION.                          *
C*      MM--------NO. OF LOG CYCLE  IN THE DEGREE OF CONSOLIDATION VS.  *
C*                TIME FACTOR PLOT.                                     *
C*      MMK-------NO. OF LOG CYCLE IN THE STRAIN VS. TIME (MINUTE) PLOT. *
C*      NM--------NO. OF LOG CYCLE  IN THE EXCESS PORE PRESSURE VS.     *
C*                TIME FACTOR PLOT.                                     *
C*      ISTART----0, NO RESTART, 1, RESTART.                            *
C*      KR--------THE NO. OF ITERATION AT WHICH RESTART BEGINS.         *
C*                                                                      *
C*    TO RESTART THE FOLLOWING ADDITIONAL DATA , WHICH CAN BE FOUND FROM *
C*      THE PREVIOUS PRINTOUT, HAVE TO BE GIVEN.                        *
C*                                                                      *
C*    FIRST GROUP  OF DATA FOR RESTART-----------FORMAT (E20.10,I10)    *
C*                                                                      *
C*      DT--------TIME INCREMENT.                                       *
C*      IIIN------NO. OF LOG TIME INCREMENT TO BE USED BETWEEN CURRENT  *
C*                TIME FACTOR AND THE TIME FACTOR 1.                    *
C*                                                                      *
C*    SECOND GROUP OF DATA FOR RESTART-----------FORMAT (3F20.10)       *
C*                                                                      *
C*      TIME(I)---TIME FACTOR AT RESTART ITERATION.                     *
C*      DEGV(I)---DEGREE OF CONSOLIDATION AT RESTART ITERATION.         *
```

Reproduced from
best available copy.

```
C*        UM(I)-----EXCESS PORE PRESSURE AT RESTART ITERATION.            *
C*                                                                        *
C*      THIRD  GROUP OF DATA FOR RESTART-----------FORMAT (2E20.10)       *
C*                                                                        *
C*        W(I)------VALUE OF W AT RESTART ITERATION.                      *
C*        V(I)------VALUE OF V AT RESTART ITERATION.                      *
C*                                                                        *
C*************************************************************************
      DIMENSION W(2,12),V(2,12),WW(2,12),VV(2,12),PF(2,12),QF(2,12),
     1   F(2,12),TIME(4000),EMIT(4000),UM(4000),DENV(4000),PHI1(12),
     2 PHI2(12)
      CALL BGNPLT(99)
      READ 5, ISET
5     FORMAT (I10)
C*                                                                        *
C*    NSET CONTROLS THE NUMBER OF DATA SET.                               *
C*                                                                        *
      NSET=0
C*                                                                        *
C*    MCOUNT INDICATES THE NUMBER OF ITERATION IN WHICH THE LOG TIME      *
C*    INCREMENT IS TOO LARGE.                                             *
C*                                                                        *
6     MCOUNT=0
C*                                                                        *
C*    ICOUNT INDICATES THE NUMBER OF ITERATION.                           *
C*                                                                        *
      KM=0
      ICOUNT=2
      NCOUNT=0
      NN=0
      ISTART=0
C*                                                                        *
C*    LCOUNT CONTROLS THE NUMBER OF ITERATION  FOR WHICH THE TIME FACTOR  *
C*    HAS BEEN DECREASED.                                                 *
C*                                                                        *
      LCOUNT = 0
C*                                                                        *
C*    JCOUNT INDICATES THE NUMBER OF THE ITERATION AT WHICH UM IS LESS    *
C*    THAN .01.                                                           *
C*                                                                        *
      JCOUNT=0
      LL=0
C*                                                                        *
C*    NCOUNT CONTROLS THE NUMBER OF THE ITERATION AT WHICH TIME FACTOR IS *
C*    GREATER THAN 0.001.                                                 *
C*                                                                        *
      NJ=0
      NCOUN=0
      LJ=0
      LCOUN=0
      KJ=0
      KCOUN=0
      IJ=0
      ICOUN=0
C*                                                                        *
C*    READ INPUT PARAMETERS.                                              *
C*                                                                        *
66    READ 10, DK,EO,RM,HO,AO,BO,PO,ETOF,EOF ,PP,AA,BB,XKK,RVO,EK
```

```
10    FORMAT (4F20.10)
      EPTOF=ETOF/(1.0+EO)
      EPOF=EOF/(1.0+EO)
      XN=EPTOF/EPOF
      AVO=-(EPOF*(1.0+EO))/(PO*ALOG(PP))
      R=DK*(1.0+EO)/(RW*AVO*HO*HO*AO*PO)
      R=-R
      TF=R*AO*PO
      D=XN/(1.-XN)
      PRINT 9, R,TF
9     FORMAT (2E20.10)
C*                                                                     *
C*    KCOUNT CONTROLS THE NUMBER OF ITERATION BETWEEN W(2,1) AND WW(2,1). *
C*                                                                     *
      KCOUNT=0
      UM(1)=1.0
C*                                                                     *
C*    ALSO READ INPUT PARAMETERS.                                      *
C*                                                                     *
      READ 176,IT,DELX,TIMEF,TTIMEF,MM,NMN,NM,ISTART,MR,VO,VF
176   FORMAT (I10,F10.5,2E20.10,2I10/3I10,2F20.10)
      PRINT 30,  DK,EO,RW,HO,AO,BO,PO,ETOF,EOF,PP,AA,BB,XKK,RVO,EK
30    FORMAT(4E20.5)
      PRINT 4, IT,DELX,TIMEF,TTIMEF,MM,NMN,NM,ISTART,MR,VO,VF
4     FORMAT (I10,F10.5,2E20.10,5I10/2F20.10)
C*                                                                     *
C*      IIMAX IS THE THE NUMBER OF INTERVAL IN THE X-COORDINATE.       *
C*                                                                     *
      IIMAX=1.0/DELX+0.001
      IMAX=IIMAX+1
      PRINT  40, IMAX
40    FORMAT (5X,* IMAX =  *, I10)
C*                                                                     *
C*      SET UP INITIAL BOUNDARY CONDITIONS HERE FOR BOTH W AND V.      *
C*                                                                     *
      IF (ISTART.EQ.0)  41,44
41    DO 60   I=1,IMAX
      W(1,I)=0.
      V(1,I)=0.
60    CONTINUE
      W(1,IMAX)=1.0
      CHECK=BO/(PP-1.)
C*                                                                     *
C*      CHECK WHETHER THE INITIAL VALUE OF V AT T=0 SHOULD BE 0 OR 1.  *
C*                                                                     *
      IF (CHECK.LT.100.)  61,62
61    V(1,IMAX)=0.
      GO TO 63
62    V(1,IMAX)=1.
63    DO 65 I=1,IT
C*                                                                     *
C*      CALCULATE THE INITIAL TIME INCREMENT FOR THE ITERATION.        *
C*                                                                     *
65    TIME(I)=0.
      PF(1,IMAX)=FP(W(1,IMAX),V(1,IMAX),XKK,XN,PP,R,EPTOF,EPOF,BO,
     1   AA,BB,IMAX,IIMAX,EO)
      DT=.004*DELX*DELX/( PF(1,IMAX) +3./(1.0-XN))
      PRINT 5005, DT
```

```
5005  FORMAT (/5X,*DT IS =*, E20.10/)
      JKM=2
      GO TO 43
C*                                                                      *
C*    RESTART IS NECESSARY. THREE ADDITIONAL GROUPS OF DATA ARE READ.   *
C*                                                                      *
44    MRM=MR+1
      READ 45,  DT,ITIN
45    FORMAT (E20.10,I10)
      DO 10061 I=2,MR
      READ 46,  TIME(I),DEWV(I),UM(I)
46    FORMAT (3E20.10)
      IF (TIME(I).GT..001)  10062,10061
10062 IF (NN.EQ.0)  10064,10061
10064 NCOUNT=I
      NN=NN+1
10061 CONTINUE
      ICOUNT=MR
      READ 47,  (W(1,I),V(1,I),I=1,IMAX)
47    FORMAT (2E20.10)
      JKM=MRM
43    EPBF=EPOF-EPTOF
      EC=EO/((1.0+EO)*EPBF)
      WGR=RVO/(1.7*62.4)
      EKTF=-EK/TF
      CX=(1.0+EO)*EPBF
      CY=1.0/EPBF
      PRINT 77789, EPTOF,EPOF,XN,AVO,D
77789 FORMAT (5E20.10)
      PRINT 77790, EPBF,EC,WGR,EKTF,CX,CY
77790 FORMAT (6E20.10)
      DO 231  M=JKM,IT
C*                                                                      *
C*      CALCULATE THE FUNCTIONS P AND Q FOR THE INITIAL VALUES OF W AND V.*
C*                                                                      *
70    DO 200 I=1,IMAX
      PF(1,I)=FP(W(1,I),V(1,I),XKK,XN,PP,R,EPTOF,EPOF,BO,AA,BB,IMAX,
     1   IIMAX,EO)
      QF(1,I)=FQ(W(1,I),V(1,I),PP,R,EPTOF,BO,AA,BB,IMAX,IIMAX)
200   CONTINUE
C*                                                                      *
C*      FIRST APPROXIMATION OF W AND V FOR THE NEXT TIME INCREMENT.     *
C*                                                                      *
C*                                                                      *
C*      SPECIFY THE VALUES OF W AND V ON THE DRAINAGE BOUNDARY.         *
C*                                                                      *
90    TIME(M)=TIME(M-1) + DT
      DO 80 J=1,IIMAX
      I=IIMAX-(J-1)
      IF (I.EQ.1)  52,54
52    PHI1(1)=PH(W(1,1),V(1,1),D,EC,WGR,EKTF,CX,CY,EK,TIME(M-1),TF)
      F(1,1)=PF(1,1)*(2.*W(1,2)-2.*W(1,1))/(DELX*DELX)-D*QF(1,1)
     1   +PHI1(1)
      W(2,1)=W(1,1)+DT*F(1,1)
      IF (W(2,1).GT.1.0)  W(2,1)=1.0
      V(2,1)=V(1,1)+DT*QF(1,1)
      IF (V(2,1).GT.1.0)  V(2,1)=1.0
      GO TO 80
```

```
C*                                                                        *
C*      CALCULATE THE W AND V OF DRAINAGE BOUNDARY FOR NEXT TIME          *
C*    INCREMENT.                                                          *
C*                                                                        *
54    PHI1(I)=PH(W(1,I),V(1,I),D,EC,WGR,EKTF,CX,CY,EK,TIME(M-1),TF)
      F(1,I)=(PF(1,I+1)-PF(1,I-1))*(W(1,I+1)-W(1,I-1))/(4.
     1 *DELX*DELX)+PF(1,I)*(W(1,I+1)-2.*W(1,I)+W(1,I-1))/(DELX*DELX)
     2  -D*QF(1,I)+PHI1(I)
      W(2,I)=W(1,I)+DT*F(1,I)
      IF (W(2,I).GT.1.0)  W(2,I)=1.0
      V(2,I)=V(1,I)+DT*QF(1,I)
      IF (V(2,I).GT.1.0)  V(2,I)=1.0
80    CONTINUE
      V(2,IMAX)=FV(W(1,IMAX),V(1,IMAX),PP,R,EPTOF,BO,AA,BB,DT,IMAX,
     1  IIMAX)
      W(2,IMAX)=1.0
      IF (V(2,IMAX).GT.1.0)  V(2,IMAX)=1.0
949   PF(2,IMAX)=FP(W(2,IMAX),V(2,IMAX),XKK,XN,PP,R,EPTOF,EPOF,BO,AA,
     1  BB,IMAX,IIMAX,EO)
      QF(2,IMAX)=FQ(W(2,IMAX),V(2,IMAX),PP,R,EPTOF,BO,AA,BB,IMAX,IIMAX)
C*                                                                        *
C*     ·CALCULATE FUNCTION F IN ORDER TO GET BETTER APPROX OF W AND V AT  *
C*    T+DT.                                                               *
C*                                                                        *
110   DO 1079 J=1,IIMAX
      I=IIMAX-(J-1)
      PF(2,I)=FP(W(2,I),V(2,I),XKK,XN,PP,R,EPTOF,EPOF,BO,AA,BB,IMAX,
     1   IIMAX,EO)
      QF(2,I)=FQ(W(2,I),V(2,I),PP,R,EPTOF,BO,AA,BB,IMAX,IIMAX)
1079  CONTINUE
C*                                                                        *
C*         CALCULATE FUNCTION F AT T+DT.                                  *
C*                                                                        *
      DO 190 J=1,IIMAX
      I=IIMAX-(J-1)
      IF (I.EQ.1) 192,194
192   PHI2(1)=PH(W(2,1),V(2,1),D,EC,WGR,EKTF,CX,CY,EK,TIME(M),TF)
      F(2,1)=PF(2,1)*(2.*W(2,2)-2.*W(2,1))/(DELX*DELX)-D*QF(2,1)+PHI2(1)
      GO TO 190
194   PHI2(I)=PH(W(2,I),V(2,I),D,EC,WGR,EKTF,CX,CY,EK,TIME(M),TF)
      F(2,I)=(PF(2,I+1)-PF(2,I-1))*(W(2,I+1)-W(2,I-1))/(4.*DELX*DELX)
     1 +PF(2,I)*(W(2,I+1)-2.*W(2,I)+W(2,I-1))/(DELX*DELX)-D*QF(2,I)
     2  +PHI2(I)
190   CONTINUE
C*                                                                        *
C*         GET BETTER APPROXIMATION OF W AND V AT T+DT.                   *
C*                                                                        *
       DO 120 IJ=1,IIMAX
      WW(2,IJ)=W(1,IJ)+DT*0.5*F(1,IJ)+0.5*F(2,IJ)*DT
      VV(2,IJ)=V(1,IJ)+DT*0.5*QF(1,IJ)+0.5*DT*QF(2,IJ)
120   CONTINUE
      WW(2,IMAX)=W(2,IMAX)
      VV(2,IMAX)=V(2,IMAX)
      KCOUNT=KCOUNT+1
C*                                                                        *
C*      CHECK THE VALUES OF W AND V AT T+DT ARE ACCURATE ENOUGH.          *
C*                                                                        *
      DO 140 I=1,IIMAX
      IF(ABS(WW(2,I)-W(2,I)).LT.0.0001.AND.ABS(VV(2,I)-V(2,I)).LT.
     1  0.0001)  122,124
122   IF (I.EQ.IIMAX)  850,140
124   IF(ABS(WW(2,I)).GT.1.0.OR.ABS(VV(2,I)).GT.1.0.OR.KCOUNT.GT.6)
     1  128,126
126   IF (I.EQ.IIMAX)  852,140
140   CONTINUE
852   DO 150  I=1,IIMAX
      W(2,I)=WW(2,I)
150   V(2,I)=VV(2,I)
C*                                                                    *
C*    THIS BRANCH MEANS THAT W AND V ARE NOT ACCURATE ENOUGH BUT NO   *
C*       DIVERGENCE OCCURS.                                           *
C*                                                                    *
      GO TO 949
128   IF (KM.EQ.0)  113,115
C*                                                                    *
C*    TIME INCREMENT IS TOO LARGE AND THE SOLUTION DOES NOT CONVERGE. *
C*    THEREFORE, TIME INCREMENT HAS TO BE HALVED.                     *
C*                                                                    *
113   MCOUNT=M
      PRINT 48,  MCOUNT
48    FORMAT (/5X,*MCOUNT=*,I10)
      KM=KM+1
115   DT=0.5*DT
      LCOUNT=LCOUNT+1
      IF (LCOUNT.GT.10) GO TO 178
      KCOUNT=0
      GO TO 90
178   PRINT 179,  DT,M,TIME(M)
179   FORMAT (2X,*DT=*,E20.10,*M=*,I10,*TIME(M)=*,E20.10)
1113  PRINT 5706, LCOUNT
5706  FORMAT (5X,*TIME HAS BEEN DECREASED FOR MORE THAN ≠*,I3,*≠TIMES,
     1  COMPUTER PROGRAM HAS STOPPED TO SEE WHAT≠S WRONG*)
C*                                                                    *
C*      THE ITERATION PROCEDURE DOES NOT CONVERGE. THE PROGRAM IS STOPPED.*
C*                                                                    *
      IT=M-1
      GO TO 9991
C*                                                                    *
C*      THIS BRANCH MEANS THAT W AND V ARE NOT ACCURATE ENOUGH AND    *
C*      DIVERGENCE OCCURS.                                            *
C*                                                                    *
850   IF ((M-2)/10*10.EQ.(M-2))  3001,299
C*                                                                    *
C*      SELECT PRINT OUT (EVERY TENTH ITERATION).                     *
C*                                                                    *
3001  PRINT 6105,  M,LCOUNT,KCOUNT
6105  FORMAT (5X,*THE NO. OF ITERATION IS=*,I10,*LCOUNT=*,I10,*KCOUNT=
     1  *,I10)
299   IF (TIME(M) .GE. .001)  301,304
301   IF(NN.EQ.0)  303,304
303   NCOUNT=ICOUNT
      NN=NN+1
304   IF (MCOUNT.EQ.0)  305,306
305   IF (ISTART.EQ.0)  10066,10067
10066 IF (ICOUNT.EQ.2)  10068,20
10068 TI=1000
```

```
      GO TO 18
10067 IF (ICOUNT.EQ.MR)  10071,20
10071 TI=ITIN
C*                                                                        *
C*    THE LOG TIME INCREMENT IS CALCULATED.                               *
C*                                                                        *
18    TLI=ALOG10(TIME(M))
      TLF=ALOG10(TIMEF)
      DIFF=ABS(TLI-TLF)/TI
20    TLID=TLI+DIFF
      TLIDA=ABS(TLID)
      TLIA=ABS(TLI)
      IF (TLI.GE.0.0.AND.TLID.GE.0.0)   GO TO 401
      IF (TLI.LE.0.0.AND.TLID.LE.0.0)   GO TO 402
      IF (TLI.LE.0.0.AND.TLID.GE.0.0)   GO TO 404
401   DT=ABS(10.**TLIDA-10.**TLIA)
      GO TO 403
402   DT=ABS(1.0/  10.**TLIDA-1.0/10.**TLIA)
      GO TO 403
404   DT=ABS(10.**TLIDA-1.0/10.**TLIA)
403   TLI=TLID
306   ICOUNT=ICOUNT+1
      DO 127 I=1,IIMAX
      W(2,I)=WW(2,I)
127   V(2,I)=VV(2,I)
      IF ((M-2)/10*10.EQ.(M-2))  3003,3004
3003  PRINT 129, TIME(M),(W(2,I),I=1,IMAX),(V(2,I),I=1,IMAX)
129   FORMAT(5X,*  TIME = *,E20.10,/5X,4E20.10,/5X,4E20.10,/5X,3E20.10,
     1  //5X,4E20.10,/5X,4E20.10,/5X,3E20.10)
3004  DEW=(DELX/3.)*(W(2,1)+4.*W(2,2)+2.*W(2,3)+4.*W(2,4)+2.*W(2,5)+
     1  4.*W(2,6)+2.*W(2,7)+4.*W(2,8)+2.*W(2,9)+4.*W(2,10)+W(2,11))
      DEV=(DELX/3.)*(V(2,1)+4.*V(2,2)+2.*V(2,3)+4.*V(2,4)+2.*V(2,5)+
     1  4.*V(2,6)+2.*V(2,7)+4.*V(2,8)+2.*V(2,9)+4.*V(2,10)+V(2,11))
      DEWV(M)=(1.0-XN)*DEW+XN*DEV
      UM(M)=(PO*PP-PO*PP**DEW    )/(PO*PP-PO)
      IF ((M-2)/10*10.EQ.(M-2))  3007,3008
3007  PRINT 6197, DEW,DEV,DEWV(M),UM(M)
6197  FORMAT (5X,*DEW=*,E15.9,2X,*DEV=*,E15.9,2X,*DEWV=*,E15.9,
     1  2X,*UM=*,E15.9)
      PUNCH 18181, TIME(M),DEWV(M),UM(M)
18181 FORMAT (3E20.10)
C*                                                                        *
C*    THE CONSOLIDATION PROCESS IS FINISHED WHEN DEGREE OF CONSOLIDATION  *
C*    IS GREATER THAN .999.                                               *
C*                                                                        *
3008  IF (DEWV(M).GE..999)  GO TO 900
C*                                                                        *
C*    THE PRIMARY CONSOLIDATION IS FINISHED WHEN THE EXCESS PORE PRESSURE *
C*    IS LESS THAN .01.                                                   *
C*                                                                        *
      IF (UM(M).LE..01)   891,895
891   IF (LL.EQ.0) 893,895
893   JCOUNT=M-1
      PRINT 10091, JCOUNT
10091 FORMAT (5X,*JCOUNT=*,I10)
      LL=LL+1
      GO TO 910
895   IF (LCOUNT.LE.3)  158,159
```

```
C*                                                                            *
C*    TIME INCREMENT IS SUFFICIENTLY SMALL AND CAN BE DOUBLED.                *
C*                                                                            *
158   DT=DT*2.0
159   LCOUNT=0
      KCOUNT = 0
      DO 160 I=1,IMAX
      W(1,I)=WW(2,I)
160   V(1,I)=VV(2,I)
231   CONTINUE
      GO TO 9991
900   PRINT 5501, DEWV(M)
5501  FORMAT (/5X,* CONSOLIDATION IS FINISHED, DEWV= *,E20.10)
C*                                                                            *
C*      THIS BRANCH MEANS THE CONSOLIDATION PROCESS IS FINISHED.              *
C*                                                                            *
      IT=M
      GO TO 9991
C*                                                                            *
C*    THE EXCESS PORE PRESSURE IS LESS THAN .01 AND IT IS IN THE              *
C*    SECONDARY STAGE.                                                        *
C*                                                                            *
910   J=M+1
      W1=1.0
      V1=DEV
      DO 825  K=J,IT
C*                                                                            *
C*    ONLY 500 LOG TIME INCREMENTS WILL BE USED IN THE SECONDARY STAGE.       *
C*                                                                            *
      IF (K.EQ.J)  520,525
520   TLI=ALOG10(TIME(M))
      TLF=ALOG10(TTIMEF)
      TTI=IT-M
      IF (TTI.GE. 500) 527,529
527   TTI= 500
      IT=M+ 500
C*                                                                            *
C*    THE LOG TIME INCREMENTS OF THE SECONDARY STAGE ARE CALCULATED.          *
C*                                                                            *
529   DIFF=ABS(TLI-TLF)/TTI
525   TLID=TLI+DIFF
      TLIDA=ABS(TLID)
      TLIA=ABS(TLI)
      IF (TLI.GE.0.0.AND.TLID.GE.0.0)   GO TO 531
      IF (TLI.LE.0.0.AND.TLID.LE.0.0)   GO TO 533
      IF (TLI.LE.0.0.AND.TLID.GE.0.0)   GO TO 532
531   DT=ABS(10.**TLIDA-10.**TLIA)
      GO TO 535
533   DT=ABS(1.0/10.**TLIDA-1.0/10.**TLIA)
      GO TO 535
532   DT=ABS(10.**TLIDA-1.0/10.**TLIA)
535   TLI=TLID
C*                                                                            *
C*    ONLY CREEP EQUATION WILL BE SOLVED IN THE SECONDARY STAGE.              *
C*                                                                            *
      TIME(K)=TIME(K-1)+DT
      PHI3=PH(W1,V1,0,EC,WGR,EKTF,CX,CY,EK,TIME(K-1),TF)
      OF3=FO(W1,V1       ,PP,R,EPTOF,BO,AA,BB,IMAX,IIMAX)
      FF1=+PHI3+  QF3
      V2=V1+DT*FF1
      DO 83951  II=1,4
      PHI4=PH(W1,V2,D,EC,WGR,EKTF,CX,CY,EK,TIME(K)   ,TF)
      QF4=FQ(W1,V2 ,PP,R,EPTOF,30,AA,BB,IMAX,IIMAX)
      FF2=+PHI4+  QF4
      VV2=V1+0.5*DT*QF3+0.5*DT*QF4
      V2=VV2
83951 CONTINUE
      DEW=W1
      DEV=VV2
      DEWV(K)=(1.0-XN)*DEW+XN* DEV
      IF ((K-2)/10*10.EQ.(K-2))  3005,3006
3005  PRINT 5702, K
5702  FORMAT (5X,*THE NO. OF ITERATION (IITER) IS = *,I10)
      PRINT 5703, TIME(K)
5703  FORMAT (5X,*TIME=*,E20.10)
      PRINT 5704,  DEW,DEV,DEWV(K)
5704  FORMAT (5X,*DEW=*,E20.10,5X,*DEV=*,E20.10,5X,*DEWV(K)=*,E20.10)
      PRINT 21190,  PHI3,QF3,FF1,PHI4,QF4,FF2
21190 FORMAT (6E20.10)
      PUNCH 17171,  TIME(K),DEWV(K)
17171 FORMAT (2E20.10)
3006  IF (TIME(K) . GE. .001)   7301,7305
7301  IF (NN.EQ.0) 7303,7305
7303  NCOUNT=ICOUNT
      NN=NN+1
C*                                                                       *
C*    THE CONSOLIDATION PROCESS IS FINISHED WHEN THE DEGREE OF           *
C*    CONSOLIDATION IS GREATER THAN .999.                                *
C*                                                                       *
7305  IF (DEWV(K).GT..999)  GO TO 989
      ICOUNT=ICOUNT+1
      IF (ICOUNT.GE.IT)   GO TO 912
      V1=VV2
825   CONTINUE
912   PRINT 915, IT
915   FORMAT(/5X,*IT     = *,I10)
519   IT=K
      GO TO 9991
989   IT=K-1
      PRINT 988, DEWV(K)
C*                                                                       *
C*      THE CONSOLIDATION PROCESS IS FINISHED.                           *
C*                                                                       *
988   FORMAT(/5X,*CONSOLIDATION HAS BEEN COMPLETED, DEWV IS =*,E20.10)
C*                                                                       *
C*       PLOT DEGREE OF CONSOLIDATION VS. TIME FACTOR.                   *
C*                                                                       *
9991  CALL PLOT (0.0,2.0,3)
      CALL PLOT (10.0,2.0,2)
      CALL PLOT (10.0,8.0,2)
      CALL PLOT (0.0,8.0,2)
      CALL PLOT (0.0,2.0,2)
C*                                                                       *
C*    LABEL HORIZONTAL AXIS AND MAKE HORIZONTAL TICK MARKS.              *
C*                                                                       *
      XM=MM
      CYCLE=10./XM
      ALOC=-CYCLE
      N=MM+1
      DO 100 J=1,N
      ALOC=ALOC+CYCLE
      BALOC=ALOC-0.10
      CALL NUMBER(BALOC,1.75,0.10,10,0.0,2HI2)
      INUM=J-4
      CALOC=ALOC+0.05
      CALL NUMBER(CALOC,1.83,.07,INUM,0.0,2HI3)
      IF(J.EQ.N)  GO TO 99
      DO 50 I=1,9
      CC=I
      DXLOG=ALOG10(CC)*CYCLE
      AALOC=ALOC+DXLOG
      CALL PLOT(AALOC,2.0,3)
      IF (I.EQ.1)  10001,10002
10001 CALL PLOT (AALOC,2.1,2)
      GO TO 50
10002 CALL PLOT (AALOC,2.05,2)
50    CONTINUE
99    CONTINUE
100   CONTINUE
      ALOC =-CYCLE
      DO 10003 J=1,N
      ALOC =ALOC+CYCLE
      IF (J.EQ.N)  GO TO 10004
      DO 10005 I=1,9
      CC=I
      DXLOG=ALOG10(CC)*CYCLE
      AALOC=ALOC+DXLOG
      CALL PLOT (AALOC,8.0,3)
      IF (I.EQ.1)  10006,10007
10006 CALL PLOT (AALOC,7.9,2)
      GO TO 10005
10007 CALL PLOT (AALOC,7.95,2)
10005 CONTINUE
10004 CONTINUE
10003 CONTINUE
C*                                                                          *
C*    LABEL VERTICAL AXIS AND MAKE VERTICAL TICK MAEKS.                     *
C*                                                                          *
      DELAX=6.0/5.0
      DEE=1.0
      YSPAC=2.0-DELAX
      ANUM=1.0/5.0
      DEL=DEE+ANUM
      DO 350  I=1,6
      YSPAC=YSPAC+DELAX
      BNUM=DEL-ANUM+0.00001
      CALL PLOT(0.0,YSPAC,3)
      CALL PLOT (0.1,YSPAC,2)
      CALL PLOT (9.9,YSPAC,3)
      CALL PLOT(10.0,YSPAC,2)
      YYSPAC=YSPAC-0.05
      CALL NUMBER(-0.5,YYSPAC,0.1,BNUM,0.0,4HF4.2)
      DEL=BNUM
350   CONTINUE
```

```
      CALL SYMBOL(-0.5,3.0,0.15,23HDEGREE OF CONSOLIDATION,90.0,23)
      CALL SYMBOL(4.0,1.5,0.15,14HTIME FACTOR, T, 0.0,14)
      CALL PLOT (0.0,2.0,-3)
      KK=NCOUNT
      DO 319 J=KK,IT
      I=J-KK+1
        TIME(I)=ALOG10(TIME(J))
      UM(I)=UM(J)
319    DEWV(I)=1.0-DEWV(J)
        TIME(IT-KK+2)=-3.0
        TIME(IT-KK+3)=XM/10.0
       DEWV(IT-KK+2)=0.
       DEWV(IT-KK+3)=1.0/6.0
      L=IT-NCOUNT+1
      LO=L
      PRINT 9998, L,NCOUNT
9998  FORMAT (2X,*L=*,I10,2X,*NCOUNT=*,I10)
      PRINT 1013, (  TIME(I), DEWV(I),I=1,L,10)
1013  FORMAT (2X,*TIMELG=*,E20.5,2X,*DDEWV=*,E20.5,
     1         2X,*TIMELG=*,E20.5,2X,*DDEWV=*,E20.5)
      CALL LINE(  TIME, DEWV,L,1,0,26)
      CALL PLOT (15.0,-2.0,-3)
      DO 3  I=1,LO
C     PUNCH 833, L
C     PUNCH 2, (TIME(I),DEWV(I),I=1,L)
3     EMIT(I)=TIME(I)
2     FORMAT (2E20.10,2E20.10)
C*                                                                     *
C*       PLOT STRAIN VS. TIME ( IN YEARS ).                            *
C*                                                                     *
      TFL=ALOG10(+TF)
      DO 12  I=1,LO
      TIME(I)=TIME(I)-TFL
      IF  (TIME(I).GE.-9.0)  3010,3040
3010  IF (NJ.EQ.0)  3030,3040
3030  NCOUN =I
      NJ=NJ+1
3040  IF (TIME(I).GT.3.0)  GO TO 9990
12    CONTINUE
      GO TO 1990
9990  LO=I-1
1990  CALL PLOT (0.0,2.0,3)
      CALL PLOT (10.0,2.0,2)
      CALL PLOT (10.0,8.0,2)
      CALL PLOT (0.0,8.0,2)
      CALL PLOT (0.0,2.0,2)
C*                                                                     *
C*    LABEL HORIZONTAL AXIS AND MAKE HORIZONTAL TICK MARKS.            *
C*                                                                     *
      XM=MM
      CYCLE=10./XM
      ALOC=-CYCLE
      N=MM+1
      DO 1001  J=1,N
      ALOC=ALOC+CYCLE
      BALOC=ALOC-0.10
      CALL NUMBER(BALOC,1.75,0.10,10.0,0.0,2HI2)
      INUM=J-9
```

Reproduced from
best available copy.

```
      CALOC=ALOC+0.0*
      CALL NUMBER(CALOC,1.83,.07,INUM,0.0,2HI3)
      IF (J.EQ.N)   GO TO 399
      DO 569  I=1,9
      CC=I
      DXLOG=ALOG10(CC)*CYCLE
      AALOC=ALOC+DXLOG
      CALL PLOT(AALOC,2.0,3)
      IF (I.EQ.1)   10009,10010
10009 CALL PLOT (AALOC,2.1,2)
      GO TO 569
10010 CALL PLOT (AALOC,2.05,2)
509   CONTINUE
399   CONTINUE
1001  CONTINUE
      ALOC =-CYCLE
      DO 10011 J=1,N
      ALOC =ALOC+CYCLE
      IF (J.EQ.N)   GO TO 10012
      DO 10013 I=1,9
      CC=I
      DXLOG=ALOG10(CC)*CYCLE
      AALOC=ALOC+DXLOG
      CALL PLOT (AALOC,8.0,3)
      IF (I.EQ.1)   10014,10015
10014 CALL PLOT (AALOC,7.9,2)
      GO TO 10013
10015 CALL PLOT (AALOC,7.95,2)
10013 CONTINUE
10012 CONTINUE
10011 CONTINUE
C*                                                                      *
C*    LABEL VERTICAL AXIS AND MAKE VERTICAL TICK MAEKS.                 *
C*                                                                      *
      DELAX=6.0/5.0
      DEE=0.5
      YSPAC=2.0-DELAX
      ANUM=0.5/5.0
      DEL=DEE+ANUM
      DO 3569  I=1,6
      YSPAC=YSPAC+DELAX
      BNUM=DEL-ANUM+0.0001
      CALL PLOT(0.0,YSPAC,3)
      CALL PLOT (0.1,YSPAC,2)
      CALL PLOT (9.9,YSPAC,3)
      CALL PLOT(10.0,YSPAC,2)
      YYSPAC=YSPAC-0.05
      CALL NUMBER(-0.5,YYSPAC,0.1,BNUM,0.0,4HF4.2)
      DEL=BNUM
3569  CONTINUE
      CALL SYMBOL(-0.4,4.0,0.15,6HSTRAIN,90.0,6)
      CALL SYMBOL(4.0,1.5,0.15,16HTIME, (IN YEARS),0.0,16)
      CALL PLOT (0.0,2.0,-3)
1992  KK=KCOUN
      DO 3199   J=KK,LD
      I=J-KK+1
      TIME(I)=TIME(J)
3199  DEHV(I)=0.5-(1.0-DEHV(J))*EPOF
```

```
      TIME(LD-KK+2)=-8.0
      TIME(LD-KK+3)=YM/10.0
      DEWV(LD-KK+2)=0.0
      DEWV(LD-KK+3)=0.5/6.0
      L=LD-NCOUN +1
      PRINT 99910, L
99910 FORMAT (2X,*L=*,I10)
      CALL LINE(TIME,DEWV,L,1,0,26)
      CALL PLOT (15.0,-2.0,-3)
C*                                                                     *
C*       PLOT STRAIN VS. TIME ( IN MINUTES ).                          *
C*                                                                     *
      YRMIN=ALOG10(525600.)
      DO 6300  I=1,LD
      TIME(I)=TIME(I)+YRMIN
      IF (TIME(I).GE.-2.0)  6301,6304
6301  IF (LJ.EQ.0)  6303,6304
6303  LCOUN =I
      LJ=LJ+1
6304  IF (TIME(I).GE.6.0)  GO TO 9992
6300  CONTINUE
      GO TO 1994
9992  LD=I-1
1994  CALL PLOT (0.0,2.0,3)
      CALL PLOT (7.5,2.0,2)
      CALL PLOT (7.5,7.0,2)
      CALL PLOT (0.0,7.0,2)
      CALL PLOT (0.0,2.0,2)
C*                                                                     *
C*    LABEL HORIZONTAL AXIS AND MAKE HORIZONTAL TICK MARKS.            *
C*                                                                     *
      XM =NMN
      CYCLE=7.5/XM
      ALOC=-CYCLE
      N=NMN+1
      DO 6111  J=1,N
      ALOC=ALOC+CYCLE
      BALOC=ALOC-0.10
      CALL NUMBER (BALOC,1.75,0.10,10.0.0,2HI2)
      INUM=J-3
      CALOC=ALOC+.08
      CALL NUMBER (CALOC,1.93,.07,INUM,0.0,2HI3)
      IF (J.EQ.N) GO TO 699
      DO 650  I=1,9
      CC=I
      DXLOG=ALOG10(CC) *CYCLE
      AALOC=ALOC+DXLOG
      CALL PLOT (AALOC,2.0,3)
      IF (I.EQ.1)  10017,10018
10017 CALL PLOT (AALOC,2.1,2)
      GO TO 650
10018 CALL PLOT (AALOC,2.05,2)
650   CONTINUE
699   CONTINUE
6111  CONTINUE
      ALOC=-CYCLE
      DO 10019 J=1,N
      ALOC=ALOC+CYCLE
```

Reproduced from
best available copy.

```
      IF (J.EQ.N)  GO TO 10020
      DO 10021 I=1,9
      CC=I
      DXLOG=ALOG10(CC)*CYCLE
      AALOC=ALOC+DXLOG
      CALL PLOT (AALOC,7.0,3)
      IF (I.EQ.1)  10022,10023
10022 CALL PLOT (AALOC,6.9,2)
      GO TO 10021
10023 CALL PLOT (AALOC,6.95,2)
10021 CONTINUE
10020 CONTINUE
10019 CONTINUE
C*                                                                      *
C*    LABEL VERTICAL AXIS AND MAKE VERTICAL TICK MAEKS.                 *
C*                                                                      *
      DELAX=5.0/5.0
      DEE=0.5
      YSPAC=2.0-DELAX
      ANUM=0.5/5.0
      DEL=DEE+ANUM
      DO 6350 I=1,6
      YSPAC = YSPAC + DELAX
      BNUM=DEL-ANUM+0.0001
      CALL PLOT (0.0,YSPAC,3)
      CALL PLOT (0.1,YSPAC,2)
      CALL PLOT (7.4,YSPAC,3)
      CALL PLOT (7.5,YSPAC,2)
      YYSPAC = YSPAC - 0.05
      CALL NUMBER (-0.7,YYSPAC,0.1,BNUM,0.0,4HF6.3)
      DEL=BNUM
6350  CONTINUE
      CALL SYMBOL (-0.40,4.0,0.15,6HSTRAIN,90.0,6)
      CALL SYMBOL (2.5,1.5,0.15,16HTIME,  (MINUTES),0.0,16)
      CALL PLOT (0.0,2.0,-3)
      KK=LCOUN
      DO 6500  J=LCOUN ,LD
      I=J-KK+1
      TIME(I)=TIME(J)
6500  DEWV(I)=DEWV(J)
      TIME(LD-KK+2)=-2.0
      TIME(LD-KK+3)=XM/7.5
      DEWV(LD-KK+2)=0.0
      DEWV(LD-KK+3)=0.5/5.0
      L=LD-KK+1
      CALL LINE(TIME,DEWV,L,1,0,26)
      CALL PLOT(15.0,-2.0,-3)
C*                                                                      *
C*       PLOT VOID RATIO VS. TIME ( IN MINUTES ).                       *
C*                                                                      *
      CALL PLOT (0.0,2.0,3)
      CALL PLOT (7.5,2.0,2)
      CALL PLOT (7.5,7.0,2)
      CALL PLOT (0.0,7.0,2)
      CALL PLOT (0.0,2.0,2)
C*                                                                      *
C*    LABEL HORIZONTAL AXIS AND MAKE HORIZONTAL TICK MARKS.             *
C*                                                                      *
```

```
      XM =NMN
      CYCLE=7.5/XM
      ALOC=-CYCLE
      N=NMN+1
      DO 86111 J=1,N
      ALOC=ALOC+CYCLE
      BALOC=ALOC-0.10
      CALL NUMBER (BALOC,1.75,0.10,10.0,0.0,2HI2)
      INUM=J-3
      CALOC=ALOC+.38
      CALL NUMBER (CALOC,1.83,.07,INUM,0.0,2HI3)
      IF (J.EQ.N) GO TO 8699
      DO 8650 I=1,9
      CC=I
      DXLOG=ALOG10(CC) *CYCLE
      AALOC=ALOC+DXLOG
      CALL PLOT (AALOC,2.0,3)
      IF (I.EQ.1)  10025,10026
10025 CALL PLOT (AALOC,2.1,2)
      GO TO 8650
10026 CALL PLOT (AALOC,2.05,2)
8650  CONTINUE
8699  CONTINUE
86111 CONTINUE
      ALOC=-CYCLE
      DO 10027 J=1,N
      ALOC=ALOC+CYCLE
      IF (J.EQ.N)  GO TO 10028
      DO 10029 I=1,9
      CC=I
      DXLOG=ALOG10(CC)*CYCLE
      AALOC=ALOC+DXLOG
      CALL PLOT (AALOC,7.0,3)
      IF (I.EQ.1)  10030,10031
10030 CALL PLOT (AALOC,6.9,2)
      GO TO 10029
10031 CALL PLOT (AALOC,6.95,2)
10029 CONTINUE
10028 CONTINUE
10027 CONTINUE
C*                                                                     *
C*    LABEL VERTICAL AXIS AND MAKE VERTICAL TICK MAEKS.                *
C*                                                                     *
      DELAX=5.0/5.0
      DEE=VF
      YSPAC=2.0-DELAX
      ANUM=(VG-VF)/5.0
      DEL=DEE-ANUM
      DO 86350  I=1,6
      YSPAC = YSPAC + DELAX
      BNUM=DEL+ANUM+.000001
      CALL PLOT (0.0,YSPAC,3)
      CALL PLOT (0.1,YSPAC,2)
      CALL PLOT (7.4,YSPAC,3)
      CALL PLOT (7.5,YSPAC,2)
      YYSPAC = YSPAC - 0.05
      CALL NUMBER (-0.7,YYSPAC,0.1,BNUM,0.0,4HF6.3)
      DEL=BNUM
```

Reproduced from
best available copy.

```
86350 CONTINUE
      CALL SYMBOL (-0.40,3.7,0.15,11HVOID RATIO.,90.0,11)
      CALL SYMBOL (2.5,1.5,0.15,16HTIME,  (MINUTES),0.0,16)
      CALL PLOT (0.0,2.0,-3)
      IC=0
      IIC=0
      DO 86500 I=1,LD
      DEWV(I)=EO-(1.0+EO)*(0.5-DEWV(I))
      IF (DEWV(I).LE.VO)  65001,65004
65001 IF (IC.EQ.0)  65003,65004
65003 ICC=I
      IC=IC+1
      GO TO 86500
65004 IF (DEWV(I).LT.VF)  65005,86501
65005 IF (IIC.EQ.0)  65006,86500
65006 IICC=I-1
      IIC=IIC+1
      KK=ICC
      LD=IICC
      GO TO 65011
86501 IF (I.EQ.LD)  65006,86500
86500  CONTINUE
65011 DO 65014  J=KK,LD
      I=J-KK+1
      TIME(I)=TIME(J)
65014  DEWV(I)=DEWV(J)
      TIME(LD-KK+2)=-2.0
      TIME(LD-KK+3)=XM/7.5
      DEWV(LD-KK+2)=VF
      DEWV(LD-KK+3)=(VO-VF)/5.0
      L=LD-KK+1
      CALL LINE(TIME,DEWV,L,1,0,26)
      DO 10033 I=1,L
      IF (TIME(I).GE.0.)  10034,10035
10034 TIME(I)=10.**TIME(I)
      GO TO 10033
10035 TIME(I)=1.0/(10.**(-TIME(I)))
10033 CONTINUE
C     PUNCH 833, L
C     PUNCH 2, (TIME(I),DEWV(I),I=1,L)
 833  FORMAT (I10)
      CALL PLOT(15.0,-2.0,-3)
C*                                                                         *
C*       PLOT UM VS. TIME FACTOR.                                          *
C*                                                                         *
      CALL PLOT (0.0,2.0,3)
      CALL PLOT (10.0,2.0,2)
      CALL PLOT (10.0,9.0,2)
      CALL PLOT (0.0,9.0,2)
      CALL PLOT (0.0,2.0,2)
C*                                                                         *
C*    LABEL HORIZONTAL AXIS AND MAKE HORIZONTAL TICK MARKS.                *
C*                                                                         *
      XM=NM
      CYCLE=10./XM
      ALOG=-CYCLE
      N=NM+1
      DO 6800 J=1,N
      ALOC=ALOC+CYCLE
      BALOC=ALOC-0.10
      CALL NUMBER(BALOC,1.75,0.10,10,0.0,2HI2)
      INUM=J-4
      CALOC=ALOC+0.09
      CALL NUMBER(CALOC,1.83,.07,INUM,0.0,2HI3)
      IF(J.EQ.N)  GO TO 689
      DO 680 I=1,9
      CC=I
      DXLOG=ALOG10(CC)*CYCLE
      AALOC=ALOC+DXLOG
      CALL PLOT(AALOC,2.0,3)
      IF (I.EQ.1)  10037,10038
10037 CALL PLOT (AALOC,2.1,2)
      GO TO 680
10038 CALL PLOT (AALOC,2.05,2)
680   CONTINUE
689   CONTINUE
6800  CONTINUE
      ALOC =-CYCLE
      DO 10039 J=1,N
      ALOC =ALOC+CYCLE
      IF (J.EQ.N)  GO TO 10040
      DO 10041 I=1,9
      CC=I
      DXLOG=ALOG10(CC)*CYCLE
      AALOC=ALOC+DXLOG
      CALL PLOT (AALOC,8.0,3)
      IF (I.EQ.1)  10042,10043
10042 CALL PLOT (AALOC,7.9,2)
      GO TO 10041
10043 CALL PLOT (AALOC,7.95,2)
10041 CONTINUE
10040 CONTINUE
10039 CONTINUE
C*                                                                     *
C*    LABEL VERTICAL AXIS AND MAKE VERTICAL TICK MAEKS.                *
C*                                                                     *
      DELAX=6.0/5.0
      DEE=0.0
      YSPAC=2.0-DELAX
      ANUM=1.0/5.0
      DEL=DEE-ANUM
      DO 6358 I=1,6
      YSPAC=YSPAC+DELAX
      BNUM=DEL+ANUM+0.00001
      CALL PLOT(0.0,YSPAC,3)
      CALL PLOT (0.1,YSPAC,2)
      CALL PLOT (9.9,YSPAC,3)
      CALL PLOT(10.0,YSPAC,2)
      YYSPAC=YSPAC-0.05
      CALL NUMBER(-0.5,YYSPAC,0.1,BNUM,0.0,4HF4.2)
      DEL=BNUM
6358  CONTINUE
      CALL SYMBOL(-0.8,3.5,0.15,18HPORE PRESSURE U/UO,90.0,18)
      CALL SYMBOL(4.0,1.5,0.15,14HTIME FACTOR, T, 0.0,14)
      CALL PLOT (0.0,2.0,-3)
      IF (LL.GT.0)  IT=JCOUNT-NCOUNT+1
      IKKK=0
      JKKK=IT
      DO 13  I=1,IT
13    TIME(I)=EMIT(I)
      DO 13001 J=1,IT
      IF (TIME(J).GT.1.0)  13002,13001
13002 IF (IKKK.EQ.0)  13003,13001
13003 IKKK=IKKK+1
      JKKK=J-1
13001 CONTINUE
      IT =JKKK
      TIME(IT+1)=-3.0
      TIME(IT+2)=XM/10.0
      UM(IT+1)=0.
      UM(IT+2)=1.0/6.0
      L=IT
      LU=L
      PRINT 6999, L
6999  FORMAT(2X,*L=*,I10)
      PRINT 61013,(  TIME(I), UM(I),I=1,L,10)
61013 FORMAT (2X,*TIMELG=*,E20.5,2X,*UUM=*,E20.5,
     1          2X,*TIMELG=*,E20.5,2X,*UUM=*,E20.5)
      CALL LINE (  TIME, UM,L,1.0,26)
      CALL PLOT (15.0,-2.0,-3)
C     PUNCH 833,  L
C     PUNCH 2, (  TIME(I),            UM(I),I=1,L)
C*                                                                *
C*       PLOT UM VS. TIME ( IN YEARS ).                           *
C*                                                                *
      DO 14   I=1,LU
      TIME(I)=TIME(I)-TFL
      IF (TIME(I).GE.-4.0)  311,314
311   IF (KJ.EQ.0)  313,314
313   KCOUN =I
      KJ=KJ+1
314   IF (TIME(I).GT.3.0)   GO TO 9993
14    CONTINUE
      GO TO 1995
9993    LU=I-1
1995  CALL PLOT (0.0,2.0,3)
      CALL PLOT (10.0,2.0,2)
      CALL PLOT (10.0,8.0,2)
      CALL PLCT (0.0,8.0,2)
      CALL PLOT (0.0,2.0,2)
C*                                                                *
C*    LABEL HORIZONTAL AXIS AND MAKE HORIZONTAL TICK MARKS.       *
C*                                                                *
      XM=MM
      CYCLF=10./XM
      ALOC=-CYCLE
      N=MM+1
      DO 4100 J=1,N
      ALOC=ALOC+CYCLF
      BALOC=ALOC-0.1
      CALL NUMBER(BALOC,1.75,0.10,10.,0.0,2HI2)
      INUM=J-9
      CALOC=ALOC+0.09
      CALL NUMBER(CALOC,1.93,.07,INUM,0.0,2HI3)
```

Reproduced from
best available copy.

```
      IF(J.EQ.N)  GO TO 499
      DO 450 I=1,9
      CC=I
      DXLOG=ALOG10(CC)*CYCLE
      AALOC=ALOC+DXLOG
      CALL PLOT(AALOC,2.0,3)
      IF (I.EQ.1)  10045,10046
10045 CALL PLOT (AALOC,2.1,2)
      GO TO 450
10046 CALL PLOT (AALOC,2.05,2)
450   CONTINUE
499   CONTINUE
4100  CONTINUE
      ALOC =-CYCLE
      DO 10047 J=1,N
      ALOC =ALOC+CYCLE
      IF (J.EQ.N)  GO TO 10048
      DO 10049 I=1,9
      CC=I
      DXLOG=ALOG10(CC)*CYCLE
      AALOC=ALOC+DXLOG
      CALL PLOT (AALOC,8.0,3)
      IF (I.EQ.1)  10050,10051
10050 CALL PLOT (AALOC,7.9,2)
      GO TO 10049
10051 CALL PLOT (AALOC,7.95,2)
10049 CONTINUE
10048 CONTINUE
10047 CONTINUE
C*
C*    LABEL VERTICAL AXIS AND MAKE VERTICAL TICK MARKS.
C*
      DELAX=6.0/5.0
      DEE=0.0
      YSPAC=2.0-DELAX
      ANUM=1.0/5.0
      DEL=DEE-ANUM
      DO 8350 I=1,6
      YSPAC=YSPAC+DELAX
      BNUM=DEL+ANUM+0.00001
      CALL PLOT(0.0,YSPAC,3)
      CALL PLOT (0.1,YSPAC,2)
      CALL PLOT (9.9,YSPAC,3)
      CALL PLOT(10.0,YSPAC,2)
      YYSPAC=YSPAC-0.05
      CALL NUMBER(-0.5,YYSPAC,0.1,BNUM,0.0,4HF4.2)
      DEL=BNUM
8350  CONTINUE
      CALL  SYMBOL(-0.9,3.3,0.15,23HMID-PLANE PORE PRESSURE,90.0,23)
      CALL SYMBOL(4.0,1.5,0.15,16HTIME, (IN YEARS),0.0,16)
      CALL PLOT (0.0,2.0,-3)
      KK=KCOUN
      DO 6389 J=KK,LU
      I=J-KK+1
       UM(I)=UM(J)
6389  TIME(I)=TIME(J)
        TIME(LU-KK+2)=-9.0
        TIME(LU-KK+3)=XM/10.0
       UM(LU-KK+2)=0.
       UM(LU-KK+3)=1.0/6.0
      L=LU-KCOUN +1
      PRINT 69990,L
69990 FORMAT (2X,*L=*,I10)
      CALL LINE (  TIME, UM,L,1,0,26)
      CALL PLOT (15.0,-2.0,-3)
C*                                                                      *
C*       PLOT UM VS. TIME ( IN MINUTE ).                                *
C*                                                                      *
      DO 7400  I=1,LU
      TIME(I)=TIME(I)+VRMIN
      IF (TIME(I).GE.-2.0)   73010,73040
73010 IF (IJ.EQ.0)  73030,73040
73030 ICOUN =I
      IJ=IJ+1
73040 IF (TIME(I).GT.6.0)  GO TO 9996
7400  CONTINUE
      GO TO 1996
9996  LU=I-1
C     MAKE BORDER
1996  CALL PLOT (0.0,2.0,3)
      CALL PLOT (7.5,2.0,2)
      CALL PLOT (7.5,7.0,2)
      CALL PLOT (0.0,7.0,2)
      CALL PLOT (0.0,2.0,2)
C*                                                                      *
C*    LABEL HORIZONTAL AXIS AND MAKE HORIZONTAL TICK MARKS.             *
C*                                                                      *
      XM=NMN
      CYCLE=7.5/XM
      ALOC=-CYCLE
      N=NMN+1
      DO 7100   J=1,N
      ALOC=ALOC+CYCLE
      BALOC=ALOC-0.10
      CALL NUMBER (BALOC,1.75,0.10,10,0.0,2HI2)
      INUM=J-3
      CALOC=ALOC+.38
      CALL NUMBER (CALOC,1.83,.07,INUM,0.0,2HI3)
      IF (J.EQ.N) GO TO 799
      DO 750  I=1,9
      CC=I
      DXLOG=ALOG10(CC) *CYCLE
      AALOC=ALOC+DXLOG
      CALL PLOT (AALOC,2.0,3)
      IF (I.EQ.1)  10053,10054
10053 CALL PLOT (AALOC,2.1,2)
      GO TO 750
10054 CALL PLOT (AALOC,2.05,2)
750    CONTINUE
799   CONTINUE
7100  CONTINUE
      ALOC=-CYCLE
      DO 10055 J=1,N
      ALOC=ALOC+CYCLE
      IF (J.EQ.N)  GO TO 10056
      DO 10057 I=1,9
```

Reproduced from
best available copy.

```
      CC=I
      DXLOG=ALOG10(CC)*CYCLE
      AALOC=ALOC+DXLOG
      CALL PLOT (AALOC,7.0,3)
      IF (I.EQ.1)  10058,10059
10058 CALL PLOT (AALOC,6.9,2)
      GO TO 10057
10059 CALL PLOT (AALOC,6.95,2)
10057 CONTINUE
10056 CONTINUE
10055 CONTINUE
C*                                                                      *
C*    LABEL VERTICAL AXIS AND MAKE VERTICAL TICK MAEKS.                 *
C*                                                                      *
      DELAX=5.0/5.0
      DEE=0.0
      YSPAC=2.0-DELAX
      ANUM=1.0/5.0
      DEL=DEE-ANUM
      DO 7350 I=1,6
      YSPAC=YSPAC+DELAX
      BNUM=DEL+ANUM+0.00001
      CALL PLOT(0.0,YSPAC,3)
      CALL PLOT (0.1,YSPAC,2)
      CALL PLOT (7.4,YSPAC,3)
      CALL PLOT( 7.5,YSPAC,2)
      YYSPAC=YSPAC-0.05
      CALL NUMBER(-0.5,YYSPAC,0.1,BNUM,0.0,4HF4.2)
      DEL=BNUM
7350  CONTINUE
      CALL SYMBOL(-0.8,2.8,0.15,23HMID-PLANE PORE PRESSURE,90.0,23)
      CALL SYMBOL(2.5,1.5,0.15,17HTIME (IN MINUTES),0.0,17)
      CALL PLOT (0.0,2.0,-3)
      KK=ICOUN
      DO 7319 J=KK,LU
      I=J-KK+1
       UM(I)=UM(J)
7319  TIME(I)=TIME(J)
      TIME(LU-KK+2)=-2.0
        TIME(LU-KK+3)=XM/7.5
       UM(LU-KK+2)=0.
       UM(LU-KK+3)=1.0/5.0
      L=LU-ICOUN +1
      CALL LINE (  TIME, UM,L,1,0,26)
32    NSET=NSET+1
      IF (NSET.EQ.ISET) 4188,6188
6188  ICOUNT=0
      NN=0
      GO TO 6
4188  CONTINUE
      CALL ENDPLT
      END
C*                                                                      *
C*             THE FUNCTION SUBROUTINE FOR CALCULATING Q                *
C*                                                                      *
```

```
      FUNCTION FQQ(W,V,PP,R,EPTOF,BO,AA,BB,IMAX,IIMAX)
      AAV=AA**V
      BBV=BB**V
      PPW=PP**W
      PPV=PP**V
      DD=BO/(PP-1.)*BBV*(PPW-PPV)
      IF (DD.GT.120.)  GO TO 242
      IF (DD.LT.-240.)  GO TO 243
      GO TO 250
242   DD=120.
      GO TO 250
243   DD=-200.
250   EE=EXP(DD)
      EEE=1./EE
      SSINH=0.5*(EE-EEE)
      CCOSH=0.5*(EE+EEE)
      FQQ=+(PP-1.)/(R*EPTOF)*SSINH*AAV*ALOG(AA)+AAV/(R*EPTOF)*CCOSH*BO
     1  *((PPW-PPV)*BBV*ALOG(BB)-BBV*PPV*ALOG(PP))
      RETURN
      END
C*                                                                      *
C*                FUNCTION SUBROUTINE FOR CALCULATING P                 *
C*                                                                      *
      FUNCTION FQ(W,V,PP,R,EPTOF,BO,AA,BB,IMAX,IIMAX)
      AAV=AA**V
      BBV=BB**V
      PPW=PP**W
      PPV=PP**V
      DD=BO/(PP-1.)*BBV*(PPW-PPV)
      IF (DD.GT.120.)  GO TO 242
      IF (DD.LT.-240.)  GO TO 243
      GO TO 250
242   DD=120.
      GO TO 250
243   DD=-200.
250   EE=EXP(DD)
      EEE=1./EE
      SSINH=0.5*(EE-EEE)
      FQ=+(PP-1.)/(R*EPTOF)*AAV*SSINH
      RETURN
      END
C*                                                                      *
C*                FUNCTION SUBROUTINE FOR CALCULATING QQ                *
C*                                                                      *
      FUNCTION FP(W,V,XKK,XN,PP,R,EPTOF,EPOF,BO,AA,BB,IMAX,IIMAX,EO)
      PPW=PP**W
      XNWV=(1.-XN)*W+XN*V
      XKKWV=XKK**XNWV
      FP=XKKWV*PPW/((1.0-XN)*(1.0-EPOF*XNWV))
      RETURN
      END
C*                                                                      *
C*                FUNCTION SUBROUTINE FOR CALCULATING V                 *
C*                                                                      *
      FUNCTION FV(W,V,PP,R,EPTOF,BO,AA,BB,DT,IMAX,IIMAX)
      QF=FQ(W,V,PP,R,EPTOF,BO,AA,BB,IMAX,IIMAX)
      QQF=FQQ(W,V,PP,R,EPTOF,BO,AA,BB,IMAX,IIMAX)
      FV=V+DT *QF*(1.0+0.5*DT *QQF)
      RETURN
      END
C*                                                                      *
C*                FUNCTION SUBROUTINE FOR CALCULATING PH                *
C*                                                                      *
```

Reproduced from
best available copy.

```
FUNCTION PH(H,V,D,EC,WGR,EKTF,CX,CY,EK,TIME,TF)
EKTTF=-EK*TIME/TF
DVSDT=WGR*EKTF*EXP(EKTTF)
PH=(EC-(H+D*V))*DVSDT*CX*(CY-(H+D*V))
RETURN
END
```

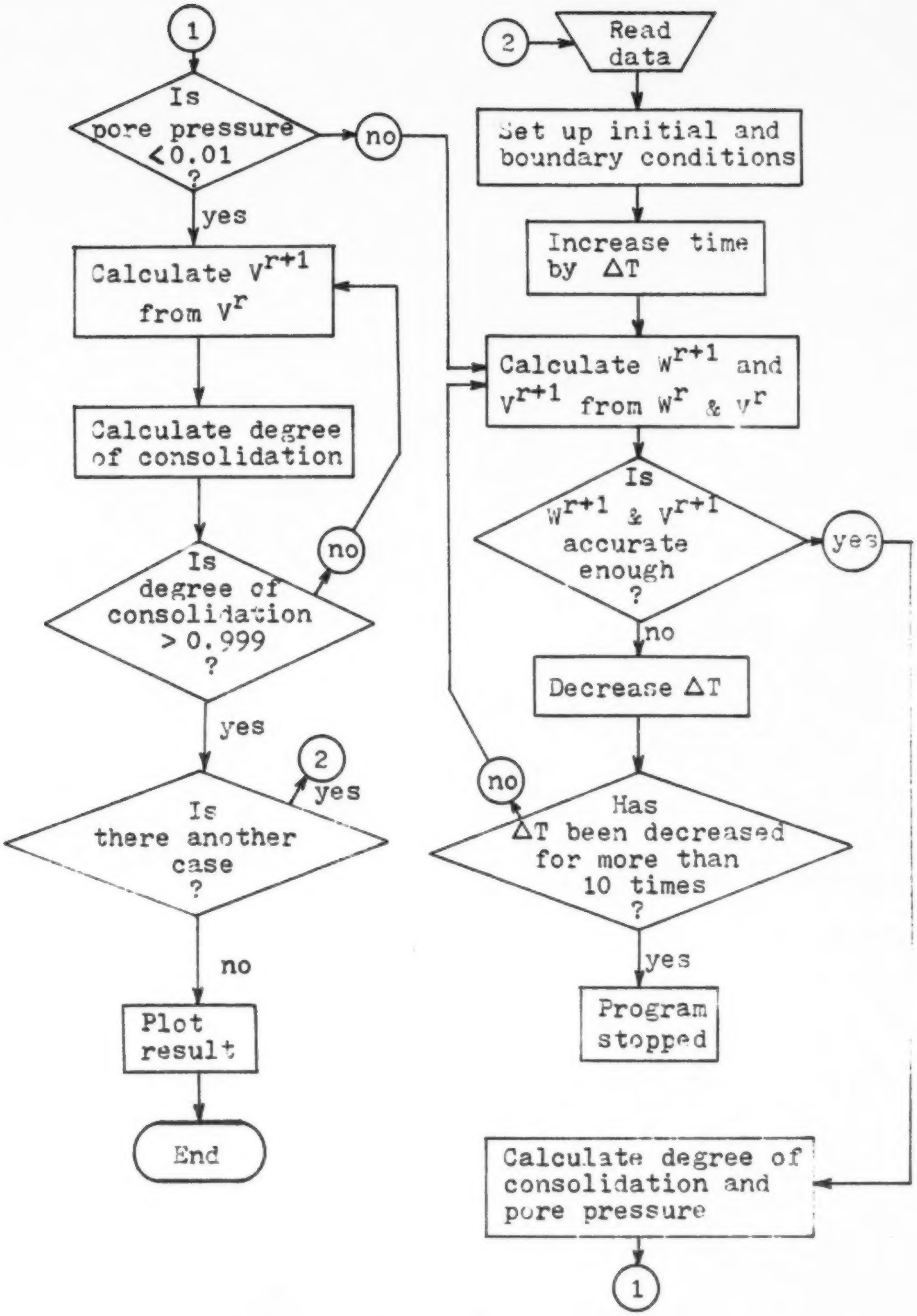
1
Is pore pressure <0.01 ?
no
yes
Calculate V^{r+1} from V^r
Calculate degree of consolidation
Is degree of consolidation > 0.999 ?
no
yes
Is there another case ?
2
yes
no
Plot result
End
2
Read data
Set up initial and boundary conditions
Increase time by ΔT
Calculate W^{r+1} and V^{r+1} from W^r & V^r
Is W^{r+1} & V^{r+1} accurate enough ?
yes
no
Decrease ΔT
Has ΔT been decreased for more than 10 times ?
no
yes
Program stopped
Calculate degree of consolidation and pore pressure
1

Flow chart for computer program

Appendix C

COMPUTER INPUT DATA FOR THE SAMPLES TESTED

Sample : A2-2-1

OK	EO	RW	HO	AO	BO	PO	ETOF	EOF	AA	BB	XKK
380	2.585	62.4	0.142	$1.557x10^{-6}$	15.0	144	0.241	.326	.500	.250	.566

VSO	EK	IT	DELX	TIMEF	TTIMEF	MM	NMN	NM	ISTART	MR	VO	VF
18.461	.01497	3902	.1	1.0	10^8	11	8	4	0	2	2.58	2.28

Sample : A2-2-2

OK	EO	RW	HO	AO	BO	PO	ETOF	EOF	AA	BB	XKK
300	2.443	62.4	0.136	$8.433x10^{-6}$	16.0	288	0.251	.351	.500	.500	.550

VSO	EK	IT	DELX	TIMEF	TTIMEF	MM	NMN	NM	ISTART	MR	VO	VF
18.461	.01497	3902	.1	1.0	10^8	11	8	4	0	2	2.44	2.10

Sample : A2-4-1

OK	EO	RW	HO	AO	BO	PO	ETOF	EOF	AA	BB	XKK
330	2.498	62.4	.140	2.130×10^{-6}	13.0	144	.322	.509	.250	.250	.450

VSO	EK	IT	DELX	TIMEF	TTIMEF	MM	NMN	NM	ISTART	MR	VO	VF
18.655	.01497	3902	.1	1.0	10^8	11	8	4	0	2	2.49	1.99

Sample : A2-4-2

OK	EO	RW	HO	AO	BO	PO	ETOF	EOF	AA	BB	XKK
210	2.228	62.4	.129	5.994×10^{-7}	15.0	576	.334	.723	.250	.500	.286

VSO	EK	IT	DELX	TIMEF	TTIMEF	MM	NMN	NM	ISTART	MR	VO	VF
18.655	.01497	3902	.1	1.0	10^8	11	8	4	0	2	2.22	1.12

Sample : A2-8-1

OK	EO	RW	HO	AO	BO	PO	ETOF	EOF	AA	BB	XKK
330	2.495	62.4	0.138	2.771×10^{-6}	12.0	144	0.418	0.891	.125	.354	.212

VSO	EK	IT	DELX	TIMEF	TTIMEF	MM	NMN	NM	ISTART	MR	VO	VF
18.383	.01497	3902	.1	1.0	10^8	11	8	4	0	2	2.49	1.60

Sample : A2-16-1

OK	EO	RW	HO	AO	BO	PO	ETOF	EOF	AA	BB	XKK
140	2.035	62.4	0.129	3.292×10^{-6}	15.0	144	0.432	1.108	.063	.250	.150

VSO	EK	IT	DELX	TIMEF	TTIMEF	MM	NMN	NM	ISTART	MR	VO	VF
19.938	.01497	3902	.1	1.0	10^8	11	8	4	0	2	2.00	1.10

Sample : A3-2-1

OK	EO	RW	HO	AO	BO	PO	ETOF	EOF	AA	BB	XKK
355	2.543	62.4	0.216	1.758×10^{-6}	15.0	144	0.269	0.313	.500	.250	.577

VSO	EK	IT	DELX	TIMEF	TTIMEF	MM	NMN	NM	ISTART	MR	VO	VF
18.082	.01497	3902	.1	1.0	10^8	11	8	4	0	2	2.54	2.30

Sample : A3-2-2

OK	EO	RW	HO	AO	BO	PO	ETOF	EOF	AA	BB	XKK
295	2.154	62.4	0.209	8.509×10^{-7}	14.0	288	0.253	0.283	.500	.250	.610

VSO	EK	IT	DELX	TIMEF	TTIMEF	MM	NMN	NM	ISTART	MR	VO	VF
18.082	.01497	3902	.1	1.0	10^8	11	8	4	0	2	2.43	2.23

Sample : A3-4-1

OK	EO	RW	HO	AO	BO	PO	ETOF	EOF	AA	BB	XKK
560	2.808	62.4	0.230	1.021×10^{-6}	16.0	144	.168	.380	.250	.500	.518

VSO	EK	IT	DELX	TIMEF	TTIMEF	MM	NMN	NM	ISTART	MR	VO	VF
17.555	.01497	3902	.1	1.0	10^8	11	8	4	0	2	2.80	2.30

Sample : A3-4-2

OK	EO	RW	HO	AO	BO	PO	ETOF	EOF	AA	BB	XKK
340	2.521	62.4	.213	6.036×10^{-7}	20.0	576	.367	.773	.250	.500	.265

VSO	EK	IT	DELX	TIMEF	TTIMEF	MM	NMN	NM	ISTART	MR	VO	VF
17.555	.01497	3902	.1	1.0	10^8	11	8	4	0	2	2.52	1.74

Sample : A3-8-1

OK	EO	RW	HO	AO	BO	PO	ETOF	EOF	AA	BB	XKK
345	2.533	62.4	.216	2.525×10^{-6}	15.0	144	.381	.754	.125	.354	.276

VSO	EK	IT	DELX	TIMEF	TTIMEF	MM	NMN	NM	ISTART	MR	VO	VF
18.555	.01497	3902	.1	1.0	10^8	11	8	4	0	2	2.50	1.80

Sample : A3-16-1

OK	EO	RW	HO	AO	BO	PO	ETOF	EOF	AA	BB	XKK
430	2.668	62.4	.223	2.596×10^{-6}	15.0	144	.411	1.304	.063	.250	.107

VSO	EK	IT	DELX	TIMEF	TTIMEF	MM	NMN	NM	ISTART	MR	VO	VF
18.004	.01497	3902	.1	1.0	10^8	11	8	4	0	2	2.60	1.45

Sample : A4-2-1

OK	EO	RW	HO	AO	BO	PO	ETOF	EOF	AA	BB	XKK
540	2.799	62.4	.305	1.403×10^{-6}	15.0	144	.235	.370	.500	.707	.222

VSO	EK	IT	DELX	TIMEF	TTIMEF	MM	NMN	NM	ISTART	MR	VO	VF
17.456	.01497	3902	.1	1.0	10^8	11	8	4	0	2	2.77	2.44

Sample : A4-2-2

OK	EO	RW	HO	AO	BO	PO	ETOF	EOF	AA	BB	XKK
380	2.334	62.4	.288	6.441×10^{-2}	20.0	288	.120	.251	.500	.500	.645

VSO	EK	IT	DELX	TIMEF	TTIMEF	MM	NMN	NM	ISTART	MR	VO	VF
17.456	.01497	3902	.1	1.0	10^8	11	8	4	0	2	2.58	2.30

Sample : A4-4-1

OK	EO	RW	HO	AO	BO	PO	ETOF	EOF	AA	BB	XKK
420	2.652	62.4	.292	1.672×10^{-6}	15.0	144	.264	.468	.250	.250	.452

VSO	EK	IT	DELX	TIMEF	TTIMEF	MM	NMN	NM	ISTART	MR	VO	VF
17.788	.01497	3902	.1	1.0	10^8	11	8	4	0	2	2.65	2.15

Sample : A4-4-2

OK	EO	RW	HO	AO	BO	PO	ETOF	EOF	AA	BB	XKK
260	2.374	62.4	.270	8.219×10^{-7}	16.0	576	.479	.819	.250	.250	.242

VSO	EK	IT	DELX	TIMEF	TTIMEF	MM	NMN	NM	ISTART	MR	VO	VF
17.788	.01497	62.4	.1	1.0	10^8	11	8	4	0	2	2.35	1.55

Sample : A4-8-1

OK	EO	RW	HO	AO	BO	PO	ETOF	EOF	AA	BB	XKK
210	2.241	62.4	.263	4.469×10^{-6}	20.0	144	.626	.993	.125	.125	.181

VSO	EK	IT	DELX	TIMEF	TTIMEF	MM	NMN	NM	ISTART	MR	VO	VF
19.613	.01497	3902	.1	1.0	10^8	11	8	4	0	2	2.24	1.24

Sample :

OK	EO	RW	HO	AO	BO	PO	ETOF	EOF	AA	BB	XKK

VSO	EK	IT	DELX	TIMEF	TTIMEF	MM	NMN	NM	ISTART	MR	VO	VF

Sample : R3-2-1

OK	EO	RW	HO	AO	BO	PO	ETOF	EOF	AA	BB	XKK
330	2.049	62.4	.224	$2.437\text{x}10^{-6}$	15.0	144	.375	.462	.500	.250	1445

VSO	EK	IT	DELX	TIMEF	TTIMEF	MM	NMN	NM	ISTART	MR	VO	VF
---	---	3902	.1	1.0	10^8	11	8	4	0	2	2.50	2.20

Sample : R3-2-2

OK	EO	RW	HO	AO	BO	PO	ETOF	EOF	AA	BB	XKK
250	2.340	62.4	.213	$1.961\text{x}10^{-6}$	15.0	288	.566	.695	.500	.250	.296

VSO	EK	IT	DELX	TIMEF	TTIMEF	MM	NMN	NM	ISTART	MR	VO	VF
---	---	3902	.1	1.0	10^8	11	8	4	0	2	2.32	1.92

Sample : R3-4-1											
OK	EO	RW	HO	AO	BO	PO	ETOF	EOF	AA	BB	XKK
260	2.377	62.4	.216	$4.861\mathrm{x}10^{-6}$	18.0	144	.709	.975	.250	.250	.192

VSO	EK	IT	DELX	TIMEF	TTIMEF	MM	NMN	NM	ISTART	MR	VO	VF
---	---	3902	.1	1.0	10^8	11	8	4	0	2	2.50	1.60

Sample : R3-4-2											
OK	EO	RW	HO	AO	BO	PO	ETOF	EOF	AA	BB	XKK
100	1.82	62.4	.180	$1.463\mathrm{x}10^{-6}$	18.0	576	.713	1.046	.250	.250	.165

VSO	EK	IT	DELX	TIMEF	TTIMEF	MM	NMN	NM	ISTART	MR	VO	VF
---	---	3902	.1	1.0	10^8	11	8	4	0	2	1.80	0.80

Sample : R3-8-1

OK	EO	RW	HO	AO	BO	PO	ETOF	EOF	AA	BB	XKK
290	2.435	62.4	.219	4.725×10^{-6}	16.0	144	.701	1.153	.125	.354	.141

VSO	EK	IT	DELX	TIMEF	TTIMEF	MM	NMN	NM	ISTART	MR	VO	VF
---	---	3902	.1	1.0	10^8	11	8	4	0	2	2.43	1.53

Sample : R3-16-1

OK	EO	RW	HO	AO	BO	PO	ETOF	EOF	AA	BB	XKK
320	2.485	62.4	.223	4.812×10^{-6}	16.0	144	.725	1.472	.063	.250	.078

VSO	EK	IT	DELX	TIMEF	TTIMEF	MM	NMN	NM	ISTART	MR	VO	VF
---	---	3902	.1	1.0	10^8	11	8	4	0	2	2.40	1.20

Appendix D

RESULTS OF THE PARAMETER STUDY OF CREEP MODELS

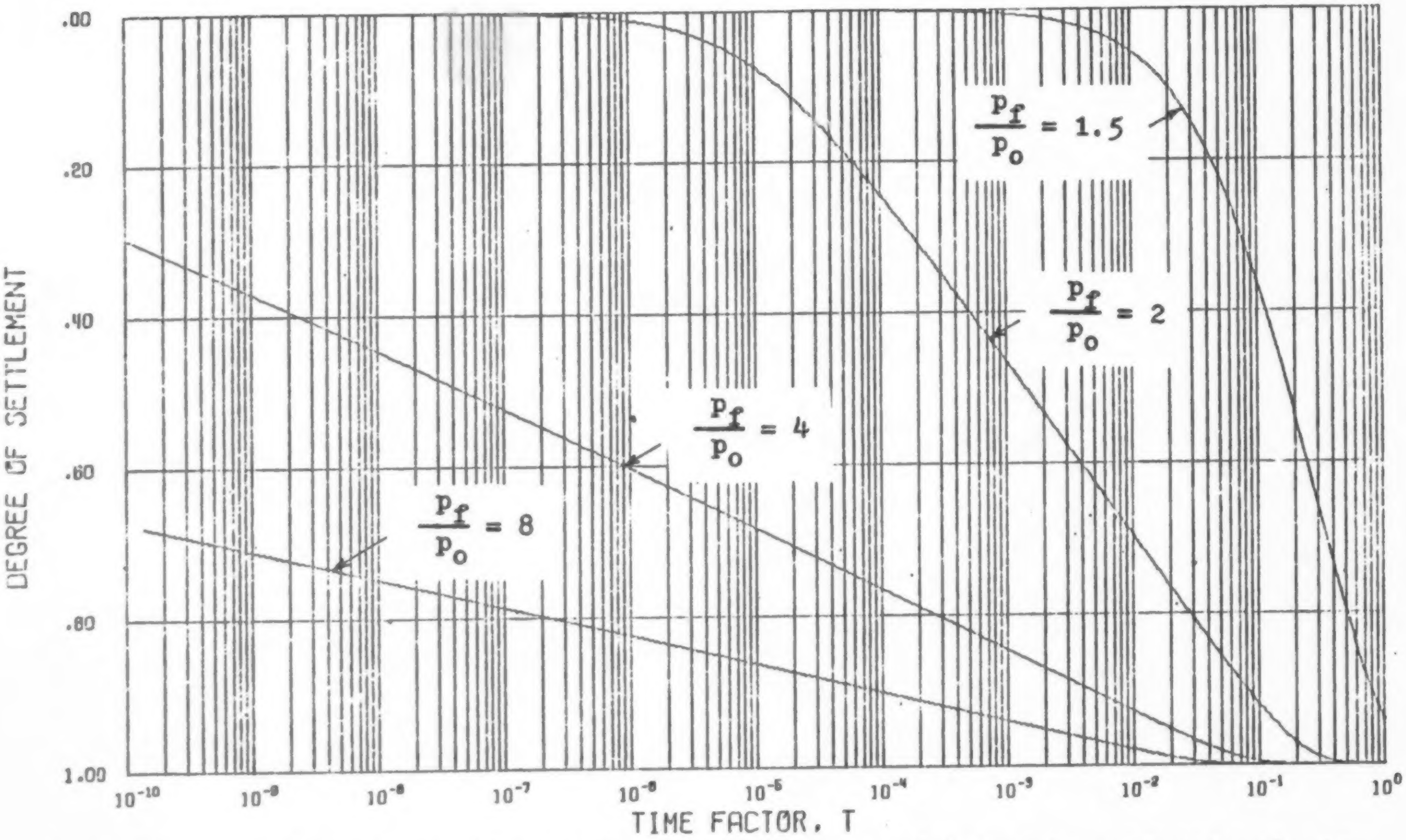

Fig. D-1. Settlement vs. time factor of the creep model based on structural viscosity for various values of stress increment: $\alpha_o p_o = 10$, $(p_f/p_o)(\alpha_f/\alpha_o)^{0.5} = 1$

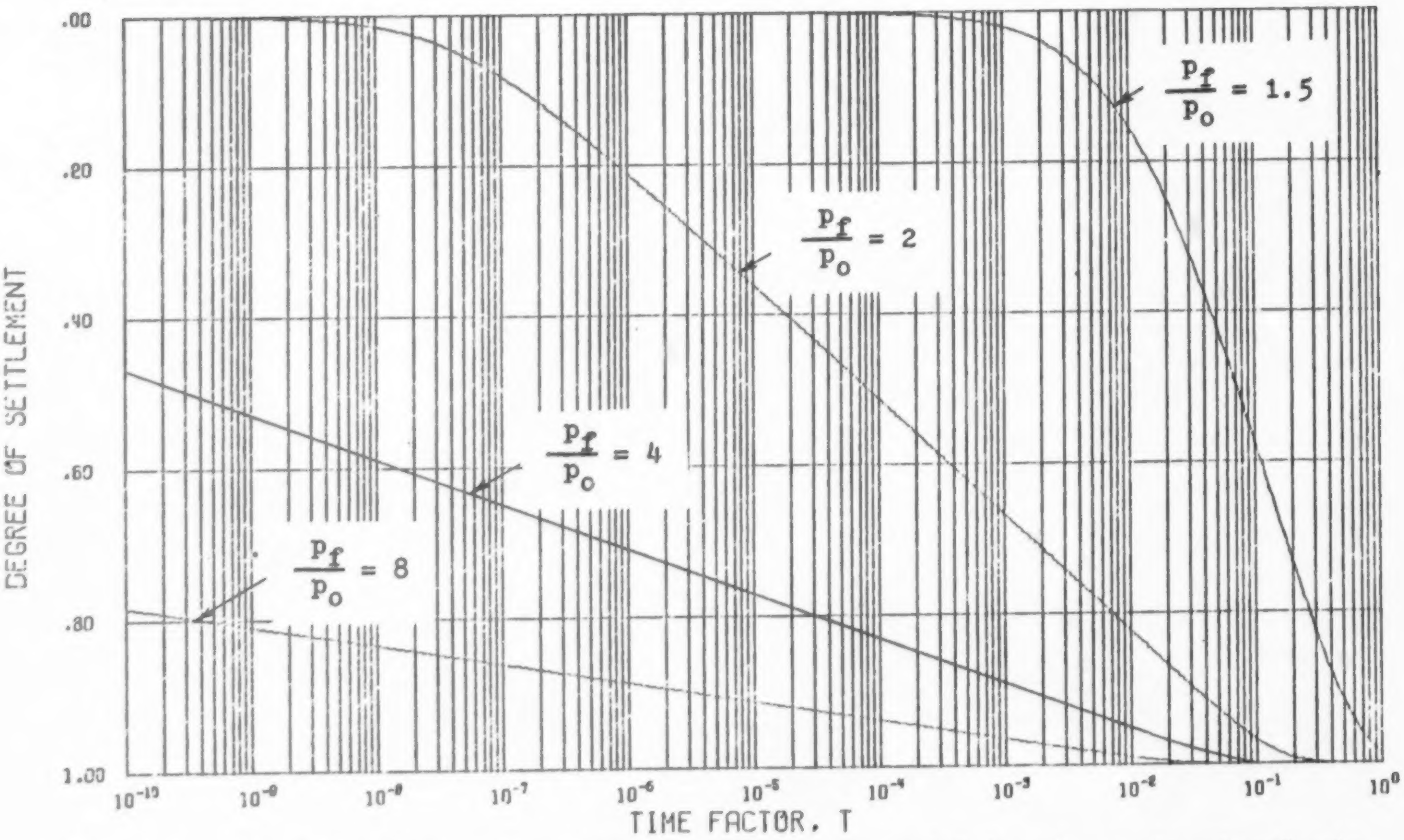

Fig. D-2. Settlement vs. time factor of the creep model based on structural viscosity for various values of stress increment: $\alpha_o p_o = 15$, $(p_f/p_o)(\alpha_f/\alpha_o)^{0.5} = 1$

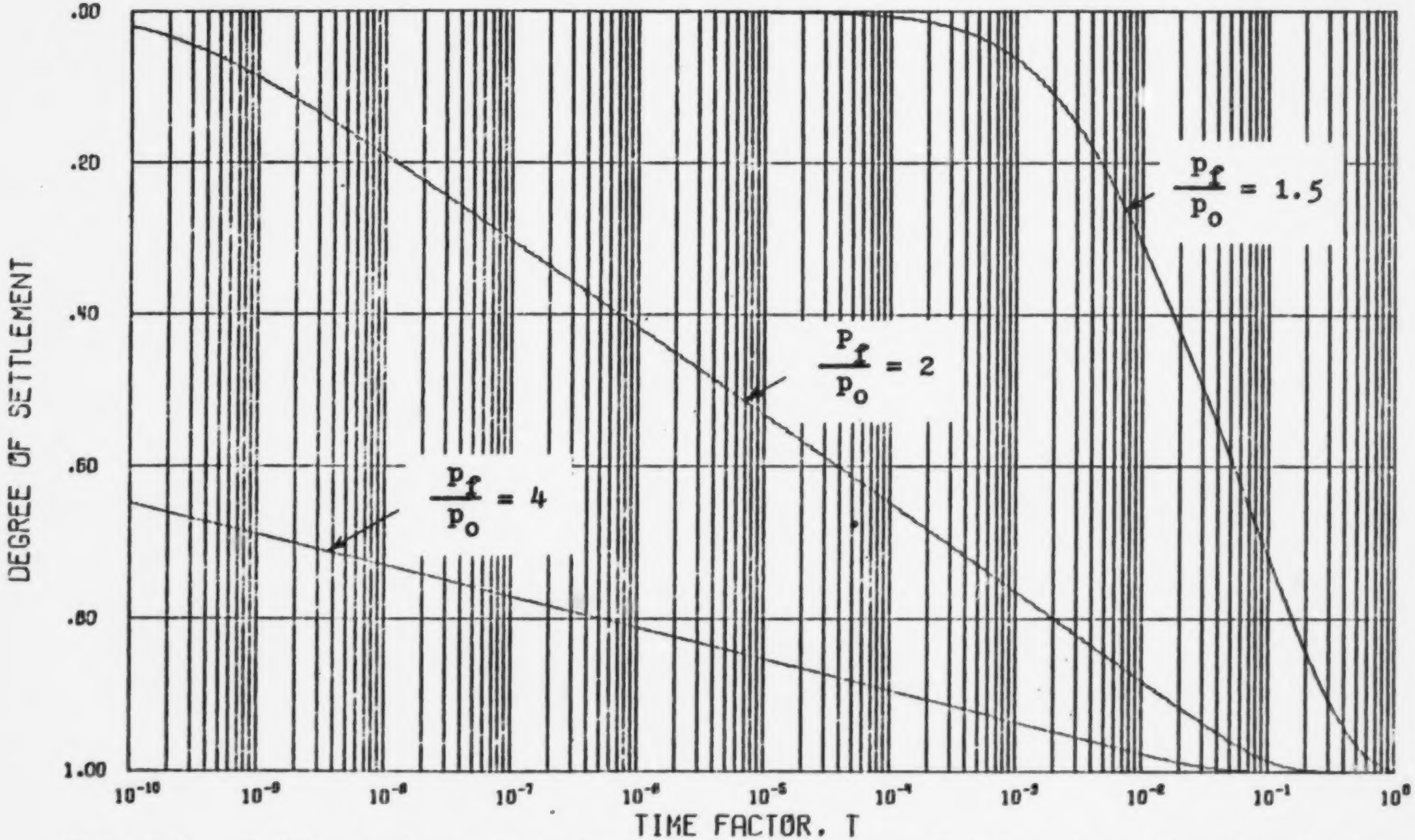

Fig. D-3. Settlement vs. time factor of the creep model based on structural viscosity for various values of stress increment: $\alpha_o p_o = 20$, $(p_f/p_o)(\alpha_f/\alpha_o)^{0.5} = 1$

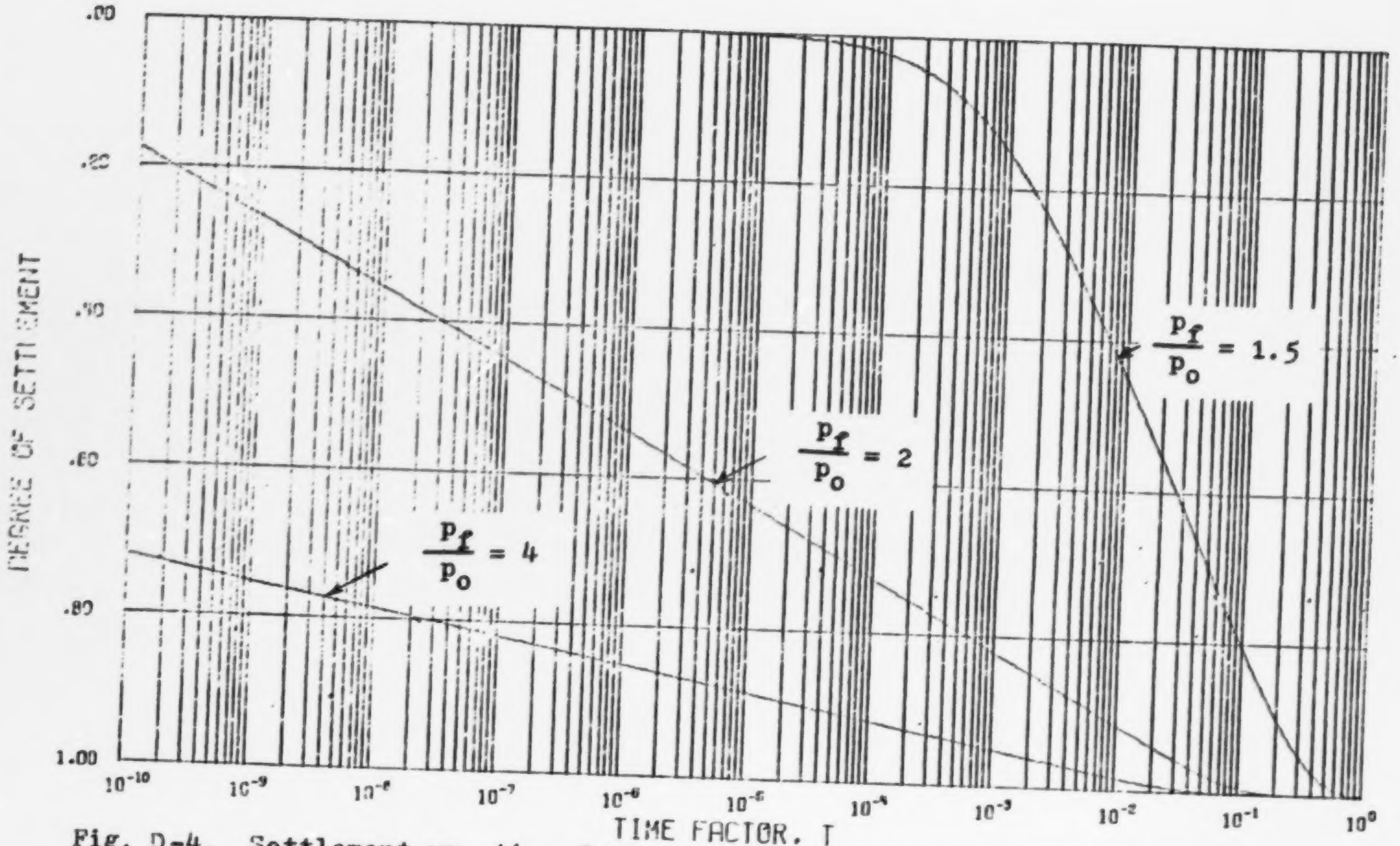

Fig. D-4. Settlement vs. time factor of the creep model based on structural viscosity for various values of stress increment: $\alpha_o p_o = 25$, $(p_f/p_o)(\alpha_f/\alpha_o)^{0.5} = 1$

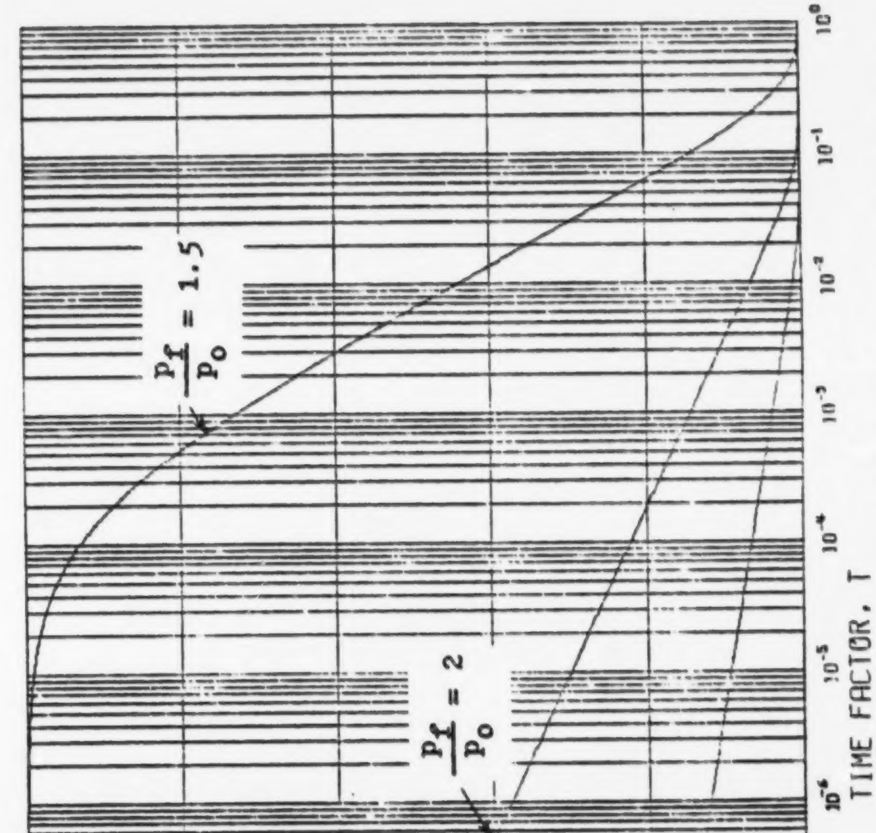

Fig. D-5. Settlement vs. time factor of the creep model based on structural viscosity for various values of stress increment: $a_o p_o = 30$, $(p_f/p_o)(a_f/a_o)^{0.5} = 1$

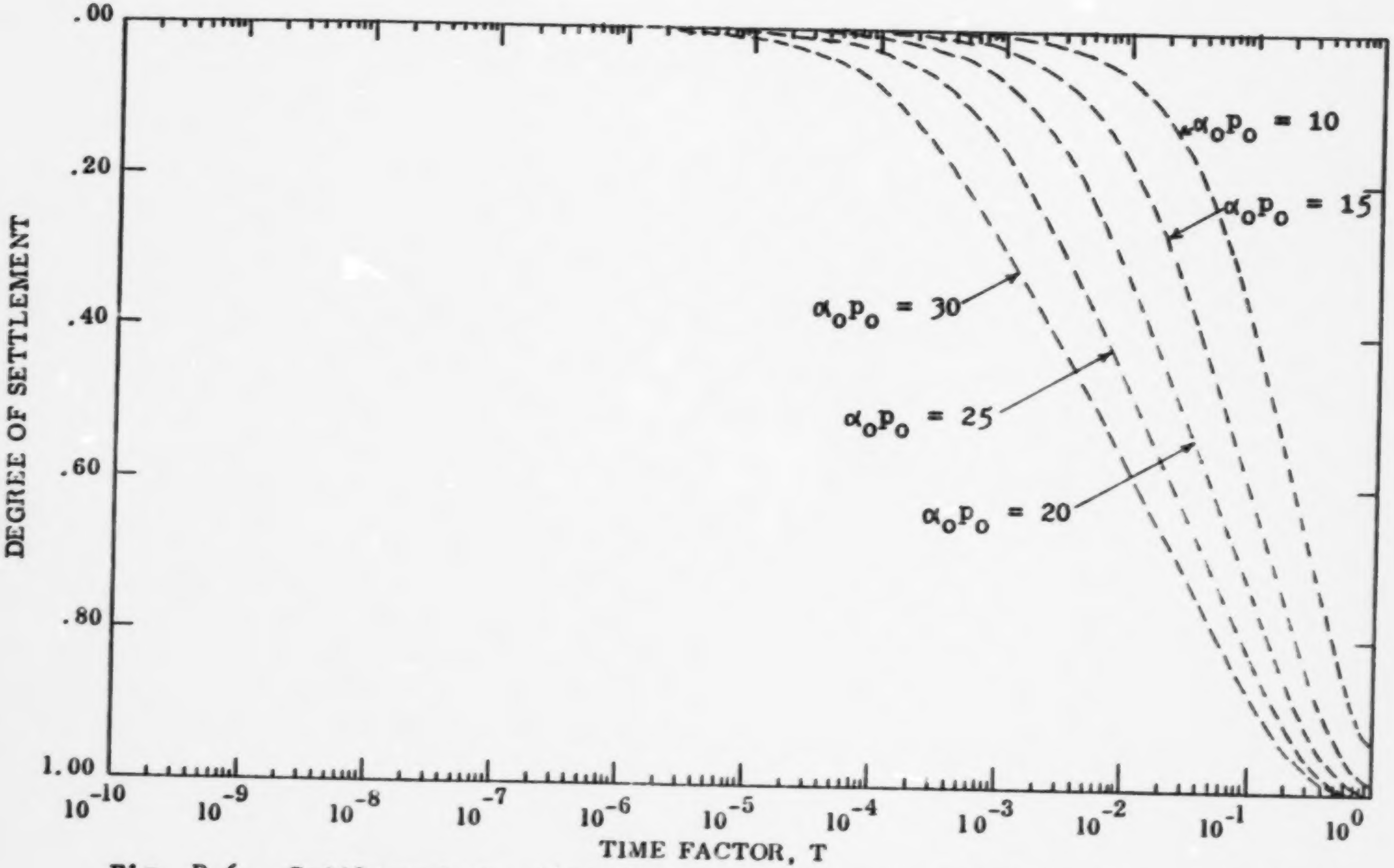

Fig. D-6. Settlement vs. time factor of the creep model based on structural viscosity for various values of $\alpha_o p_o$, $(p_f/p_o) = 1.5$, $(p_f/p_o)(\alpha_f/\alpha_o)^{0.5} = 1$.

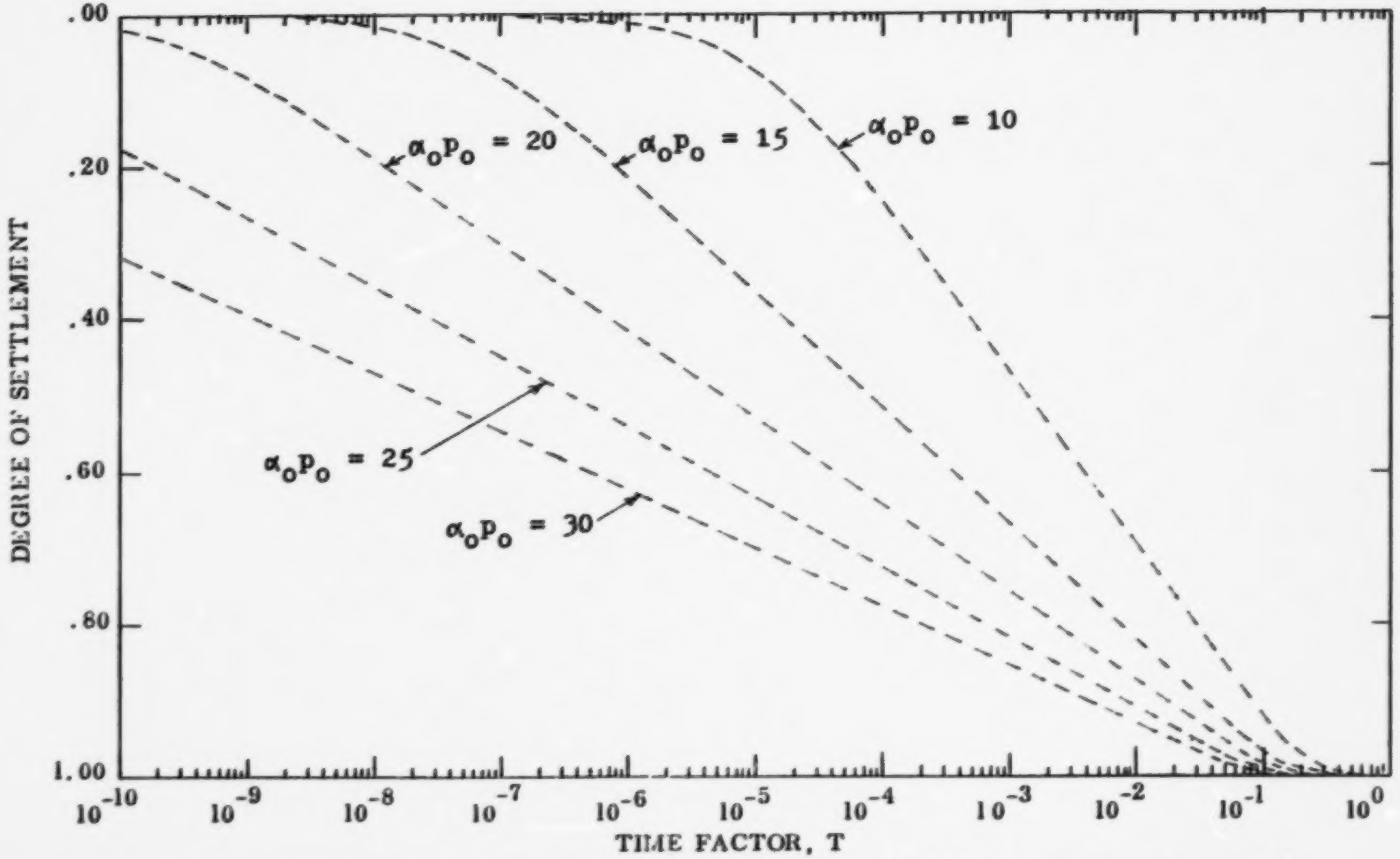

Fig. D-7. Settlement vs. time factor of the creep model based on structural viscosity for various values of $\alpha_o p_o$: $(p_f/p_o) = 2$, $(p_f/p_o)(\alpha_f/\alpha_o)^{0.5} = 1$

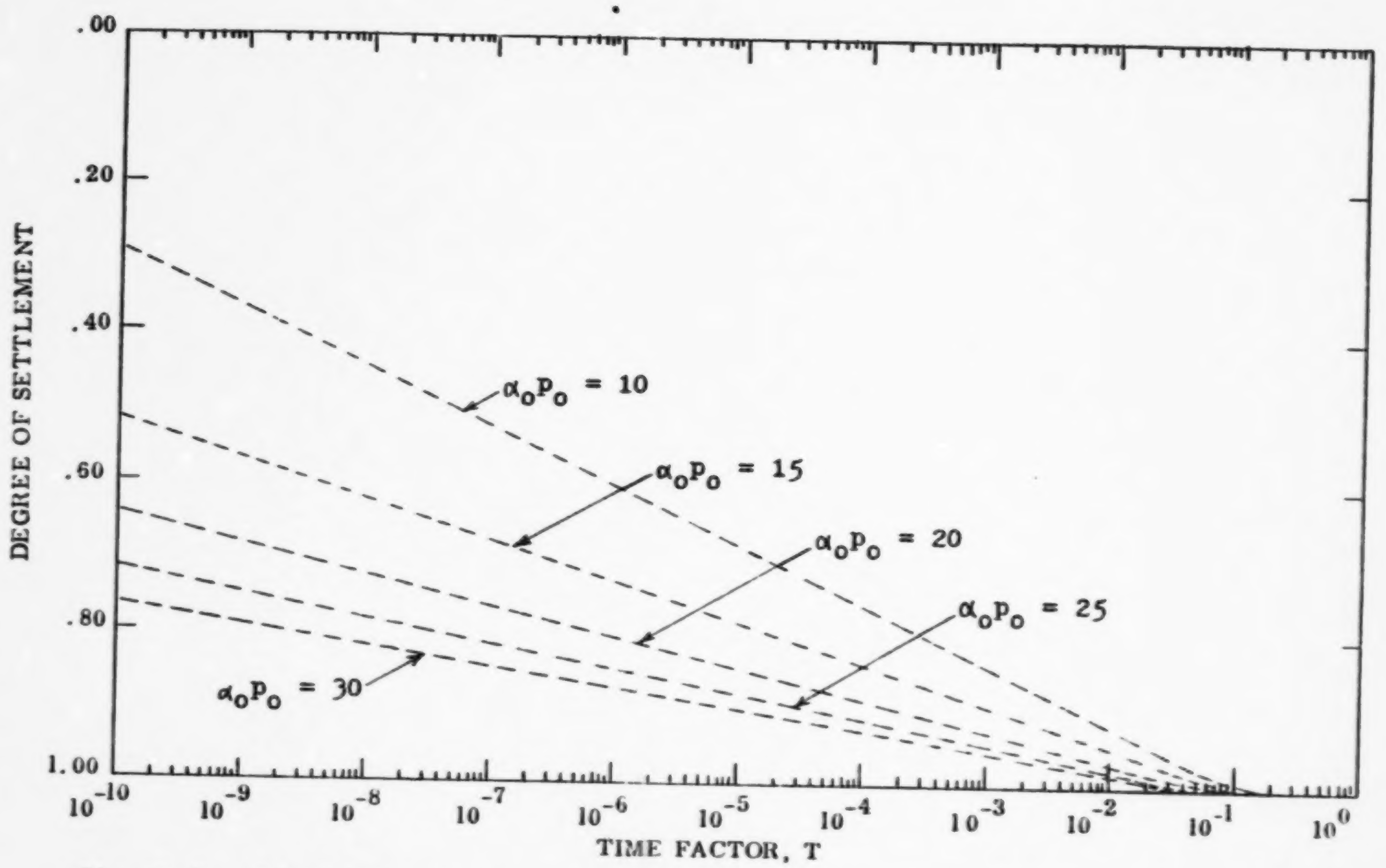

Fig. D-8. Settlement vs. time factor of the creep model based on structural viscosity for various values of $\alpha_o p_o$; $(p_f/p_o) = 4$, $(p_f/p_o)(\alpha_f/\alpha_o)^{0.5} = 1$

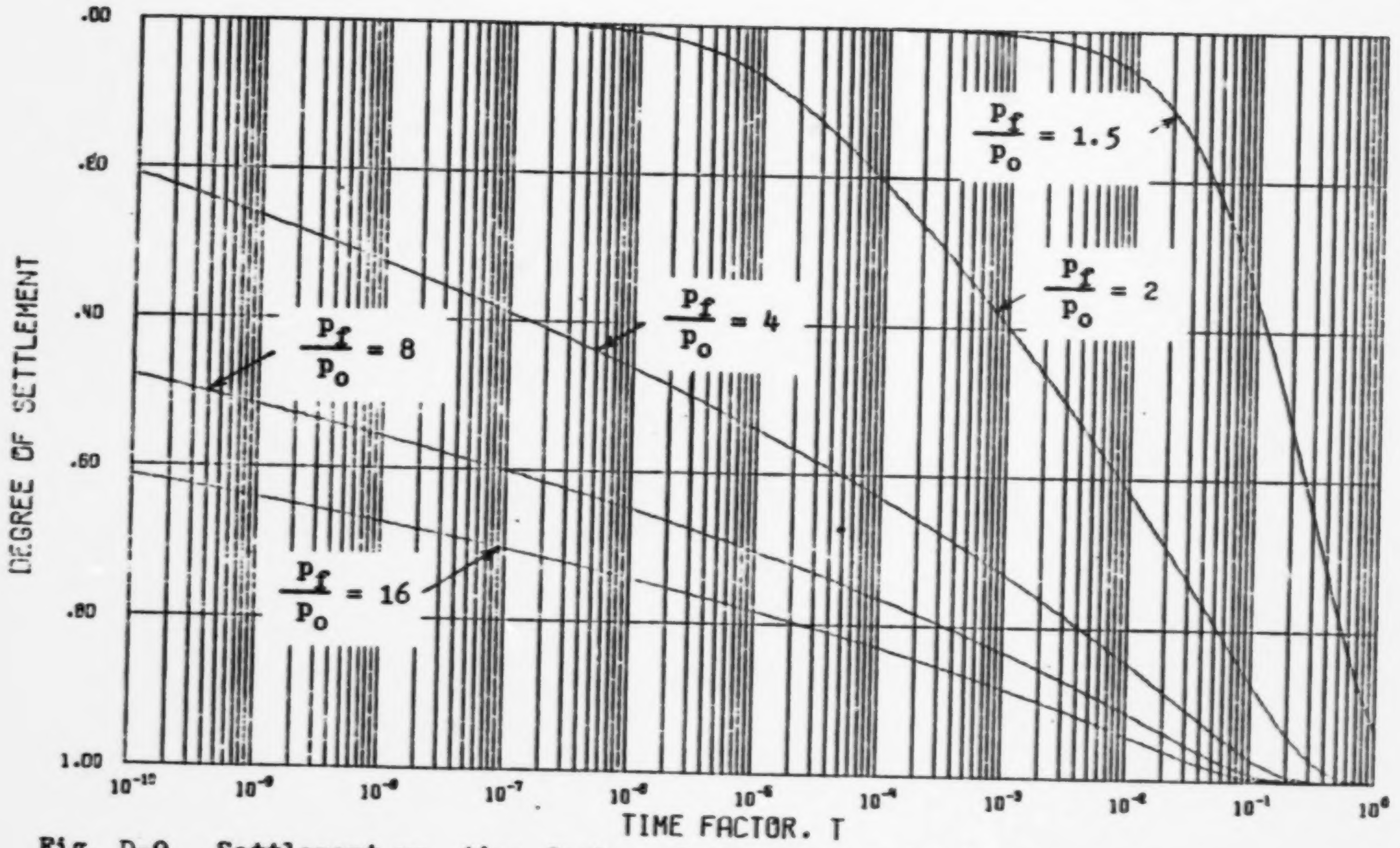

Fig. D-9. Settlement vs. time factor of the creep model based on structural viscosity for various values of stress increment: $\alpha_o p_o = 10$, $(p_f/p_o)(\alpha_f/\alpha_o) = 1$.

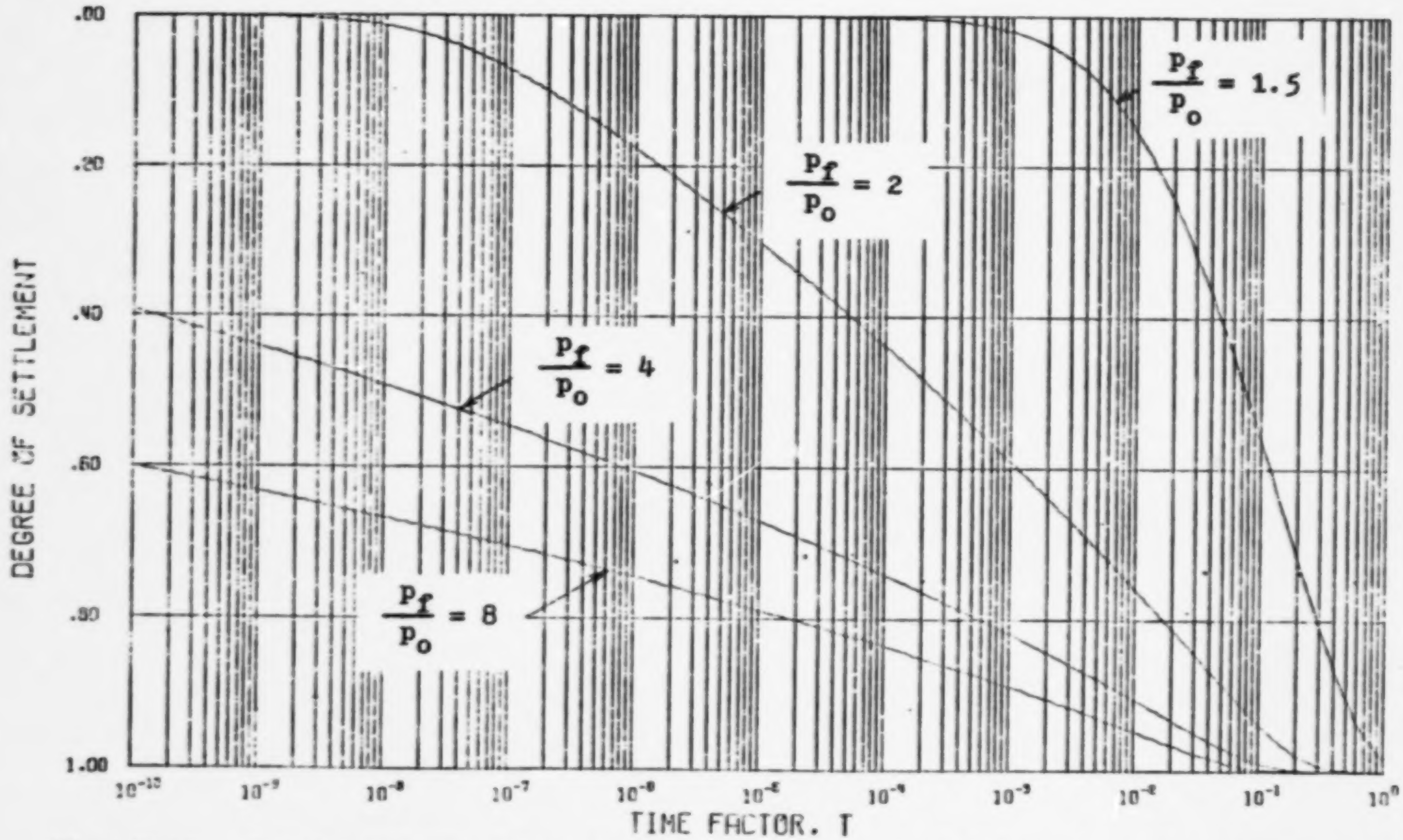

Fig. D-10. Settlement vs. time factor of the creep model based on structural viscosity for various values of stress increment: $\alpha_o p_o = 15$, $(p_f/p_o)(\alpha_f/\alpha_o) = 1$

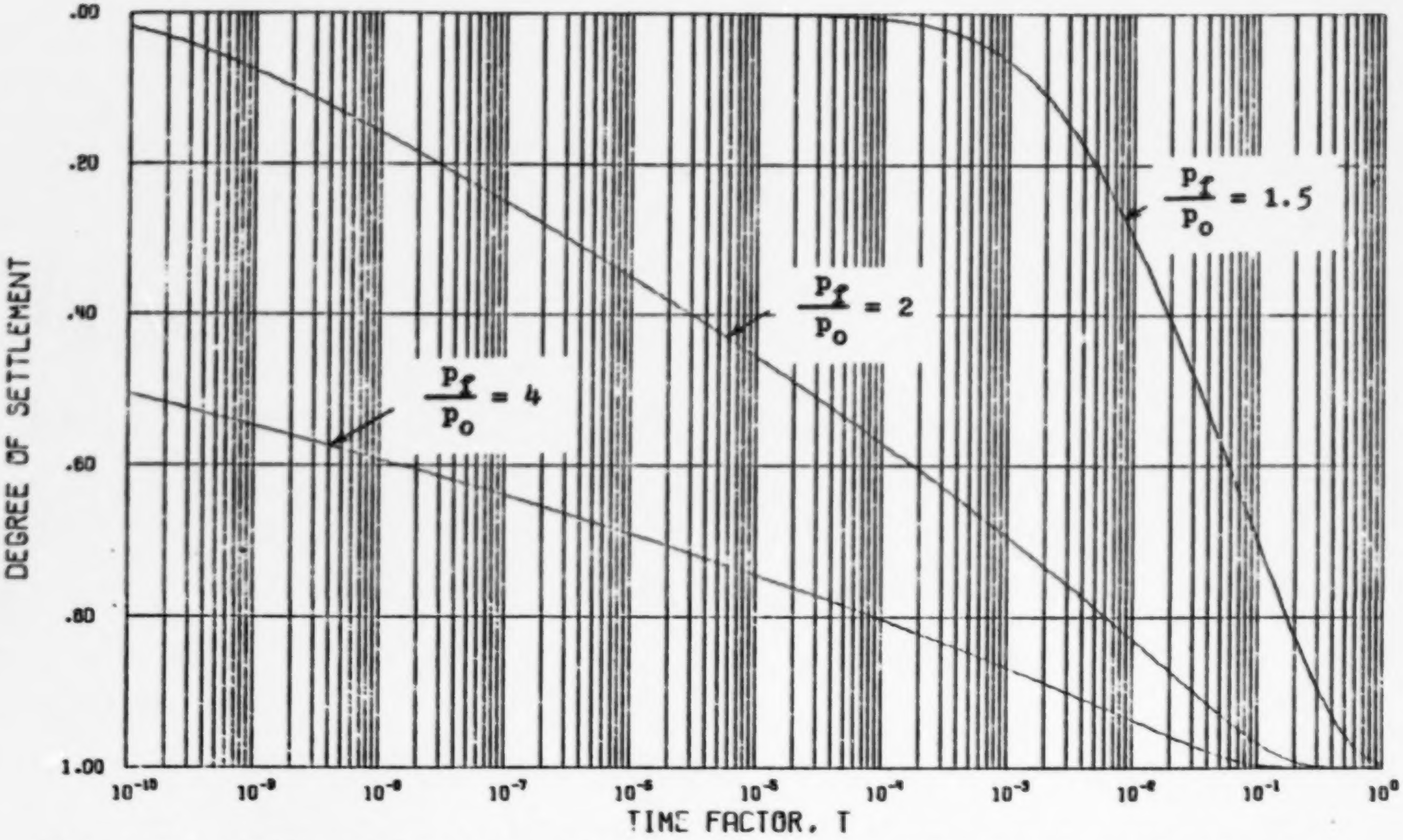

Fig. D-11. Settlement vs. time factor of the creep model based on structural viscosity for various values of stress increment: $\alpha_o p_o = 20$, $(p_f/p_o)(\alpha_f/\alpha_o) = 1$

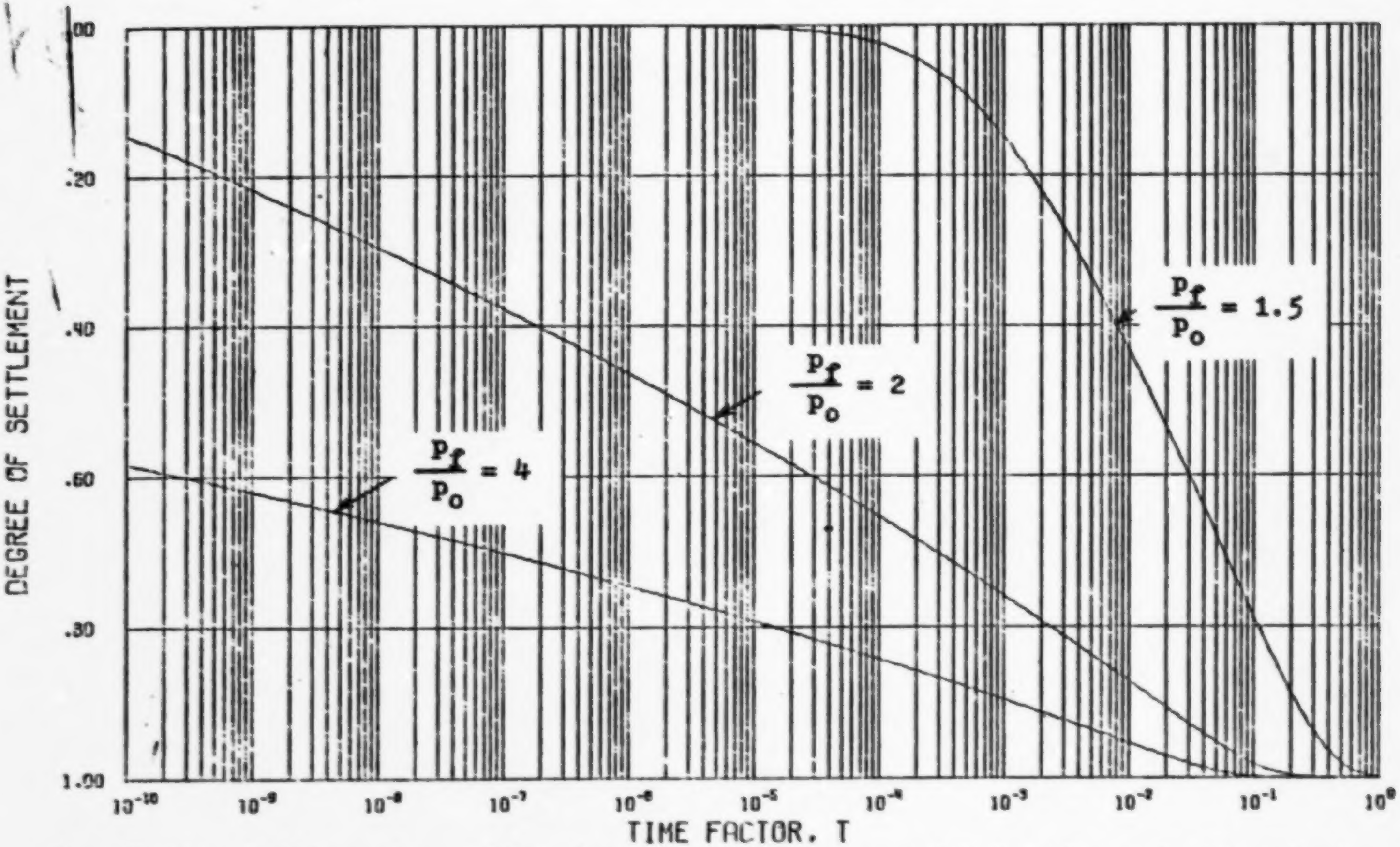

Fig. D-12. Settlement vs. time factor of the creep model based on structural viscosity for various values of stress increment: $\alpha_o p_o = 25$, $(p_f/p_o)(\alpha_f/\alpha_o) = 1$

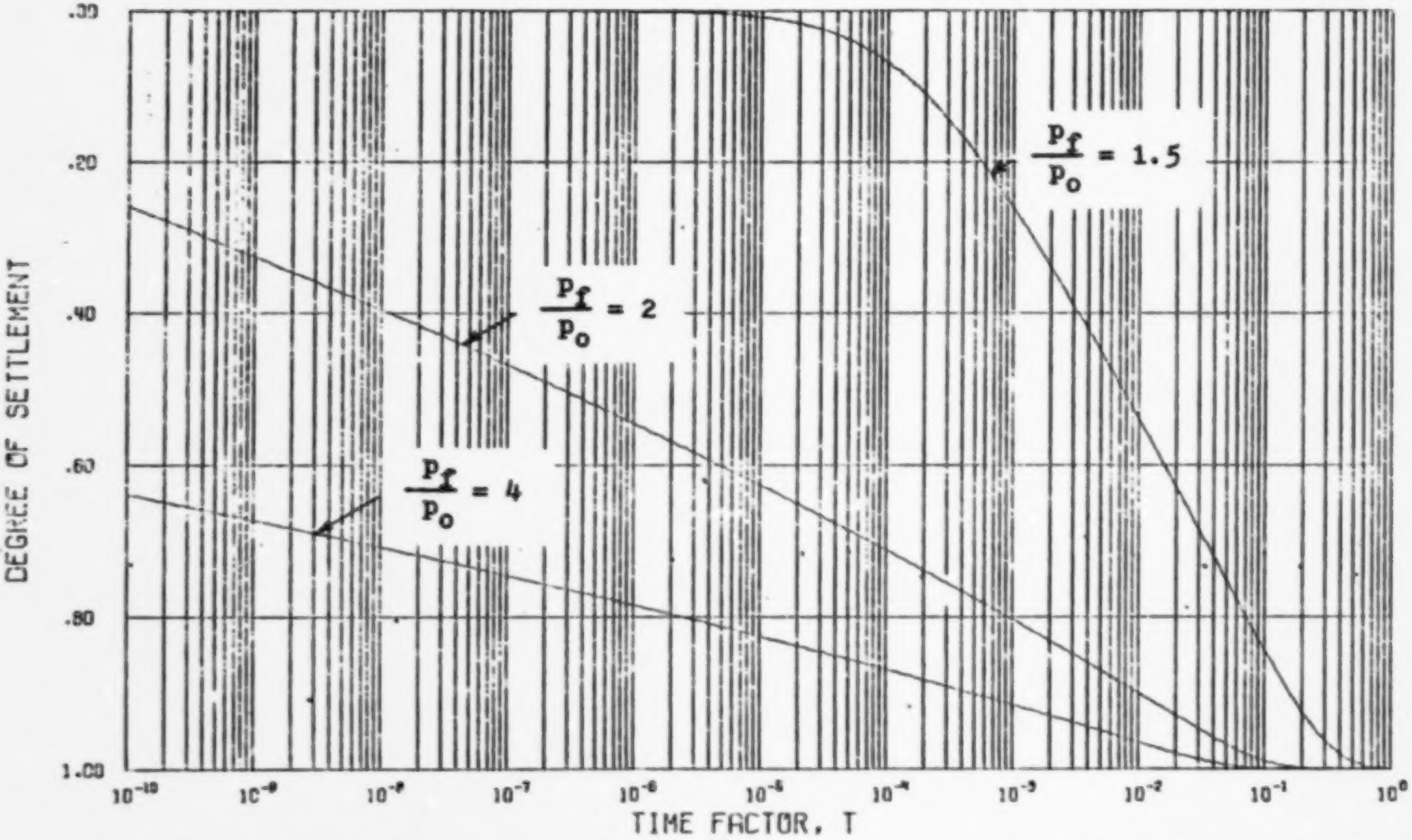

Fig. D-13. Settlement vs. time factor of the creep model based on structural viscosity for various values of stress increment: $\alpha_o p_o = 30$, $(p_f/p_o)(\alpha_f/\alpha_o) = 1$

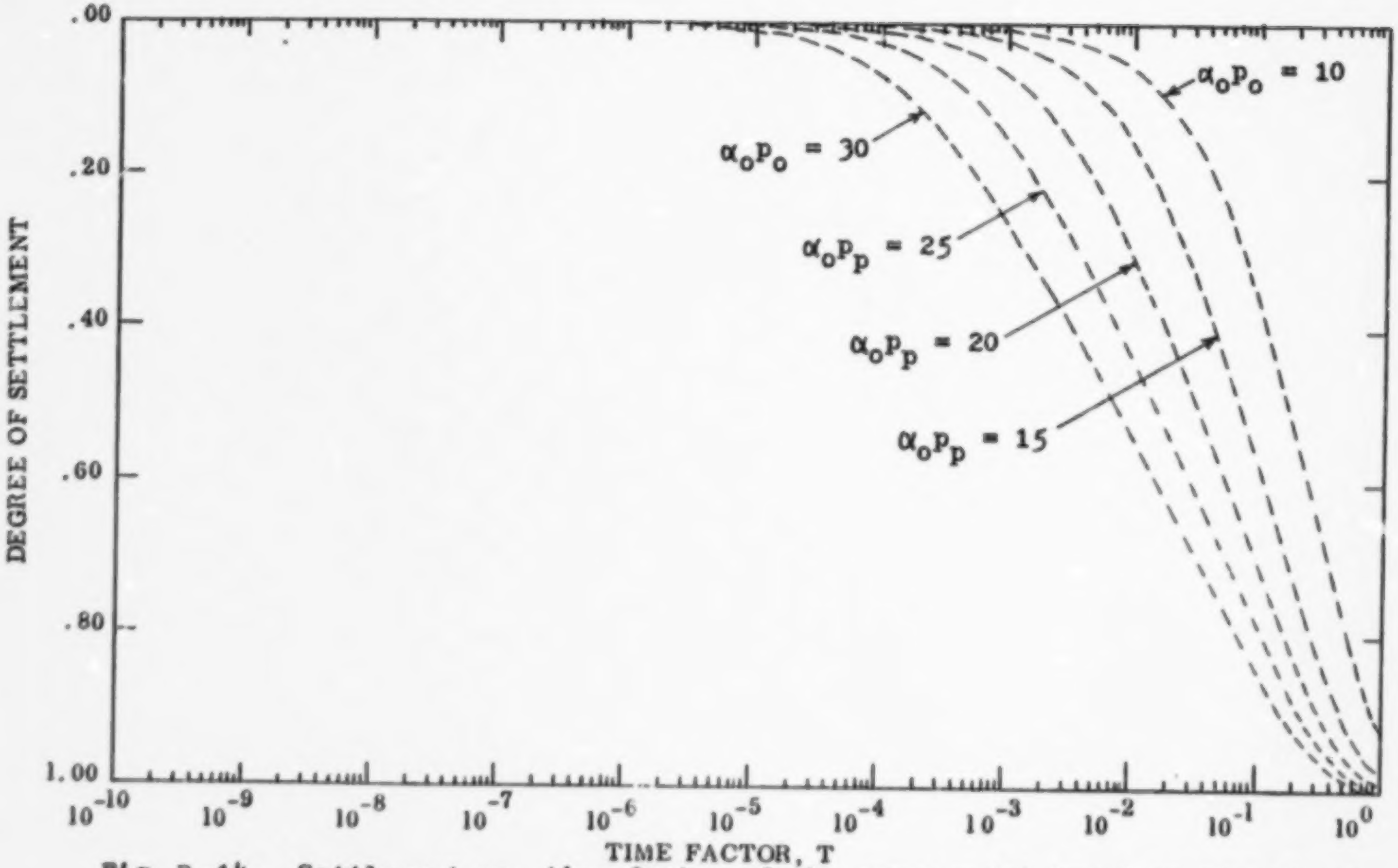

Fig. D-14. Settlement vs. time factor of the creep model based on structural viscosity for various values of $\alpha_o p_o$, $p_f/p_o = 1.5$, $(p_f/p_o)(\alpha_f/\alpha_o) = 1$.

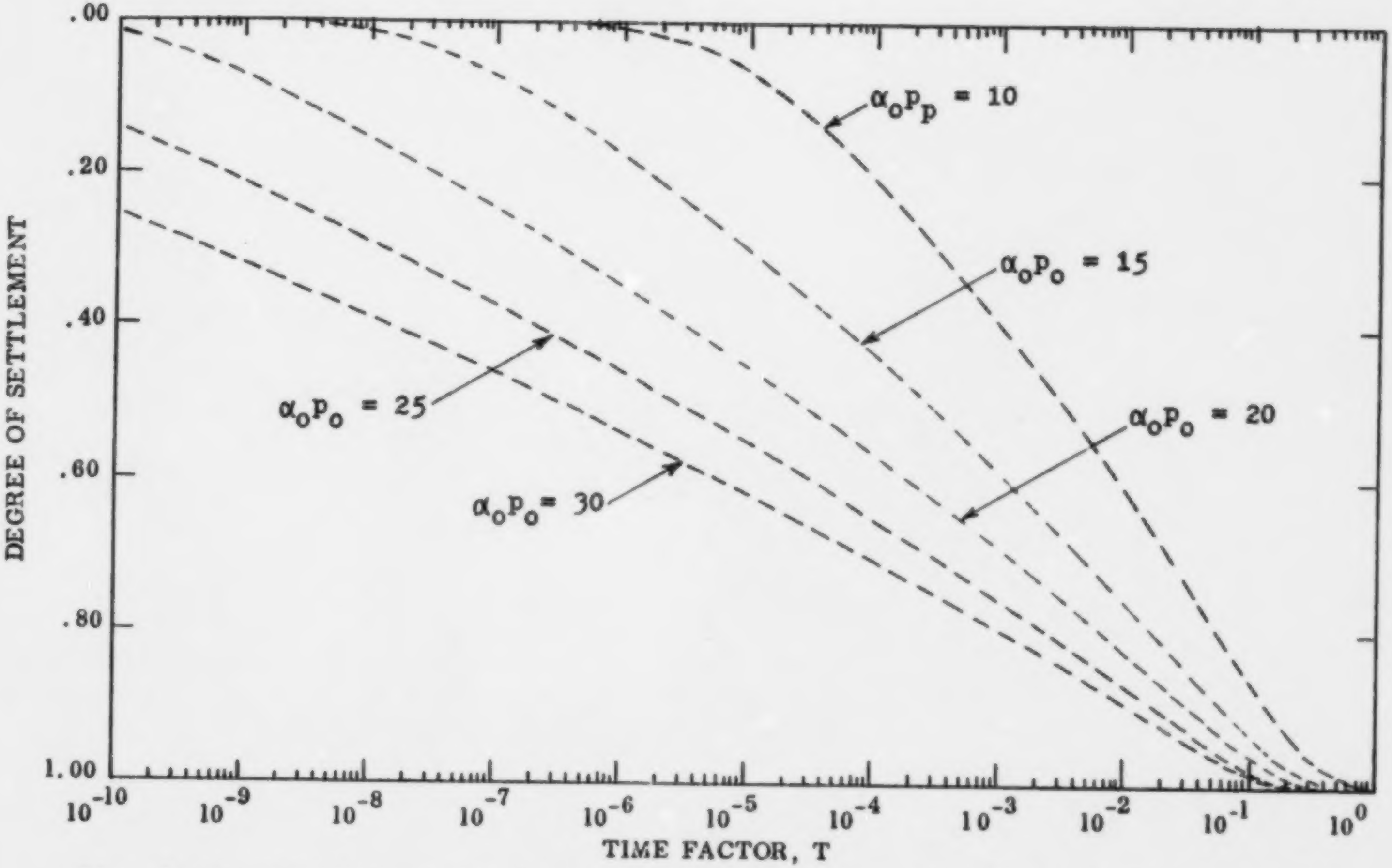

Fig. D-15. Settlement vs. time factor of the creep model based on structural viscosity for various values of $\alpha_o p_o$: $p_f/p_o = 2$, $(p_f/p_o)(\alpha_f/\alpha_o) = 1$

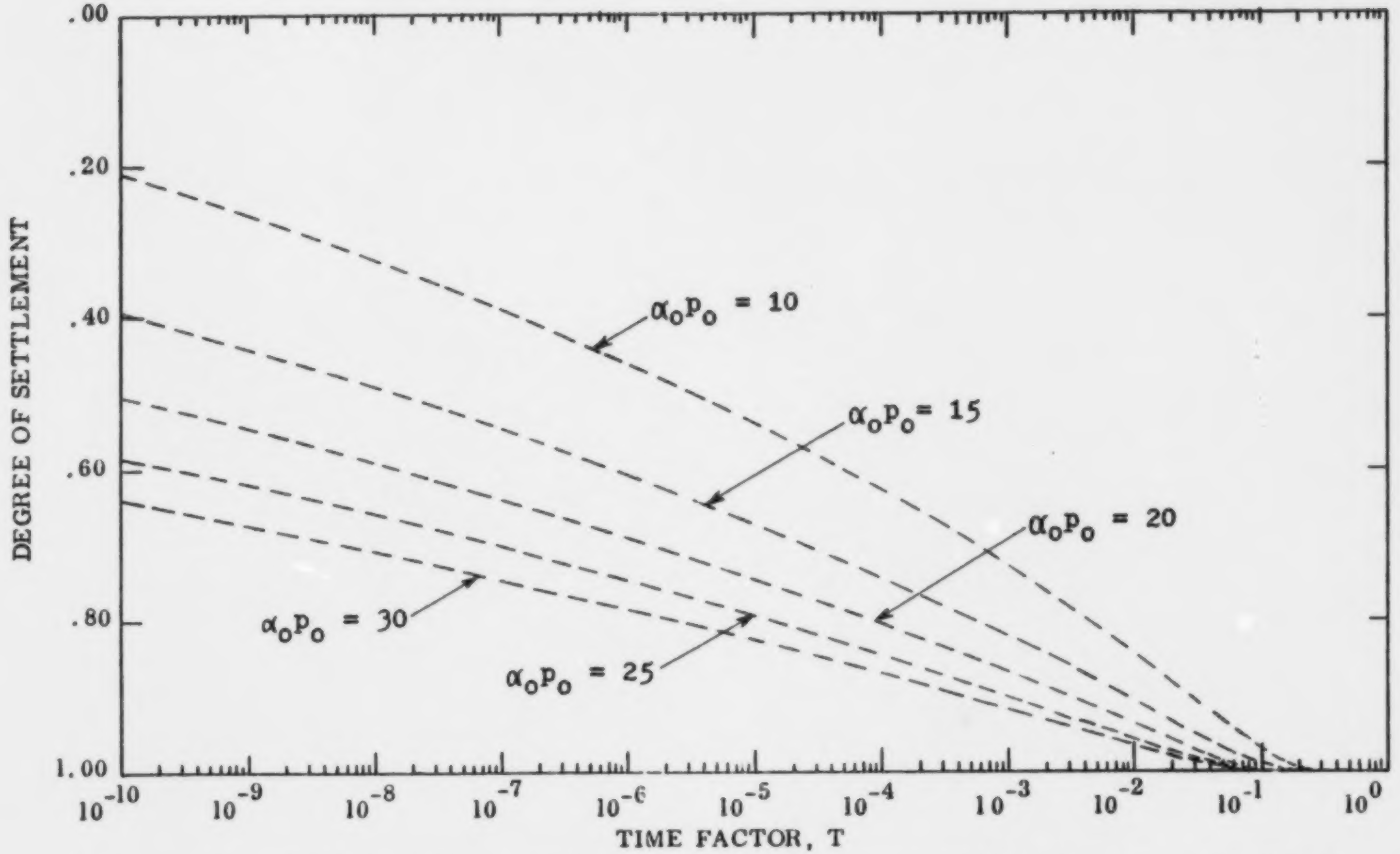

Fig. D-16. Settlement vs. time factor of the creep model based on structural viscosity for various values of $\alpha_o p_o$; $p_f/p_o = 4$, $(p_f/p_o)(\alpha_f/\alpha_o) = 1$

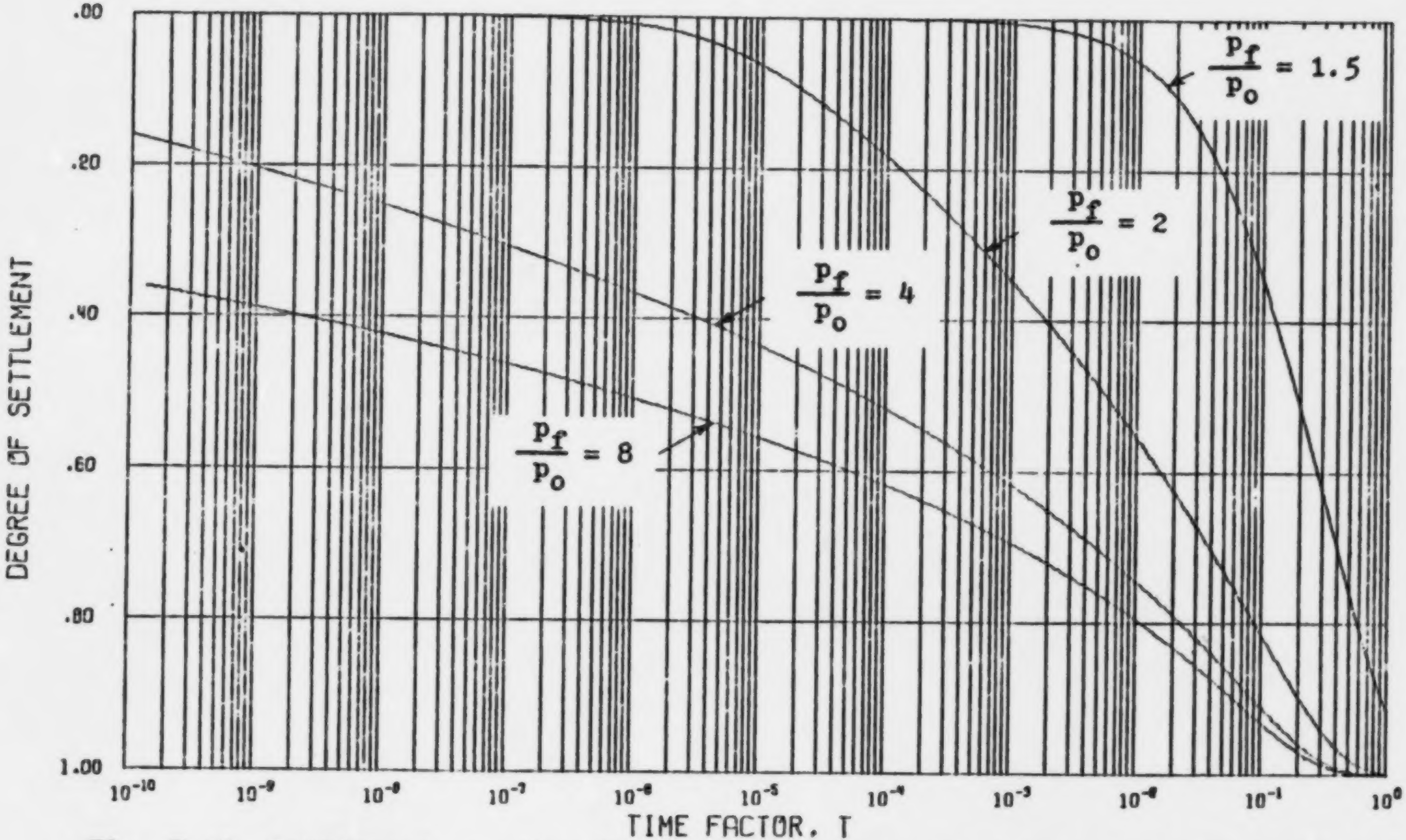

Fig. D-17. Settlement vs. time factor of the creep model based on structural viscosity for various values of stress increment: $\alpha_o p_o = 10$, $(p_f/p_o)(\alpha_f/\alpha_o)^{1.5} = 1$.

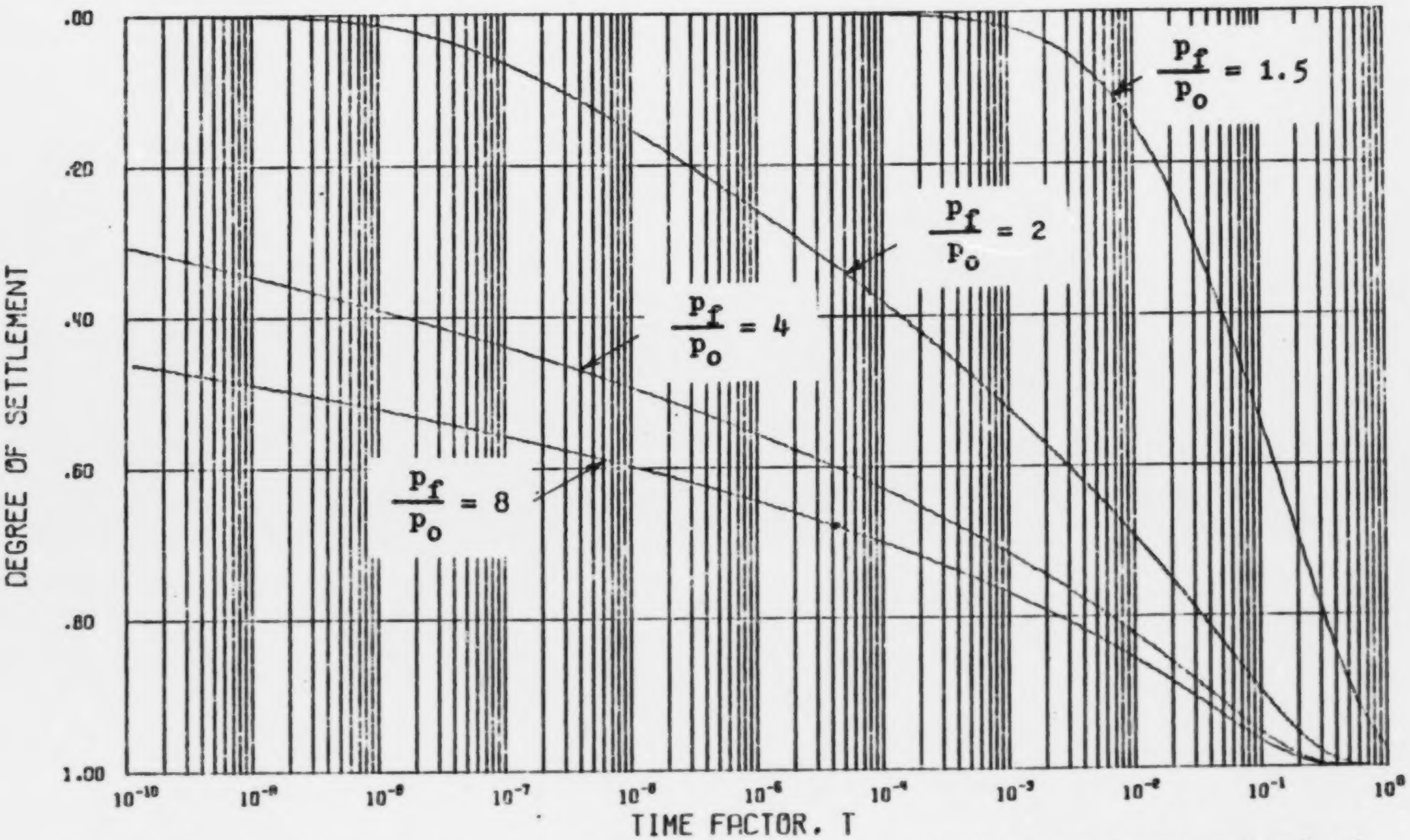

Fig. D-18. Settlement vs. time factor of the creep model based on structural viscosity for various values of stress increment: $\alpha_o p_o = 15$, $(p_f/p_o)(\alpha_f/\alpha_o)^{1.5} = 1$

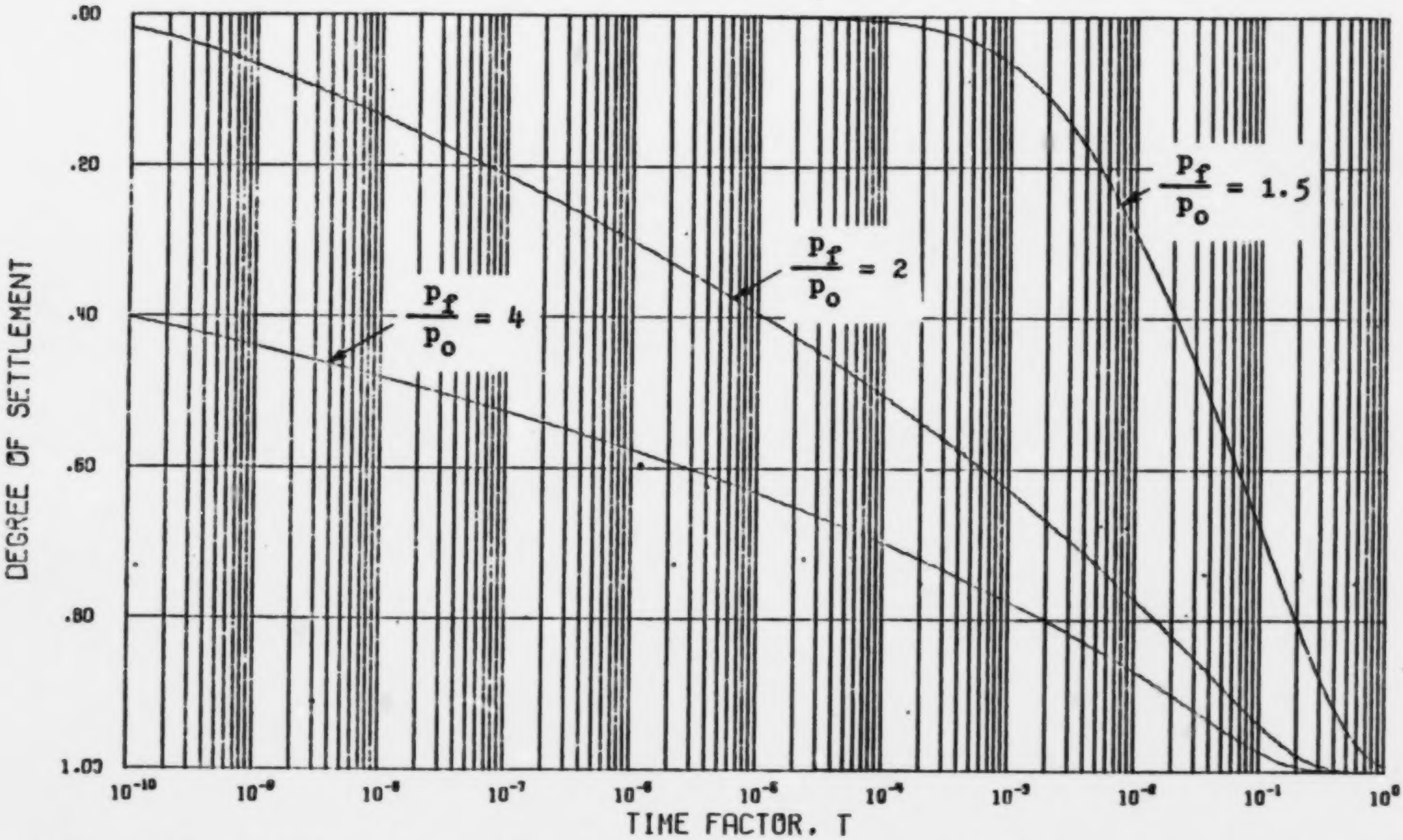

Fig. D-19. Settlement vs. time factor of the creep model based on structural viscosity for various values of stress increment: $\alpha_o p_o = 20$, $(p_f/p_o)(\alpha_f/\alpha_o)^{1.5} = 1$

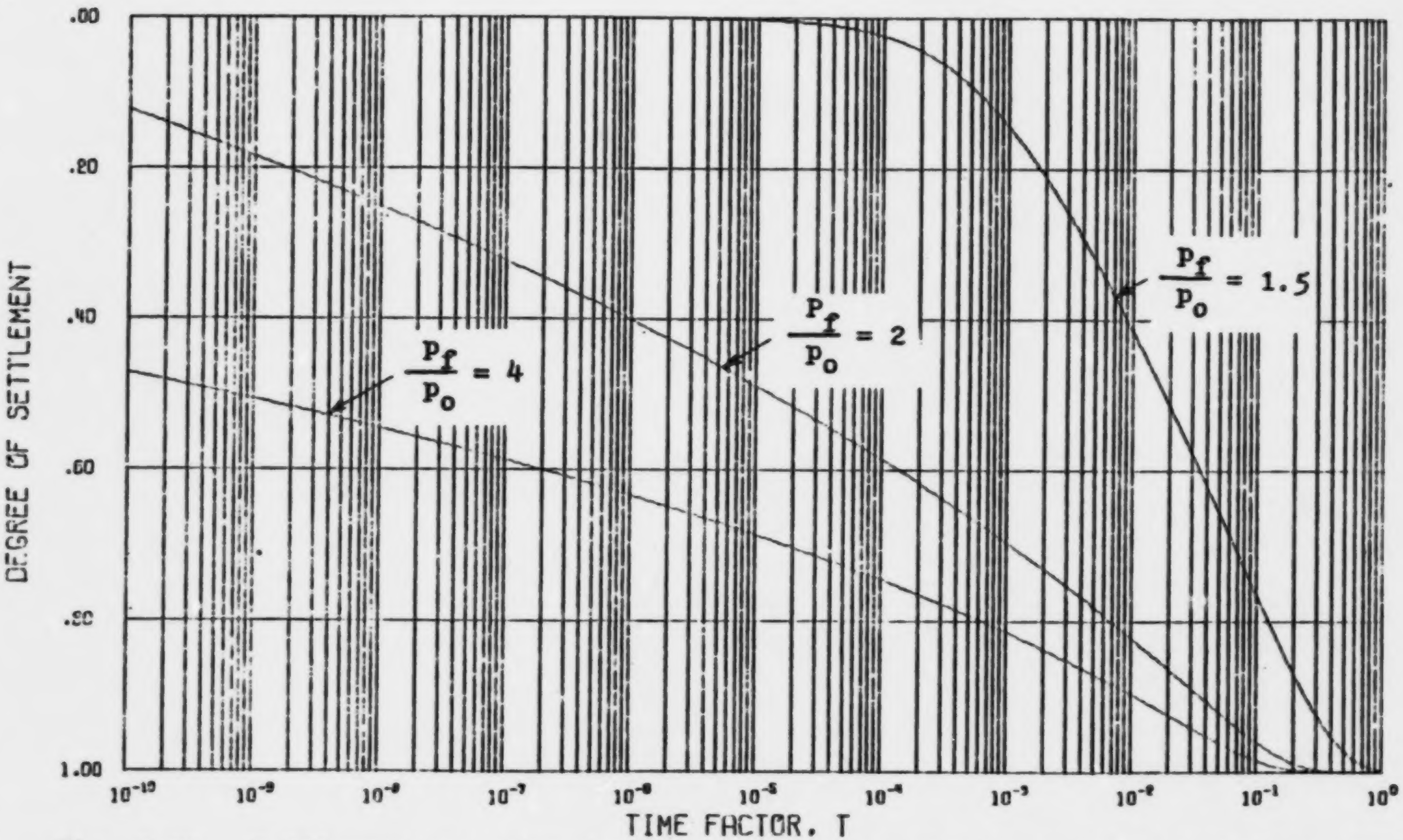

Fig. D-20. Settlement vs. time factor of the creep model based on structural viscosity for various values of stress increment: $\alpha_o p_o = 25$, $(p_f/p_o)(\alpha_f/\alpha_o)^{1.5} = 1$

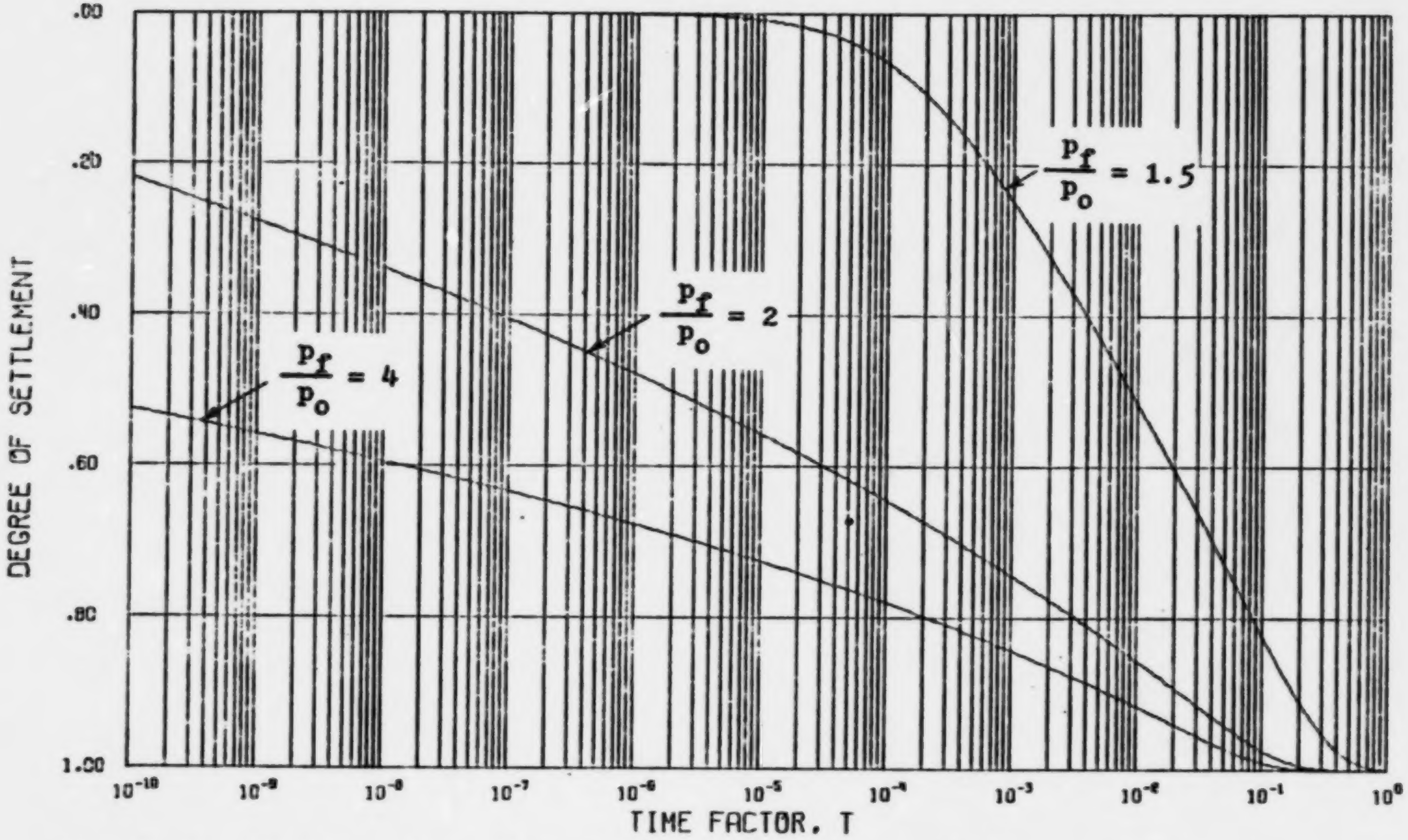

Fig. D-21. Settlement vs. time factor of the creep model based on structural viscosity for various values of stress increment: $\alpha_o p_o = 30$, $(p_f/p_o)(\alpha_f/\alpha_o)^{1.5} = 1$

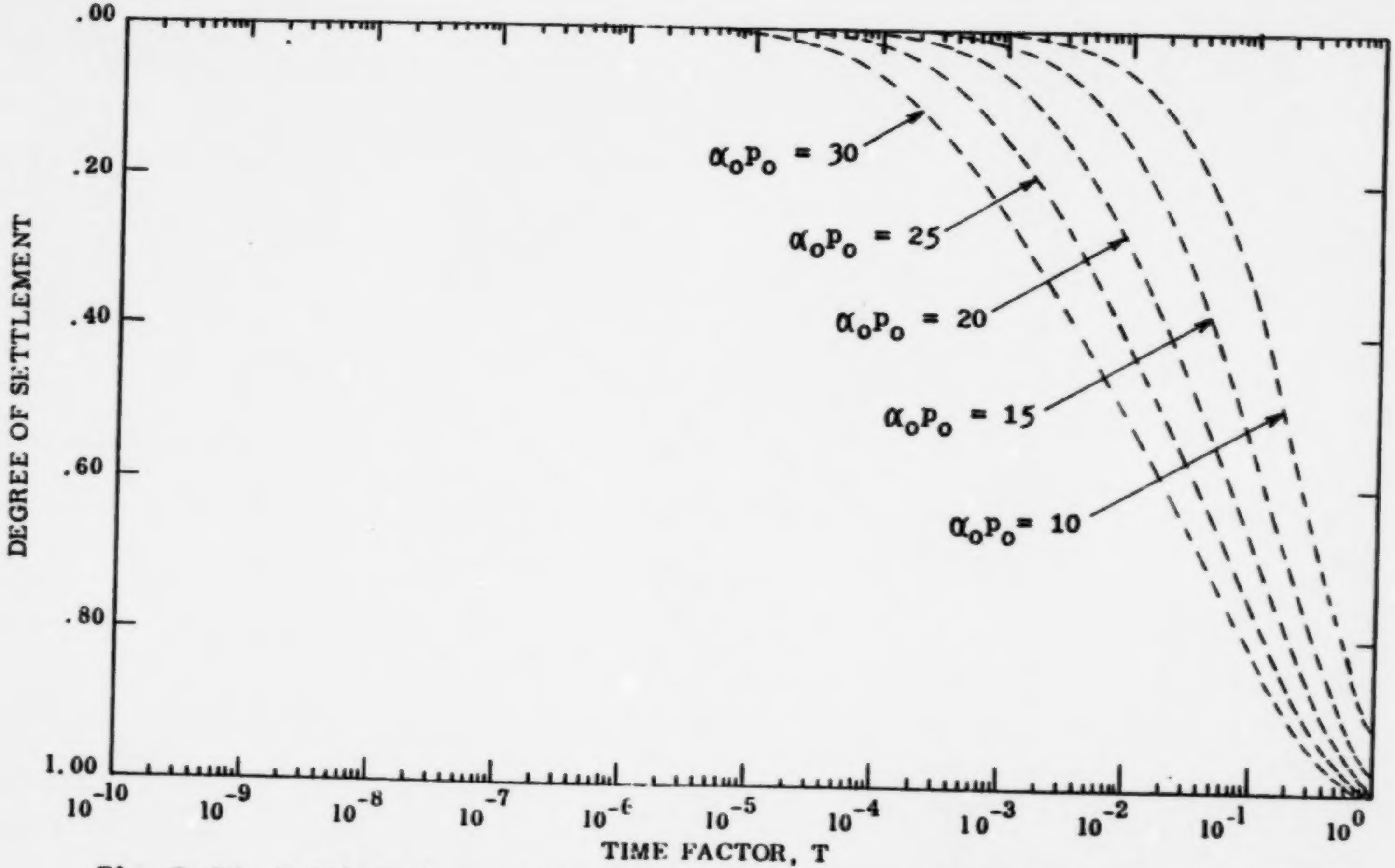

Fig. D-22. Settlement vs. time factor of the creep model based on structural viscosity for various values of $\alpha_o p_o$, $p_f/p_o = 1.5$, $(p_f/p_o)(\alpha_f/\alpha_o)^{1.5} = 1$.

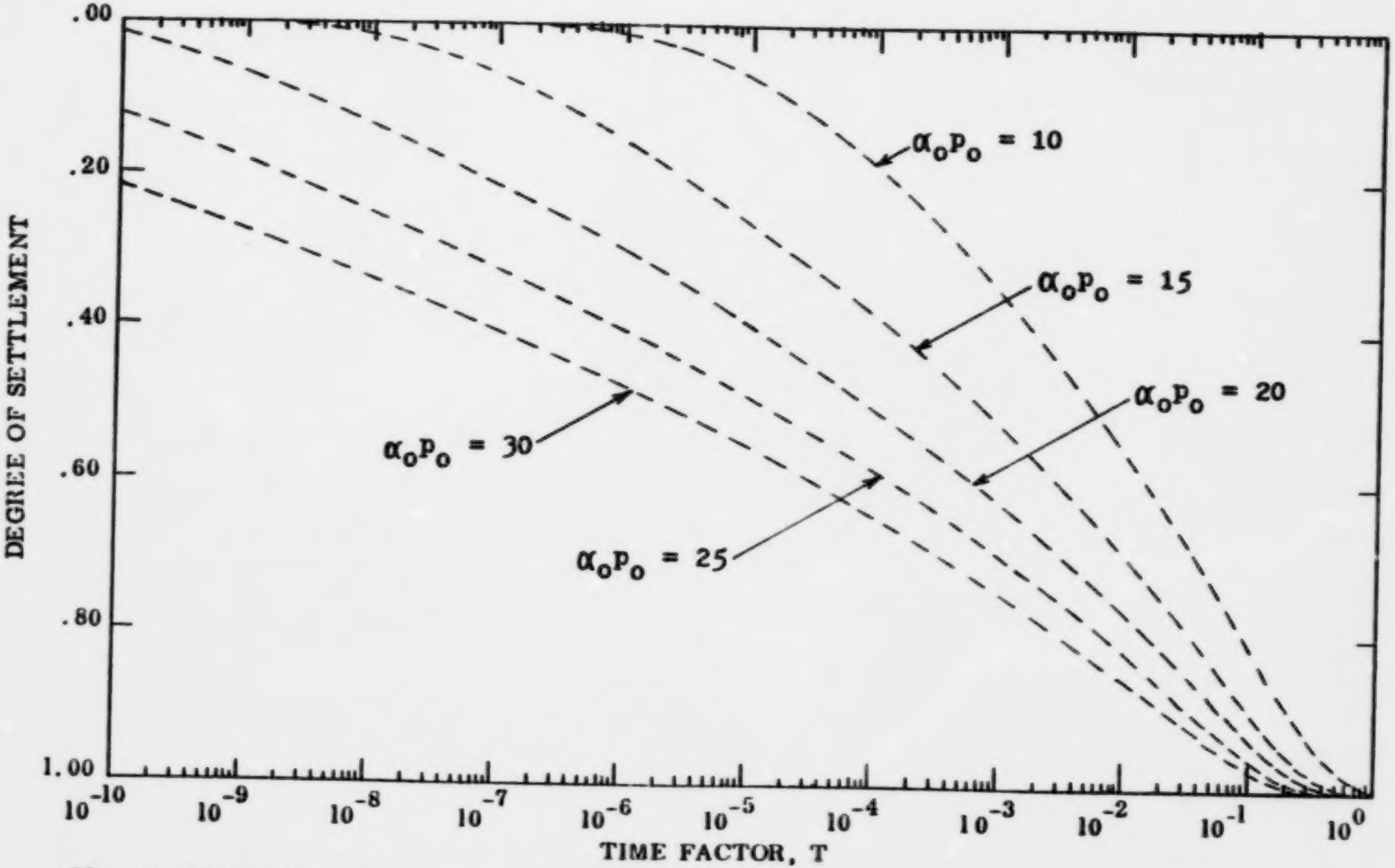

Fig. D-23 Settlement vs. time factor of the creep model based on structural viscosity for various values of $\alpha_o p_o$: $p_f/p_o = 2$, $(p_f/p_o)(\alpha_f/\alpha_o)^{1.5} = 1$

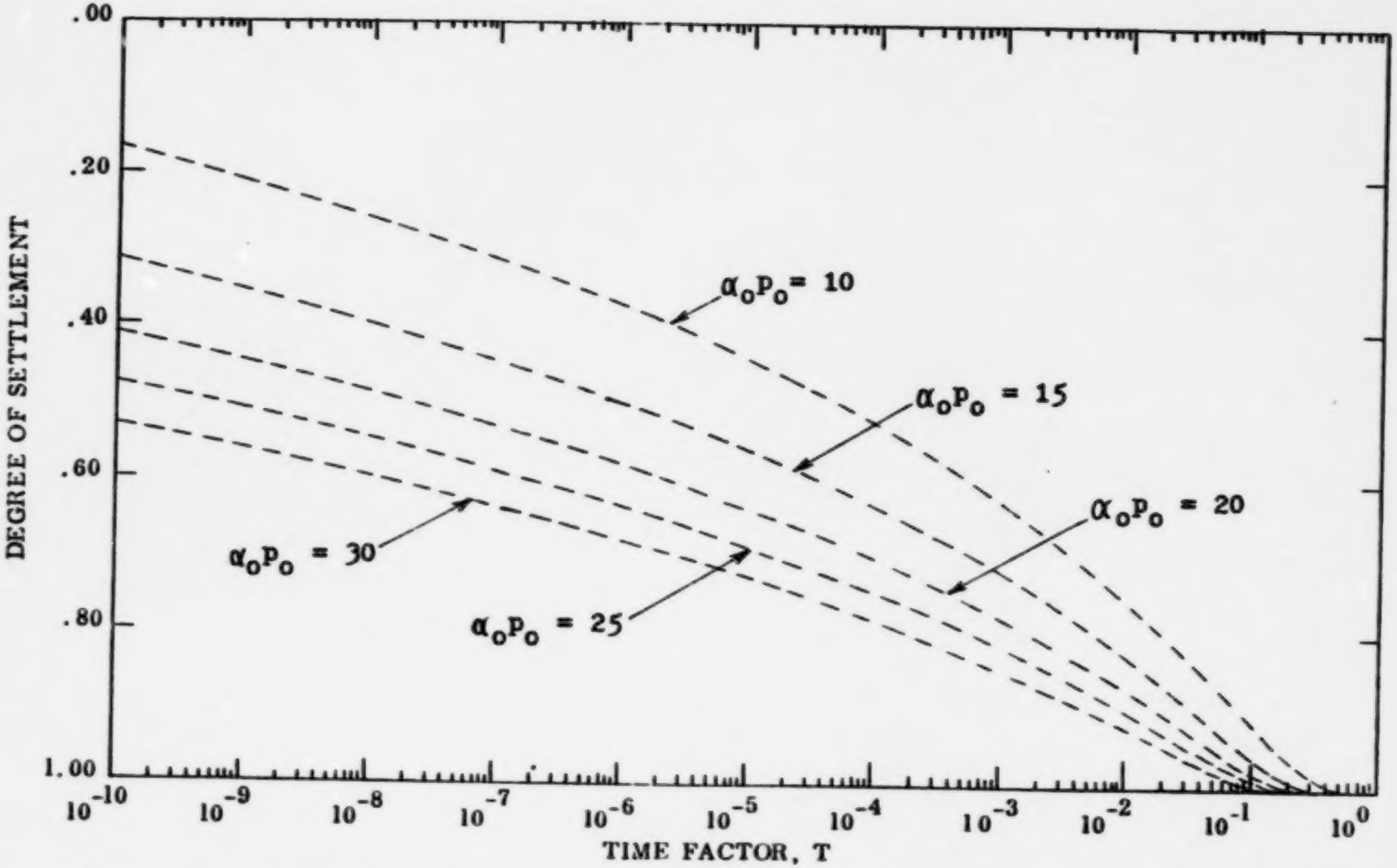

Fig. D-24. Settlement vs. time factor of the creep model based on structural viscosity for various values of $\alpha_o p_o$: $p_f/p_o = 4$, $(p_f/p_o)(\alpha_f/\alpha_o)^{1.5} = 1$

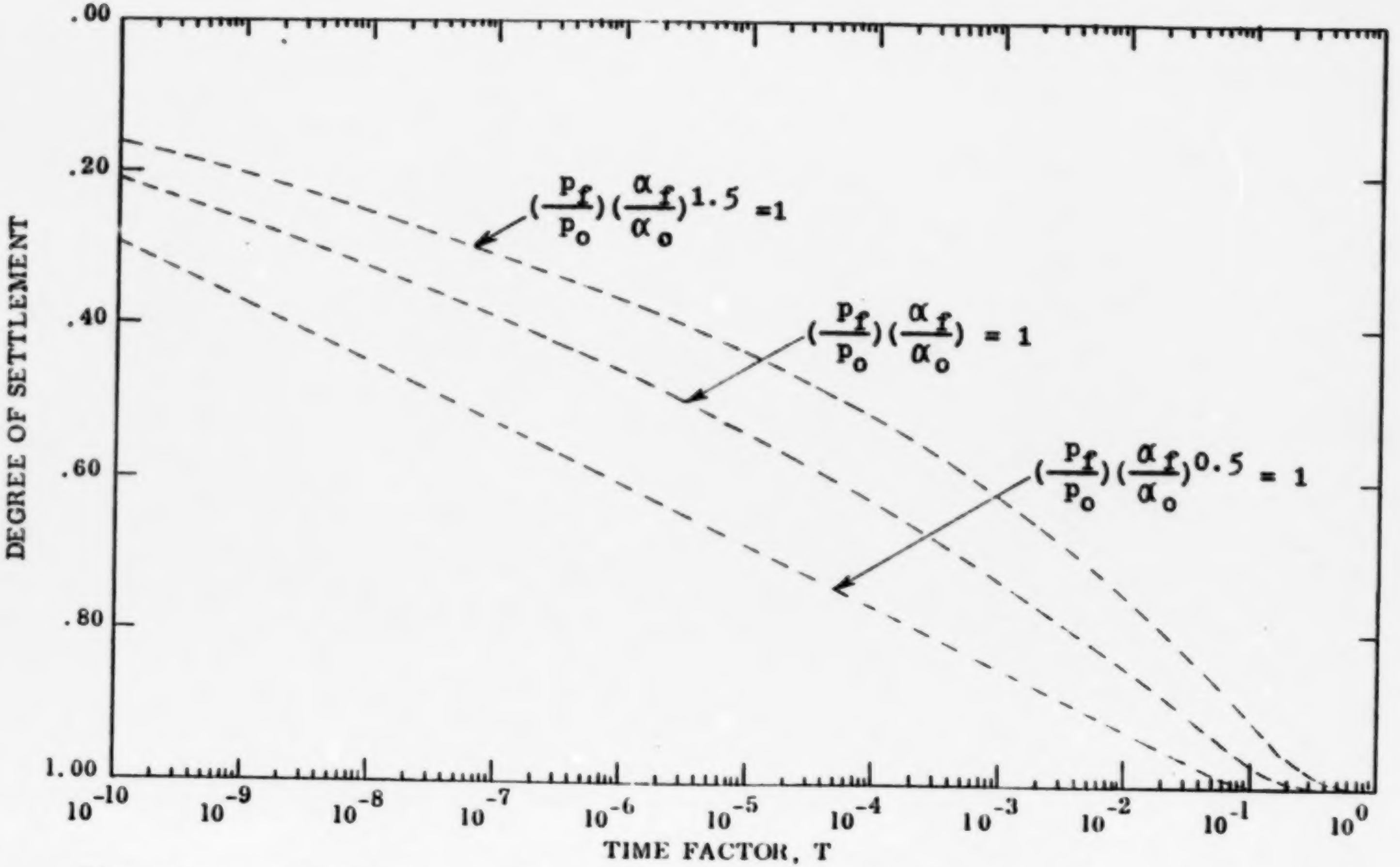

Fig. D-25. Settlement vs. time factor of the creep model based on structural viscosity for various values of the ratio of the slope of the e_b-log p line to the slope of the e_b-logα line: $\alpha_o p_o = 10$, $p_f/p_o = 4$

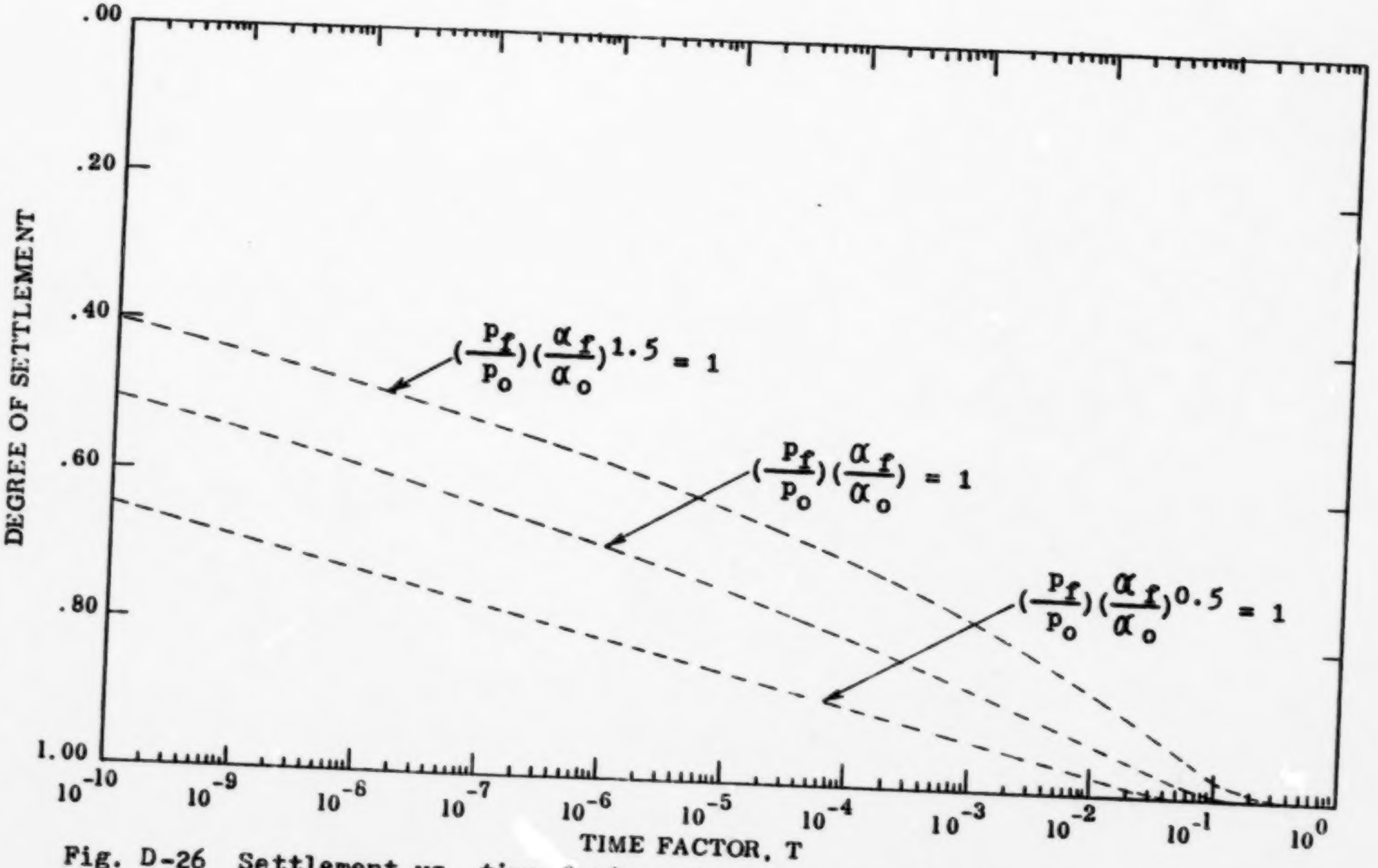

Fig. D-26 Settlement vs. time factor of the creep model based on structural viscosity for various values of the ratio of the slope of the e_b-log p line to the slope of the e_b-logα line: $\alpha_o p_o = 20$, $p_f/p_o = 4$

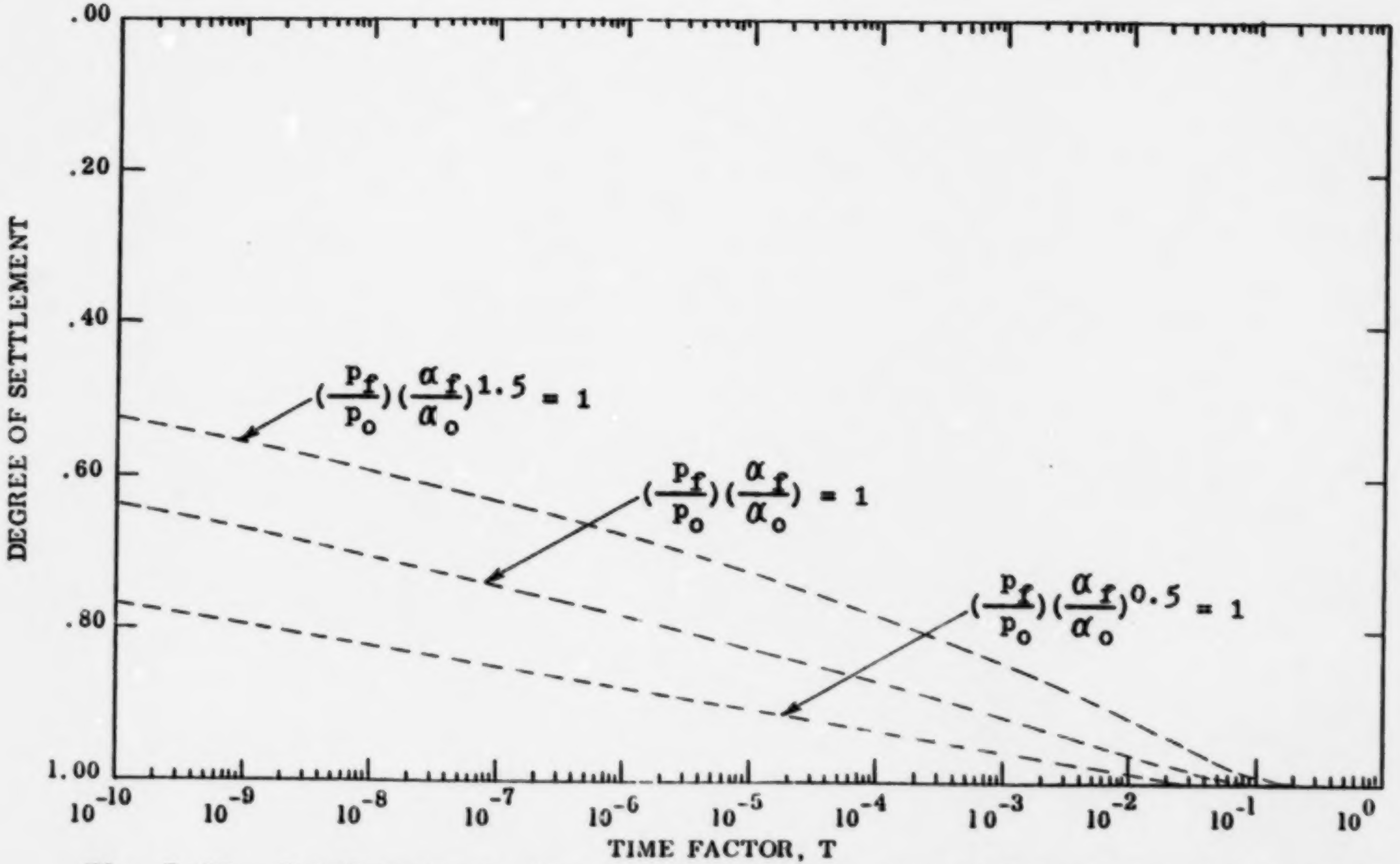

Fig. D-27. Settlement vs. time factor of the creep model based on structural viscosity for various values of the ratio of the slope of the e_b-log p line to the slope of the e_b-logα line: $\alpha_o p_o = 30$, $p_f/p_o = 4$

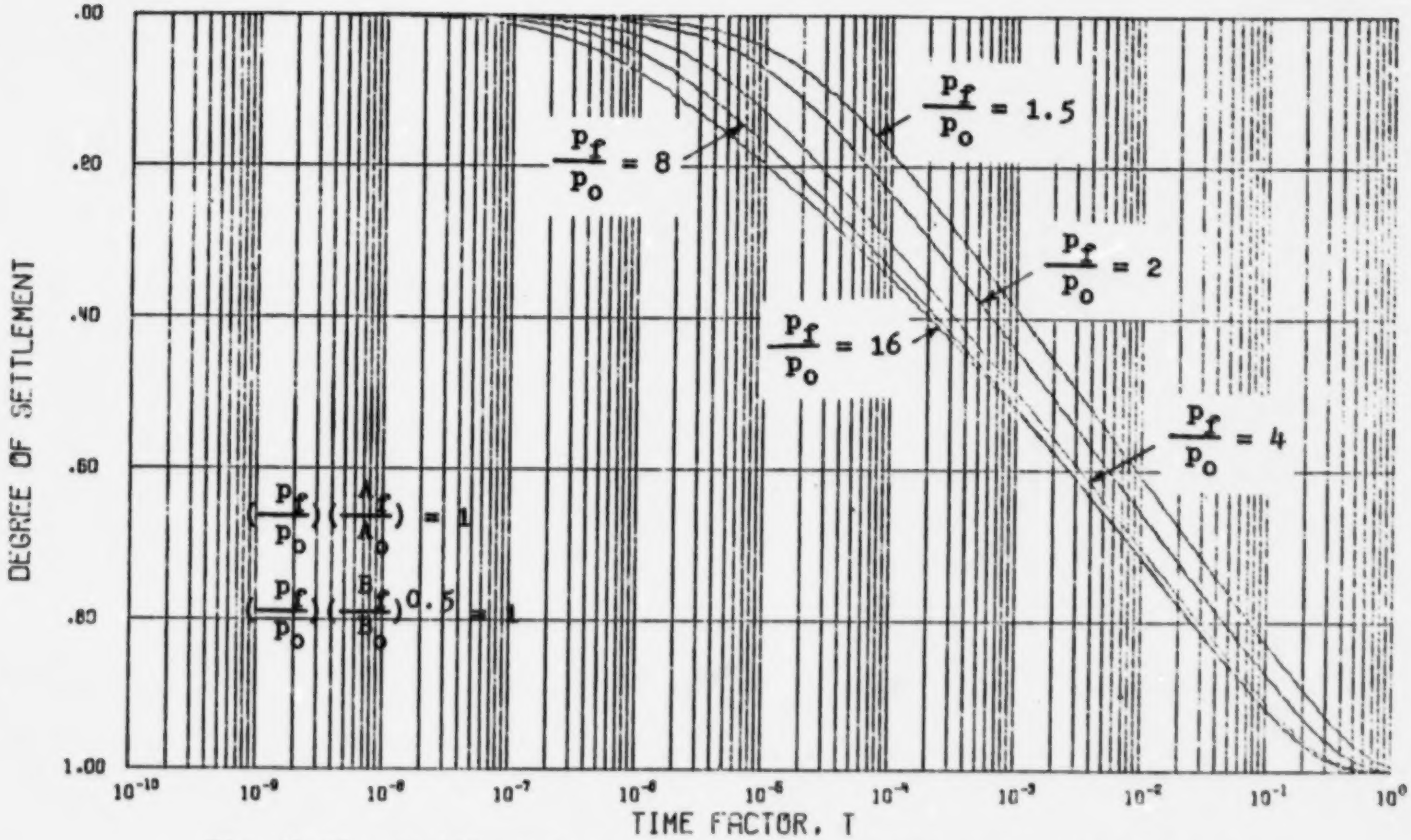

Fig. D-28. Settlement vs. time factor of the creep model based on micropore structure for various values of p_f/p_o; $B_o = 10$

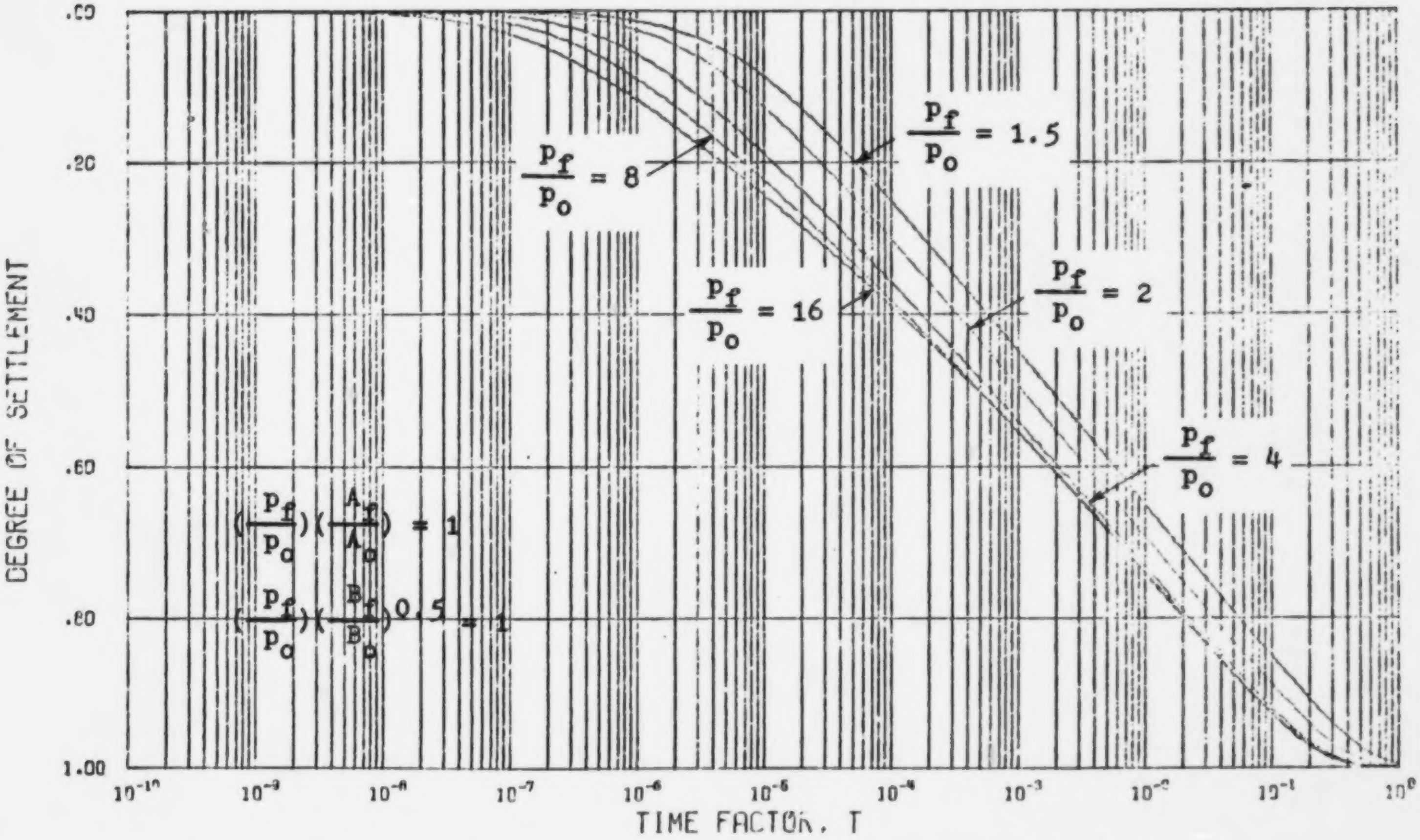

Fig. D-29. Settlement vs. time factor of the creep model based on micropore structure for various values of p_f/p_o, $B_o = 11$

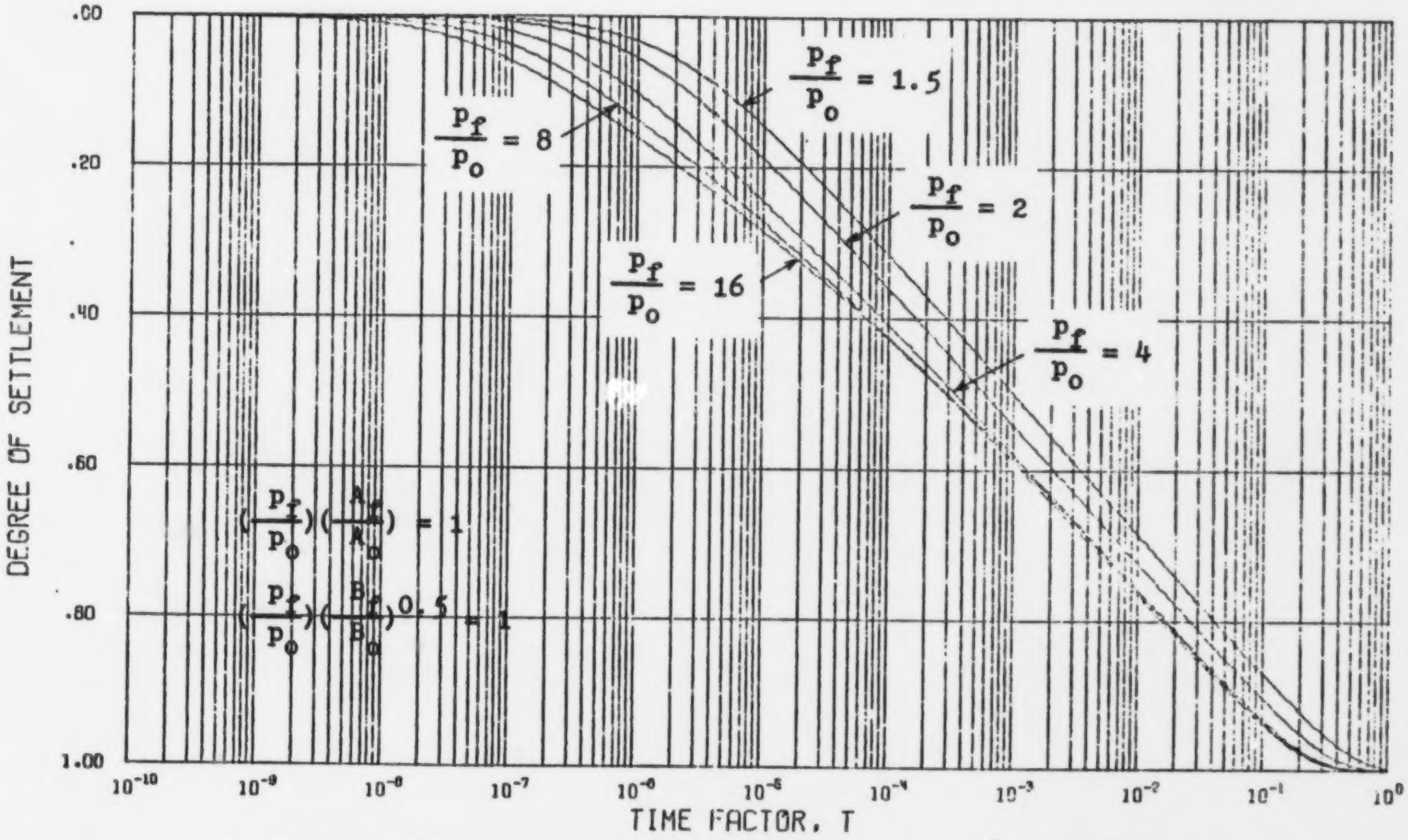

Fig. D-30. Settlement vs. time factor of the creep model based on micropore structure for various values of p_f/p_o; $B_o = 12$

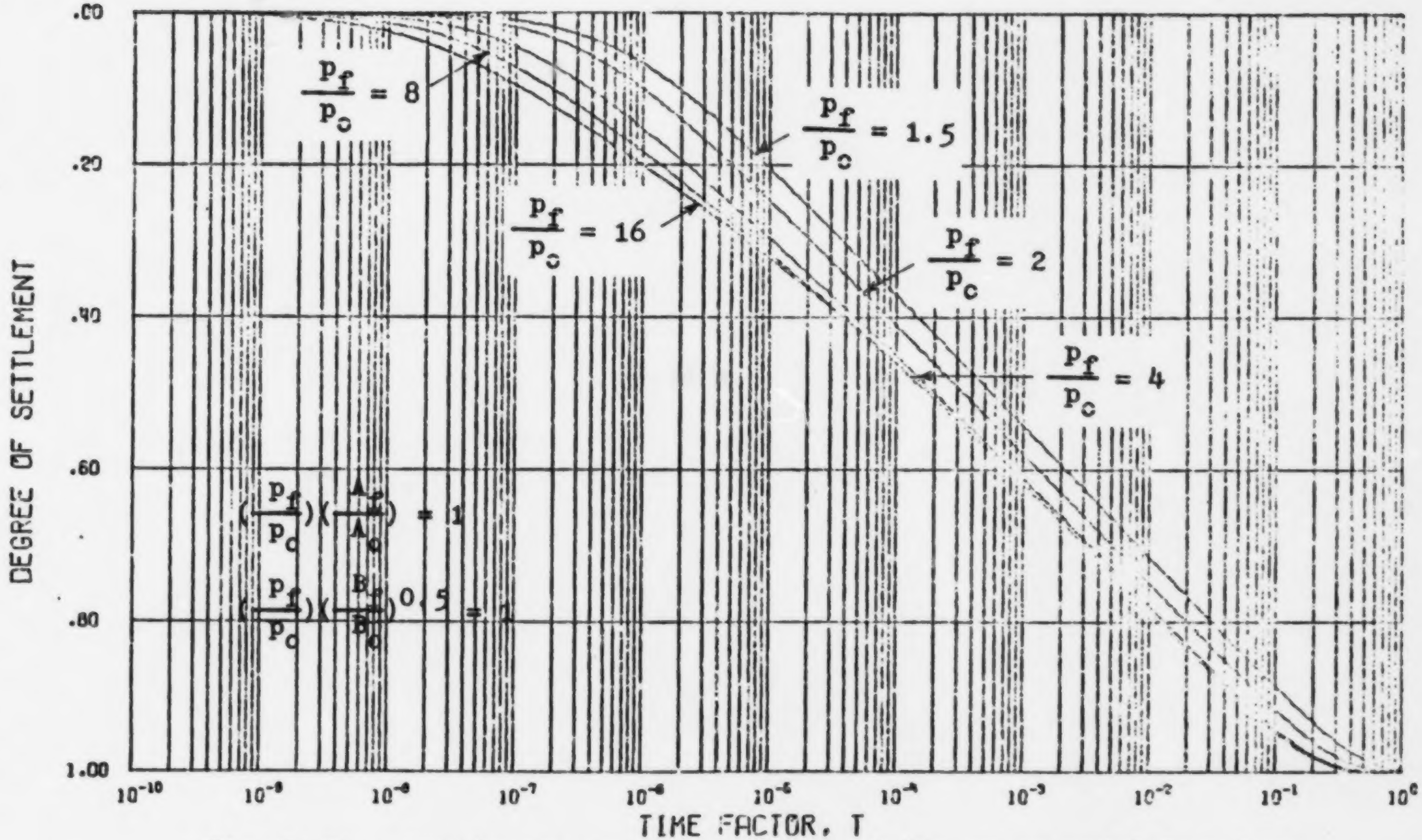

Fig. D-31. Settlement vs. time factor of the creep model based on micropore structure for various values of p_f/p_o, $B_o = 13$

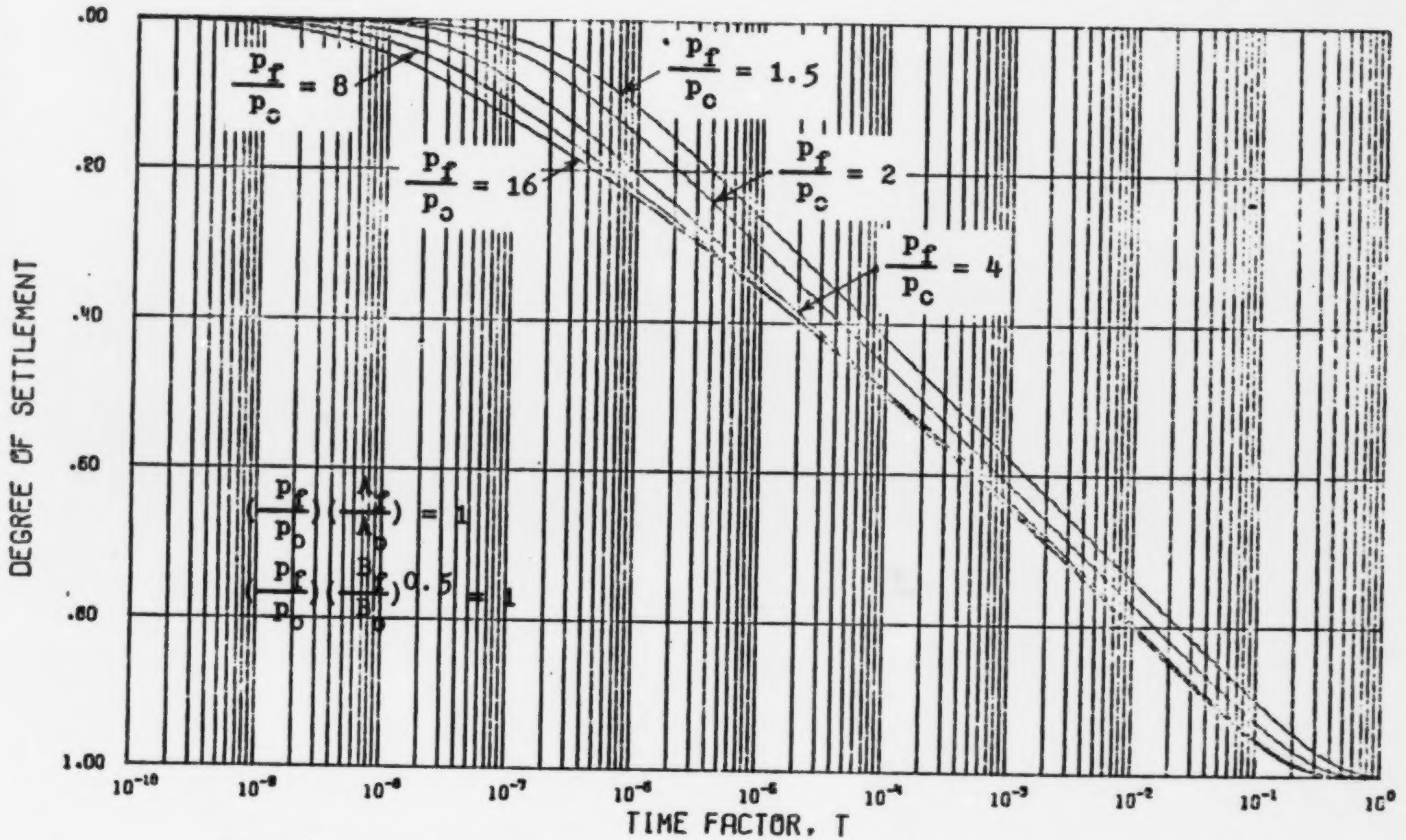

Fig. D-32. Settlement vs. time factor of the creep model based on micropore structure for various values of p_f/p_o; $B_o = 14$

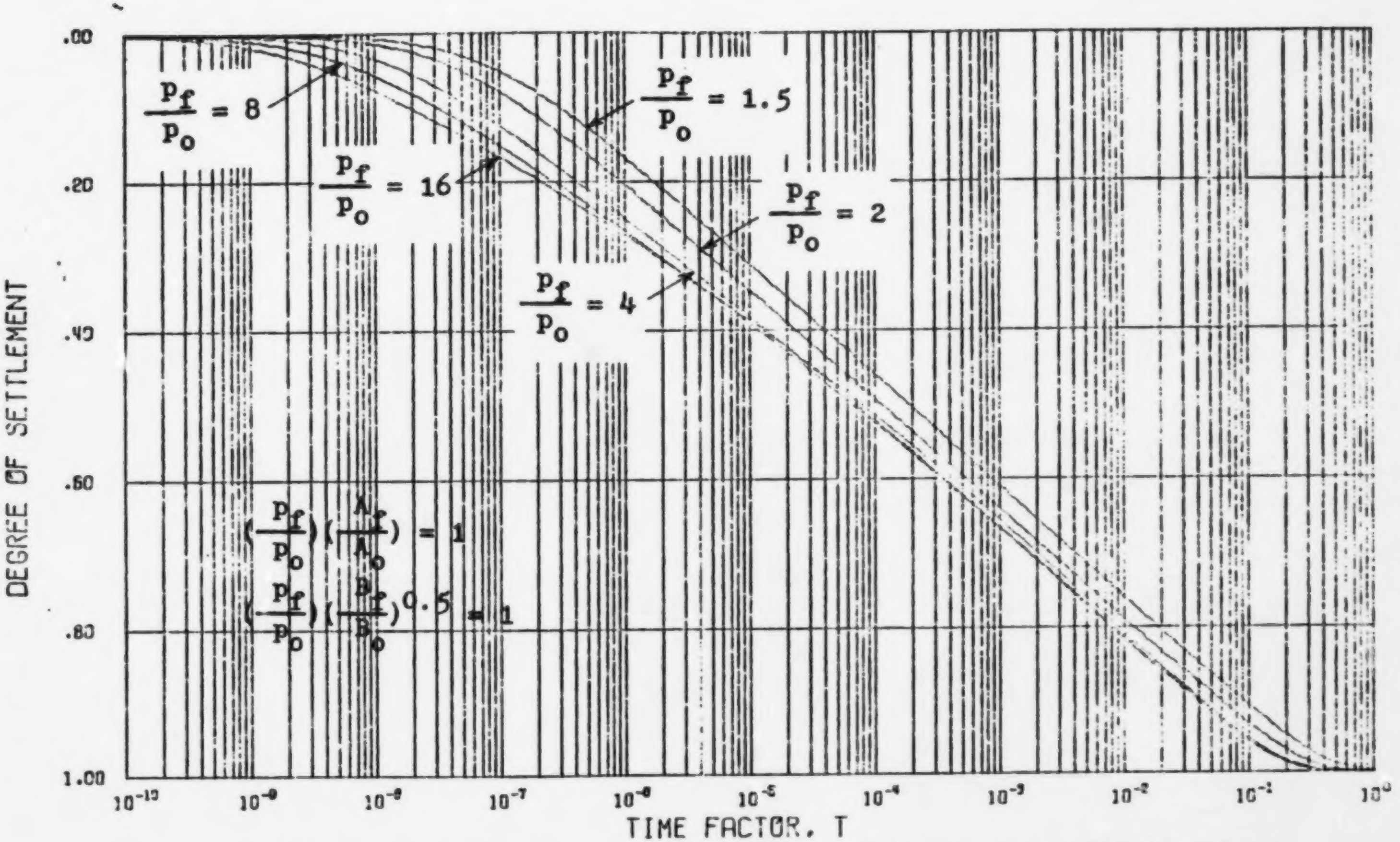

Fig. D-33. Settlement vs. time factor of the creep model based on micropore structure for various values of p_f/p_o, $B_o = 15$

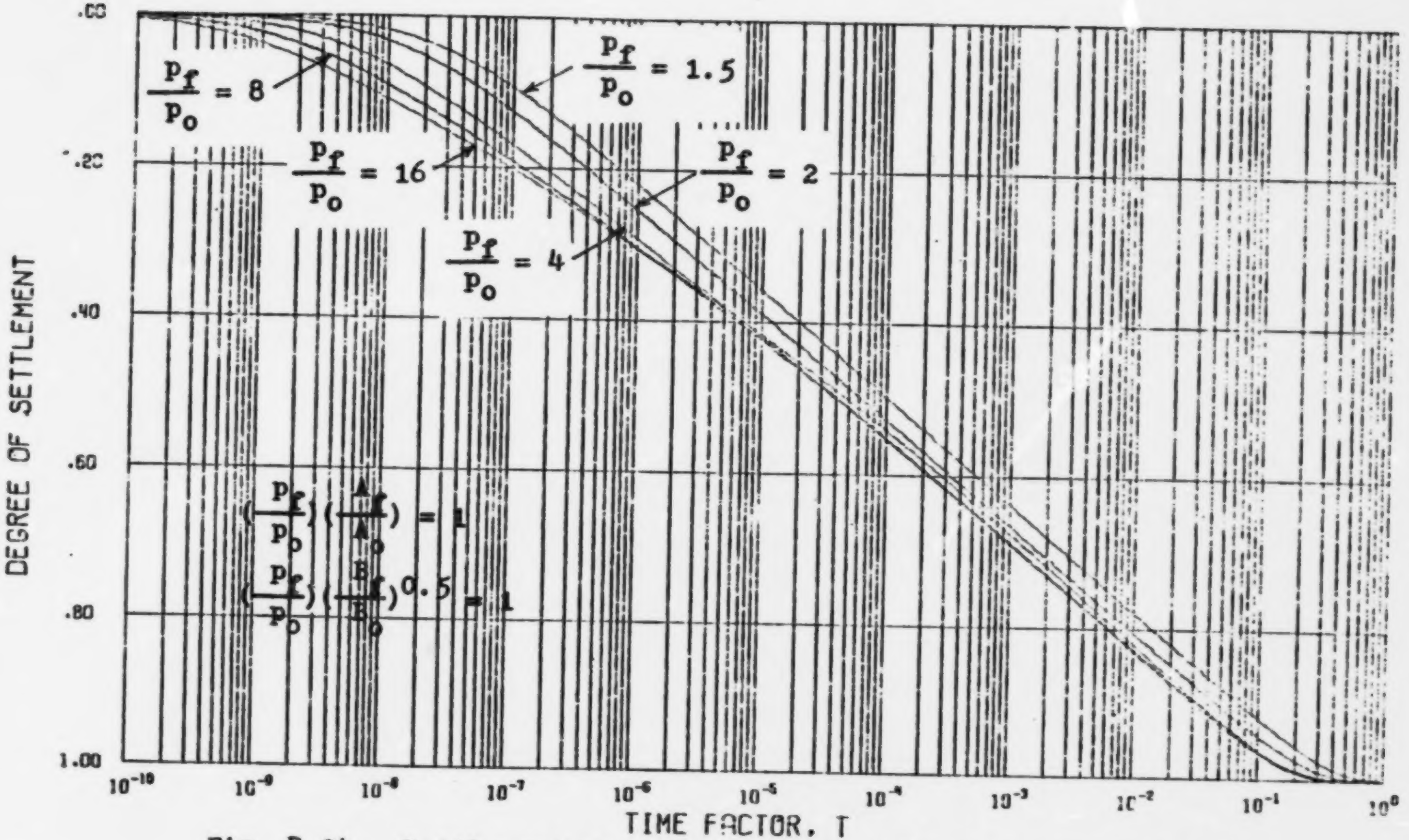

Fig. D-34. Settlement vs. time factor of the creep model based on micropore structure for various values of p_f/p_o; $B_o = 16$

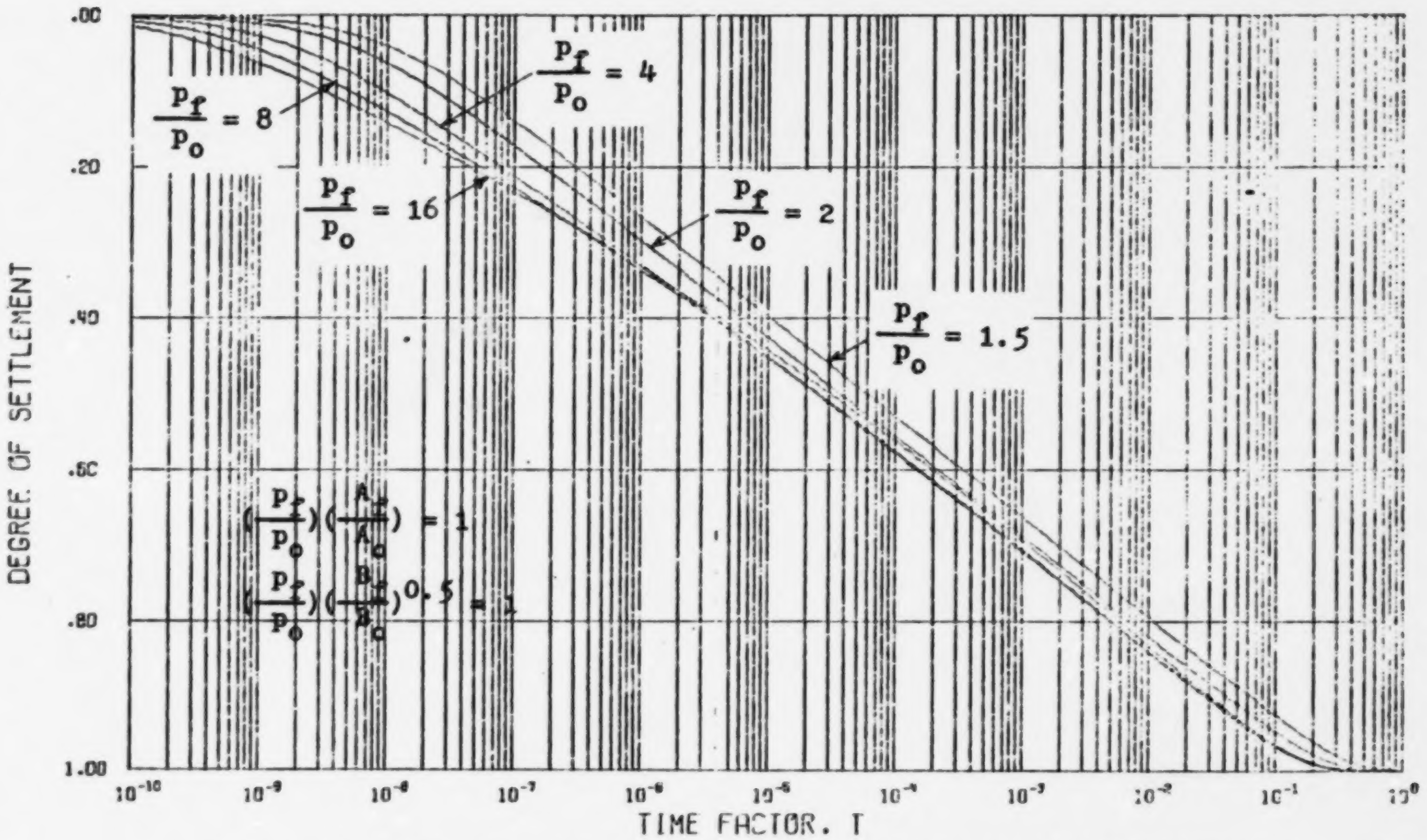

Fig. D-35. Settlement vs. time factor of the creep model based on micropore structure for various values of p_f/p_o, $B_o = 17$

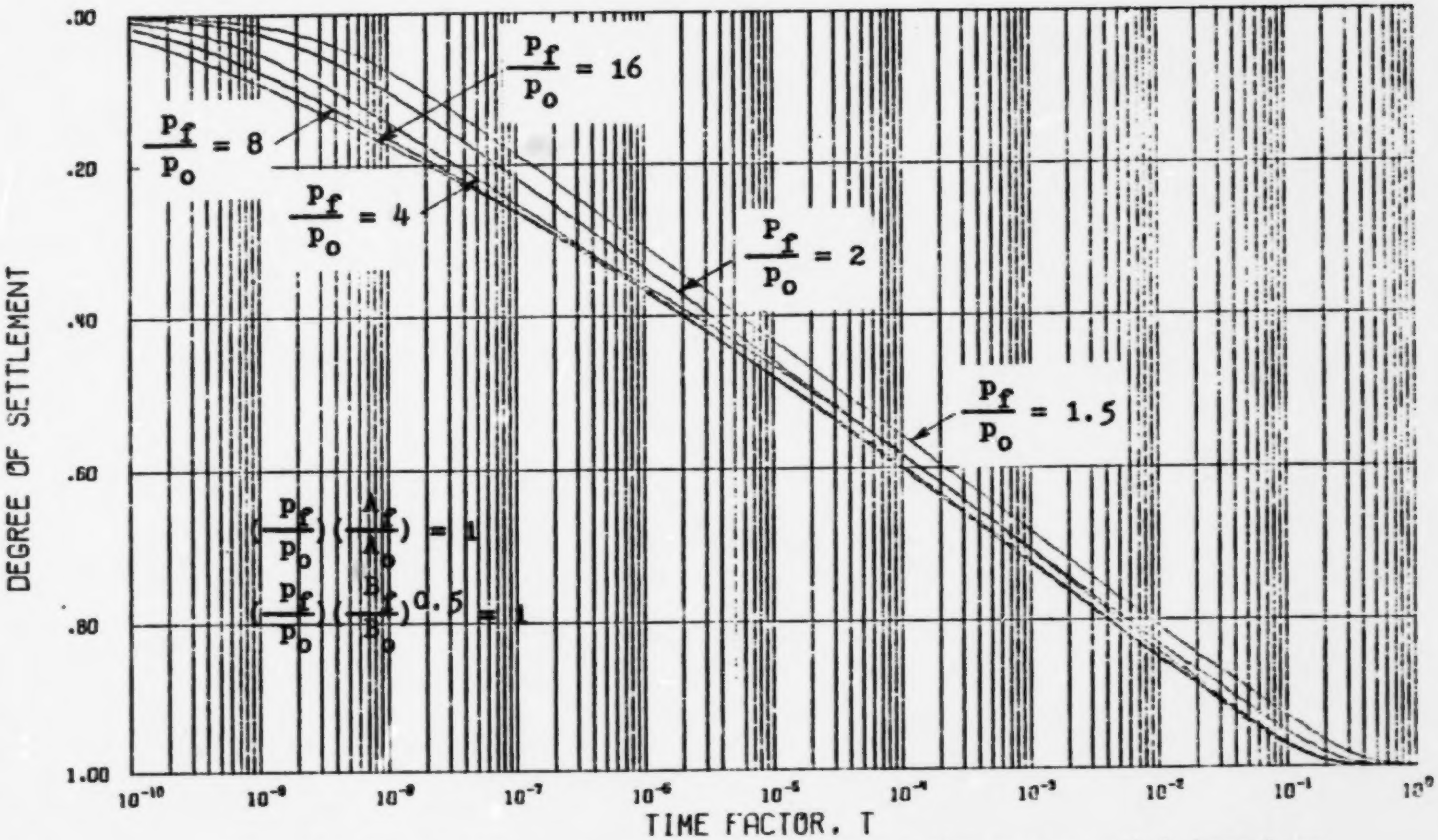

Fig. D-36. Settlement vs. time factor of the creep model based on micropore structure for various values of p_f/p_o, $B_o = 18$

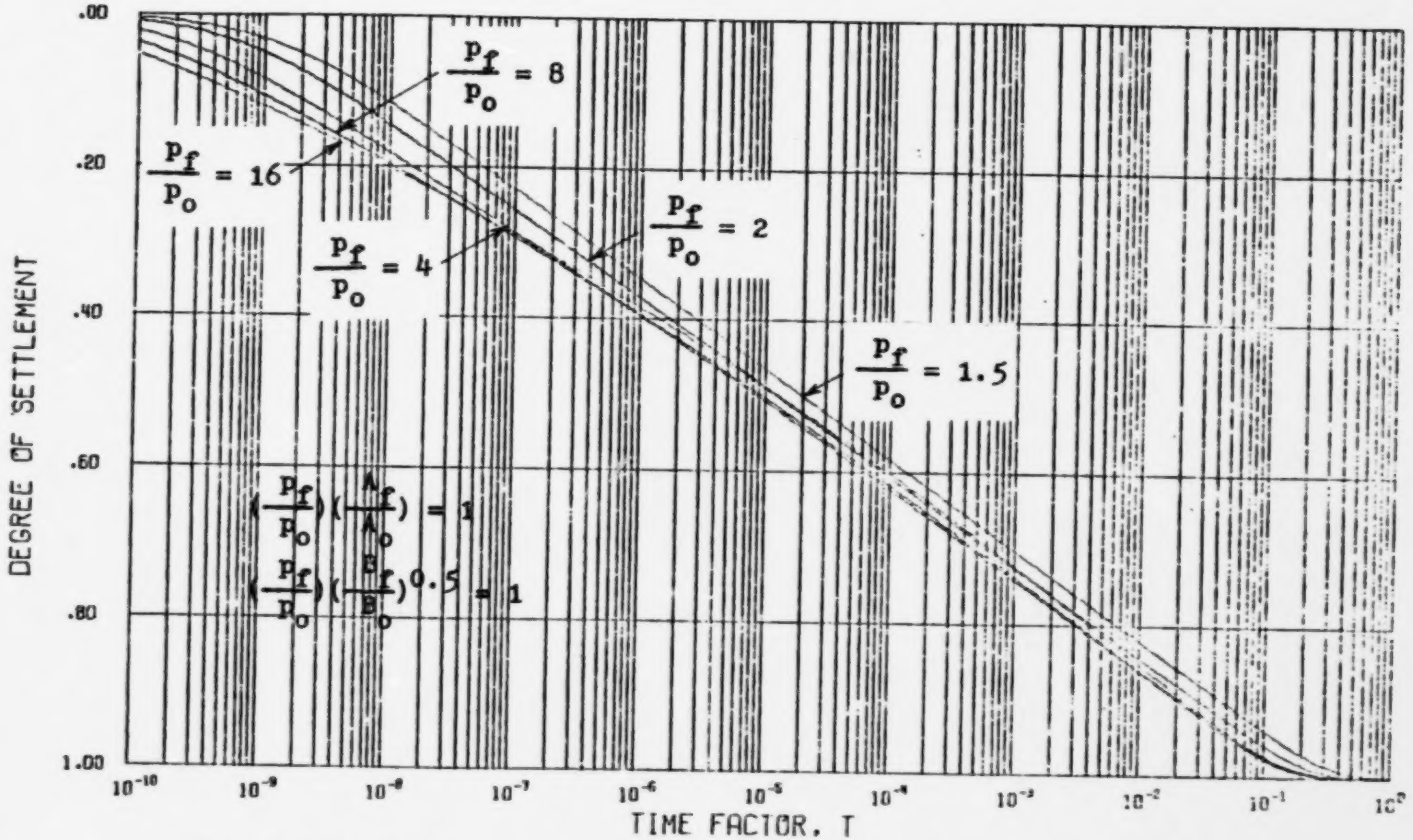

Fig. D-37. Settlement vs. time factor of the creep model based on micropore structure for various values of p_f/p_o; $B_o = 19$

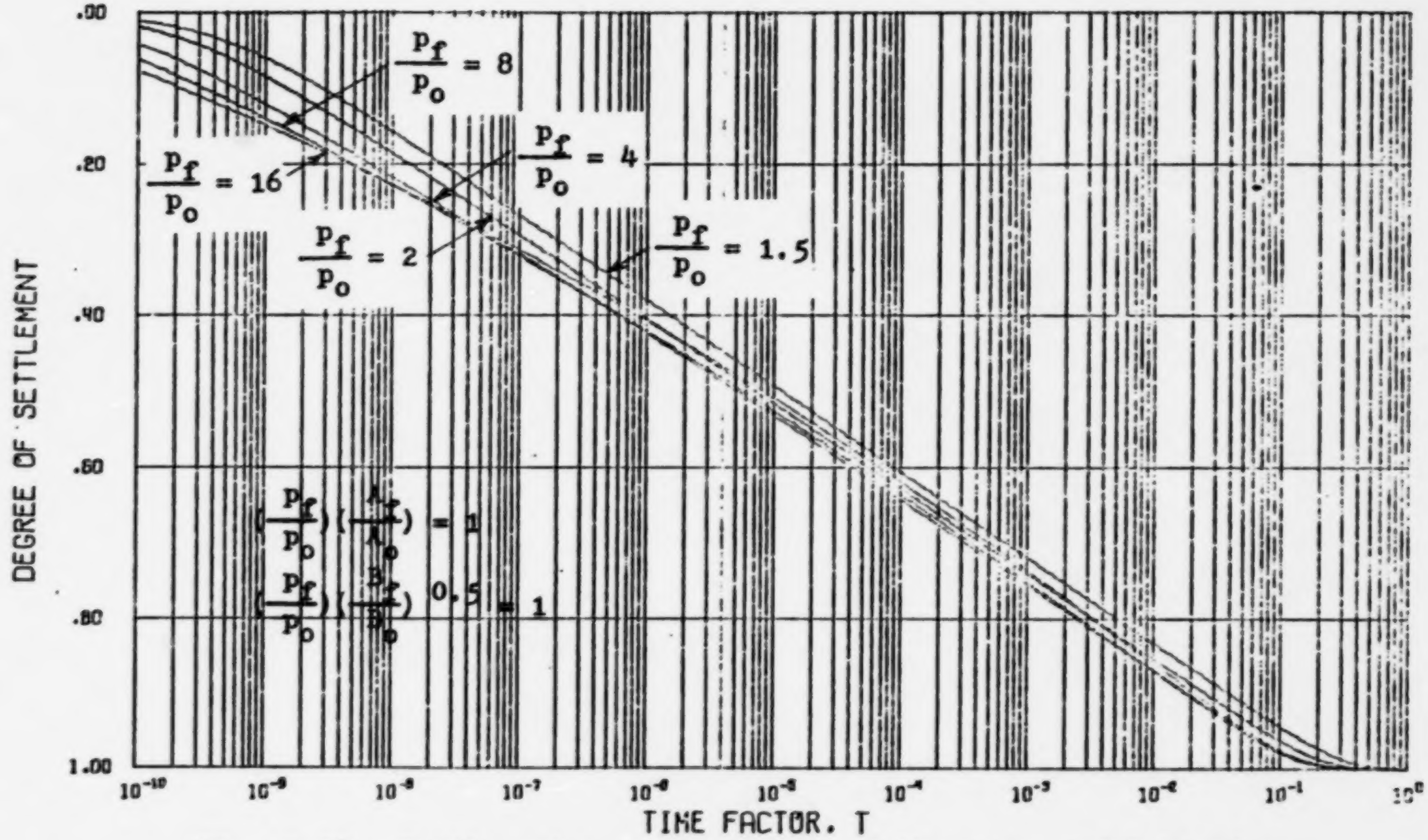

Fig. D-38. Settlement vs. time factor of the creep model based on micropore structure for various values of p_f/p_o; $B_o = 20$

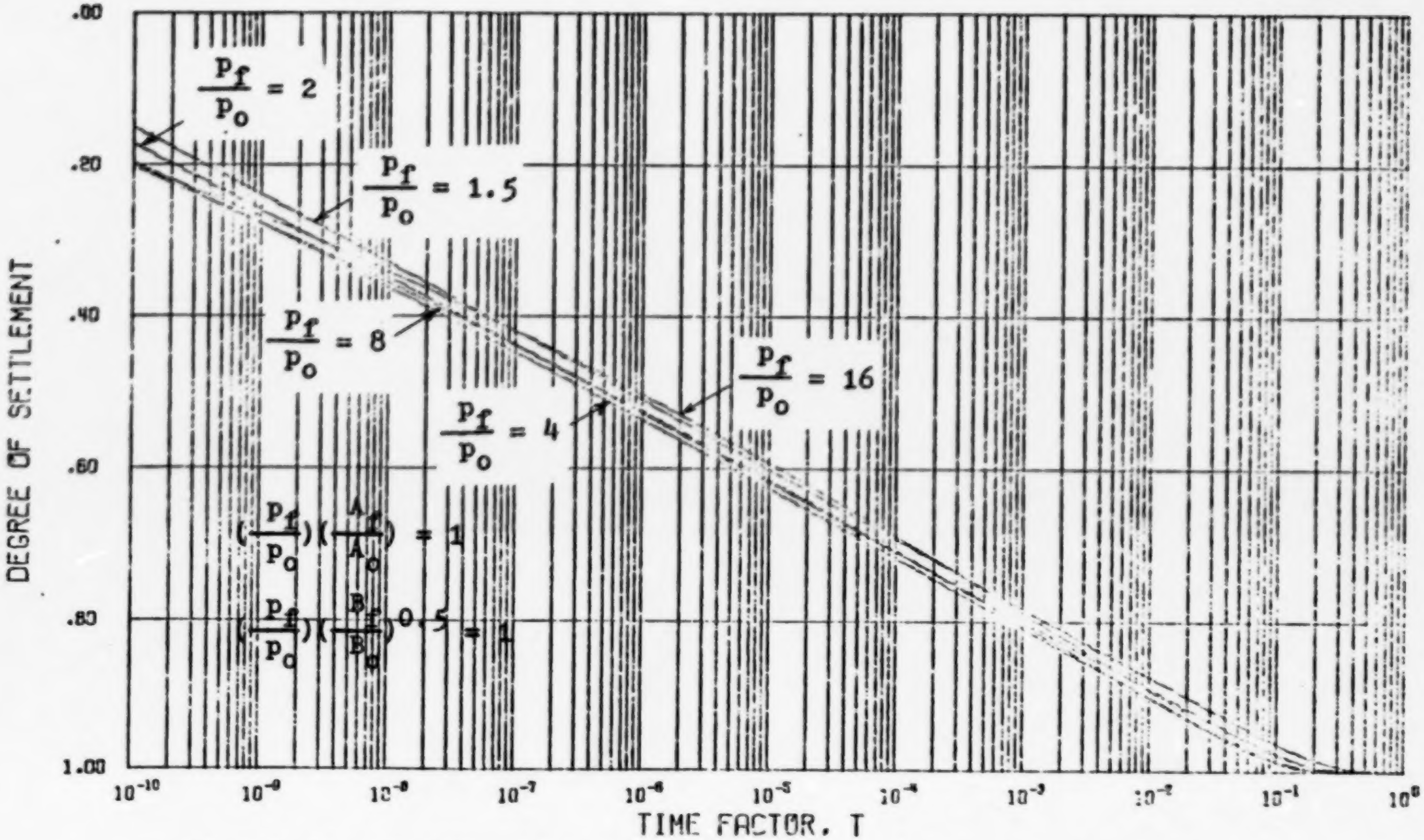

Fig. D-39. Settlement vs. time factor of the creep model based on micropore structure for various values of p_f/p_o, $B_o = 25$

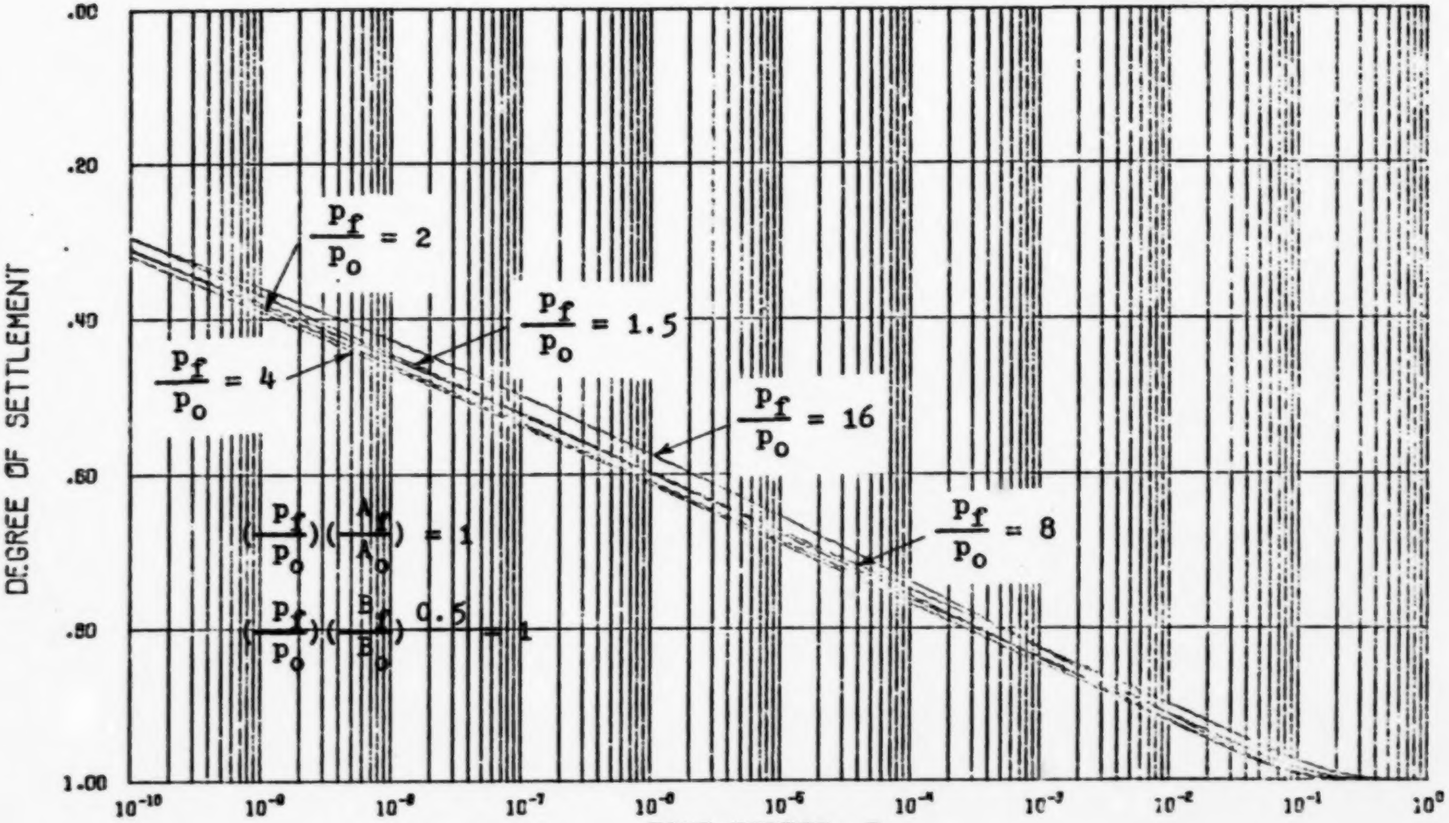

Fig. D-40. Settlement vs. time factor of the creep model based on micropore structure for various values of p_f/p_o: $B_o = 30$

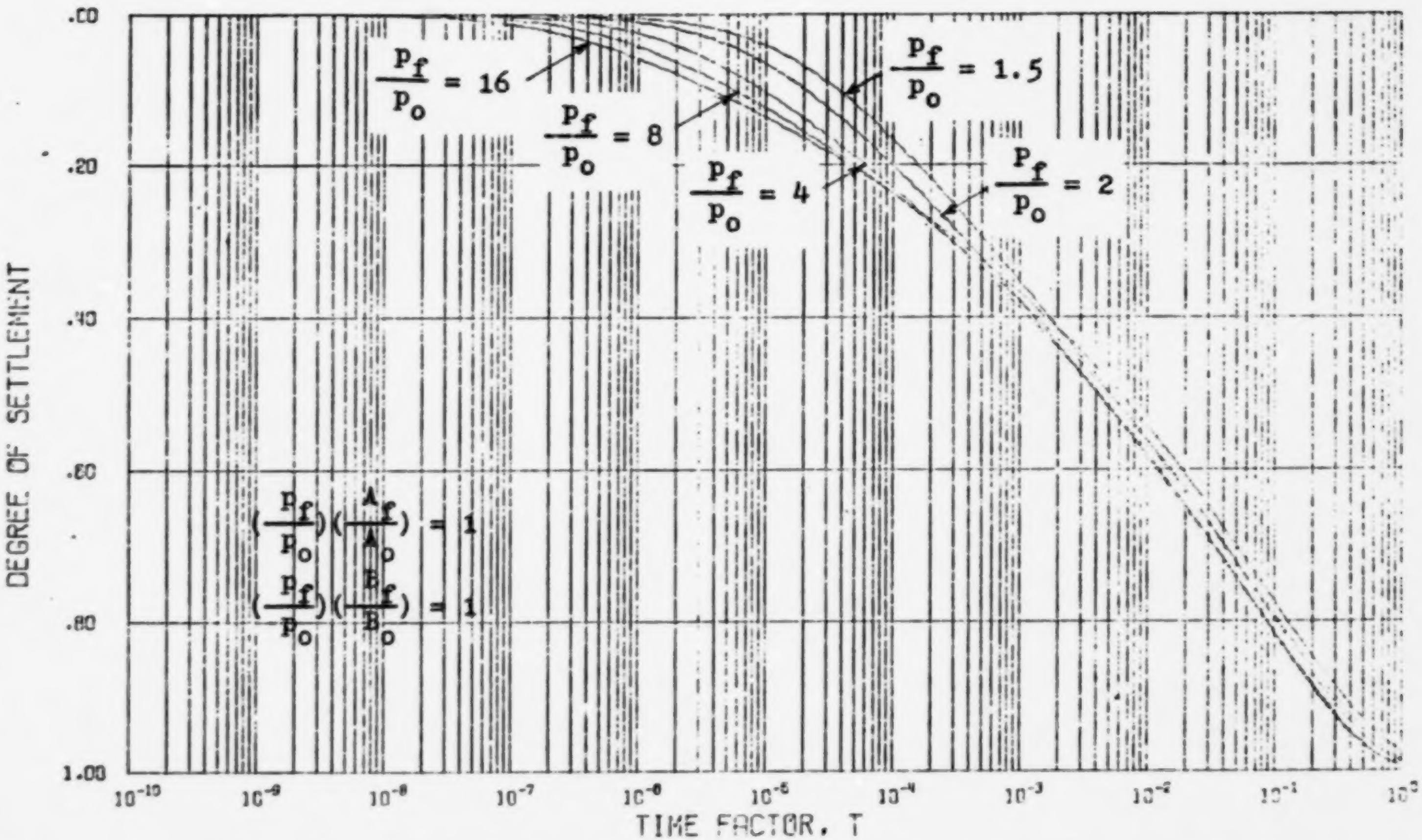

Fig. D-41. Settlement vs. time factor of the creep model based on micropore structure for various values of p_f/p_o, $B_o = 10$

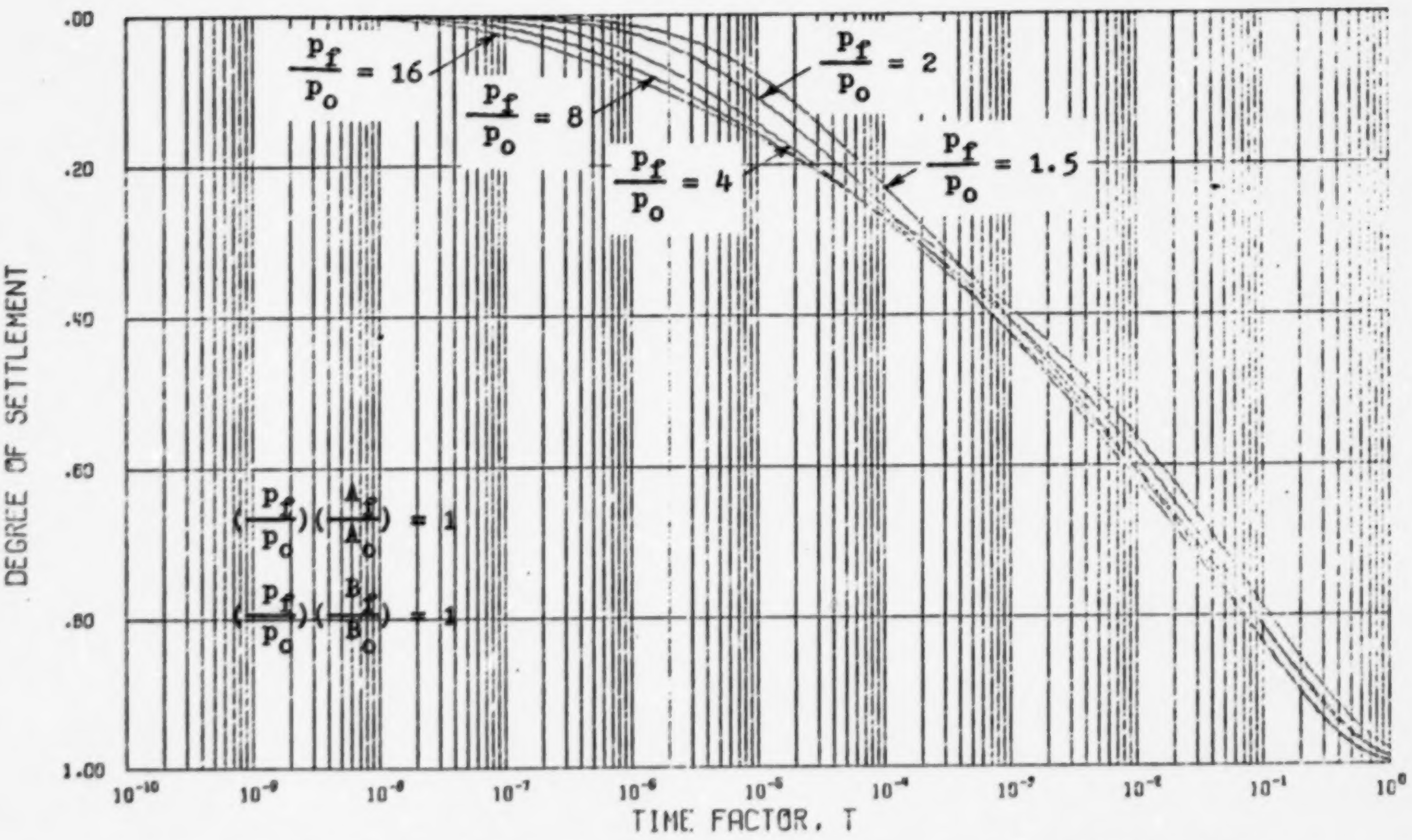

Fig. D-42. Settlement vs. time factor of the creep model based on micropore structure for various values of p_f/p_o, $B_o = 11$

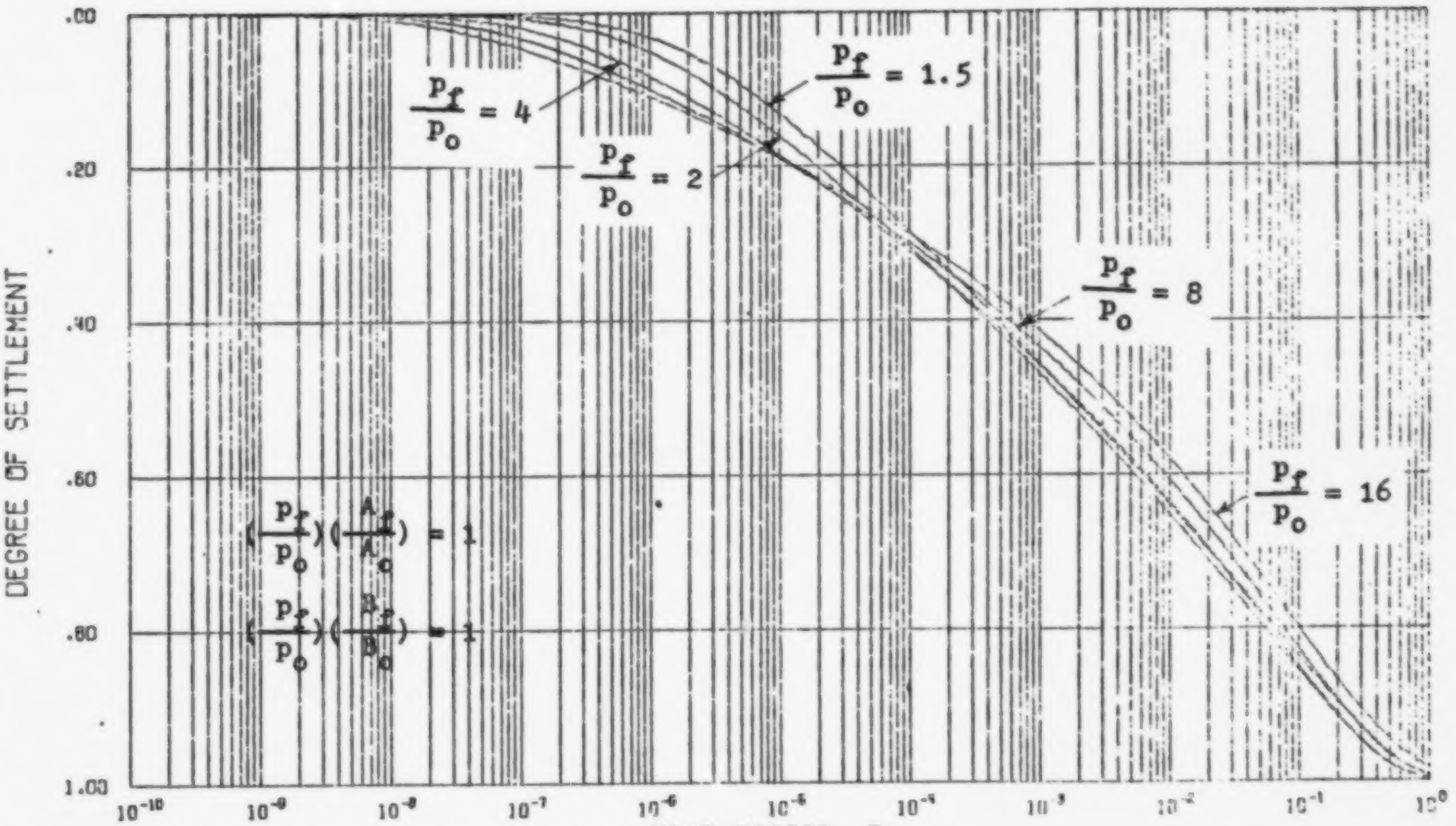

Fig. D-43. Settlement vs. time factor of the creep model based on micropore structure for various values of p_f/p_o, $B_o = 12$

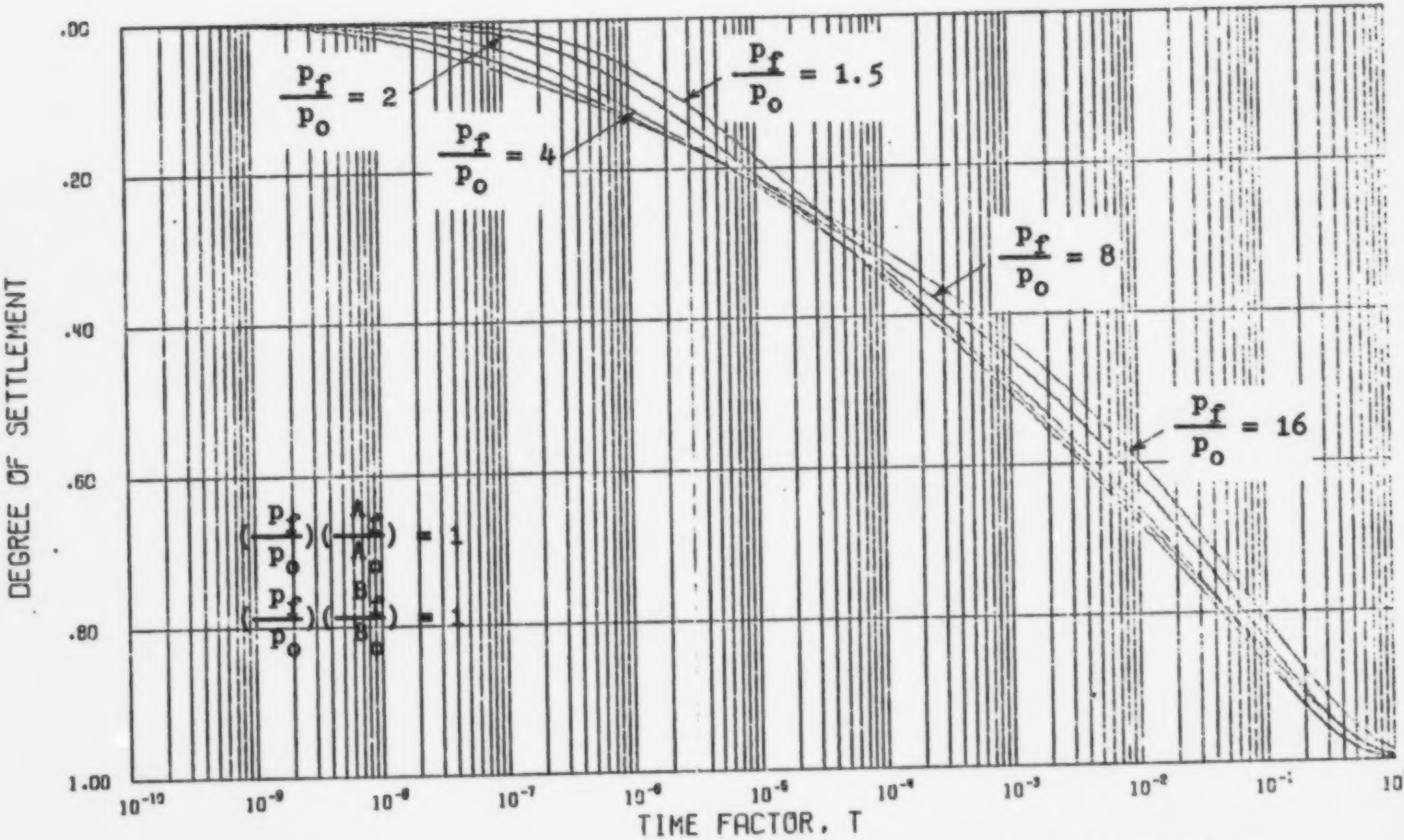

Fig. D-44. Settlement vs. time factor of the creep model based on micropore structure for various values of p_f/p_o, $B_o = 13$

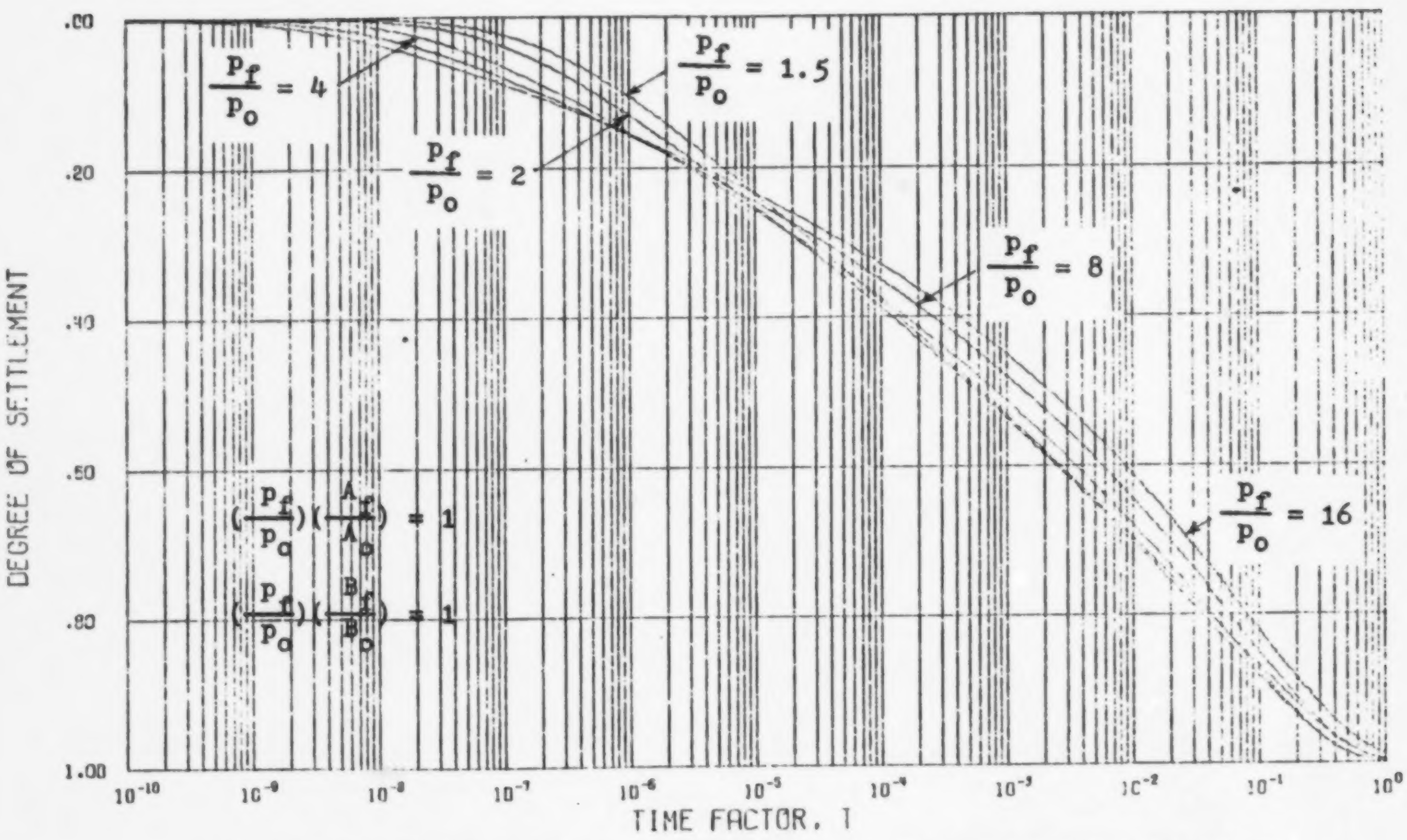

Fig. D-45. Settlement vs. time factor of the creep model based on micropore structure for various values of p_f/p_o, $B_o = 14$

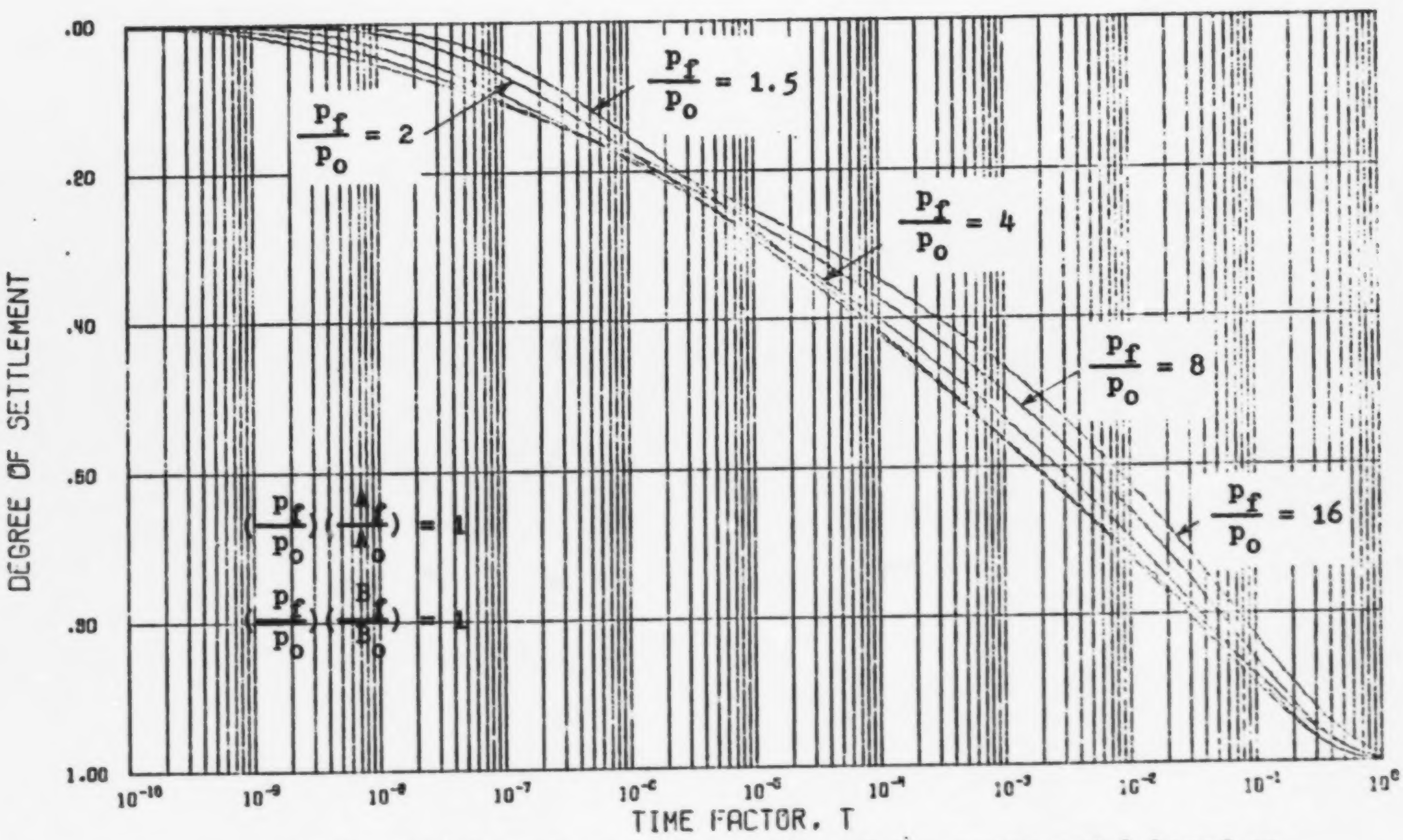

Fig. D-46. Settlement vs. time factor of the creep model based on micropore structure for various values of p_f/p_o; $B_o = 15$

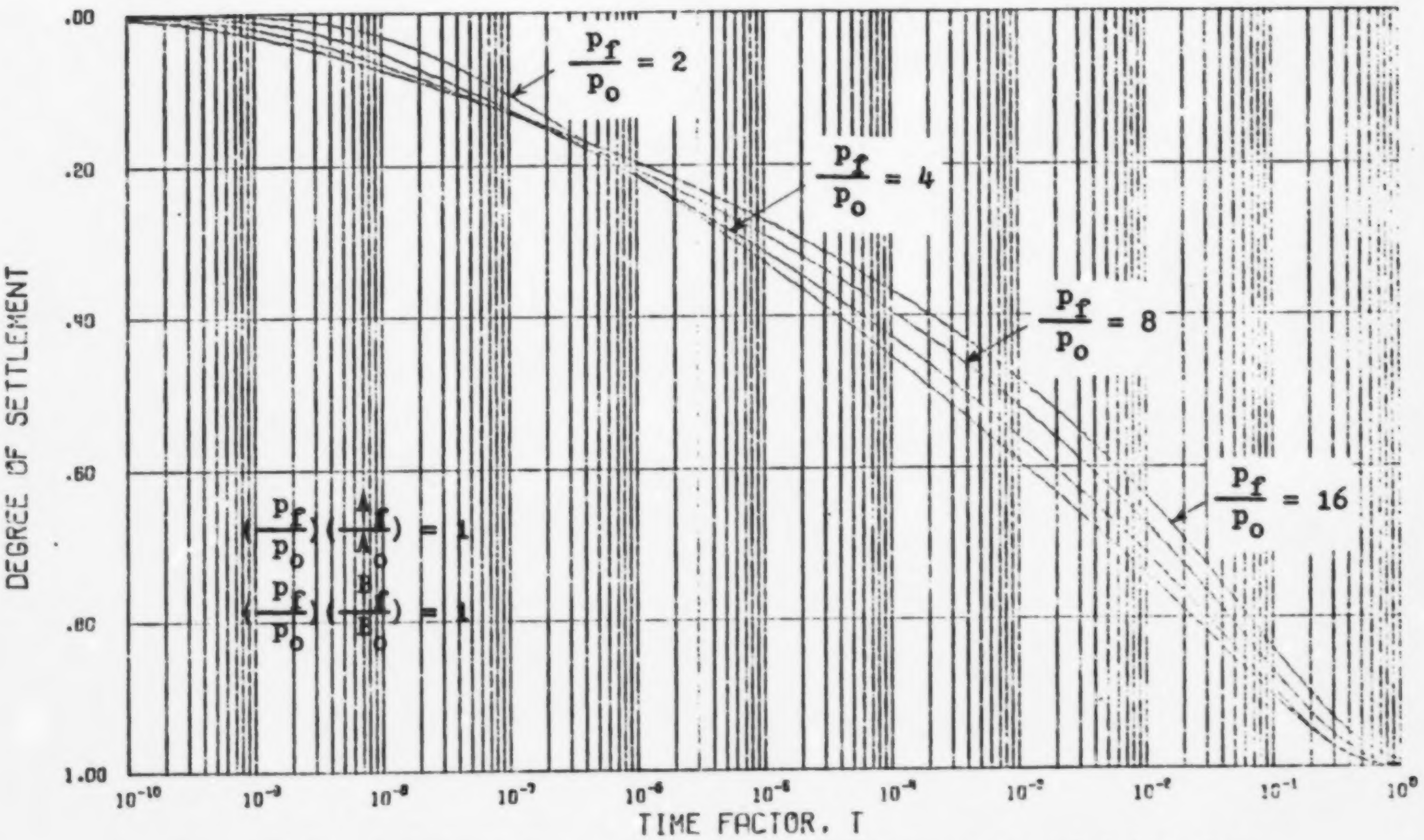

Fig. D-47. Settlement vs. time factor of the creep model based on micropore structure for various values of p_f/p_o; $B_o = 16$

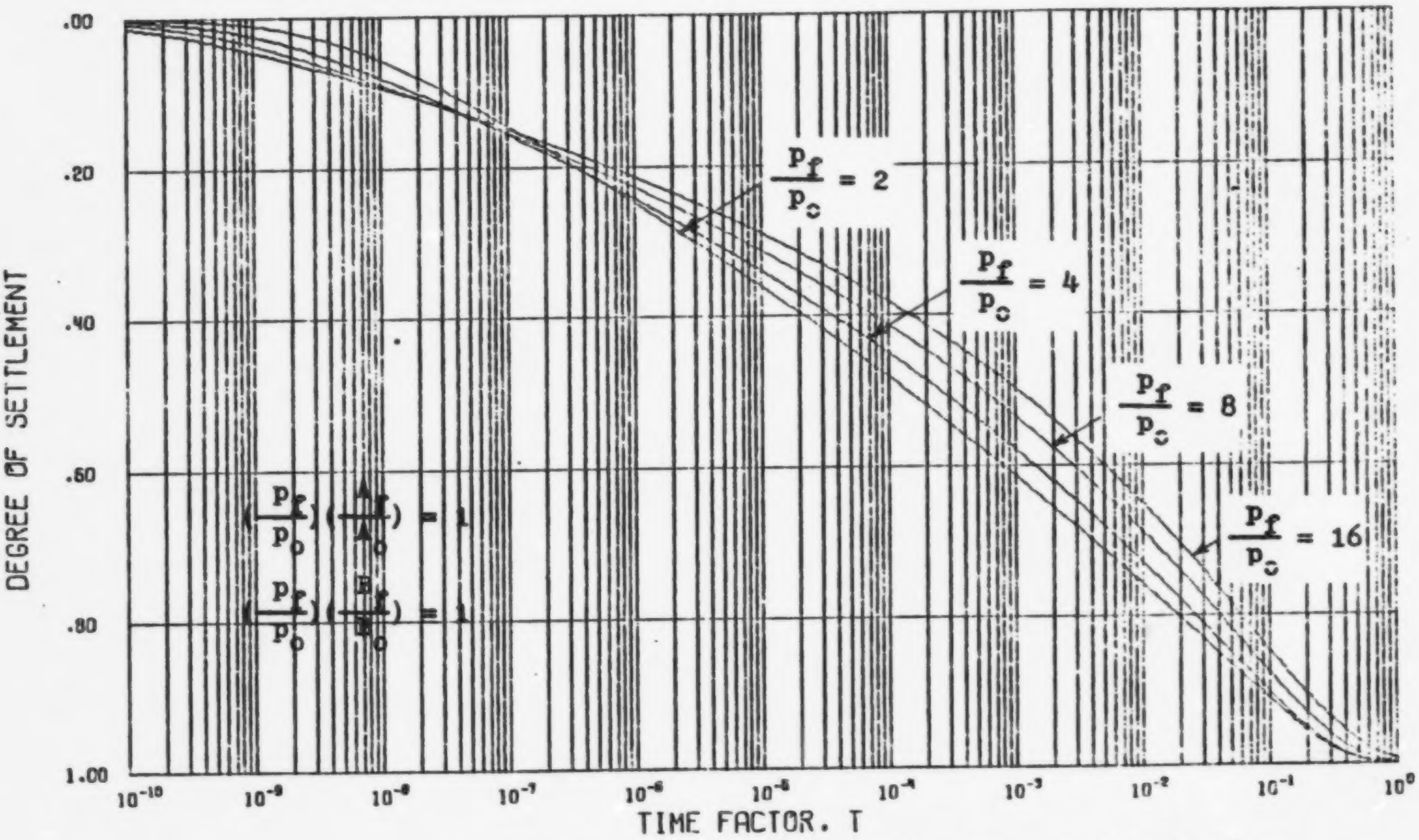

Fig. D-48. Settlement vs. time factor of the creep model based on micropore structure for various values of p_f/p_o, $B_o = 17$

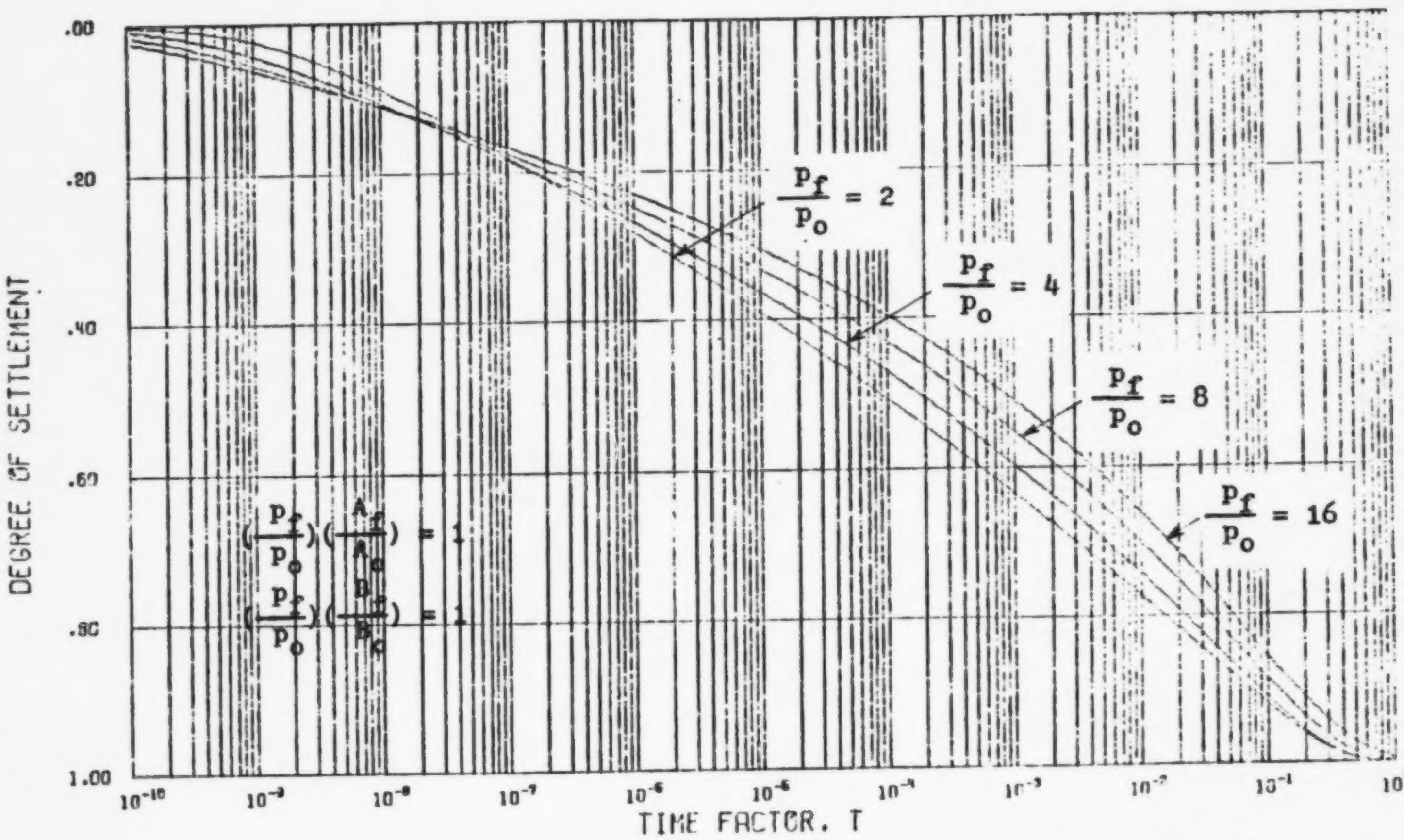

Fig. D-49. Settlement vs. time factor of the creep model based on micropore structure for various values of p_f/p_o, $B_o = 18$

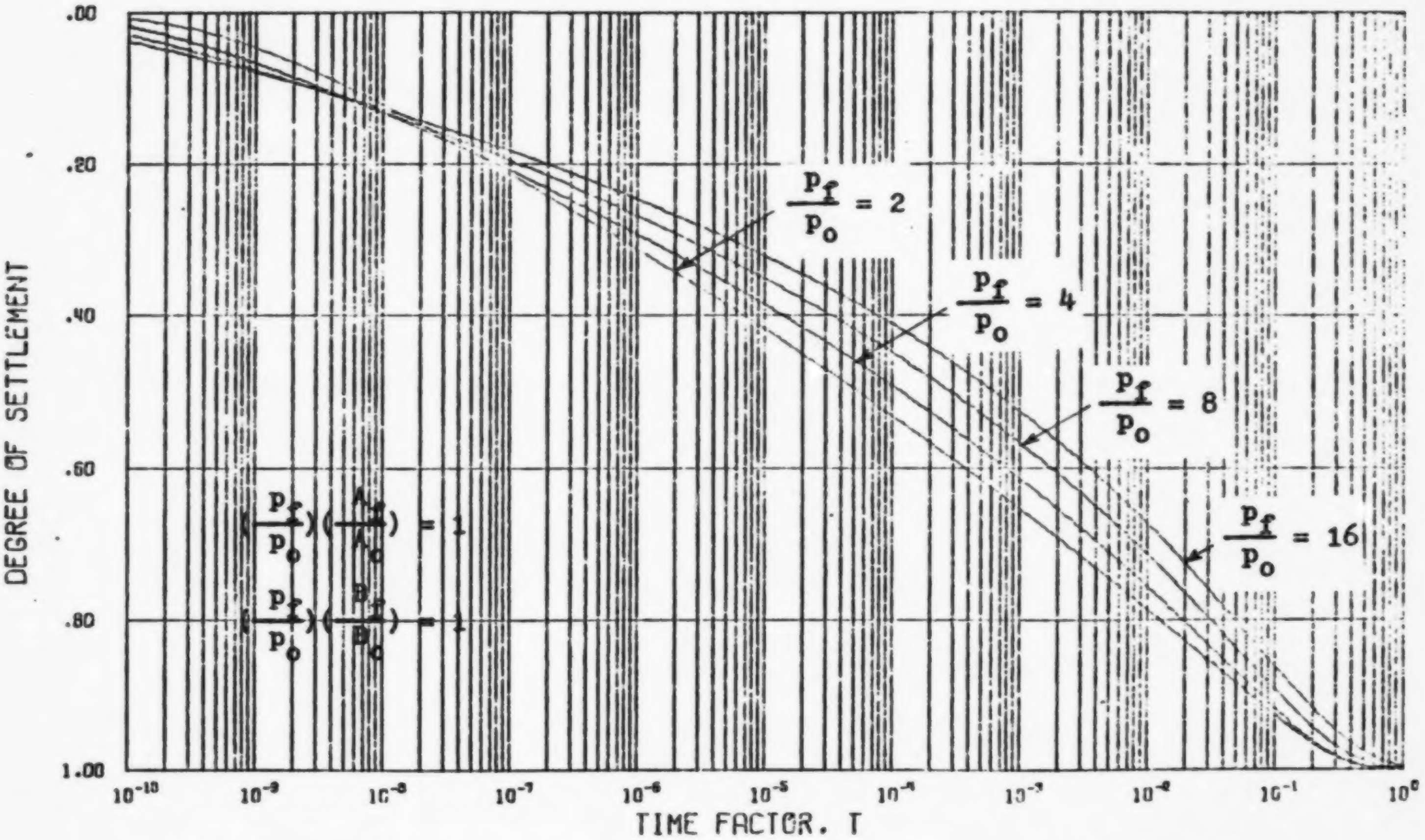

Fig. D-50. Settlement vs. time factor of the creep model based on micropore structure for various values of p_f/p_o, $B_o = 19$

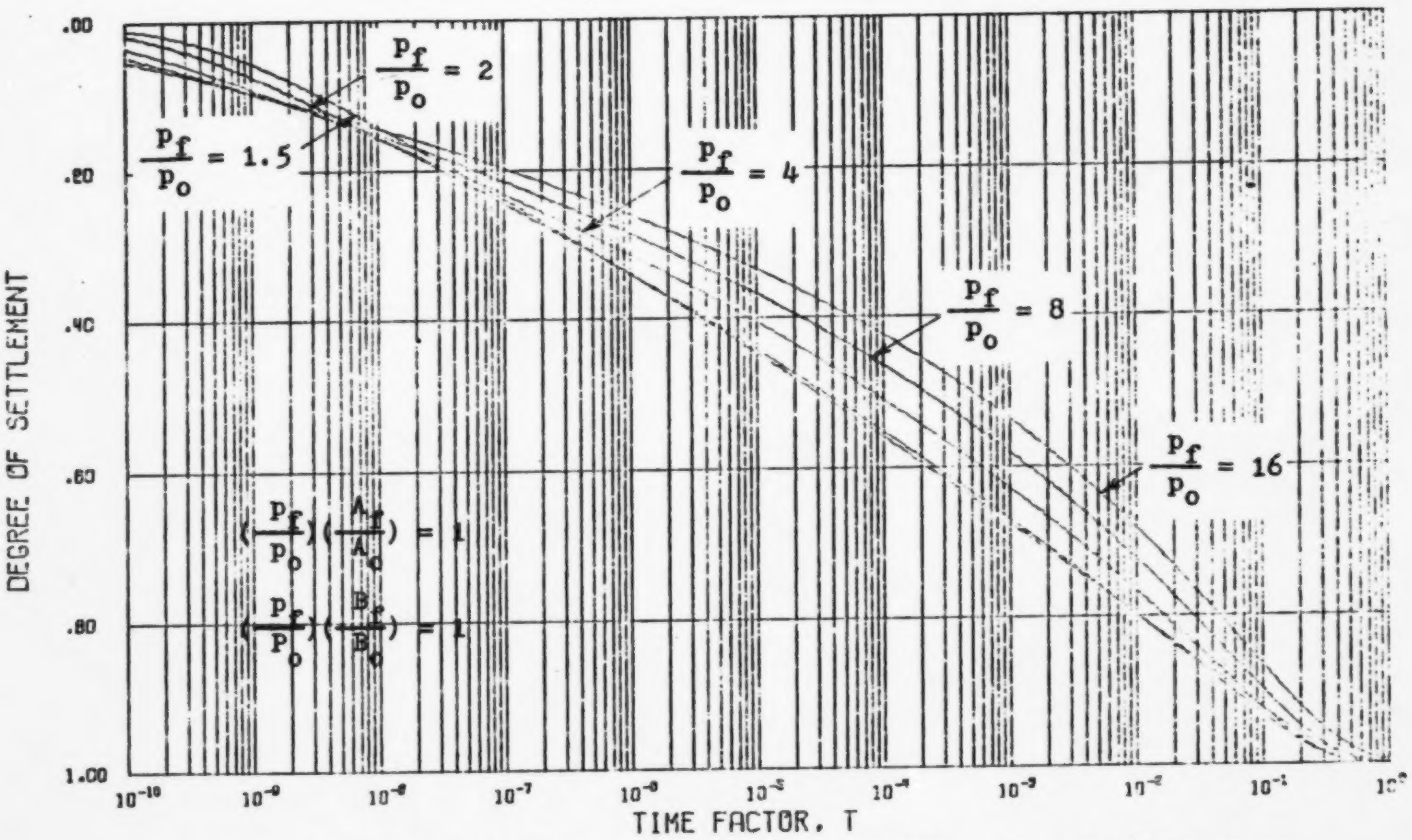

Fig. D-51. Settlement vs. time factor of the creep model based on micropore structure for various values of p_f/p_o; $B_o = 20$

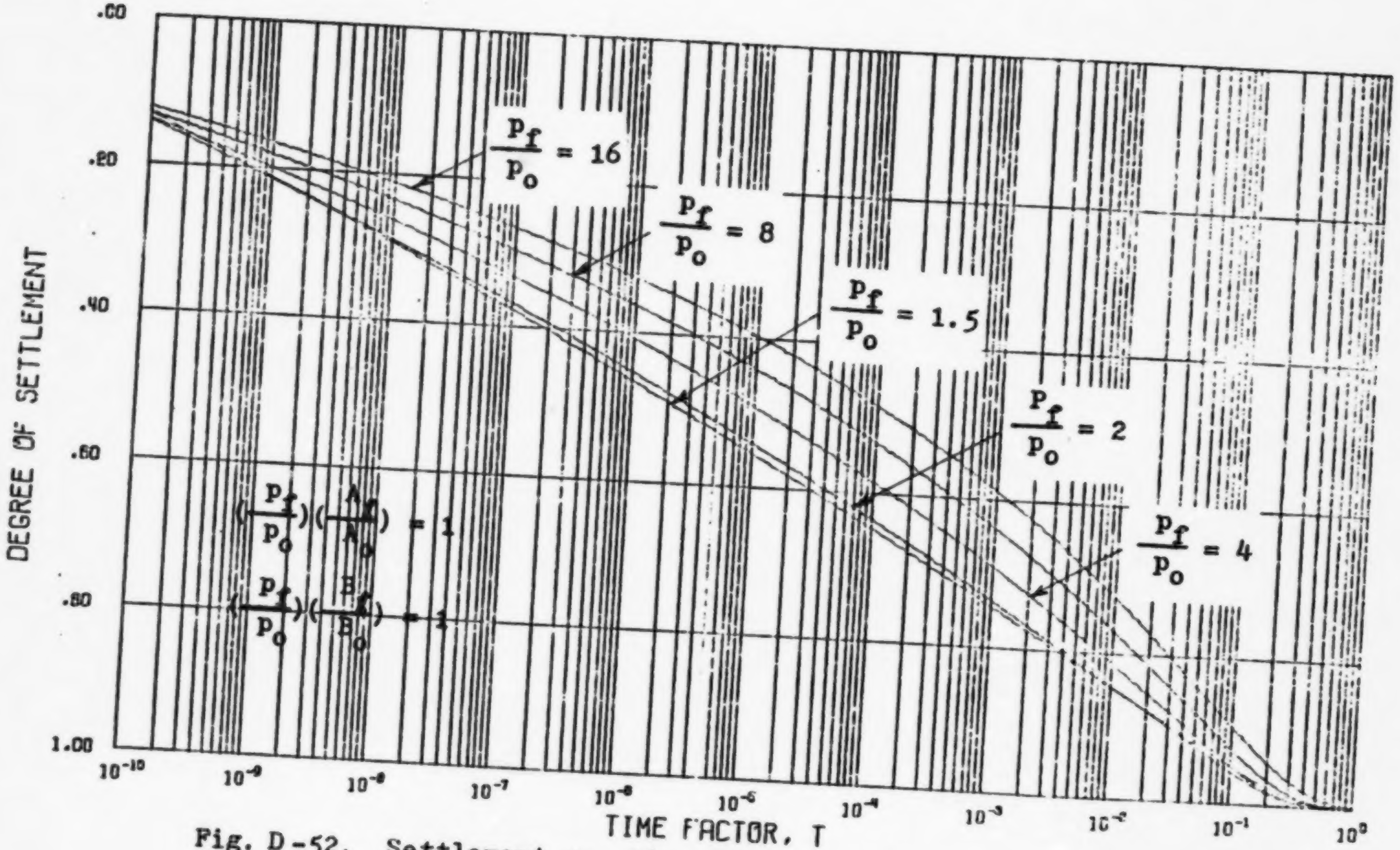

Fig. D-52. Settlement vs. time factor of the creep model based on micropore structure for various values of p_f/p_o, $B_o = 25$

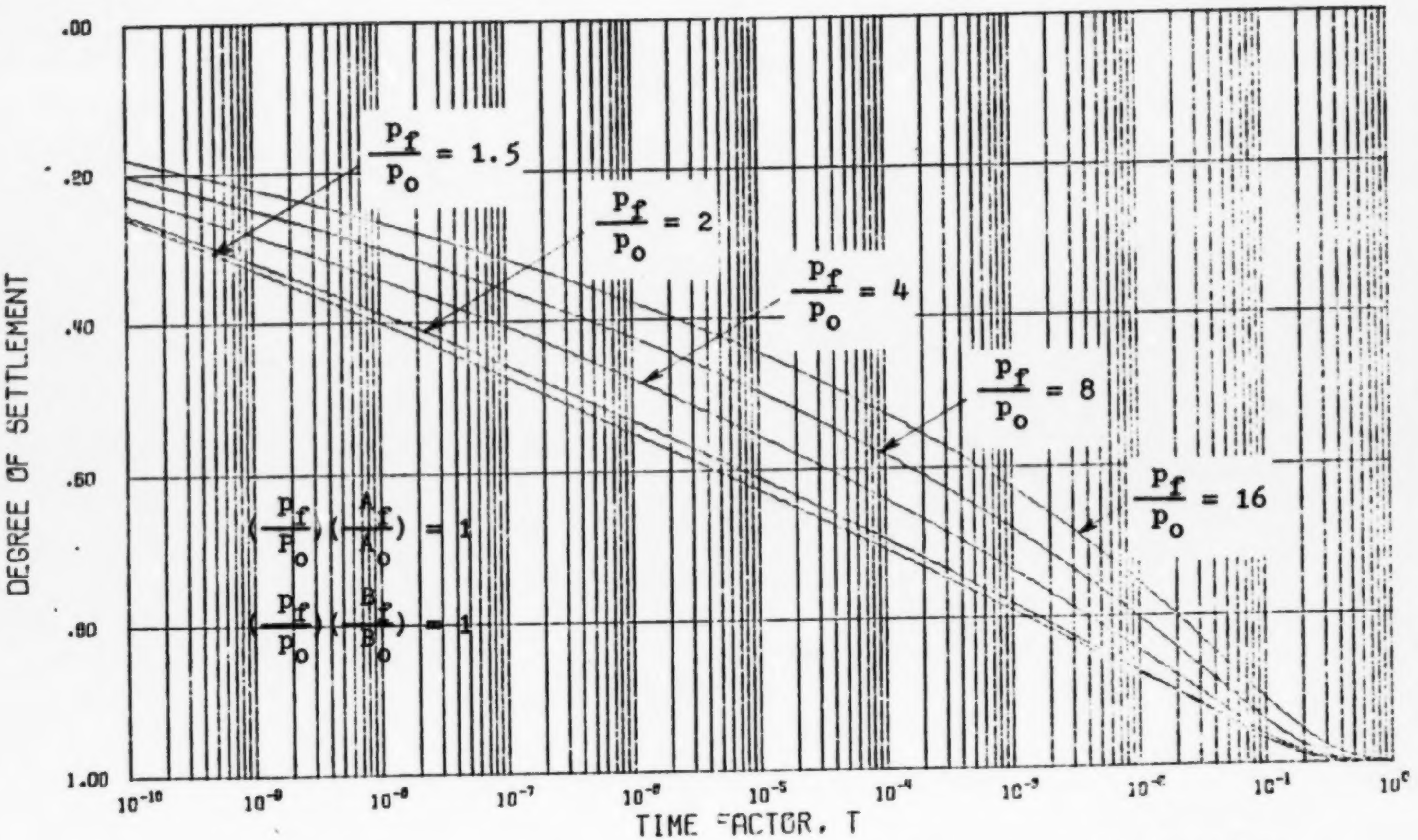

Fig. D-53. Settlement vs. time factor of the creep model based on micropore structure for various values of p_f/p_o, $B_o = 30$

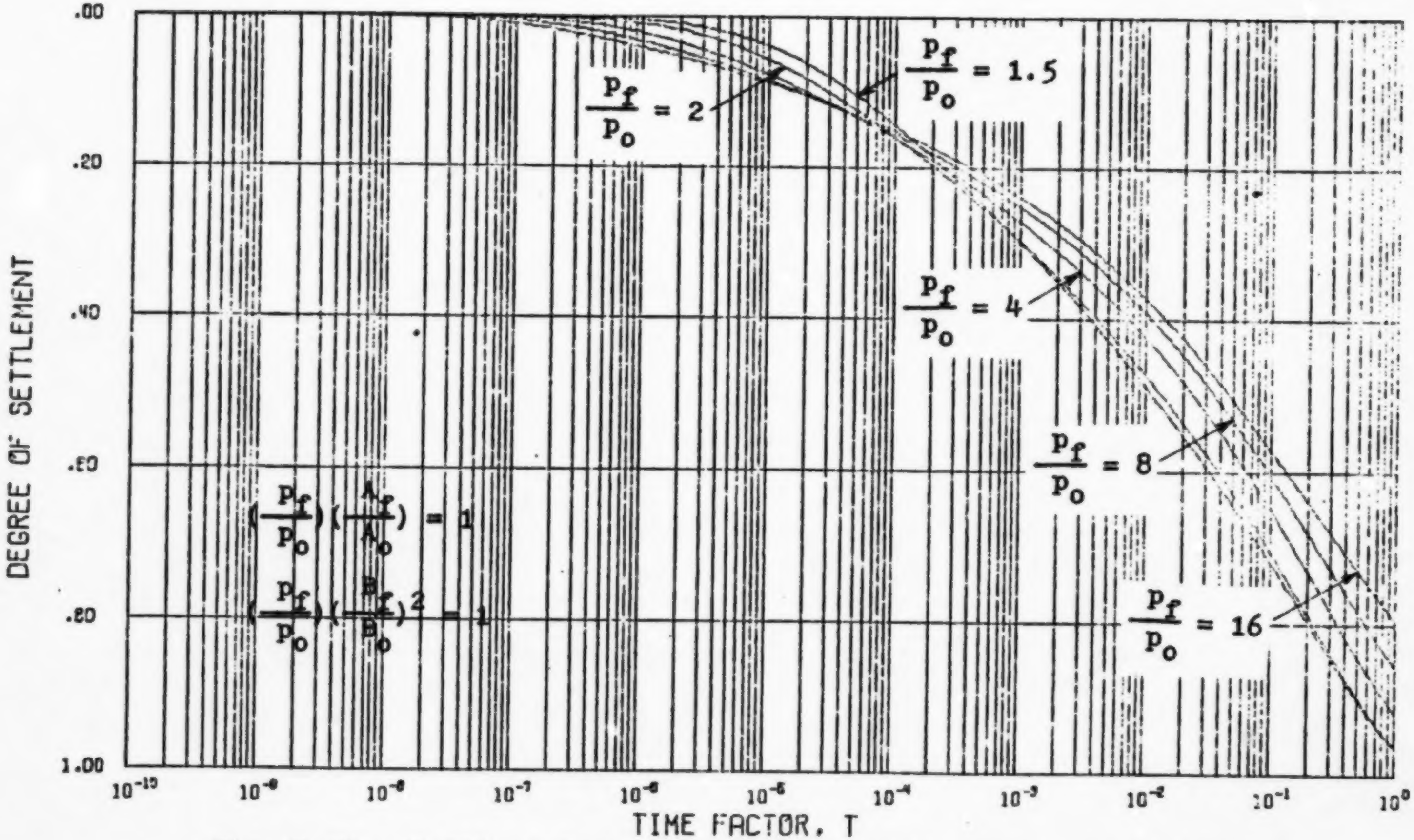

Fig. D-54. Settlement vs. time factor of the creep model based on micropore structure for various values of p_f/p_o, $B_o = 10$

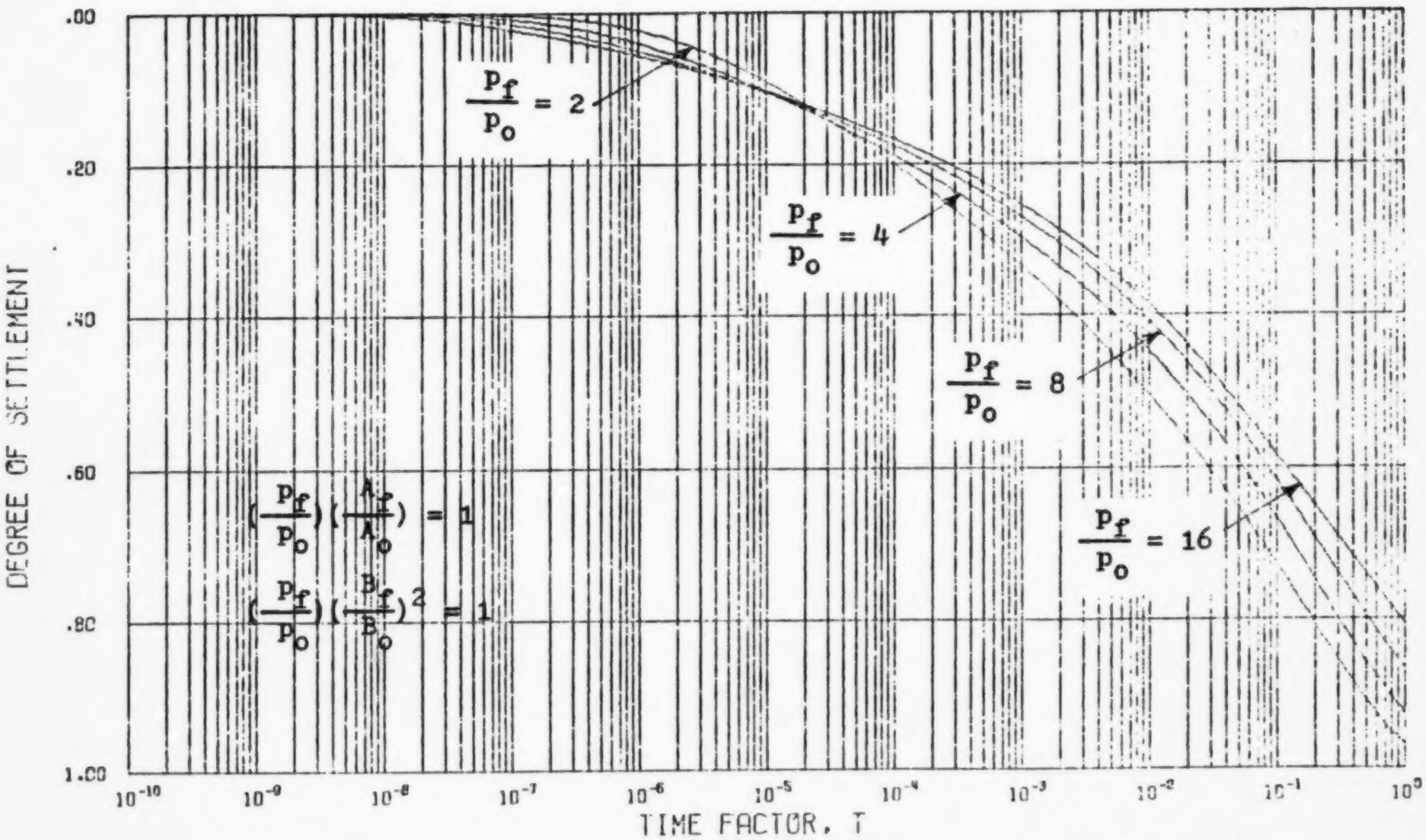

Fig. D-55. Settlement vs. time factor of the creep model based on micropore structure for various values of p_f/p_o, $B_o = 11$

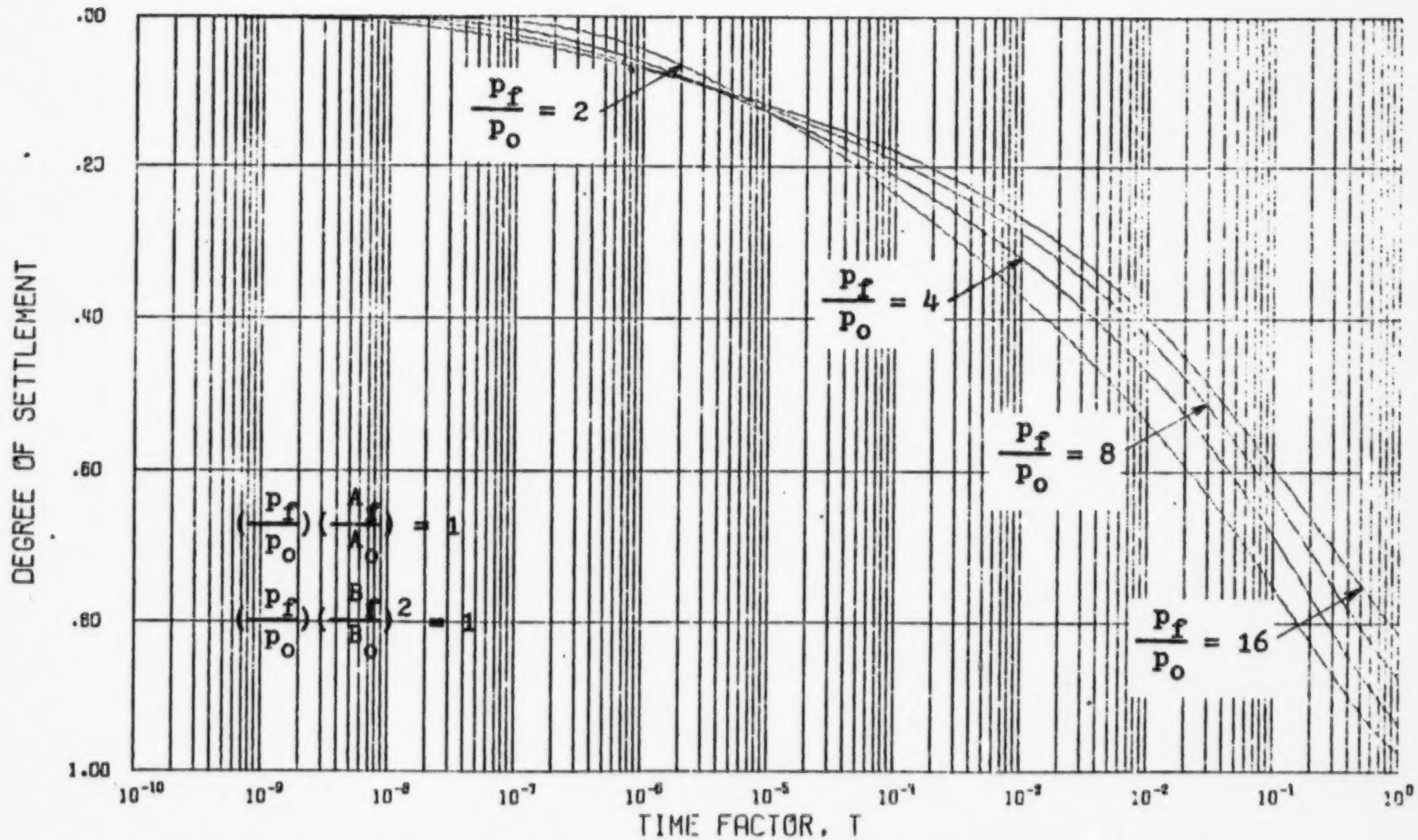

Fig. D-56. Settlement vs. time factor of the creep model based on micropore structure for various values of p_f/p_o; $B_o = 12$

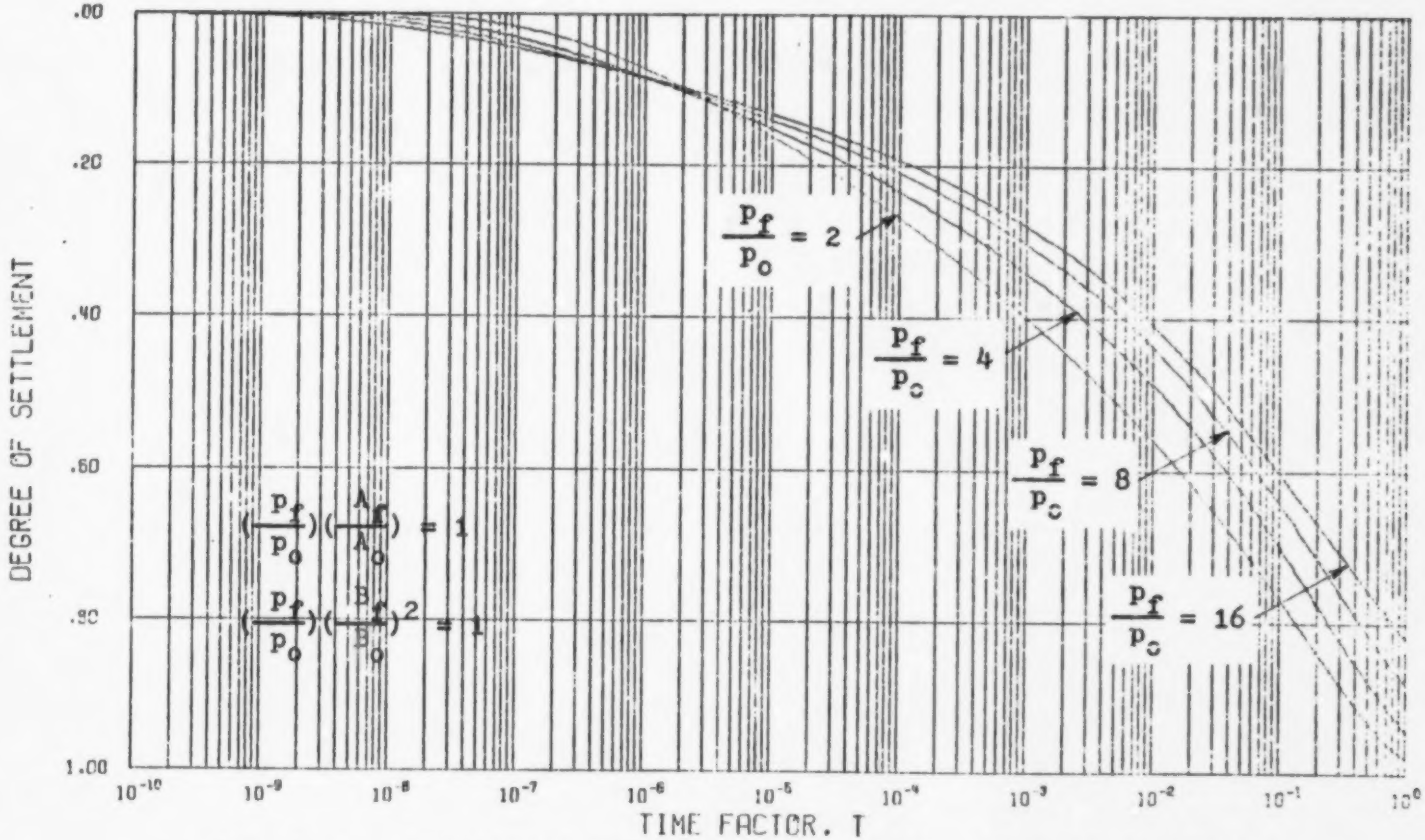

Fig. D-57. Settlement vs. time factor of the creep model based on micropore structure for various values of p_f/p_o; $B_o = 13$

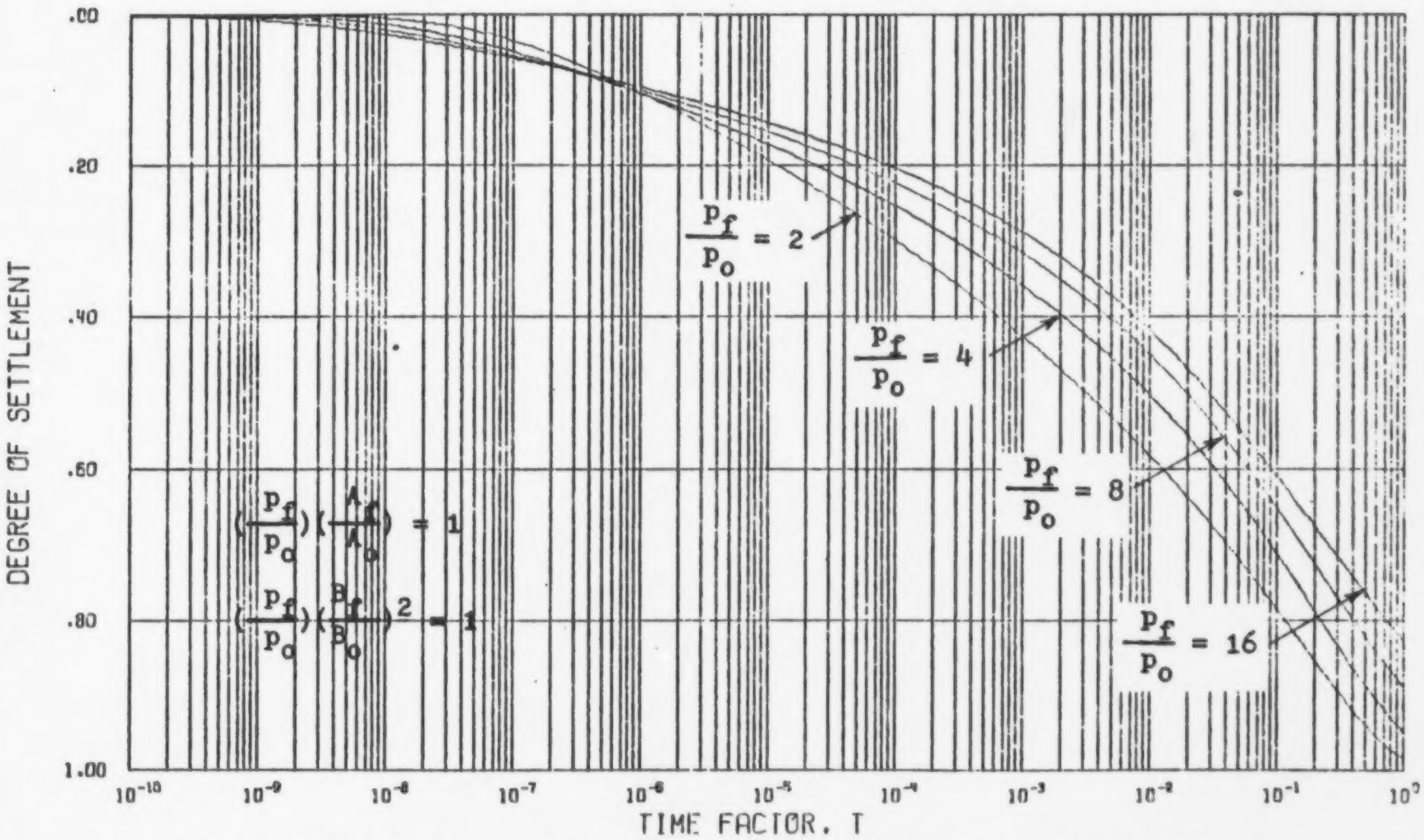

Fig. D-58. Settlement vs. time factor of the creep model based on micropore structure for various values of p_f/p_o; $B_o = 14$

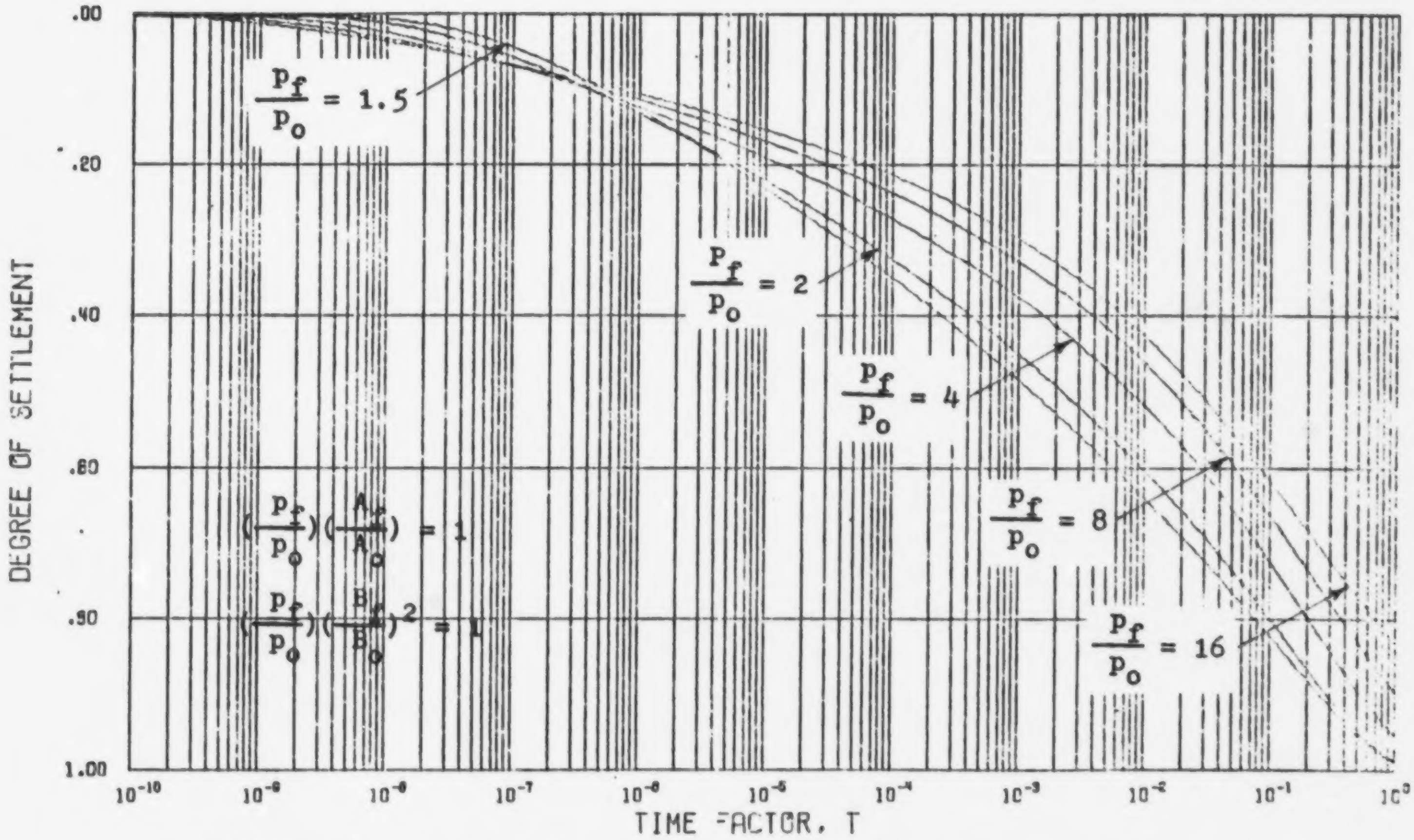

Fig. D-59. Settlement vs. time factor of the creep model based on micropore structure for various values of p_f/p_o, $B_o = 15$

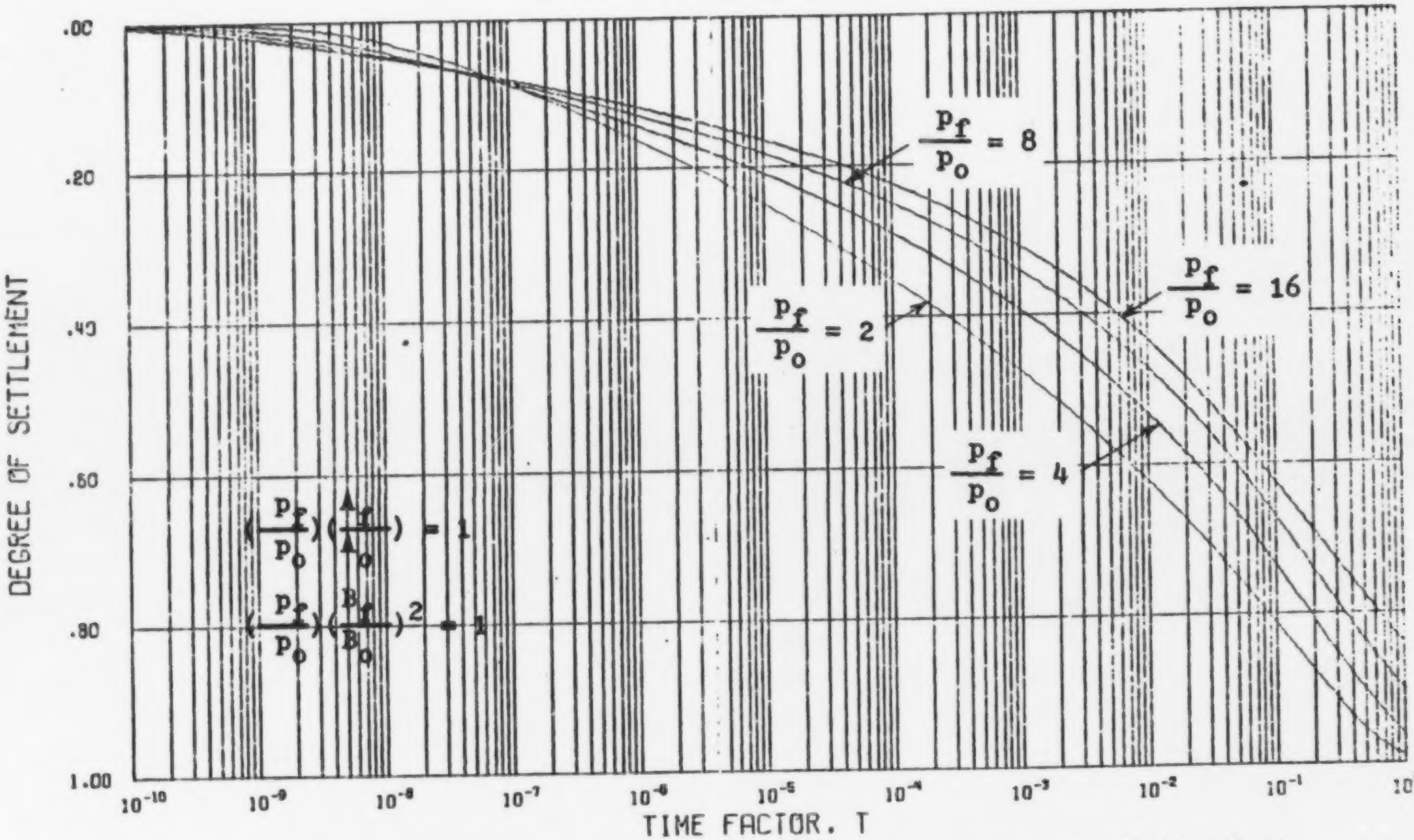

Fig. D-60. Settlement vs. time factor of the creep model based on micropore structure for various values of p_f/p_o; $B_o = 16$

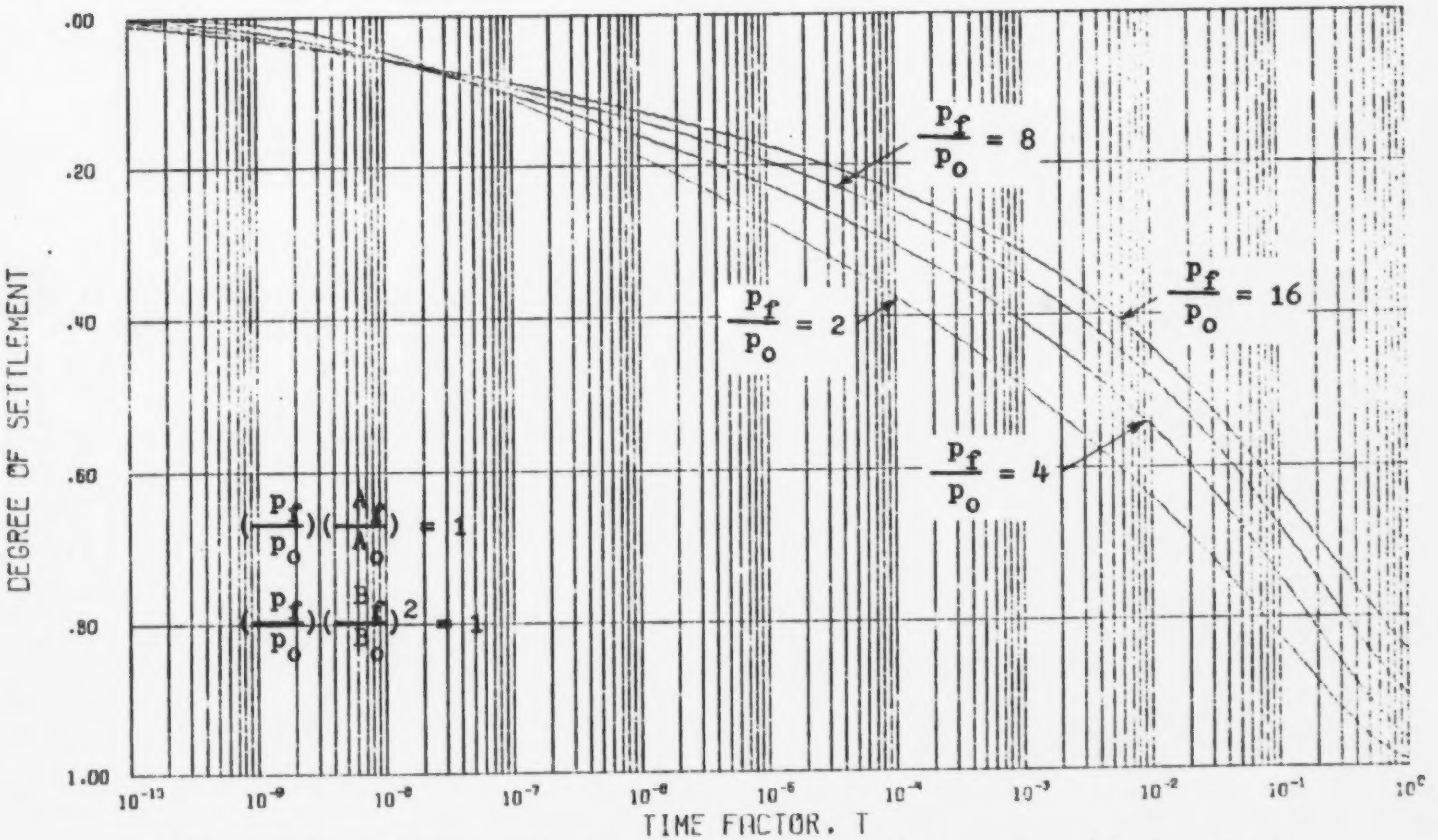

Fig. D-61. Settlement vs. time factor of the creep model based on micropore structure for various values of p_f/p_o, $B_o = 17$

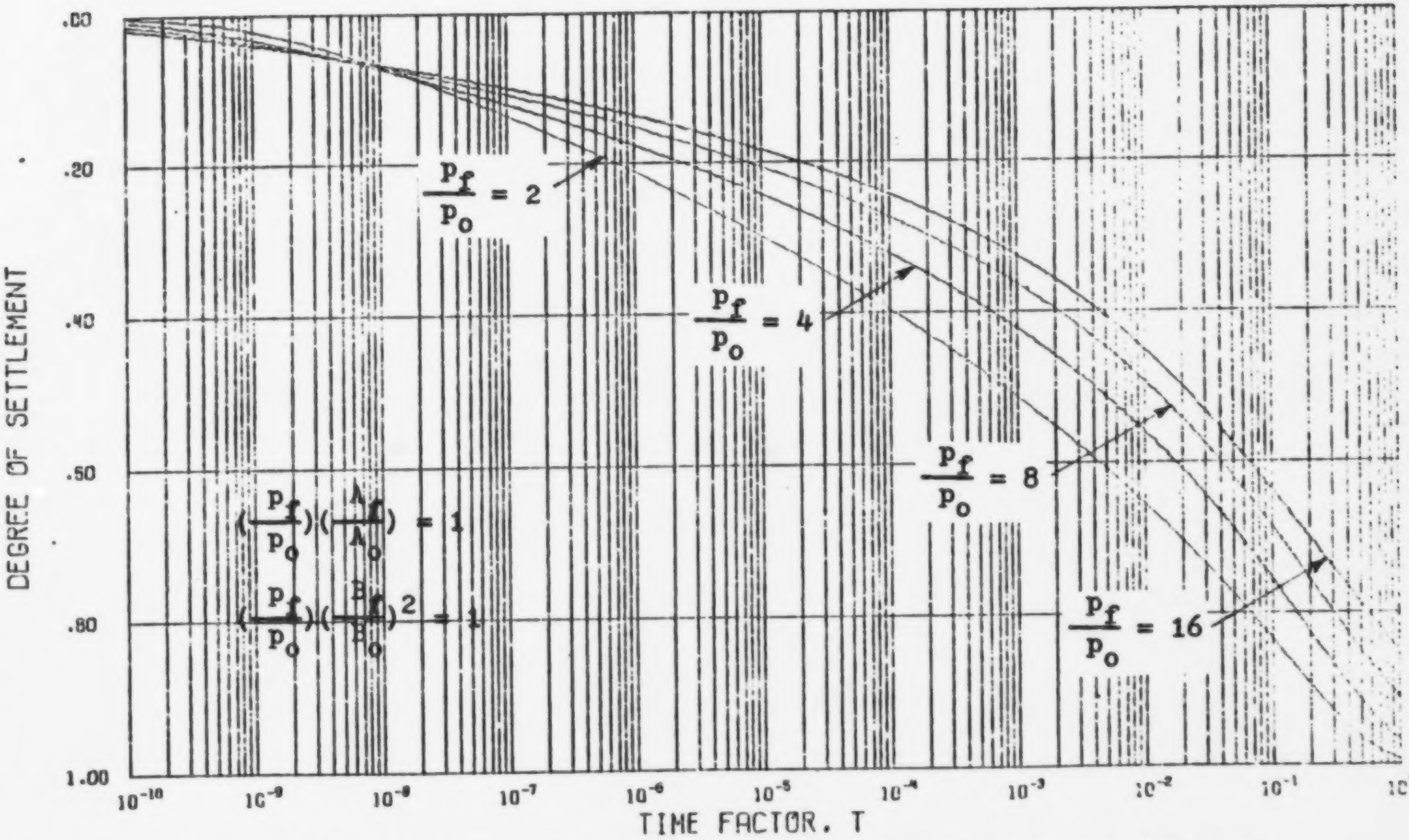

Fig. D-62. Settlement vs. time factor of the creep model based on micropore structure for various values of p_f/p_o, $B_o = 18$

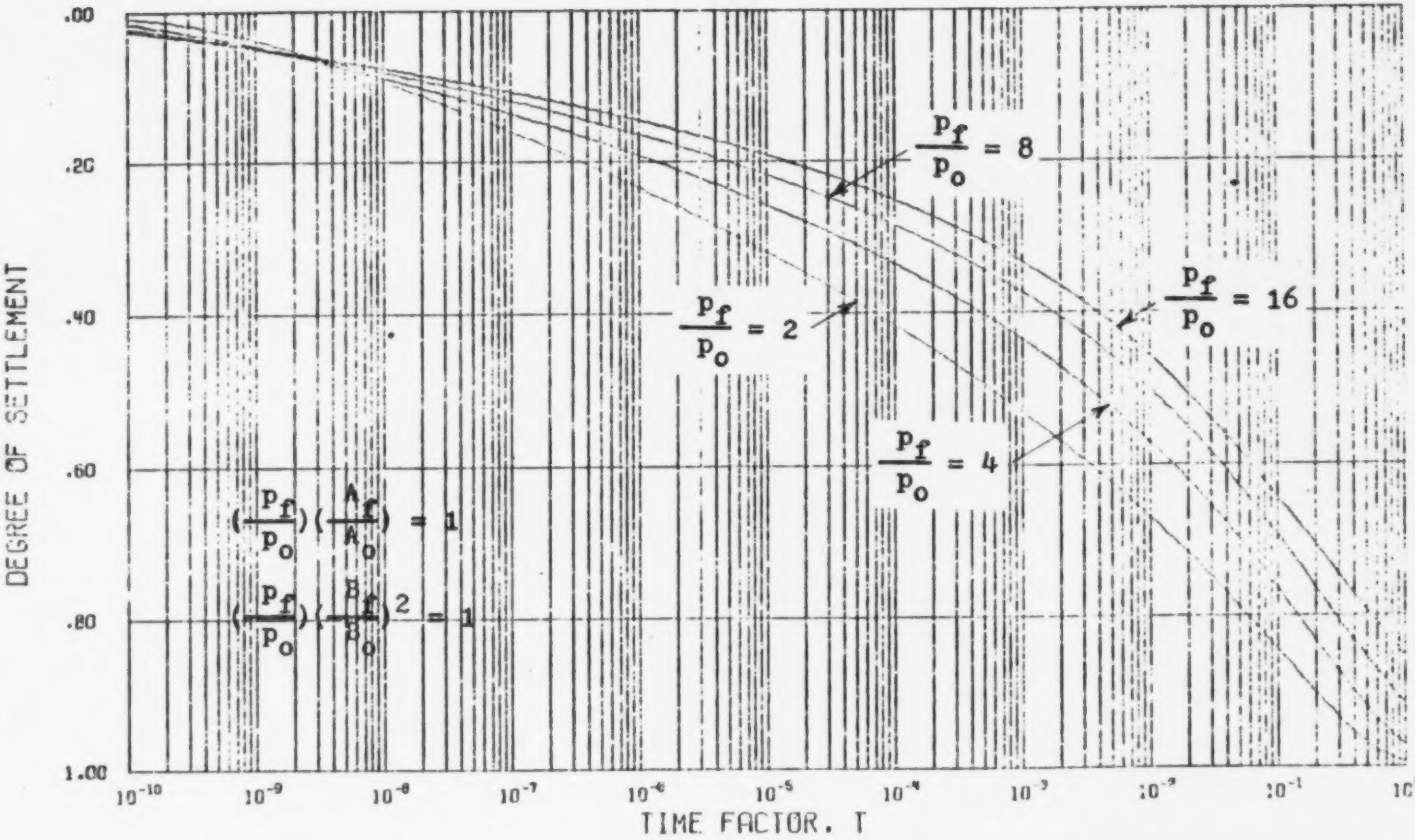

Fig. D-63. Settlement vs. time factor of the creep model based on micropore structure for various values of p_f/p_o; $B_o = 19$

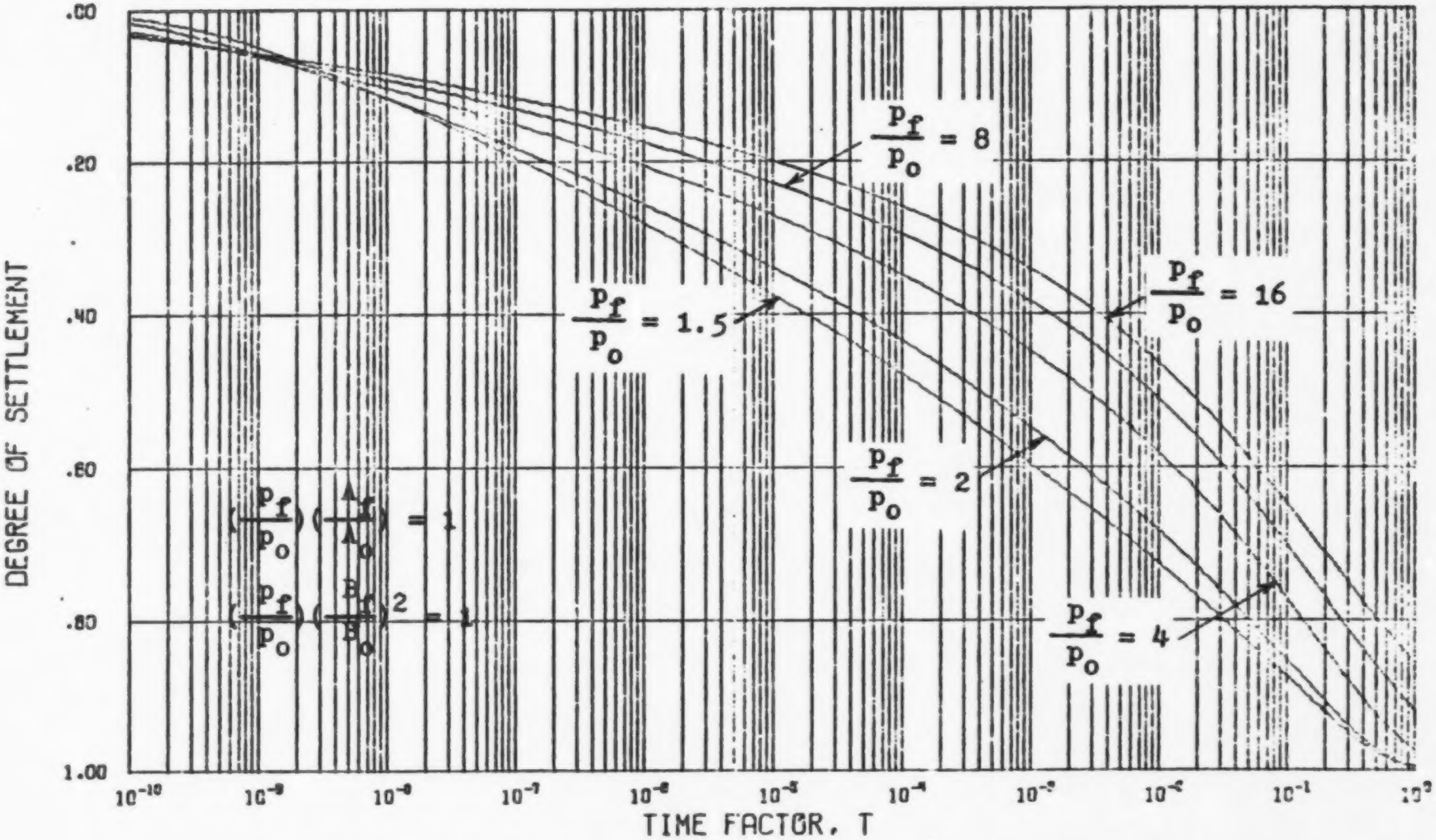

Fig. D-64. Settlement vs. time factor of the creep model based on micropore structure for various values of p_f/p_o; $B_o = 20$

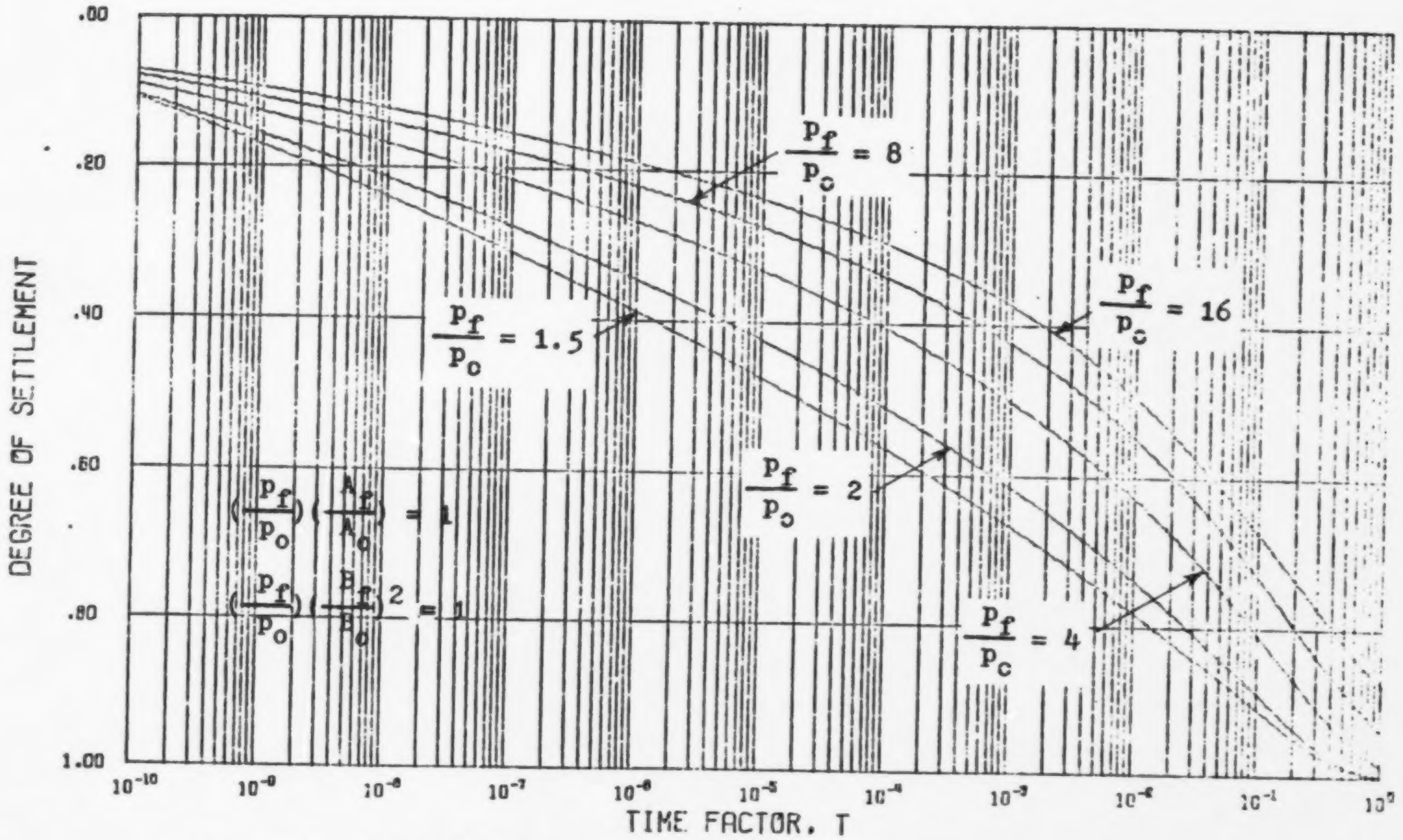

Fig. D-65. Settlement vs. time factor of the creep model based on micropore structure for various values of p_f/p_o, $B_o = 25$

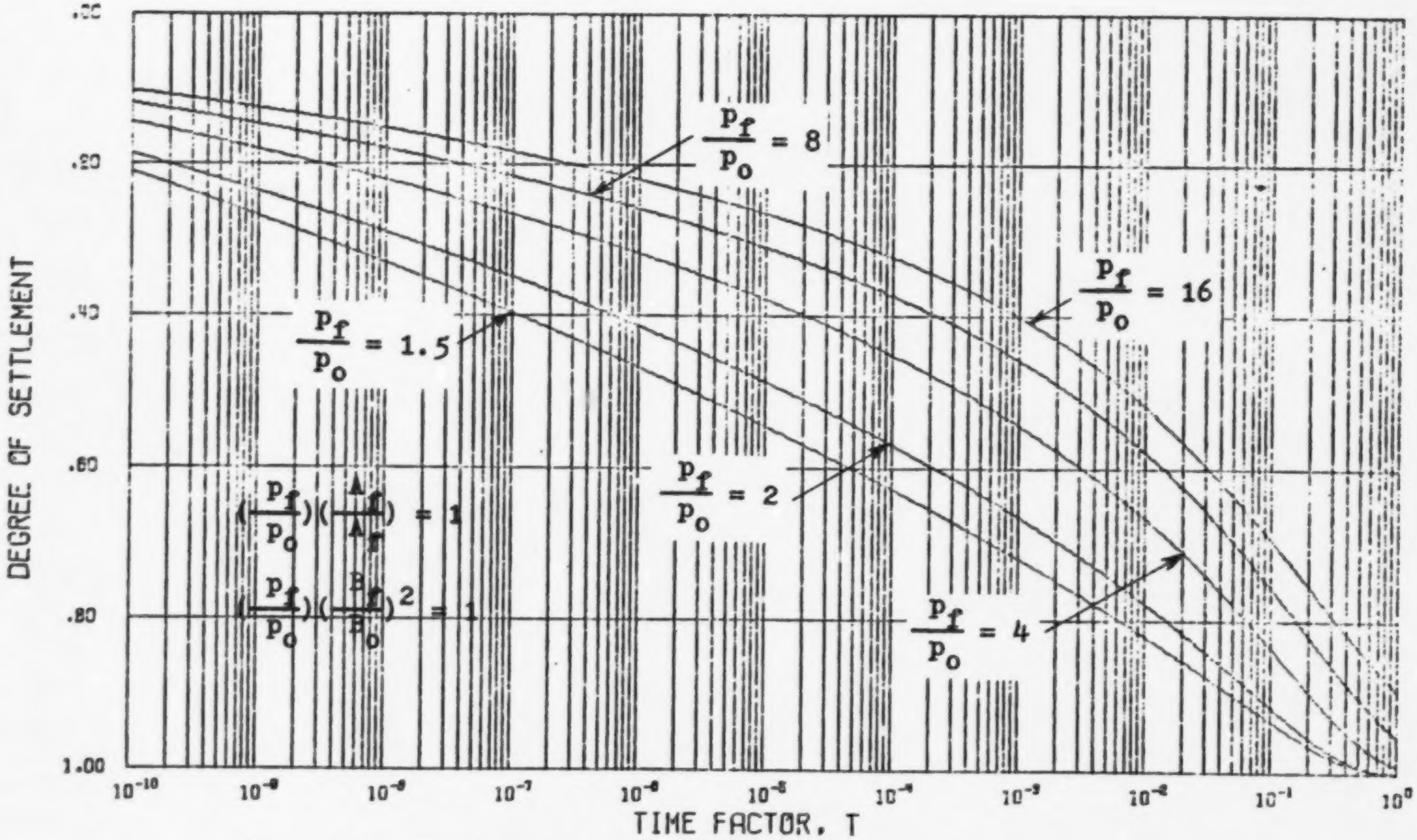

Fig. D-66. Settlement vs. time factor of the creep model based on micropore structure for various values of p_f/p_o, $B_o = 30$

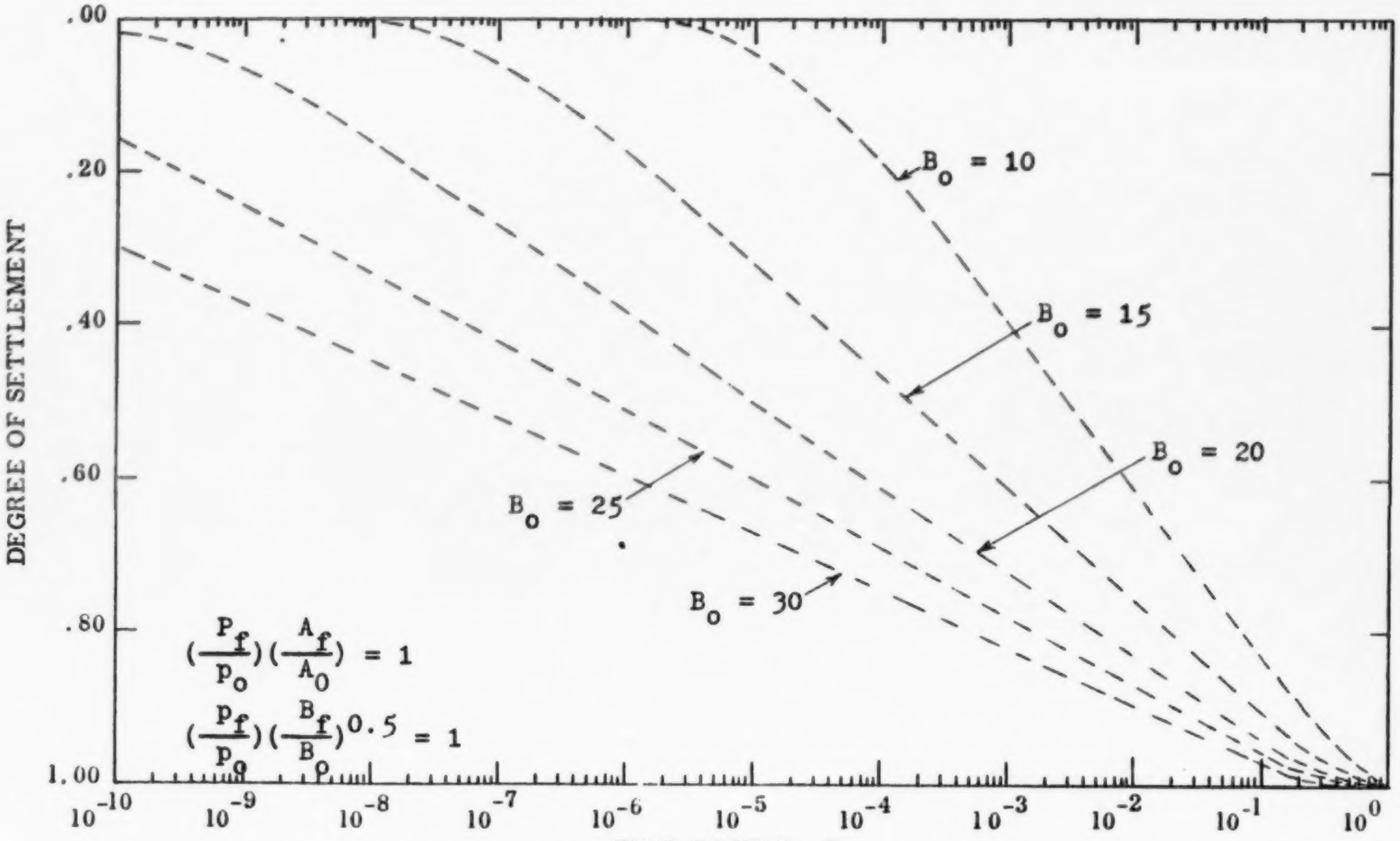

Fig. D-67. Settlement vs. time factor of the creep model based on micropore structure for various values of B_o; $p_f/p_o = 1.5$

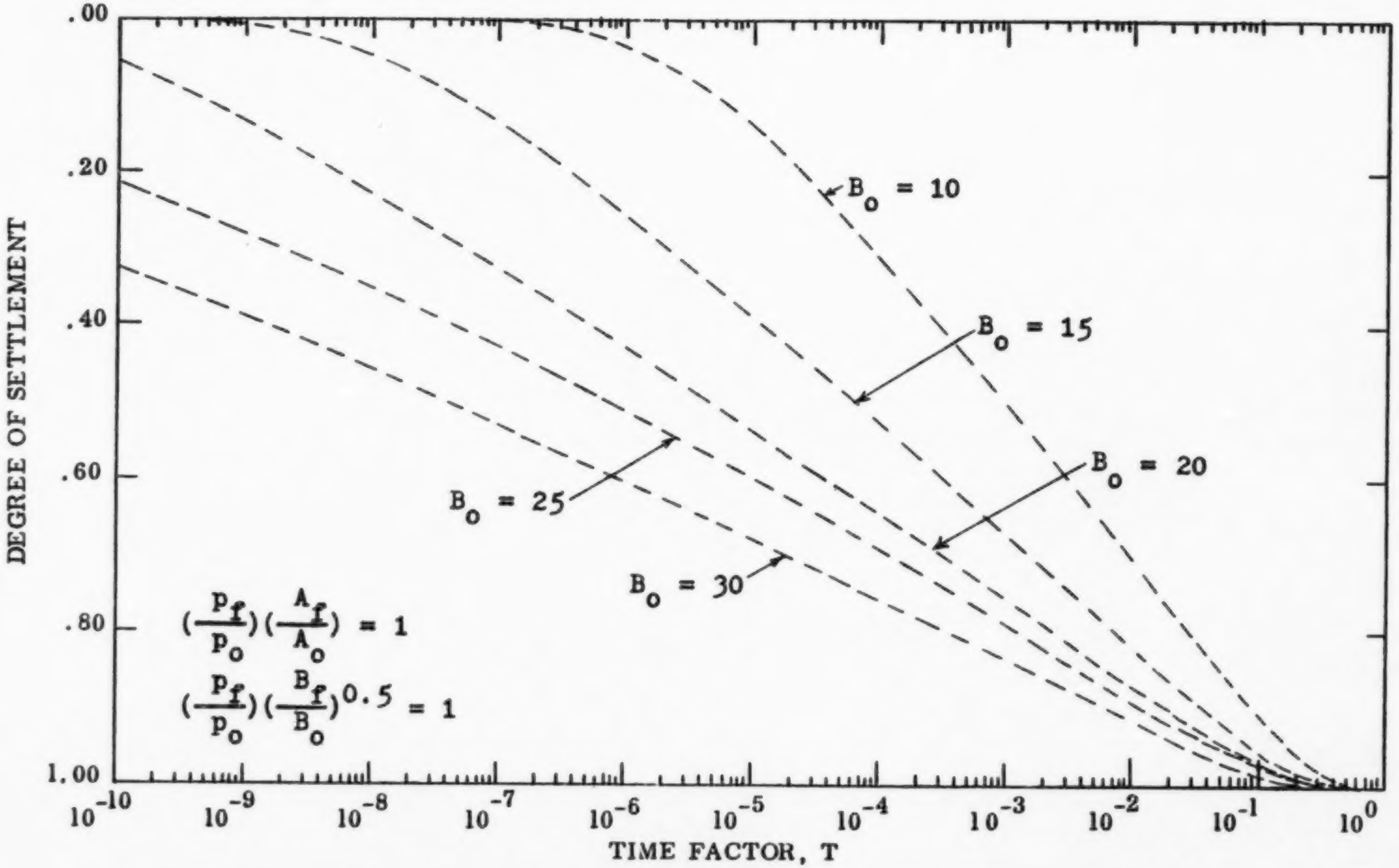

Fig. D-68. Settlement vs. time factor of the creep model based on micropore structure for various values of $B_o; p_f/p_o = 4$

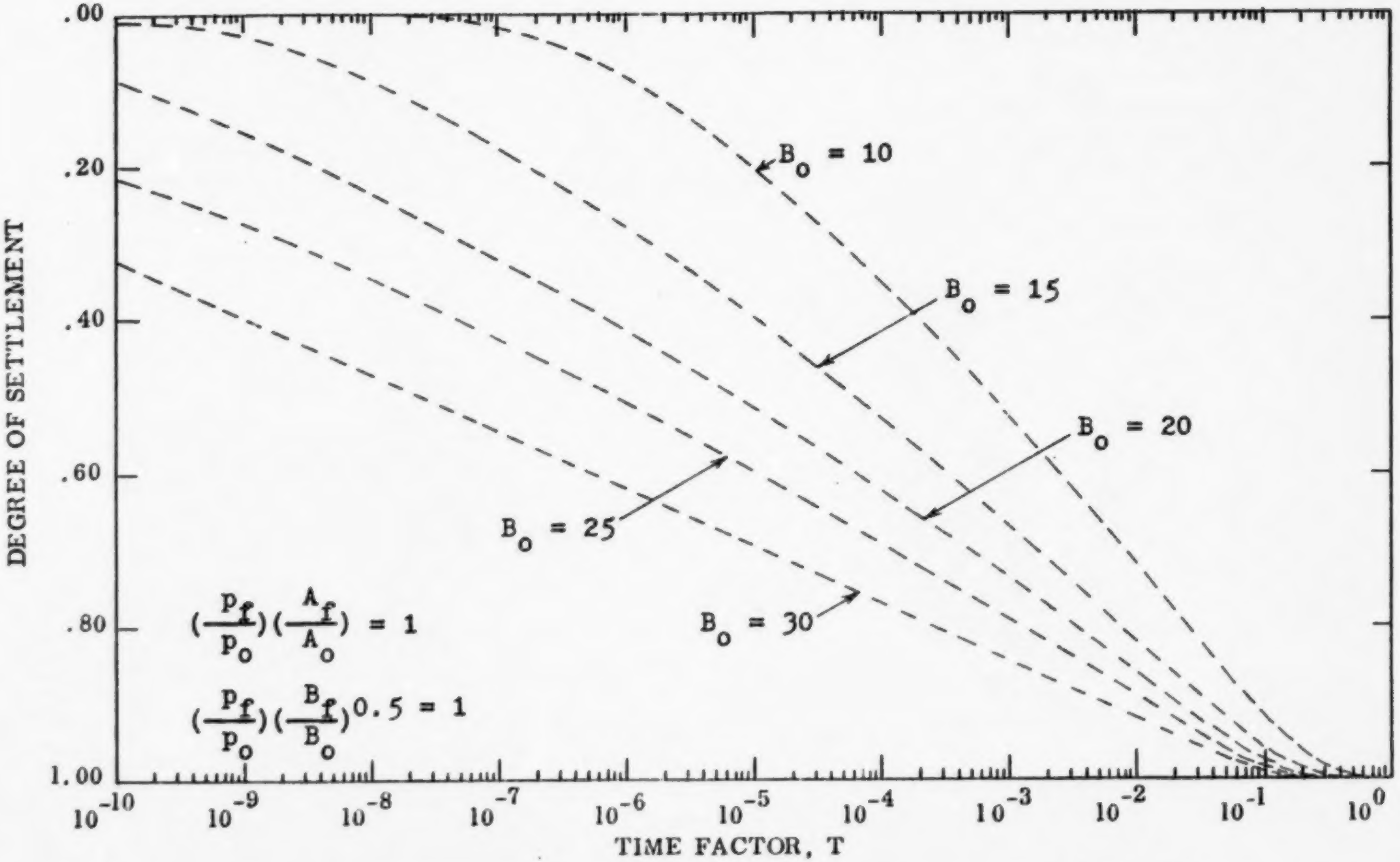

Fig. D-69. Settlement vs. time factor of the creep model based on micropore structure for various values of B_o, $p_f/p_o = 16$

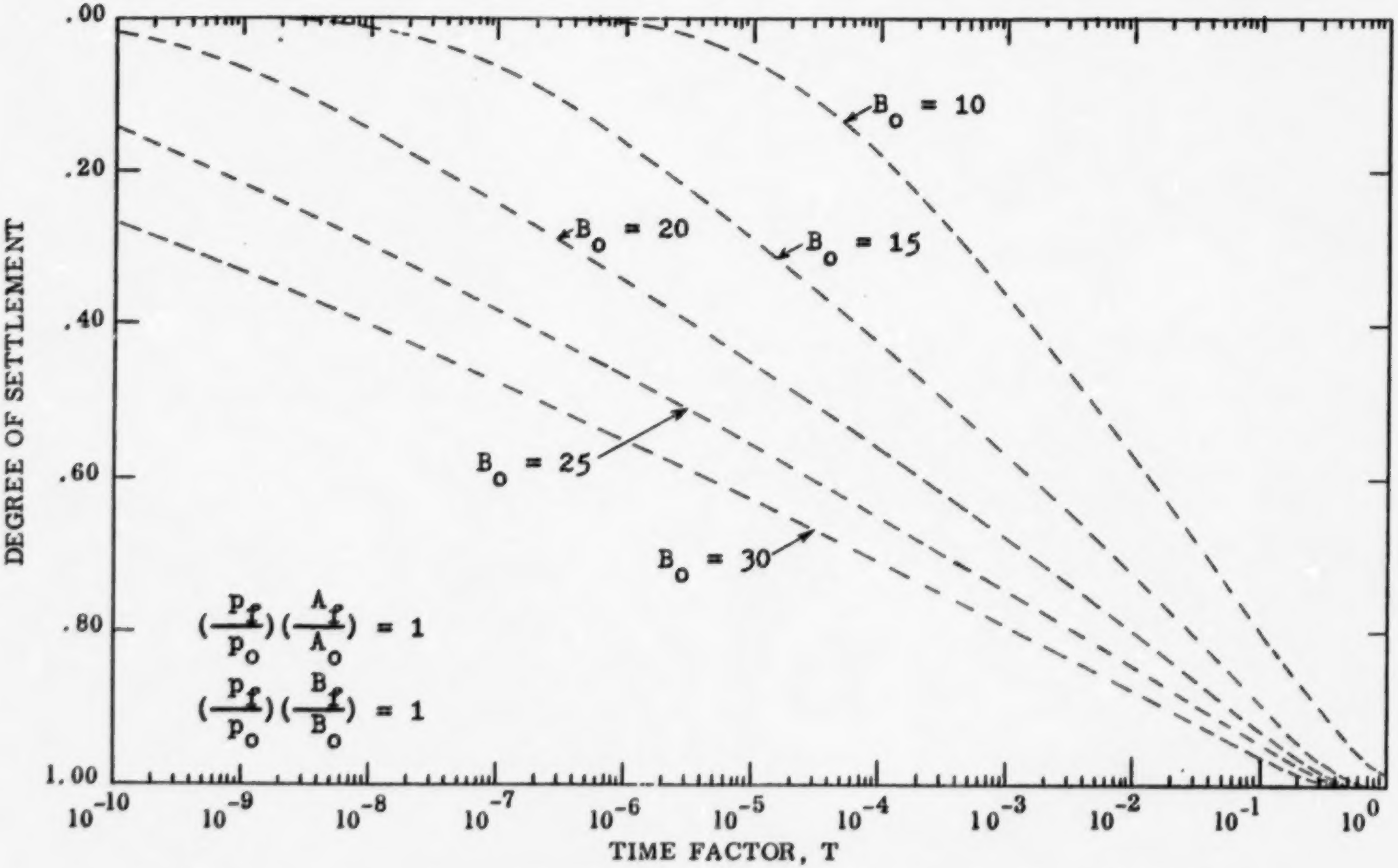

Fig. D-70. Settlement vs. time factor of the creep model based on micropore structure for various values of B_o; $p_f/p_o = 1.5$

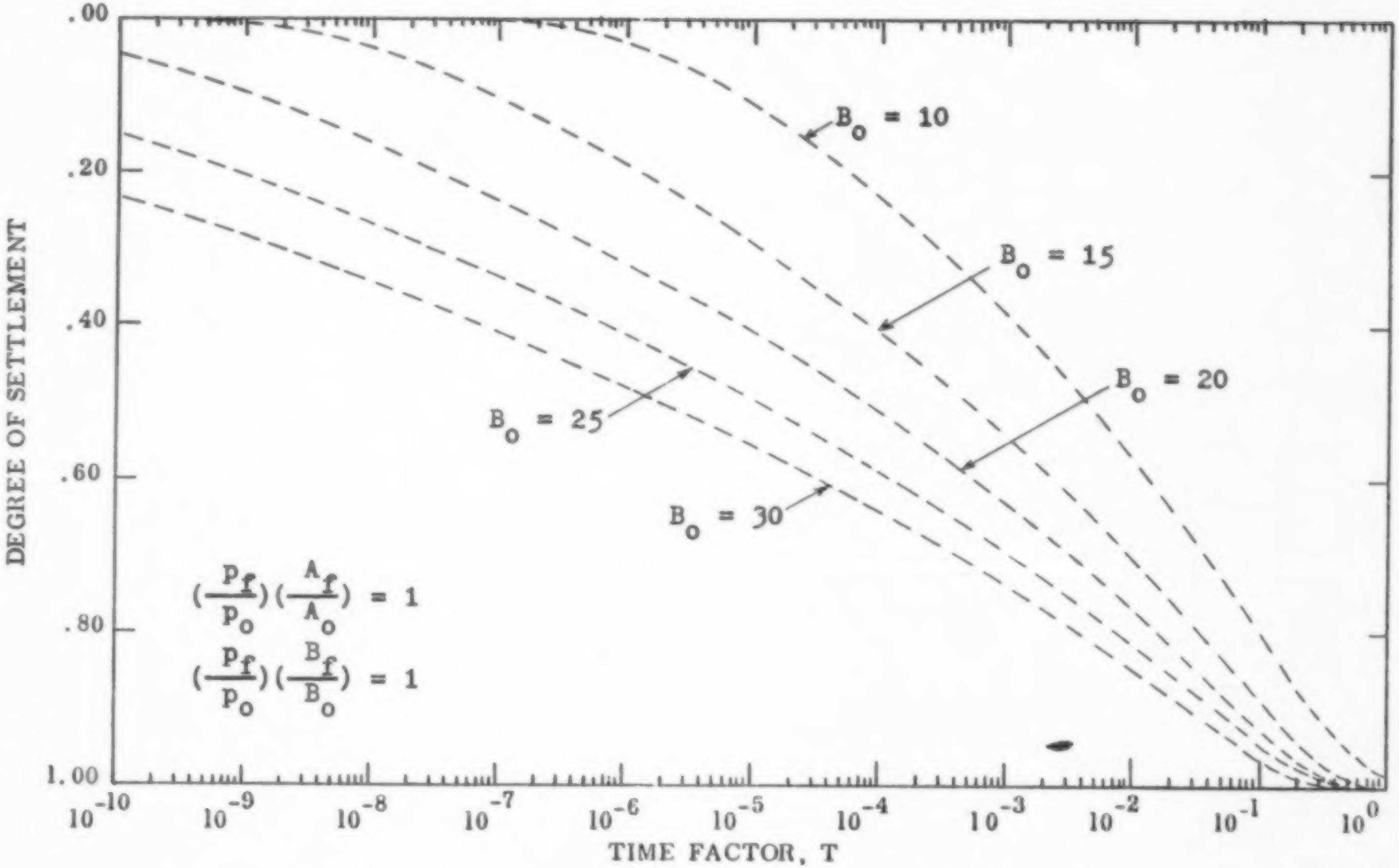

Fig. D-71. Settlement vs. time factor of the creep model based on micropore structure for various values of B_o; $p_f/p_o = 4$

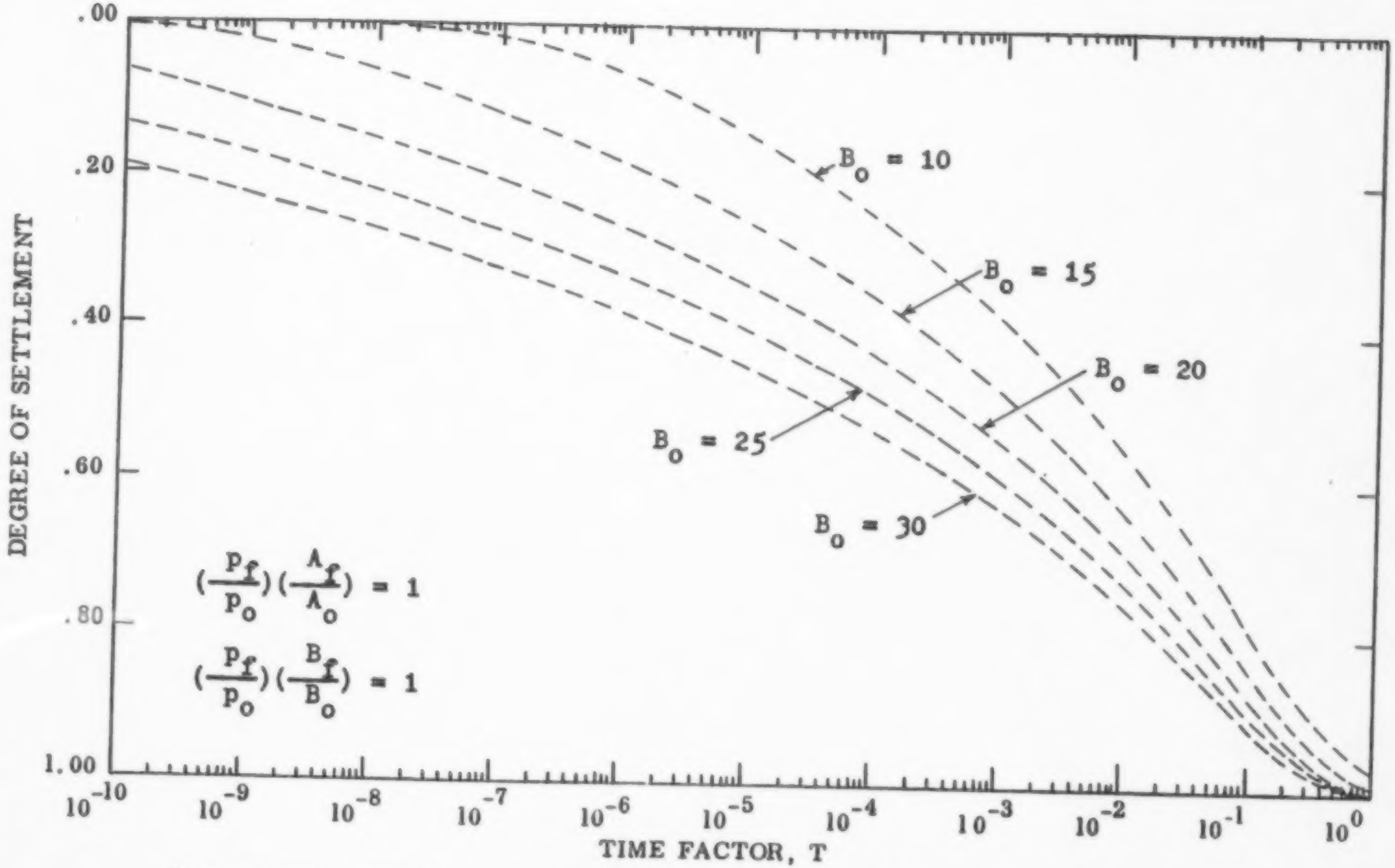

Fig. D-72. Settlement vs. time factor of the creep model based on micropore structure for various values of B_o: $p_f/p_o = 16$

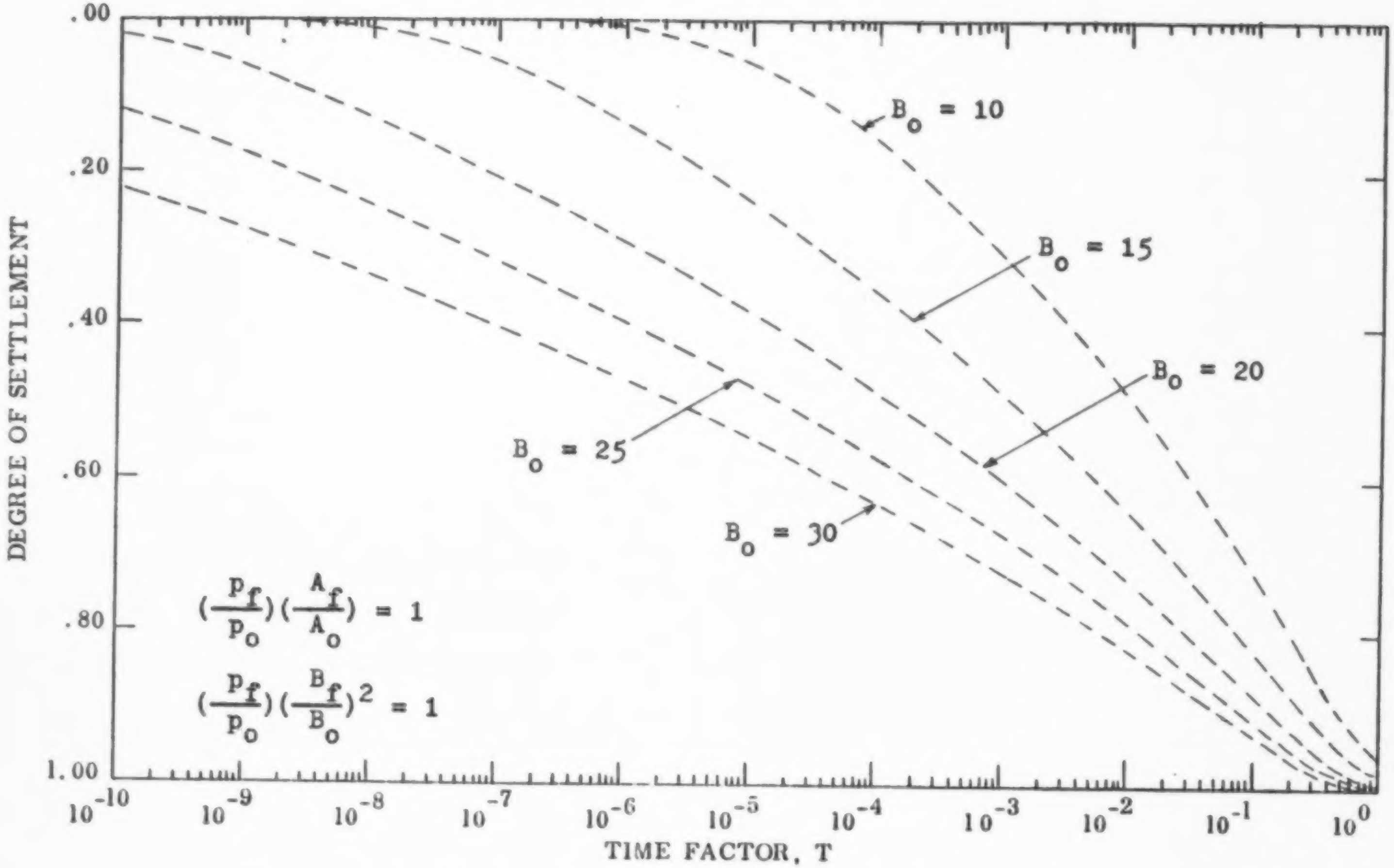

Fig. D-73. Settlement vs. time factor of the creep model based on micropore structure for various values of B_o; $p_f/p_o = 1.5$

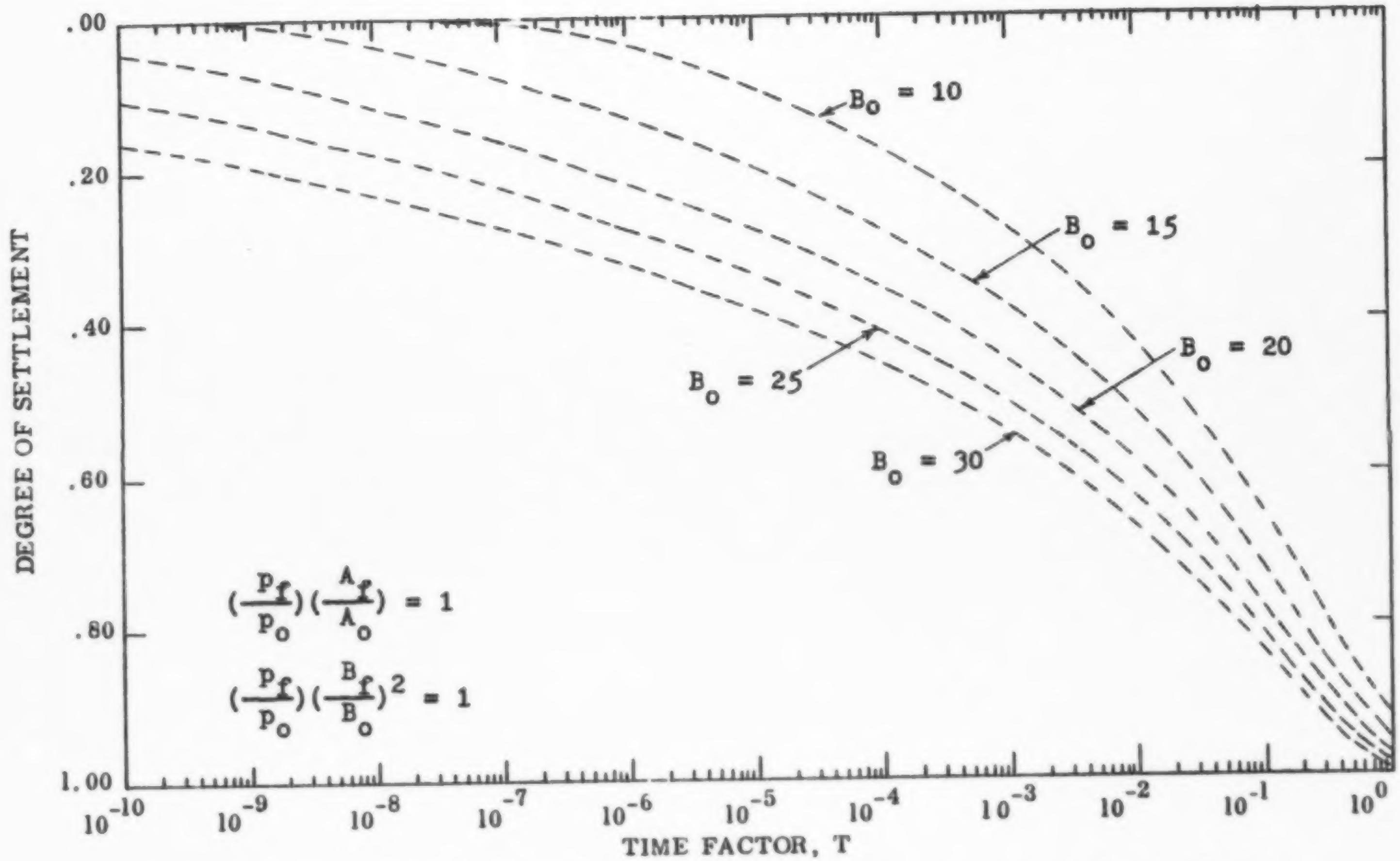

Fig. D-74. Settlement vs. time factor of the creep model based on micropore structure for various values of $B_o{}' P_f/P_o = 4$

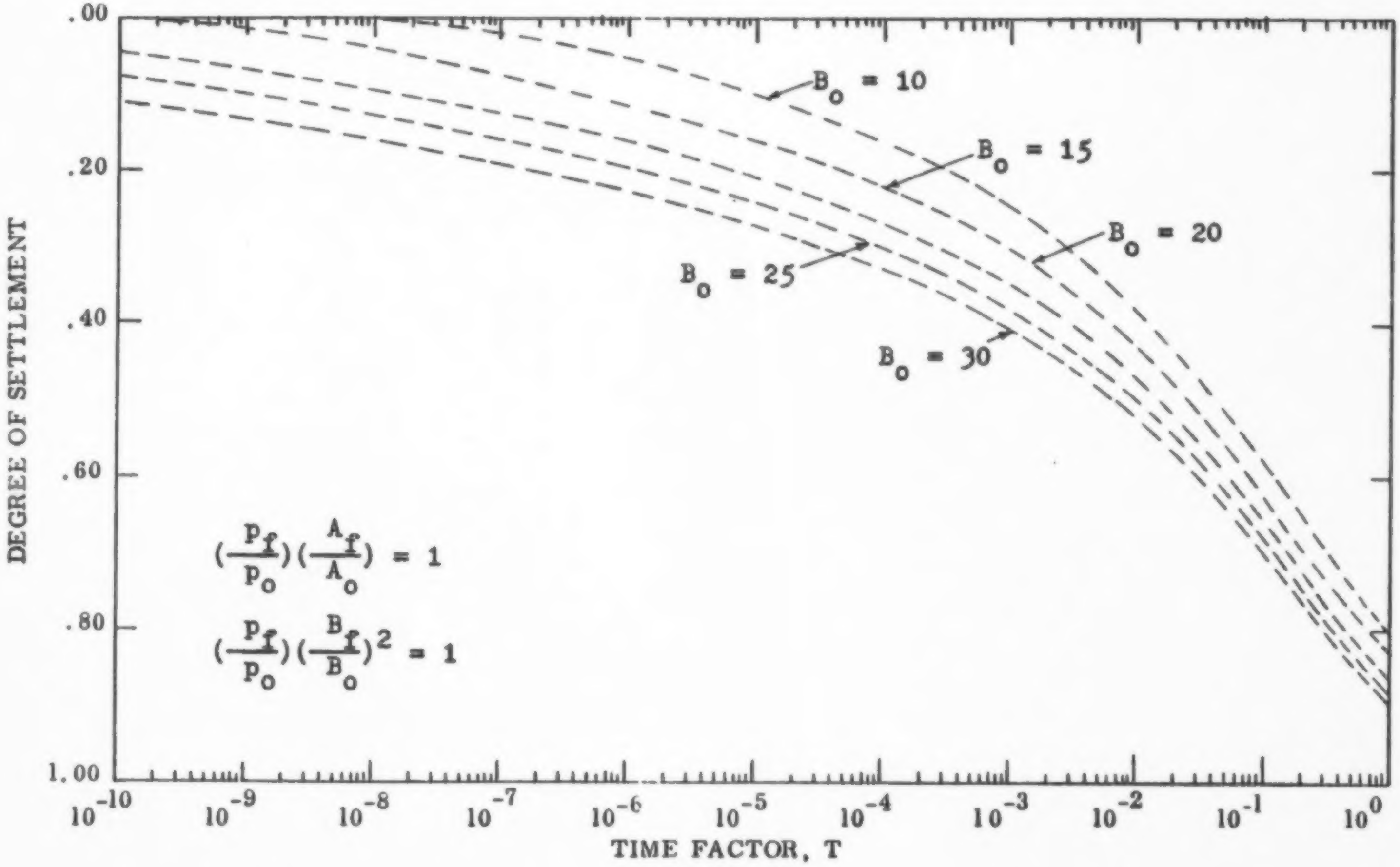

Fig. D-75. Settlement vs. time factor of the creep model based on micropore structure for various values of B_o; $p_f/p_o = 16$

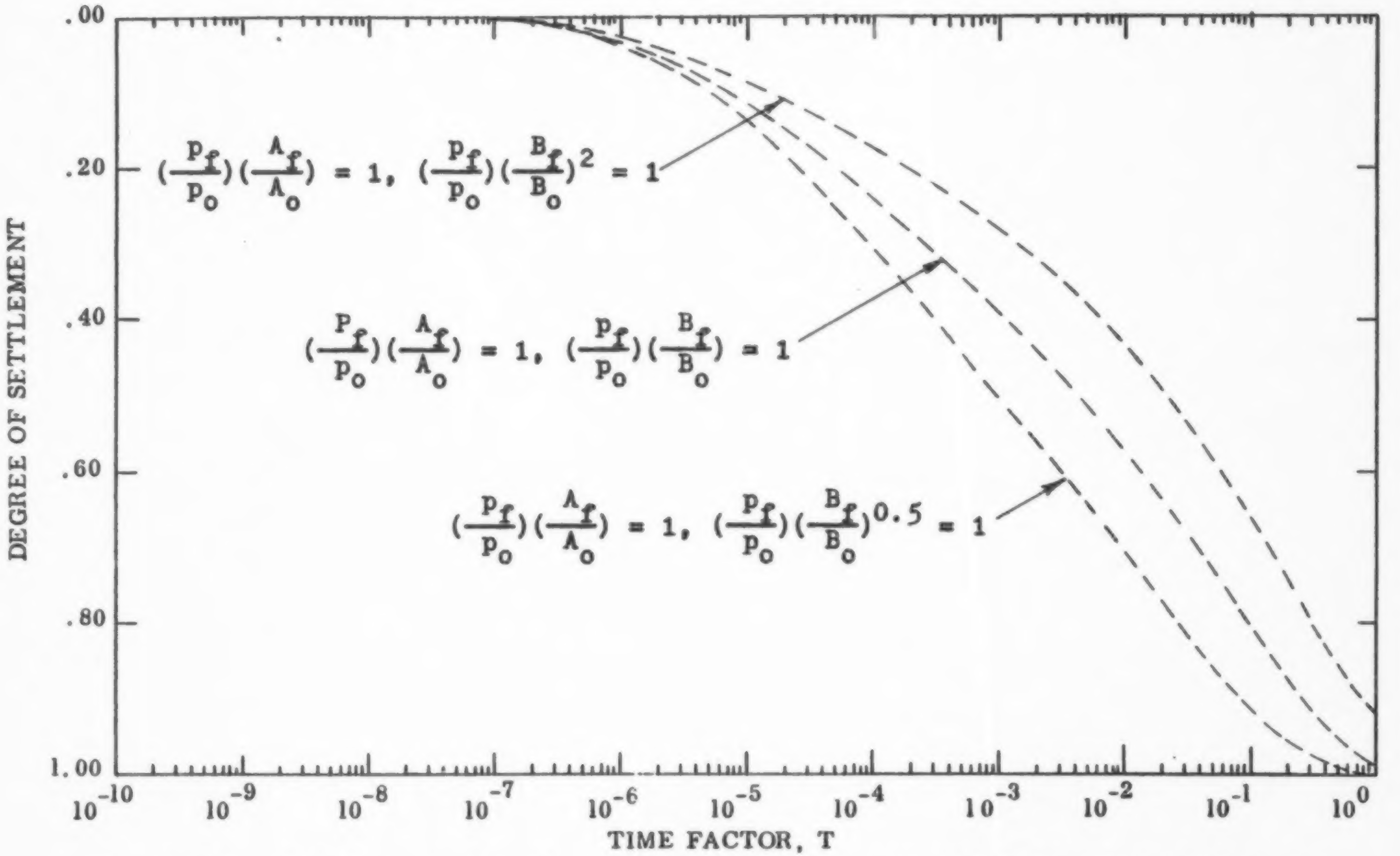

Fig. D-76. Settlement vs. time factor of the creep model based on micropore structure for various values of the ratio of the slope of the e_b-log p line to the slope of the e_b-log B line: B_o=10, p_f/p_o = 4

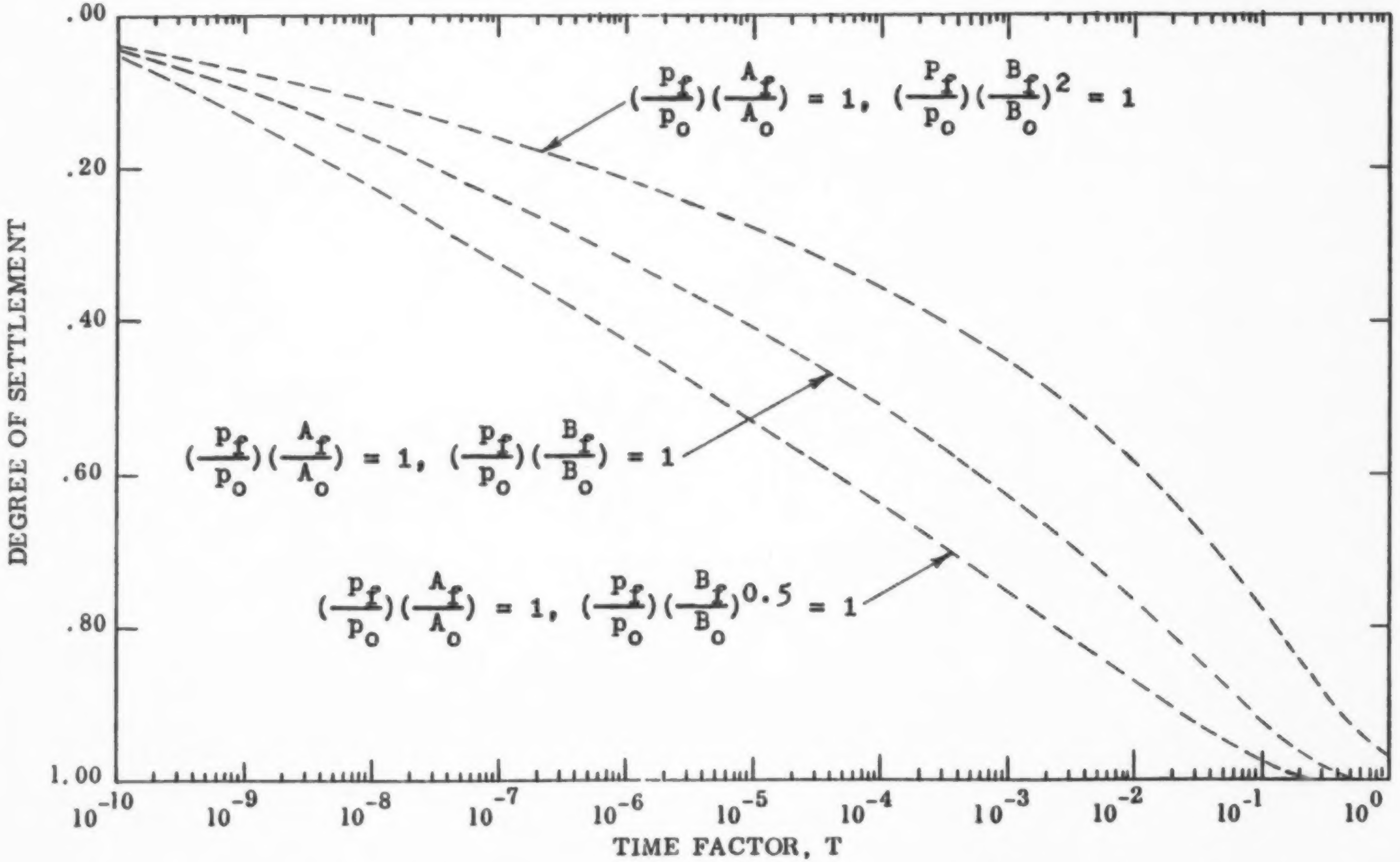

Fig. D-77. Settlement vs. time factor of the creep model based on micropore structure for various values of the ratio of the slope of the e_b-log p line to the slope of the e_b-log B line: $B_o = 20$, $p_f/p_o = 4$

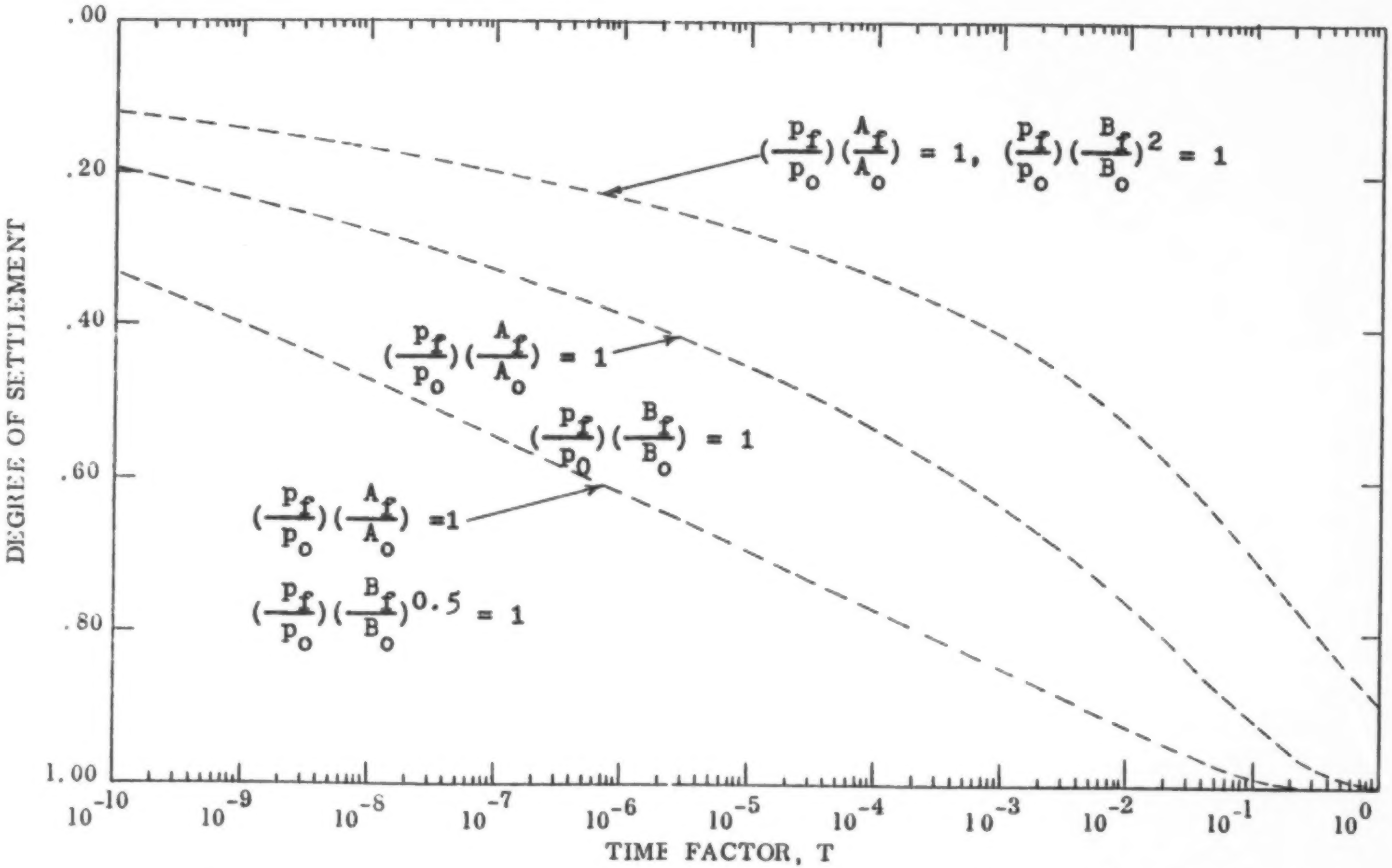

Fig. D-78. Settlement vs. time factor of the creep model based on micropore structure for various values of the ratio of the slope of the e_b-log p line to the slope of the e_b-log B line: B_o=30, p_f/p_o = 4